

University of Mons
Doctoral School MUSICS
Signal Processing

P H D T H E S I S

to obtain the title of

PhD in Engineering Sciences

of University of Mons

Specialty: BIOMEDICAL SIGNAL PROCESSING

Defended by

Matthieu DUVINAGE

**Towards Effective Non-Invasive
Brain-Computer Interfaces Dedicated
to Ambulatory Applications**

**Theoretical and practical contributions oriented to the
control of a lower limb orthosis**

Thesis Advisor: Thierry DUTOIT

Thesis Co-Advisor: Thierry CASTERMANS

prepared at University of Mons, Faculty of Engineering,
TCTS Lab

Jury:

Prof. Dr. Thierry DUTOIT	- University of Mons, Belgium
Dr. Thierry CASTERMANS	- University of Mons, Belgium
Prof. Dr. Alain VANDE WOUWER	- University of Mons, Belgium
Prof. Dr. Bernard GOSELIN	- University of Mons, Belgium
Dr. Quentin NOIRHOMME	- University of Liège, Belgium
Dr. Fabien LOTTE	- Inria Bordeaux, France

Get up, pick up your pallet and walk
Jesus

Acronyms

ANOVA	Analysis of Variance
BCI	Brain-Computer Interface
BNCI	Brain-Neuronal Computer Interfaces
BP	BereitschaftsPotential
BSS	Blind Source Separation
CCA	Canonical Correlation Analysis
CNS	Central Nervous System
CPG	Central Pattern Generator
CRT	Cathode Ray Tube
DRNN	Dynamic Recurrent Neural Network
ECoG	Electrocorticography
EEG	Electroencephalogram
EMG	Electromyogram
EOG	Electrooculography
ERD	Event-Related Desynchronization
ERP	Event-Related Potential
ERS	Event-Related Synchronization
ERSP	Event-Related Spectral Perturbation
FES	Functional Electrical Stimulation Imaging
FFT	Fast Fourier Transform
fMRI	functional Magnetic Resonance
FPR	False Positive Rate
FWER	Family-Wise Error Rate
GIA	Global Industry Analyst
GL	Gluteus Maximus
GM	Gastrocnemius Medialis
GRF	Ground Reaction Forces
HL	Lateral Hamstrings
HM	Medial Hamstrings
HS	Heel Strike
ICA	Independent Component Analysis

ITC	Inter-Trial Coherence
LCD	Liquid Crystal Display
LDA	Linear Discriminant Analysis
LED	Light Emitting Diode
LFP	Local Field Potential
LMS	Least Mean Square
M1	Primary Motor Cortex
MEG	Magnetoencephalography
MLR	Mesencephalic Locomotor Region
MRP	Movement Related Potential
MUA	Multi-Unit Activity
Nasa-TLX	Nasa Task Load Index
NFC	Normalized Frequency Control
NIRS	Near Infrared Spectroscopy
PCA	Principal Component Analysis
PCPG	Programmable Central Pattern Generator
PET	Positron Emission Tomography
PNS	Peripheral Nervous System
PWM	Pulse Width Modulation
RF	Rectus Femoris
RIC	Rehabiliation Institute Chicago
RLS	Recursive Least Square
ROC	Receiver Operator Curve
S1	Primary Somatosensory Cortex
SCI	Spinal Cord Injury
SCP	Slow Cortical Potential
SFFS	Sequential Forward Floating Search
SI	Similarity Index
SMA	Supplementary Motor Area
SNR	Signal-to-Noise Ratio
SPECT	Single Photon Emission Tomography
SPL	Sound Pressure Level
SSVEP	Steady-State Visual Evoked Potential
SUA	Single-Unit Activity
SUS	System Usability Scale
TA	Tibialis Anterior
TO	Toe Off
TTD	Though Translation Device
VEP	Visual Evoked Potential
VL	Vastus Lateralis
VM	Vastus Medialis

Acknowledgements and Non-Acknowledgements

First, I want to thank Professor Joel Hancq and Professor Thierry Dutoit for welcoming me in the TCTS Lab and participating in funding my research. I also thank the Professor Guy Cheron for giving me the possibility to use his lab for my experiments. I am also debt-full to the Fonds National de la Recherche Scientifique (FNRS) without which this PhD thesis would not have been possible.

Then, I express my deepest gratitude to Dr. Thierry Castermans, my co-supervisor and daily collaborator/psychologist, for his incredible patience, good mood and personal discussion. I also thank Professor Marc Pirlot, who introduced me to statistics. I would like to thank all my co-authors without whom this PhD thesis would not have been feasible. I also thank them for contributing to this unique experience. A special thank goes to Kevin Nis and Regis Berton for their helpful expertises in electronics and orthosis design.

I also want to thank my family for their unconditional support. First, my thanks go to my parents who worked hard to give me everything I need to be successful up to now including food, shelter, education and character. They made me like understanding, which is the basis of my success. Second, I thank my grand parents and my sister for the good moments we have lived together so far. Then, I thank my whole family for what they brought to me as experience and enjoyable moments, like the numerous mathematical courses about trigonometry with Sebastien. I am also grateful to my girlfriend, Sylvie Scolas, for having supporting me despite several tough nights and weekends dedicated to my Master thesis at FUCAM and this PhD thesis. I also thank her for helping in .doc .latex conversion. I also thank Panpan, Cheap Sheep, Simba, and all the "petits chous" for increasing my large family. I also thank Madame Berte, my speech therapist for providing essential help during my youth. Finally, I want to honour all the people that I have met in my life and who construct my personality and my way of thinking, this PhD thesis is our success.

I would like to thank my colleagues for supporting my economical, financial, political, social, technological discussions and for providing me with a lot of fun working in the TCTS Lab. I would like to address a special thank to Nathalie Durieux, my personal secretary who helped me to hide my strongly negative lab account from the authorities. By this, I would like to emphasize that she knew everything. Another special thought is addressed to the "Parrain Montois", who made me discover attention modelling and how big brother will strengthen in the near future. I am also grateful to all my master students who somehow helped in my work. I address a special thank to Jeremy Cubetta who help me recover my debugging skills in a very narrow

time. Finally, I want to thank Professor Mikael Petitjean and PhD Paollo Mazza for making me discover the wonderful world of financial economics. I also thank them for their collaborative work on financial topics and economical discussion.

Finally, I want to honour innovation and entrepreneurship. Indeed, innovation leads to productivity gains that lay the foundation of growth. But, without the help of entrepreneurship to convert innovation into innovative products, the claimed productivity gains would never be materialized. As shown by the National Bank of Belgium, these two aspects are at least more important than labour costs while speaking about competitiveness.

On top of that, I want to address some non-acknowledgements. First, my deepest contempt goes to researchers whose lack of ethics is contributing to stain research. By providing false results, blocking papers in the reviewing process to steal ideas by intensively old-boy network, they contribute to a bad resource allocation. This tends to decrease growth and increase inefficient funding attributions. Indeed, the structural European underperforming job market is partly your fault. Shame on you !

Second, I hate people who disregard manual work. Indeed, one problem of Belgium is the assumption that studies are the only way to get a good job. This way of thinking leads to consider that manual workers are less valuable than intellectual workers. It also suggests non-general high school studies as the last chance of stupid people. This is completely wrong and I believe once this problem will be fixed, job market and global happiness of Belgian people will be increased.

Third, I do not thank European politicians who are responsible for the current economic downturn. Indeed, by lacking of economic and European vision, their contributions to poverty and unemployment rates are important. I just hope that this crisis will show them how important the economy is and that only a unified and close-to-people Europe will be a key of success towards prosperity.

Fourth, by not supplying a high-quality service, the SNCB railway company has a big contribution to the disappearance of polar bears. Actually, this poor quality service is undoubtedly a major reason of the extensive car use in Belgium participating to global warming.

Fifth, people with dogmas about the state intervention in the economy are often counter-productive. Indeed, what matters is the overall efficiency. It is easily observed that Switzerland and Northern countries in Europe have been known for their strong economy and efficient job market. However, those countries have a completely different point of view when dealing with the state role and social benefits. Moreover, as discussed by Joseph E. Stiglitz, the growing inequality in the world may bring to the edge of a new revolution. Keep in mind that first and second world wars were partly an outcome of this situation. On the other hand, I can not agree with politicians that consider a country with a high level of social benefits as a social country when 15% of the population is unemployed. These benefits are not an excuse for such a personal drama.

Sixth, because education is one of the most important contribution to a strong economy, people refusing to refinance or to enhance the overall match between job market and teaching quality are responsible for unemployment rate. By providing a high-quality and affordable education system, the country is giving a chance to everybody to get an adequate job. Moreover, a properly educated population would bring a more objective assessment of policy maker actions, a more responsive population to economic stimuli and a more cost effective administration.

Abstract

Disabilities affecting mobility, in particular, often lead to exacerbated isolation and thus fewer communication opportunities, resulting in a limited participation in social life. Additionally, as costs for the health-care system can be huge, rehabilitation-related devices and lower-limb prostheses (or orthoses) have been intensively studied so far. However, although many devices are now available, they rarely integrate the direct will of the patient. Indeed, they basically use motion sensors or the residual muscle activities to track the next move.

Therefore, to integrate a more direct control from the patient, Brain-Computer Interfaces (BCIs) are here proposed and studied under ambulatory conditions. Basically, a BCI allows you to control any electric device without the need of activating muscles. In this work, the conversion of brain signals into a prosthesis kinematic control is studied following two approaches. First, the subject transmits his desired walking speed to the BCI. Then, this high-level command is converted into a kinematics signal thanks to a Central Pattern Generator (CPG)-based gait model, which is able to produce automatic gait patterns. Our work thus focuses on how BCIs do behave in ambulatory conditions. The second strategy is based on the assumption that the brain is continuously controlling the lower limb. Thus, a direct interpretation, i.e. decoding, from the brain signals is performed. Here, our work consists in determining which part of the brain signals can be used.

This manuscript consists of three different parts: ambulatory BCIs, gait modelling and gait-related spontaneous brain signals. In the first part, it is shown that for several standard BCIs based on P300 and SSVEP, the effect of gait-related artefacts is not that important. Additionally, it was demonstrated that an online application using SSVEP and P300 are definitely feasible, while the SSVEP interface is much more accepted by subjects based on subjective questionnaires. A comparison between the low-cost Emotiv EPOC Headset and a medical device shows that the former system has the potential to increase the BCI use among end-users. To expand control interfaces to eye movements, electrooculographic signal based recognition methods have been intensively reviewed showing that little difference exists between the standard and modified approaches.

In the second part, two gait model approaches are studied. A modified Programmable Central Pattern Generator (PCPG) algorithm is proposed to fit at best the actual patient movement. First, the parameters of the model are continuously adapted depending on the speed thanks to a polynomial interpolation. Then, as gait is not perfectly periodic, a new soft-phase resetting method was proposed and assessed. Second, a Dynamic Recurrent Neural Network combined with sinusoidal inputs is shown to provide a better fit than the PCPG approach.

In the third part, the spontaneous gait-related signal studies are exposed. First, a deep review of the current knowledge in gait-related spontaneous signal is provided. Then, an experiment of artefact free gait-like movements sitting on a chair shows significant brain activities synchronized to feet movement. Afterwards, using an accelerometer and a hardware prototype system, it was shown that current gait-related studies should be affected by artefacts. Finally, a review of gait intent detection methods was proposed.

As perspective, a major focus would be to properly disentangle artefacts and brain signals. Given the phase-locking trick between both signals, the use of phase-locked based decomposition methods is suggested.

Keywords: Brain-Computer Interfaces, Ambulatory Conditions, Artefacts, Gait Model, Central Pattern Generator, Electroencephalography, Electrooculography, Eye Movement Detection, SSVEP, P300, SUS, NASA-TLX, Gait, Readiness Potential, Dynamic Recurrent Neural Network, Artefact Removal Techniques, Event-Related (De)synchronisation.

Contents

1 General Introduction	1
1.1 Brain Control of a Lower Limb Prosthesis	1
1.1.1 Context	1
1.1.2 Description of the Gait Cycle	2
1.1.3 The Ankle-Foot Device Market	3
1.2 Brain-Computer Interfaces (BCIs)	10
1.2.1 Measuring Brain Activity	10
1.2.2 Standard Brain-Neuronal Computer Interfaces (BNCIs)	15
1.3 Strategies and contributions	25
1.3.1 Strategies	25
1.3.2 Artefact Problematic	27
1.3.3 Organization of The Manuscript	28
I Central-Pattern Generator Based Gait Modelling	39
2 PCPG Gait Model and Orthosis Implementation	41
2.1 Introduction	44
2.2 Gait Model	44
2.2.1 PCPG Description	44
2.2.2 Experimental and methodological approaches	47
2.2.3 Results and discussion	48
2.3 Orthosis Design and Control	50
2.3.1 Orthosis Hardware	50
2.3.2 Gait cycle control strategies	52
2.4 Practical needs	53
2.4.1 Frequency adaptation	53
2.4.2 Phase-resetting	54
2.5 Simulation Results	55
2.6 Conclusion and Future Work	57
2.6.1 Conclusion	57
2.6.2 Future Work	57

3 DRNN-based Gait Model	61
3.1 Introduction	63
3.2 Background	63
3.3 Methods	65
3.3.1 Experimental Setup	65
3.3.2 Dynamical Recurrent Neuronal Network	66
3.3.3 Experiment 1: Proof of concept	67
3.3.4 Experiment 2: Multiple pattern learning and prediction	69
3.3.5 Neuronal properties and connectivity after learning	70
3.3.6 Statistical analysis	70
3.3.7 Computations	70
3.4 Results	73
3.4.1 Experiment 1: Proof of concept	73
3.4.2 Experiment 2: Prediction of intermediary velocities	73
3.4.3 DRNN structures from experiment 2	76
3.4.4 Neurophysiological similarity	76
3.4.5 Structural Similarities	79
3.5 Conclusion	81
II Brain-Computer Interfaces in An Ambulatory Framework	91
4 Ambulatory SSVEP Analysis	93
4.1 Introduction	95
4.2 Method	95
4.2.1 SSVEP Paradigm	95
4.2.2 Experiment Description	96
4.2.3 Performance Evaluation	96
4.3 Results and Discussion	99
4.4 Conclusions	104
5 Ambulatory P300	109
5.1 Introduction	111
5.2 BCIs in ambulatory conditions: a state of the art	111
5.2.1 Artefacts present in EEG recordings	111
5.2.2 Artefacts typically related to gait	112
5.2.3 An ambulatory BCI system based on auditory P300 potentials	112
5.2.4 An ambulatory BCI system based on steady-state evoked potentials	113
5.2.5 Proposed methods to remove gait-related artefacts	114
5.3 Experimental procedure and data analysis	116
5.3.1 Data collection	116
5.3.2 Pre-processing	117
5.3.3 Identification and correction of gait artefacts	119
5.3.4 Feature extraction	121

5.3.5	Classification	122
5.4	Results and discussion	122
5.4.1	Efficiency of the methods in terms of EEG signal properties	124
5.4.2	Efficiency of the methods in terms of P300 classification performance	124
5.4.3	Classification performance using spatial filtering	125
5.4.4	Classification Performance Using The Optimal Configuration	126
5.5	Conclusion	128
6	Online BCI Feedback	135
6.1	Introduction	137
6.2	SSVEP System	138
6.2.1	SSVEP Approach	138
6.2.2	SSVEP Pipeline	139
6.2.3	Experiment Description	141
6.3	Performance Measures	142
6.3.1	Subjective Feedback Measures	142
6.3.2	Objective Performance Measures	143
6.4	Discussion	143
6.5	Conclusions and Future Work	147
7	Performance of the Emotiv Epoc Headset	153
7.1	Introduction	155
7.2	Previous Studies	155
7.3	Acquisition systems	156
7.3.1	ANT	156
7.3.2	Emotiv EPOC	157
7.4	BCI system	157
7.4.1	P300-based approach	157
7.4.2	P300 pipeline	160
7.5	Performance evaluation	162
7.5.1	Performance measures	162
7.6	Experiment description	162
7.7	Statistical analysis	162
7.8	Results and Discussion	163
7.8.1	P300 Results	163
7.8.2	Other material considerations	165
7.9	Conclusions	167
8	Eye Movement Detection and Control	173
8.1	Introduction	175
8.2	EOG Eye Movements	175
8.2.1	EOG Measurements	175
8.2.2	Eye Movement Features	176
8.3	Whole schematic control	177

8.4	Experiment Description	178
8.4.1	Experimental Design	178
8.4.2	Evaluation Metrics	179
8.5	Saccade, Blink and Wink	180
8.5.1	R. Barea (RB)'s Work	181
8.5.2	A. Bulling (AB)'s Work	183
8.5.3	Enhancement Propositions	184
8.5.4	Wink Detection: A. Brandão's approach	186
8.5.5	Others Methods	187
8.6	Results	188
8.6.1	R. Barea (RB)'s Results	188
8.6.2	A. Bulling's results	188
8.6.3	Interface Comparison	189
8.7	Conclusion and Future work	190
III	Spontaneous Brain Gait Signal Analysis	195
9	Review of Brain-based Locomotion	197
9.1	Introduction	199
9.2	Deciphering Human Locomotion Control	199
9.2.1	Arguments in Favour of a Human CPG	199
9.2.2	Sensory Feedback Regulates the Stepping Patterns	201
9.2.3	Evidence of a Supra-spinal Control	202
9.2.4	An Overview of the Human Locomotion Machinery	203
9.3	Supra-spinal Control of Human Locomotion	205
9.3.1	Spatial Organization of Supra-spinal Control	205
9.3.2	Temporal Characteristics of Supra-spinal Control	210
9.3.3	Results from Invasive Studies	217
9.4	A BCI-based rehabilitation system	219
9.4.1	General Considerations about BCIs	219
9.4.2	Detecting the User Intent	219
9.4.3	Developing a Direct Brain Signals to Limb Kinematics Decoding	222
9.4.4	Producing a Gait/Stepping Movement in a Step by Step Approach	223
9.5	Discussion and Future Works	226
10	Gait-like Movement Preliminary Study	241
10.1	Introduction	243
10.2	Experimental procedure and data analysis	244
10.2.1	Data collection	244
10.2.2	Pre-processing	244
10.2.3	Ensemble averaged time-frequency analysis	245
10.3	Results and discussion	245
10.3.1	Description of results	245

10.3.2 Discussion	246
10.4 Conclusion	249
11 Automatic Detection of EEG-based Gait Intent	253
11.1 Introduction	255
11.2 Background	255
11.3 Experiment	256
11.3.1 Gait Intent Paradigm	256
11.3.2 Acquisition Material	256
11.3.3 Experiment Description	257
11.3.4 Statistical Note	257
11.4 Methods	258
11.4.1 Preprocessing	258
11.4.2 Feature Extraction	258
11.4.3 Classifiers	259
11.5 Results	259
11.5.1 Fundamental Analysis	259
11.5.2 MRP Analysis	259
11.5.3 Classifier Performances	260
11.6 Conclusion	268
12 Movement Artefact Estimation	273
12.1 Introduction	275
12.2 Material and Methods	275
12.2.1 Acquisition Device and Analysis Approach	275
12.2.2 Brain Electrical Model for Motion Artefact Estimation	276
12.3 Results	278
12.4 Discussion	281
12.5 Conclusion	284
13 Low-delta and High-gamma Rhythms Origins	287
13.1 Introduction	289
13.2 Material and Methods	289
13.2.1 Data Collection	289
13.2.2 Pre-Processing and Spectral Analysis	290
13.2.3 Ensemble Averaged Time-Frequency Analysis	291
13.3 Results	291
13.4 Discussion	293
13.5 Conclusions	297
IV General Conclusion	303
14 General Conclusion	305
14.1 Contributions of this thesis	305

14.2 Perspectives	309
14.3 Research Statement	312
V Other Research Contributions	317
15 IRL Applied to a Robotic Arm Control	319
16 Bacteria Hunt	321
17 The Emotionally Driven Emotiv Cinema	323
A Statistical Assessment of Investment Strategies	A-1
B RARE2012	B-1
C Saliency Model Assessment	C-1
D Publications	D-1
D.1 Book Chapter	D-1
D.2 Patents	D-1
D.3 Regular papers in Journals	D-1
D.4 Papers in Conference Proceedings	D-3

List of Figures

1.1 One standard gait cycle	3
1.2 Kinematics data at 10 different walking speeds	5
1.3 Different types of lower-limb devices	7
1.4 The Ekso exoskeleton	8
1.5 The bionic leg controlled by residual nerve	9
1.6 The invasive Braingate2 project	10
1.7 The 10-20 standard EEG cap	12
1.8 General scheme of a classical Brain-Computer Interface	16
1.9 Peaked SSVEP response	18
1.10 The SSVEP SNR response curve	20
1.11 A BP potential consists of 3 main sections	21
1.12 Homunkulus	21
1.13 Gait intent related BP potentials	22
1.14 The P300 response	23
1.15 The standard P300 speller	23
1.16 The ERD/ERS frequency bands	24
1.17 The standard eye events	25
1.18 Two gait models are available	26
1.19 Common artefacts corrupting the EEG signal	27
1.20 Neck muscle time-frequency analysis	28
1.21 Eye artefacts in the EEG	28
1.22 Movement-related artefacts	29
2.1 PCPG model	46
2.2 PCPG learning of measured kinematics	46
2.3 PCPG parameter interpolation	49
2.4 Similarity index graph	50
2.5 First prototype design	51
2.6 Second prototype design	52
2.7 Microcontroller diagram	52
2.8 Soft-phase resetting enhancement	55
2.9 Comparison of phase-resetting techniques on a step speed modification	56
2.10 Comparison of phase-resetting techniques on a chirp speed modification	56

3.1	DRNN-based central pattern generator	65
3.2	Input signal used in the DRNN model	68
3.3	Learning method for experiment 1	69
3.4	DRNN structures and related learning times	71
3.5	Planar covariation	72
3.6	FFT magnitude and frequency values	74
3.7	Learning and generation similarity index	75
3.8	Learning and generation similarity index by speeds	75
3.9	Planar covariation in intermediate velocities	77
3.10	DRNN parameters distributions	78
4.1	LED panel	97
4.2	A 32-electrode cap	97
4.3	SNR distribution using two Gaussians	98
4.4	The SNR curves	99
4.5	The SSVEP response locations	100
4.6	One subject was immune to artefact	101
4.7	Muscular artefact spectrum	101
4.8	Muscular artefact is affecting the occipital area	102
4.9	Reinforcement in SSVEP SNR distribution due to walk	103
4.10	Abnormal modification of the responsive frequencies	104
5.1	Noise canceller scheme	116
5.2	P300 interface	118
5.3	The accelerometer hardware measurement design	118
5.4	Gait-related artefact examples	119
5.5	Oz electrode EEG spectrum	122
5.6	Harmonic amplitudes in EEG spectra	123
5.7	Effect of artefact correction methods on EEG standard deviation	123
5.8	Inter-subjects classification rates with the Cz O1 O2 electrodes	124
5.9	Inter-subjects classification rates with the Cz Pz POz electrodes	125
5.10	xDawn classification rates over a different number of electrodes	126
5.11	<i>k</i> -fold results	127
5.12	Classification rates using seven electrodes	128
6.1	A four LED panel	139
6.2	Threshold selection by ROC analysis	140
6.3	SUS score distribution	142
7.1	The ANT device	157
7.2	The Emotiv EPOC headset (1)	158
7.3	The Emotiv EPOC headset (2)	158
7.4	P300 picture	159
7.5	The used P300 interface	159
7.6	The Vuzix eyewear	160

7.7	The used pipeline	161
7.8	Results showing the underperformance of the Emotiv headset	164
7.9	Oxidation of the electrodes	166
8.1	EOG measurement hardware	176
8.2	Typical eye events	177
8.3	Electrode positioning	179
8.4	Eye movement configurations	179
8.5	RB method pipeline	181
8.6	CWT derivative	182
8.7	Eye movement magnitude model	182
8.8	EOG targets	183
8.9	AB method pipeline	184
8.10	Blink removal in AB method	184
8.11	The moving-window-size moving-average filter mitigates the noise during fixations	185
8.12	Non-alignment of targets	186
8.13	Wink detector pipeline	186
8.14	Height/duration distribution of eye events	187
8.15	Barea results	188
8.16	Bulling results	189
8.17	Bitrate depending on the configuration	190
9.1	EMGs from the lower limb muscles at different speeds	200
9.2	Model of the pathways interactions between afferents and CPGs	203
9.3	Global view of the human locomotion machinery	204
9.4	Comparative study between PET and fMRI imagery	209
9.5	Illustration of the executive and planning networks of locomotion	211
9.6	LFP oscillation during a gait cycle	218
9.7	General scheme of a classical Brain-Computer Interface	220
10.1	In-phase movement experimental condition	247
10.2	Anti-phase movement experimental condition	248
11.1	Topographic BP potential view	260
11.2	MRP signal distribution	261
11.3	Representative ERSP analysis of ERD/ERS	261
11.4	2-class performance with other electrodes	262
11.5	Classification accuracies for a two-class problem	264
11.6	Classification accuracies for a three-class problem	265
11.7	Classification accuracies for sliding time windows	266
11.8	Classification accuracies based on leg EMG signals	267
11.9	Classification accuracy in a pseudo-online framework	267
12.1	Major components of the artefact measurement system	277
12.2	Time-frequency analyses of both brain and artefact signals	279

12.3 Another example of the difference between artefact and brain signals	280
12.4 Difference of both signal at 1.5 km/h	280
12.5 Gwin's results	282
12.6 Severens's results	282
12.7 Wagner's results	283
12.8 Similarities between subjects artefacts	283
13.1 Accelerometer system	290
13.2 Number of artefact harmonics across speeds	292
13.3 ERSP analyses	293
13.4 ERSP analyses after ICA cleaning	294

List of Tables

1.1	Spinal cord injury costs	2
1.2	Subdivisions of the stance and swing phases of the gait cycle.	4
1.3	Overview of the different brain recording techniques	11
1.4	An overview of the different BCI paradigms	17
1.5	Exogenous/endogenous BCI paradigm classification	17
1.6	Synchronous/asynchronous classification	18
2.1	Polynomial orders of the PCPG interpolation	48
2.2	Similarity index results of PCPG modelling	49
6.1	The SSVEP parameters per subject	140
6.2	Objective performance measures of P300 and SSVEP paradigms	144
6.3	P300 subjective measures	146
6.4	SSVEP subjective measures	146
7.1	Hedge g results	164
8.1	Subject description for EOG experiment	180
8.2	ROC analysis classes	180
9.1	Overview of past locomotion studies	206
9.2	EEG studies of human locomotion	217
9.3	Studies of EEG signals preceding lower limb motor tasks	222
9.4	Overview of several spontaneous brain signal studies	223
9.5	A few applications.	225

Chapter 1

General Introduction

Contents

1.1	Brain Control of a Lower Limb Prosthesis	1
1.1.1	Context	1
1.1.2	Description of the Gait Cycle	2
1.1.3	The Ankle-Foot Device Market	3
1.2	Brain-Computer Interfaces (BCIs)	10
1.2.1	Measuring Brain Activity	10
1.2.2	Standard Brain-Neuronal Computer Interfaces (BNCIs)	15
1.3	Strategies and contributions	25
1.3.1	Strategies	25
1.3.2	Artefact Problematic	27
1.3.3	Organization of The Manuscript	28

1.1 Why Studying Brain Control of a Lower Limb Prosthesis?

1.1.1 Context

More than 10 million people in the world live with some form of handicap caused by a central nervous system (CNS) disorder. According to a recent Eurostat survey carried out in 25 European countries, about 15% of the active population suffer from a long-term disability. This means that almost 45 million persons of working age, i.e. 15 to 64, live in such medical condition. Disabilities affecting mobility, in particular, often lead to exacerbated isolation and thus fewer communication opportunities, resulting in a limited participation in social life. Encounters with other people are made difficult as well as simply performing usual daily tasks at home, and obviously working. Lower limbs disability can have various origins, either medical (after a stroke, i.e. a rapid loss of brain function due to the disturbance in the blood supply to the brain, multiple sclerosis or Parkinson's disease for instance) or accidental (road traffic accident, sport practice accident, etc.). In these conditions, either leg muscles become inefficient or unexciting for walking, or

the brain motor signals do not even properly reach the spinal motoneurons commanding the leg muscles. The consequences are similar: the disabled person cannot properly stand up or walk anymore. Developing technological tools to empower the lower limbs of disabled people with a walking ability will drastically change their day-to-day life, as they will perform more independently most of the usual daily activities both at home and outside, thus sustaining their own inclusion in the society.

In addition to these difficulties, the cost for the society of such disabilities can be huge depending on the level and extent of lesion. For instance, as reported by the National Spinal Cord Injury (SCI) Statistics Center [1], the development of therapies for those who are already spinal cord injured and preventing new injuries could help the United States to save as much as \$400 billion on future direct and indirect lifetime costs (compared to \$157 billion in 2010 in the US for Cancer treatment [2]). Indeed, in average, the patient stays 12 days of initial hospitalization following injury and 37 days in a rehabilitation unit are required. In Table 1.1, the average yearly expenses and estimated lifetime cost by age at injury show that SCI problems are not only a disaster for the family but also a financial burden to the health care system. In addition to the reported direct cost, the indirect cost, i.e. the losses in wages, fringe benefits and productivity, averages \$70,575 depending on education, severity of injury and pre-injury employment history. This indirect cost does not include the potential destruction of innovation that the person would have been able to bring in other circumstances. This leads to a decrease of potential growth for the country. As detailed by the American Heart Association, similar conclusions can be drawn for stroke-related medical costs and disability estimated at \$73.7 billion in 2010 [3].

Table 1.1: Spinal Cord Injuries lead to huge direct costs to the society. The first year after the injury is by far the one leading to the highest expenses. Future costs are discounted at 2%.

Severity of Injury	Average Yearly Expenses		Lifetime Costs by Age at Injury	
	First year	Each Subsequent Year	25 years old	50 years old
High Tetraplegia (C1-C4)	\$1,044,197	\$181,328	\$4,633,137	\$2,546,294
Low Tetraplegia (C5-C8)	\$754,524	\$111,237	\$3,385,259	\$2,082,237
Paraplegia	\$508,904	\$67,415	\$2,265,584	\$1,486,835
Incomplete Motor Functional at Any Level	\$340,787	\$41,393	\$1,547,858	\$1,092,521

1.1.2 Description of the Gait Cycle

Human walking is composed of successive periodic and symmetric movements produced by a precise sequence of collective actions, one leg alternating with the other one. The gait cycle is usually defined as starting with the first contact (initial contact, or heel contact in normal gait) of one foot, so that the end of the cycle occurs with the next contact of the same (ipsilateral)

foot (see Figure 1.1). Each cycle begins with a stance phase (when the foot hits the ground) and proceeds through a swing phase until the cycle ends with the limb's next initial contact.

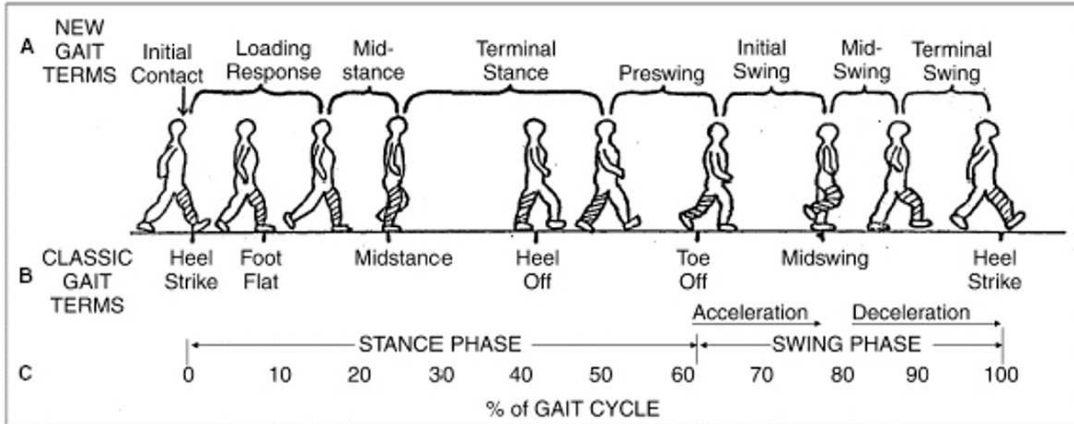


Figure 1.1: Illustration of different phases of the gait cycle (adapted from [4]).

The stance phase lasts approximately 60 % of the gait cycle, while the swing phase occurs during the remaining 40 % of the time. Each gait cycle includes two periods of double support, when both feet are in contact with the ground. The first double support begins at initial contact, and lasts for the first 10 to 12 % of the cycle. The second period of double limb support occurs in the final 10 to 12% of the stance phase.

The stance phase of gait is divided into four periods: loading response, mid-stance, terminal stance, and preswing. The swing phase is divided into three periods: initial swing, mid-swing, and terminal swing. The beginning and ending of each period are defined by specific events, listed in Table 1.2. Figure 1.2 presents the typical joint kinematics of the lower body during the gait cycle, for a range of walking speeds [5]. Although the amplitude of the hip joint movement clearly increases as a function of the walking speed, the movement pattern remains about the same, except at very slow walking speeds. A similar behaviour is found for the knee joint. Clear changes in amplitude and movement pattern occur in the ankle joint, already at speeds slower than 3.0 km/h.

1.1.3 The Ankle-Foot Device Market

Market Share

Under an economic point of view, this ankle-foot device industry is steadily growing. Indeed, the Global Industry Analysts (GIA) reported in 2011 that orthopedic orthotics market should reach \$4.7 billion by 2015 [6, 7]. Furthermore, the *Businessweek* economic magazine predicts a \$400 million annual sales of medical exoskeleton robots in 2020 [8]. These strong perspectives are favoured by an aging population in the developed countries such as the United States, Europe and Japan and increasing incidence of conditions such as diabetes, arthritis and obesity.

Thanks to technical advances and increased functionalities, the use of orthopedic support devices has been fostered [7]. On the market, several customer segments are addressed: They range

Table 1.2: Subdivisions of the stance and swing phases of the gait cycle.

Phase	Events	
Stance	Loading response [0% – 10%]	Begins with initial contact, the instant when the foot contacts the ground. Normally, the heel contacts the ground first. Loading response ends with contralateral toe off, when the opposite extremity leaves the ground. Thus, loading response corresponds to the gait cycle first period of double limb support.
	Mid-stance [10% – 30%]	Begins with contralateral toe off and ends when the center of gravity is directly over the reference foot. Note that this phase, and early terminal stance, the phase discussed next, are the only times in the gait cycle when the body's center of gravity truly lies over the base of support.
	Terminal stance [30% – 50%]	Begins when the center of gravity is over the supporting foot and ends when the contralateral foot contacts the ground. During terminal stance the heel rises from the ground.
	Preswing [50% – 60%]	Begins at contralateral initial contact and ends at toe off. Thus, preswing corresponds to the gait cycle second period of double limb support.
Swing	Initial swing [60% – 70%]	Begins at toe off and continues until maximum knee flexion (60 degrees).
	Mid-swing [70% – 80%]	Is Period from maximum knee flexion until the tibia is vertical or perpendicular to the ground.
	Terminal swing [80% – 100%]	Begins where the tibia is vertical and ends at initial contact.

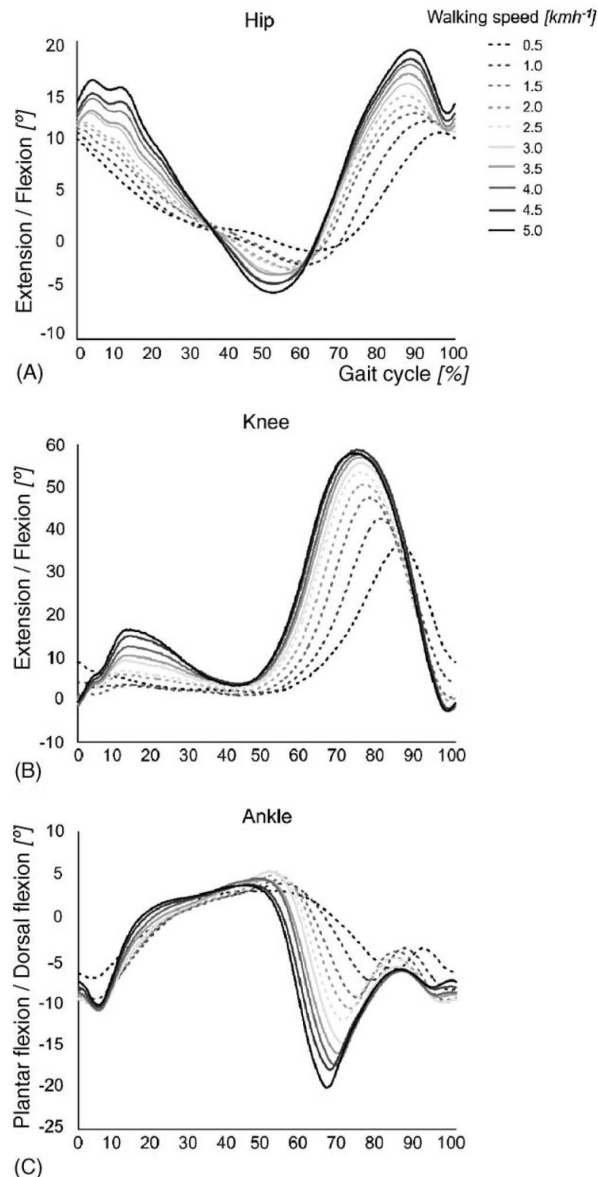


Figure 1.2: Influence of walking speed on joint trajectories. Joint trajectories of the (A) hip, (B) knee and (C) ankle joint at 10 different walking speeds (figure from [5]).

from a highly specific device to low-cost mass distribution systems. Several major aspects have been enhanced by new efficient material and modelling technologies: faster customizing and/or standardizing specifications of orthotic devices, extension of the lifespan of products, enhanced the pliability or rigidity of braces in accordance with consumer needs. Sales of orthotic braces are boosted as patients desire to maintain an active lifestyle while avoiding major risky surgery. Additionally, increasing incidence of injuries as a result of an active aging population is one of

the major factors spurring non-operative use of orthopedic braces and supports. The report also states that minimally invasive hip surgeries are gaining popularity due to the patient's desire to maintain an active lifestyle as well as their desire to avoid major surgery.

As a result, the current global orthopedic orthotics market comprises both niche companies as well as large diversified orthopedic companies. Major players profiled in the report include Biomet Inc., Bledsoe Brace Systems, BSN Medical GmbH & Co. KG, DeRoyal Industries, DJO Incorporated, Orthofix International NV, Ossur hf., and Zimmer Holdings Inc.

Available Prototypes

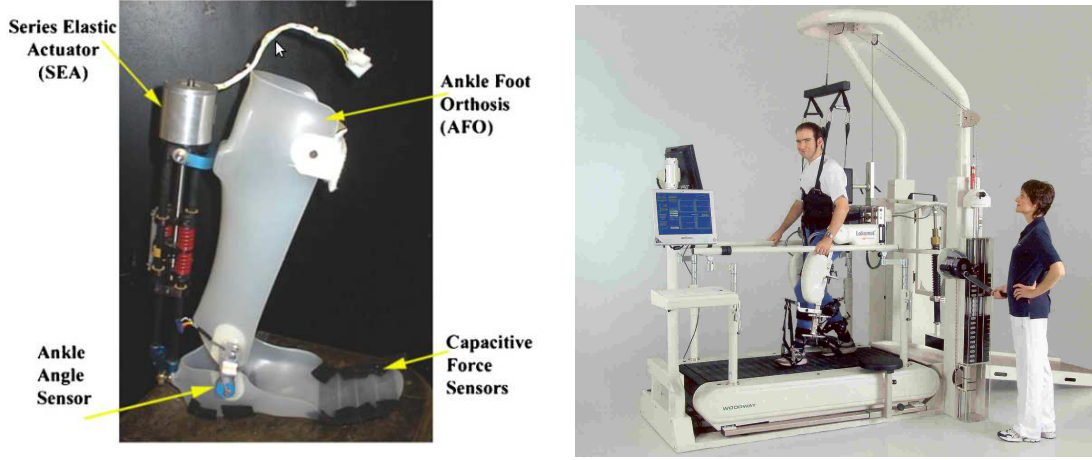
Although standard walking appears as a simple process, conservative (postural stability) and destabilizing (dynamic control of the body and limbs for forward progression) functions render the development of human locomotion devices very challenging. Indeed, this also explains why the majority of leg prostheses available on the market are equipped with passive mechanisms. As reviewed in [9], for low-speed walking, the commercial passive orthoses and prostheses can mimic the behaviour of a healthy ankle in a satisfactory way. But, for higher speeds, further energy is required at the plantar flexion phase. Therefore, amputees using passive devices have to compensate for these limitations and they are generally faced with a reduced locomotion speed, a non-natural gait, considerable fatigue and possibly harmful consequences like recurrent pain and injuries at the interface between their residual limb and the prosthesis.

During the last five decades, active prostheses have been proposed to partially solve these problems. Actually, by being powered by a battery-operated motor, they move on their own and therefore reduce the fatigue of the amputees while improving their posture. Although major advances have been realized, some practical issues explain their limited use. Portable power supplies, lightweight actuators and high-efficiency transmissions are the main components still requiring strong improvements [9].

In practice, three categories can be found among the active ankle devices: prostheses (replace the lost foot) and orthoses (help the present impaired foot), rehabilitation robots and powered exoskeletons. Although they all have similar features at the functional level, as shown in Figure 1.3, they differ in terms of control objectives and human interfaces [9]. First, for orthoses/prostheses assistive devices (see Figure 1.3(a)) to a patient with a motor pathology, user motion intent recognition and adaptation to different working conditions such as different walking speeds and surfaces are important. Moreover, contrary to prosthesis, the weight is a crucial point for orthoses design as their components are added to the present injured limb (for prosthesis, the limb has been amputated). Second, in Figure 1.3(b), rehabilitation robots aim at reproducing a given pattern in order to facilitate the patient's recovery. Therefore, the control strategy mainly relies on trajectory tracking. Third, in Figure 1.3(c), an exoskeleton is designed to enhance power capabilities of a subject.

Four control signals have been investigated so far: biomechanical signals, electromyographic (EMG) signals, implantable peripheral nervous system signals (implantable PNS) and implantable central nervous system (implantable CNS) signals.

1) Several biomechanical signals allow to control ankle devices: foot switch, Ground Reaction Forces (GRFs) estimators, joint angles measured by potentiometer-like systems. There are mainly two types of strategies with these signals: pattern generators or hierarchical with gait-



(a) An orthosis helps still present injured limb to move.
 (b) The Lokomat device is a lower-limb rehabilitation system.



(c) The Exo exoskeleton is able to enhance people's power.

Figure 1.3: Three different devices can be designed: orthosis/prostheses, rehabilitation system and exoskeleton.

phase identification. The former strategy mainly aims at tracking the trajectory adapted from a learned pattern. As proposed in [10, 11], the heel strike duration measures allows to adjust the normal-gait pattern using a polynomial function. In [12], the tibia angle and angular velocity are used to fit a mathematical function that relates the gait percent, the stride length and the ankle angle. The same authors also propose to modify the Fourier coefficients of the pattern

depending on the last gait cycle duration. In the latter strategy, a hierarchical control scheme with gait-phase identification has been investigated. It mainly models the three subparts in the stance phase by a combination of passive elements (stiffness and damping are modified according to the gait phase, gait speed, *etc.*) and power sources [13]. In [14, 15], GRFs are estimated by capacitive force transducers and used to modify the stiffness of the simulated rotary. Additionally, a foot switch detects heel strike events to properly activate the different behaviours of the orthosis. In [16], at each time, a nonlinear dynamic model of the foot-ankle system evaluates the required torque thanks to strain gauges combined with an ankle angle sensor. Based on sensor information, the current gait phase (swing or stance) is estimated by a specific algorithm. In [17], the force and movement produced by the interaction between the user and the prosthesis are used to determine the current phase using a k-nearest-neighbour classifier. In the end, a recent exoskeleton based on weight shift detection has started commercialisation: the Ekso Bionics product. According to the company website [18], Ekso, depicted in Figure 1.4, is a wearable bionic suit which enables individuals with any amount of lower extremity weakness to stand up and walk over ground with a natural, full weight bearing, reciprocal gait. Walking is achieved by the user weight shifts to activate sensors in the device which initiate steps. Battery-powered motors drive the legs, replacing deficient neuromuscular function. The Ekso device has 3 main purposes: a) it provides a means for people with as much as complete paralysis, and minimal forearm strength, to stand and walk, b) it helps patients re-learn proper step patterns and weight shifts using a functional based platform and c) it facilitates intensive step dosage over ground.



Figure 1.4: The Ekso exoskeleton product is able to help people with strong lower limb disabilities to move [8]. Its control strategy mainly relies on weight shift detection.

2) Direct motion intent recognition based on EMG signals has also been studied. For instance, in [19], the muscle activation pattern magnitude (from the soleus and/or tibialis anterior) proportionally generates a command signal to the controller. This signal then controls the pressure in the artificial muscles. In [20], a similar strategy was developed by converting EMG signals from the gastrocnemius and soleus muscles. The employed movement intent detectors were based either on a muscle model, or on a multi-layer feedforward neural-network.

3 and 4) Another type of strategy would be to restore the natural link between an orthotic device and the central nervous system, which could be performed by developing implantable PNS and CNS interfaces [21]. As these kinds of interfaces are still under development, none of the prototypes are available on the market today. PNS interface approaches include the use

of percutaneous electrodes implanted in the nerves and/or the use of implantable capsules for extraction of the EMG signals, from which neural or EMG commands can be extracted. This principle is investigated by several groups such as the Rehabilitation Institute of Chicago (RIC) or the Micera Lab at the Center of Neuroprostheses at the EPFL. The last prototype of the RIC group is depicted in Figure 1.5. CNS interfaces are using electrode arrays implanted in the cortex of the brain, from which motor commands can also be extracted. This approach paves the way to get a somatosensory feedback to the central nervous system. For instance, the Braingate2 project is focussing on helping heavily disabled people to move a robotic arm [22]. Indeed, although able-bodied monkeys have successfully controlled a robotic arm for a long time, researchers have shown in their paper that two people with long-standing tetraplegia were able to use the proposed neural interface to control a robotic arm to perform three-dimensional reach and grasp movements. Obviously, although their movements were not as quick or accurate as those of an able-bodied person, one patient was able to drink coffee from a bottle as illustrated in 1.6. These good results were obtained without explicit training, using signals decoded from a small, local population of motor cortex (M1) neurons recorded from a 96-channel microelectrode array. Additionally, one of the patients was implanted with the sensor 5 years ago. As the device is still working, it indicates the relative long-term reliability of the approach.



Figure 1.5: The bionic leg is connected to the residual nerve by a re-innervation technique [23].



Figure 1.6: By using a minimal training, a paralysed patient was able to drink coffee thanks to a robotic arm [22].

1.2 Brain-Computer Interfaces (BCIs)

1.2.1 Measuring Brain Activity

Brain imagery techniques are essential tools to investigate the spatial and temporal organization of the supra-spinal centers involved, for instance, in human locomotion control. To date, these techniques allow to monitor two types of brain activities: first, the electrophysiological activity and, second, the hemodynamic response of the brain.

Electrophysiological activity of the brain is produced both by the electro-chemical transmitters exchanging information between the neurons and by the ionic currents generated within the neurons themselves. Electrophysiological activity can be measured thanks to electroencephalography (EEG), electrocorticography (ECoG), magnetoencephalography (MEG), and invasive electrical measurements operated at the single neuron level.

The hemodynamic response of the brain allows to distinguish active from less activated neurons. Indeed, the blood releases glucose to active neurons at a greater rate than in the area of inactive neurons. The presence of glucose and oxygen results in a surplus of oxyhemoglobin in the veins of the active area. Hence, the local ratio of oxyhemoglobin to deoxyhemoglobin changes [24]. The variations of this ratio can be quantified by methods such as functional magnetic resonance (fMRI) and near infrared spectroscopy (NIRS), from which it is possible to build 3D maps of the brain activity. These methods are often considered as indirect, because they measure the hemodynamic response, which, in contrast to electrophysiological activity, does not directly characterize the neuronal activity.

In the following paragraphs, each brain imaging technique is explained. First, electrophysiological methods are discussed and then metabolic methods are described. Table 1.3 summarizes the different imaging techniques by listing in each case the type of brain activity measured, the temporal and spatial resolutions, safety and portability (adapted from [25]).

Neuroimaging method	Activity measured	Temporal resolution	Spatial resolution	Risk	Portability
EEG	Electrical	~0.001 s	~10 mm	Non-invasive	Portable
MEG	Magnetic	~0.05 s	~5 mm	Non-invasive	Non-portable
ECoG	Electrical	~0.003 s	~1 mm	Slightly invasive	Portable
Intracortical neuron recording	Electrical	~0.003 s	~0.5mm (LFP) ~0.1mm (MUA) ~0.0 5mm (SUA)	Strongly invasive	Portable
fMRI	Metabolic	~1-10 s	~1 mm	Non-invasive	Non-portable
SPECT	Metabolic	~10 s–30 min	~1 cm	Non-invasive	Non-portable
PET	Metabolic	~0.2 s	~1 mm	Non-invasive	Non-portable
NIRS	Metabolic	~1-10 s	~5 mm	Non-invasive	Portable

Table 1.3: An overview of neuroimaging methods. Direct methods detect electrical or magnetic activity of the brain while metabolic methods are considered as indirect methods of imaging (adapted from [25]).

Electroencephalography

Electroencephalography (EEG) measures the electric brain activity caused by the currents induced by neurons and during synaptic excitations of the dendrites [26]. The measurements are realized thanks to electrodes placed on the scalp, thus in a non-invasive way. This explains why EEG is by far the most widespread brain activity recording modality. With NIRS (see below), EEG is the only non-invasive acquisition technique that is really portable. Moreover, it is relatively cheap and offers a high temporal resolution (about 1 ms). However, EEG scalp electrodes are only able to measure the electrical potentials of thousands of neurons, which are weakened and smeared by the volume conduction effect of the skull [27], leading to signals of a few microvolts only and a poor global spatial resolution.

The electrodes placed over the scalp are commonly based on the International 10–20 system [28], which has been standardized by the American Electroencephalographic Society. The 10–20 system uses two reference points in the head to define the electrode location. One of these reference points is the nasion, located at the top of the nose at the same level as the eyes. The other reference point is the inion, which is found in the bony lump at the base of the skull. The transverse and median planes divide the skull from these two points. The electrode locations are determined by marking these planes at intervals of 10% and 20% (Figure 1.7). The letters in each location corresponds to specific brain regions in such a way that *A* represents the ear lobe, *C* the central region, *P_g* the nasopharyngeal, *P* the parietal, *F* the frontal, *F_p* the frontal polar and *O* the occipital area.

The weak amplitude of EEG signals renders them sensitive to electronic noise and artefacts. EEG artefacts are spurious signals present in recordings and whose origin is not cerebral. They may arise from the patient itself: the eyes, the tongue, the pharyngeal muscle, the scalp muscles, the heart or the sweat glands all produce electrical potentials which can influence the EEG mea-

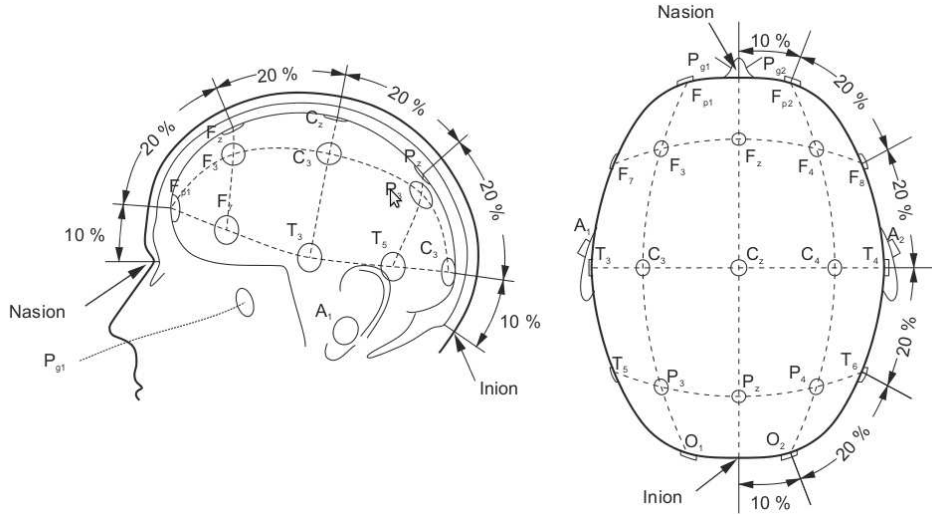


Figure 1.7: The 10-20 EEG cap standard system has a specific design and electrodes [25].

surement, especially if they are in movement. Skin resistance changes due to sweating may also badly affect the signals. Electrical interference with power line or surrounding electrical apparatus is another source of artefacts which may be induced electro-statically or electromagnetically. Finally, artefacts may also arise from faulty electrodes or the recording equipment itself.

In many cases, artefacts can be immediately identified by visual spatial analysis: high amplitude potentials appearing at only one electrode are not likely due to cerebral activity. Indeed, our brain produces potentials that exhibit a physiological distribution characterized by a maximum voltage amplitude gradually decreasing with increasing distance over the scalp. Likewise, rhythmical or repetitive irregular signals appearing simultaneously in non-adjacent brain areas strongly suggest the presence of artefacts [29].

Algorithms designed to detect and correct EEG artefacts integrate these principles and exploit techniques like temporal filtering, spatial filtering, Independent Component Analysis (ICA) [30, 31], Blind Source Separation (BSS) [32] or thresholding of meaningful parameters (e.g. channel variance) based on a prior statistical analysis [33].

EEG analysis of human locomotion is particularly complicated by experimental difficulties [34, 35]: in addition to “traditional” EEG artefacts (ocular, muscular, power line, ...), EEG recordings realized in ambulatory conditions are further degraded by additional sources of noise. Triboelectric noise is generated by movement, friction and flexion of the cable components, resulting in a static or piezoelectric movement transducer effect [36]. Electrode movements are produced by movements of the head, but also by the shocks undergone by the whole body at each step, which - albeit significantly attenuated - are transmitted to the head [37]. These movements modify the magnetic and capacitive coupling of the user and the electrode leads, leading to an alteration of the parasitic current flowing into the leads [38]. A resulting parasitic voltage drop is then produced in the electrode/gel/skin interface which interferes with the EEG signal [39]. Finally, electrode movements can also cause impedance variation which directly affects the electrode voltage offset [40].

Unfortunately, all these *motion artefacts* are not limited to a small spectral band, so they cannot be simply removed by frequency filtering. In a study conducted to assess EEG signal quality in motion environments [41], it is shown that EEG spectra in the walking (or jogging) condition exhibit frequency peaks consistent with the fundamental stride frequency as well as its harmonics. The authors also state that motion artefacts affect signal integrity most prominently at low frequencies (i.e. < 4 Hz) during steady walk. Nevertheless, the study also shows that traditional event-related potentials (ERP) elicited during a standard *auditory* discrimination task (i.e. “oddball paradigm”, in which a rare and relevant event activates a potential) are not dramatically affected by the walking condition, either in amplitude, in topographic distribution or response time (70% of acceptable trials across all participants). This is however not the case for the jogging condition, for which only 14% of trials were accepted. Analog conclusions are drawn in more recent studies where subjects are standing or walking on a treadmill while performing a *visual* oddball response task [35, 42].

Magnetoencephalography

Magnetoencephalography (MEG) detects the weak magnetic fields resulting from the intracellular electrical currents in neurons. The neurophysiological processes that produce MEG signals are the same as those that produce EEG signals. The advantage of MEG is that magnetic fields are less distorted by the skull and scalp than electric fields. This technique offers a spatial resolution of a few millimetres and a temporal resolution of a few milliseconds [43] but requires highly sensitive devices (arrays of SQUIDS – superconducting quantum interference devices) cooled to a few degrees Kelvin. Additionally, measurements must be realized in a shielded room in order to minimize interferences with magnetic fields from external sources. This non-invasive technique gives only access to shallow parts of the brain and is too bulky and expensive to become an acquisition system suitable for everyday use.

Electrocorticography

Electrocorticography (ECoG) consists in implanting electrodes under the dura matter, directly on the surface of the cortex, without penetrating it. This technique represents a partially invasive compromise, offering a good signal quality and spatial resolution [44]. Compared to EEG, ECoG provides higher temporal and spatial resolution. ECoG signals are characterized by higher amplitudes and a lower vulnerability to artefacts such as blinks and eye movement [45]. However, this technique is invasive and requires a surgical intervention in order to implant an electrode grid. This operation is thus risky. Early experiments with animals indicated that stable ECoG signals could be recorded over several months [46]. Additionally, more recent studies with monkeys also indicated that ECoG electrodes remained stable during several months [47]. Nevertheless, the long-term stability of ECoG signals remains unclear to date.

Intracortical Neuron Recording – Brain Implants

Brain implants may be directly inserted into the grey matter of the brain, in order to measure the electrical activity of single neurons. Three types of signals can be obtained with this technology: single-unit activity (SUA), multi-unit activity (MUA), and local field potentials (LFPs) [48]. The

SUA is obtained by high-pass filtering (> 300 Hz) of the signal of a single neuron. MUA contains the contribution of multiple SUA. LFPs are computed by low-pass filtering (< 300 Hz) of the neuron activity. LFPs are analog signals whereas SUA and MUA contain the spiking activity of single neurons.

Brain implants provide the best quality of signals, with a much higher spatial and temporal resolution than EEG recording. In 2005, such type of neurosurgery was done successfully with a tetraplegic who was subsequently able to move – only by thought – a cursor on a computer screen as well as an artificial hand [49]. Nevertheless, this technique requires a heavy and risky surgical operation. Additionally, such devices raise several issues like long-term viability and biocompatibility [50].

Functional Magnetic Resonance Imaging

Functional magnetic resonance imaging (fMRI) is a non-invasive technique allowing to determine the blood oxygen level variations that occur during brain activity (higher neural activity requires more glucose and oxygen). The main advantage of this technique is a high spatial resolution, of the order of the millimeter, which makes it perfectly suitable for accurately localizing active regions inside the brain [51]. fMRI suffers from a poor time resolution of about 1 or 2 seconds. On top of this, this technique is highly susceptible to head motion artefacts. Like for MEG, fMRI requires a cumbersome and very expensive equipment, which is not really suited for individual and everyday applications.

Nuclear Functional Imaging Techniques

Single-photon-emission-computed-tomography (SPECT) is an imaging technique based on the tracking of gamma rays emitted by radionuclides injected in the bloodstream of the patient. Specific chemicals (radioligands), by their particular binding properties to certain types of tissues (e.g. brain tissues), allow to concentrate the radionuclides in the region of interest of the body, thus making them visible to the gamma cameras of the system [52]. SPECT is a tomography tool that provides 3D information, and which can reconstruct an image of a thin slice along any chosen axis of the body. The spatial resolution of SPECT is about 1 cm and several dozens of seconds are needed for a single projection (a full 360° scan by 5° steps takes up to 30 minutes). When used for functional brain imaging, the system is able to assess the cerebral blood flow, which is directly linked to the local brain metabolism.

Positron-emission-tomography (PET) is relatively similar to SPECT. The radionuclides injected in the patient emit positrons, which annihilate with electrons located in the vicinity (a few mm) and, therefore, produce a pair of gamma rays emitted in opposite directions [53]. By detecting the two gammas in coincidence mode, enhanced spatial information is available for the imaging algorithms. Consequently, a better spatial resolution is reached, compared to the SPECT technique. In brain imaging applications, the active molecule generally chosen is FDG, an equivalent of glucose. Again, brain metabolism is assessed in this particular application of the technology.

Near-Infrared Spectroscopy

Near-infrared spectroscopy (NIRS) is another non-invasive acquisition technique. It determines the variations of hemoglobin concentrations linked to neural activity by detecting changes in the optical response (absorption, scattering) of cerebral tissue to near-infrared light. Infrared light penetrates the skull to a depth of approximately 1–3 cm below the surface. Thus, only the outer cortical layer can be imaged using this technique. A further limitation of the technique lies in the fact that hemodynamic response occurs a certain number of seconds after its associated neural activity [54]. The spatial resolution of this technique is of the order of the centimetre while the time resolution is of approximately 200 ms. Contrary to MEG and fMRI, NIRS is an appropriate measurement modality for everyday use, as its equipment is relatively cheap, portable [55], simple to attach and requires little user training [56].

1.2.2 Standard Brain-Neuronal Computer Interfaces (BNCIs)

Brain-Computer Interfaces (BCI) include devices or systems which respond to neural or cognitive processes. These systems enable their users – whose neural system may have been destroyed by amputation, trauma or disease – to control a computer or any robotic device by interpreting neurophysiological signals which are recorded and processed following different steps as shown in Figure 1.8. First, the brain signals are pre-processed to clean them as much as possible. Then, some features are extracted and classified so that the computer can determine in which mental state the user was. Finally, the corresponding action is produced by the system. As it is non-invasive, light and relatively cheap, electroencephalography (EEG) is the most used acquisition technique to record cerebral activity of the BCI users.

Thanks to current BCI technology, severely disabled people can communicate [57], control computers [58], or drive robotic [59] or simple prosthetic devices [60] via the power of their brain only, without activating any muscle. Nowadays, BCI applications dedicated to both disabled and healthy users are also being developed in the video game field [61]. Although functional, BCI technology offers information transfer rates that are too limited (from 1 to 100 bits/min) to control complex systems entirely. Consequently, shared control is used extensively in assistive applications. This means that the BCI user generally sends high-level commands to the system, which is able to operate all the low-level problems [62, 63].

As deeply reviewed in [25, 62], several types of EEG-based signals, i.e. standard BCI paradigms, can be decoded to enable the BCI systems to interpret the subject intention among standard BCIs: P300, Visual Evoked Potential (VEP), Slow Cortical Potential (SCP), sensorimotor rhythms. These paradigms strongly vary in the interaction mode (task performed by the subject), the physiological phenomena, the number of states that can be selected, the required subject training, the potential performance that they can provide often described in terms of bitrate (the common bitrate for speech is around 50 bits/s [65]). All the paradigms and their major characteristics are summarized in Table 1.4 from [25]. Additionally, some Brain-Neuronal Computer Interfaces (BNCIs) are also popular. These kind of interfaces extend the types of potential signals to be used: EMG and EOG. In addition to the already discussed electromyographic signal, the electroocculographic (EOG) signal is able to measure the eye movements by

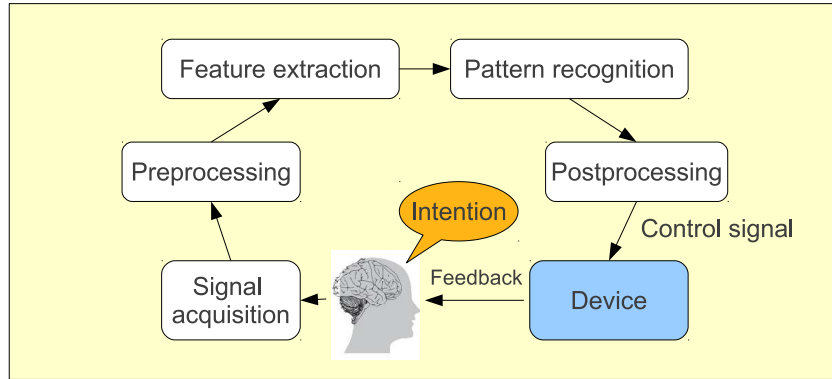


Figure 1.8: General scheme of a classical Brain-Computer Interface (BCI): first of all, the subject performs a specific mental task in order to produce a signal of interest in his brain; then this signal is acquired and generally pre-processed in order to get rid of different artefacts. Afterwards, some discriminating features are extracted and classified (pattern recognition) to determine which specific signal was produced. Finally, the identified signal is associated to a specific action to be performed by a computer or any electronic device (adapted from [64]).

recording cornea/retina potential modifications. By detecting the eye movements, the subject is able to communicate with a device.

As summarized in Table 1.5 and 1.6 from [25], BCIs can be divided according to several criteria: 1) exogenous or endogenous, 2) synchronous (cue-paced) or asynchronous (self-paced). First, exogenous BCIs such as VEPs do need an external stimulus. Because they do not require an extensive training, SSVEPs and P300 BCIs may be quickly deployed. On the contrary, endogenous BCIs do not require any external stimuli, which allows the subject to freely control the system. In rehabilitation, some BCIs may activate some frequency bands that are linked to the injury. This may enhance the recovery time [66].

Contrary to synchronous BCIs, asynchronous interfaces allow the user to control the device in a self-paced manner. Actually, a synchronous BCI requires to interact and execute the desired task at a precise moment, i.e. any signals emitted outside this time frame will be ignored (this concept is used in the Graz BCI [67]). The advantage of knowing the onset of mental activity and the matching stimulus make the design of such BCIs much easier. At the opposite, asynchronous BCIs continuously look for a user intent. Although more natural, this kind of interfaces requires a more complex and demanding signal processing pipeline: the detection of the non-control (non-action) state is essential.

Visual Evoked Potential (VEPs)

As used in Chapter 6 and in Chapter 4, VEPs are brain activity modulations that occur in the visual cortex after receiving a visual stimulus [68]. Although the VEPs can be classified according to several criteria such as the morphology of the optical stimuli, the stimulated frequency (it is possible to get a visual VEP response in the range 1-100 Hz [69]) and the field of stimulation [70], the focus here is on Steady State Visual Evoked Potential (SSVEP).

Table 1.4: Several different paradigms are available when performing a Brain-Computer Interface. They differ by their physiological phenomenon, their number of choices, their training type and their transfer rate.

Signal	Physiological phenomena	Number of choices	Training	Information transfer rate
VEP	Brain signal modulations in the visual cortex	High	No	60-100 bits/min
SCP	Slow voltages shift in the brain signals	Low (2 or 4, very difficult)	Yes	5-12 bits/min
P300	Positive peaks due to infrequent stimulus	High	No	20-25 bits/min
Sensorimotor rhythms	Modulations in sensorimotor rhythms synchronized with motor activities	Low (2,3,4,5)	Yes	3-35 bits/min

Table 1.5: BCI paradigms can be classified according to the exogenous or endogenous approach.

Approach	Brain signals	Advantages	Disadvantages
Exogenous BCI	SSVEP P300	Minimal training Control signal set-up easily and quickly High bit rate (60 bits/min) Only one EEG channel required	Permanent attention to external stimuli May cause tiredness in some users
Endogenous BCI	SCPs Sensorimotor rhythms	Independent of any stimulation Can be operated at free will Useful for users with sensory organs affected Suitable for cursor control applications	Very time-consuming training (weeks or months) Multichannel EEG recordings required for good performance Lower bit rate (20-30 bits/min)

Table 1.6: BCI paradigms can be classified according to the synchronous or asynchronous approach.

Approach	Advantages	Disadvantages
Synchronous BCI	Simple design and performance evaluation The users can avoid generating artifacts since they can perform blinks and other eye movements when brain signals are not analyzed	Does not offer a more natural mode of interaction
Asynchronous BCI	No need for waiting for external cues Offers a more natural mode of interaction	Much more complicated design More difficult evaluation

As depicted in Figure 1.9, SSVEP is a strong steady state potential that mainly arises in the occipital area, i.e. the O_x electrodes, when a subject is looking at a flickering stimulus whose frequency is usually considered to be higher than 6 Hz. This potential is a sinusoidal-like waveform oscillating at the stimulated frequency and its harmonics. The main advantage of this type of BCI is the relatively high SNR with a clear peak in the FFT occurring at the frequency of interest and some of its harmonics. Moreover, as discussed in [71], the Signal-to-Noise Ratio (SNR) SSVEP response has three main frequency bands with peaks around 15 Hz, 31 Hz and 41 Hz. Logically, this leads to a high potential bitrate that can even reach around 100 bits/min [72].

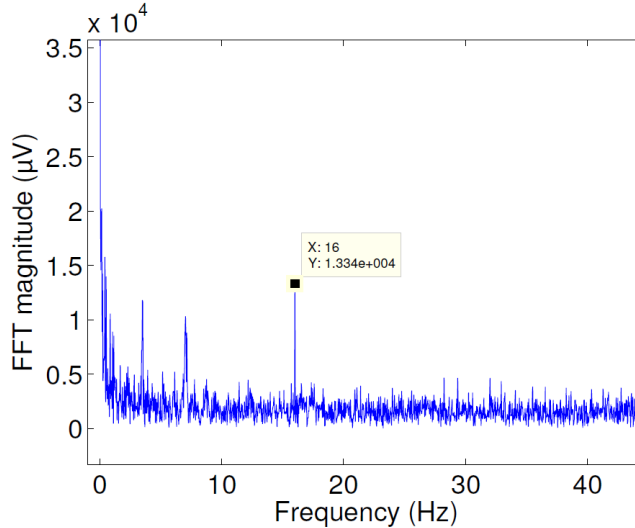


Figure 1.9: The peaked SSVEP response is obviously elicited at 16 Hz in the occipital area when a subject is looking to a flickering LED.

The flickering stimulus can be either produced by a cathode-ray tube (CRT)/liquid crystal display (LCD) screen or by a LED. From previous studies and at the same luminance and modulation depth, it is known that LEDs produce stronger fundamental SSVEP responses than LCD/CRT screens [73]. However, LEDs are much challenging to cope with a hardware and presentation (CRT/LCD can easily be connected to a PC) point of view. It is thus suggested when the number of commands is higher than 20 whereas the LCD screens are advised when less than 10 commands can be emitted. Given the so short rising and descending edges, the LED flicker spectrum has a strong fundamental, weak harmonics and a global cleaner generated signal compared to other technologies. Obviously, this leads to a cleaner SSVEP response with a stronger fundamental and weaker harmonics frequency spectrum.

Moreover, SSVEP response strength is strongly linked to the precision of the generated frequency, i.e. a small jitter can dramatically decrease the performance of such BCIs. This jitter is clearly much smaller with LED than with screens whose control depends on the operating system latency and on the computer hardware. As discussed in [73], LED technology has an intrinsic quicker response and a more stable generated light.

As for the stimuli frequencies, the response spectrum and the feeling of subjects have to be considered. As summarized in [74], SSVEP response has an optimal SNR in the 5-30 Hz range, with a peak at 15 Hz. Beyond 15 Hz, there are some risks of triggering photoepileptic seizures. Moreover, the late theta, the whole alpha band (6-13 Hz), and the early beta band (13-17 Hz) usually show better stimulus-related responses, while higher stimulation rate has proven to be reliable only when inducing a specific resonance phenomenon indicating a selective frequency preference of the neural oscillators of the subject. Additionally, as illustrated in Figure 1.10, other SSVEP resonances are present around 32 Hz and 42 Hz [71]. Because it is less disturbing than low frequency, subjects largely prefer SSVEP stimulations at high frequencies. This is why a lot of studies are now focusing on what is called high frequency SSVEP above 30 Hz [75].

Slow Cortical Potentials (SCPs)

As used in Chapter 11, Slow Cortical Potentials are slow voltage drifts in the recorded EEG that last a second to several seconds [76]. As summarized in [25], SCPs are associated with changes in the level of cortical activity (negative SCPs correlate with increased neuronal activity *and vice versa*). These kinds of signals can be self-regulated, e.g. to move a cursor and select the targets presented on a computer screen [77], or spontaneous occurring before a movement.

First, self-regulated SCPs can be converted to commands using a Thought-Translation Device (TTD). People can be trained to generate voluntary SCP changes using a thought-translation device [77]. The TTD training typically consists in displaying a vertical cursor whose position reflects the SCP amplitude shift. Although the obtained interface has a low bitrate and requires a several month training, it has been tested extensively with patients suffering from ALS [78, 79, 80].

Second, a slow surface negative signal, the Bereitschaftspotential (BP) or Movement-Related Potential (MRP), can be obtained by averaging EEG occurring before repeated self-paced movements and time-locked to the movement onset [81, 82]. BP starts about 1.5 s prior to movement

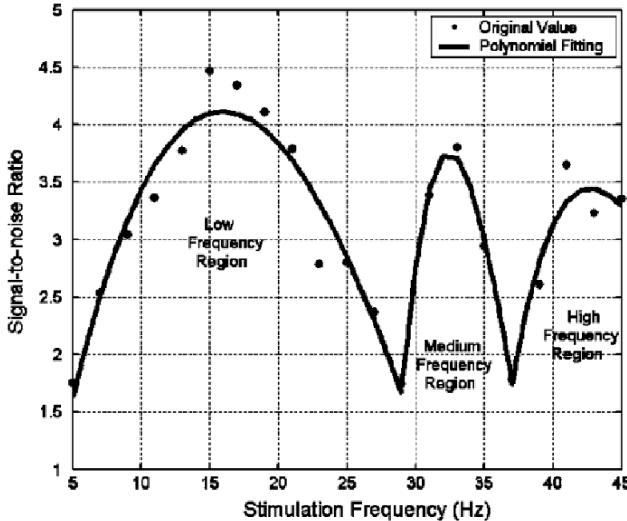


Figure 1.10: The SSVEP SNR response has three main resonances [71]. Up to now, the first resonance peak has been the most widely used. However, given the preference of subjects for high frequencies, some investigations are undertaken in the following frequency ranges.

onset and is symmetrically recorded with a maximum over the supplementary motor area (SMA) and followed by an asymmetrical negative potential starting about 0.4 s and originating from the contralateral primary motor cortex [82, 83]. As shown in Figure 1.11, the BP potential can be divided into three different parts. First, in the pre-BP section, the brain signals are not affected by the movement intent yet. Then, in the BP section or *early BP*, the negative potential slowly appears at about 1.5 s before movement onset and is more prominent in the central-medial areas. Second, a negative steeper slope (NS) or *late BP* corresponding to the activity of the primary motor cortex (M1) starts around 400 ms prior to movement onset. It was shown that these potentials are also observed in the case of imaginary movement intention and similar observed movements [84].

In a recent study [86], the BP signal was analysed during gait intent. Five different tasks were performed: gait/stepping forward, gait and stepping backward and stepping laterally. As shown in Figure 1.13 from [86], the measured potentials are slightly different and observed at the top of the head, which matches the motor and sensorimotor leg representation of the homunculus as depicted in Figure 1.12.

P300 Evoked Potentials

As used in Chapters 5 and in Chapter 6 and illustrated in Figure 1.14, the P300 evoked potential is an involuntary positive peak arising around 300 ms after the user has perceived a relevant and rare auditory, visual or somatosensory stimulus [57]. Typically, it is generated by the *odd-ball* paradigm, in which the user is requested to attend to a random sequence composed of two kind of stimuli with one stimulus much less frequent than the other one. In case the infrequent stimulus is relevant to the user and, assuming that the subject was focusing on it by, for example, silently

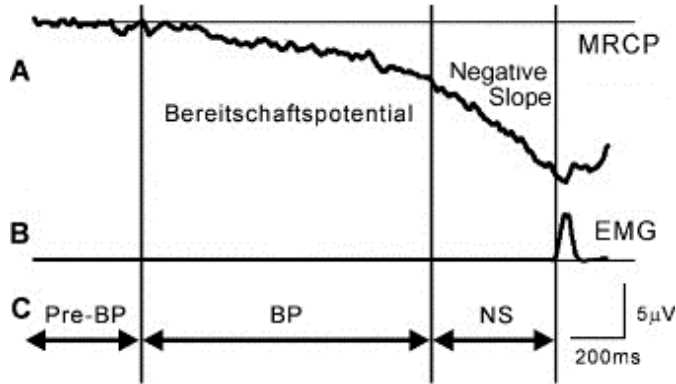


Figure 1.11: When looking at a BP signal, three main sections are observed: no potential, a slow decreasing potential *early BP* and a steeper (figure from [85]).

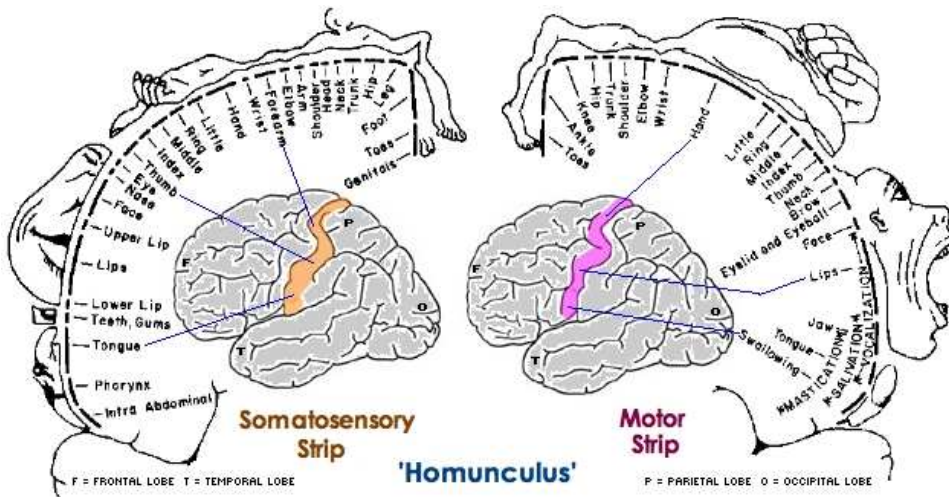


Figure 1.12: The homunculus shows the dedicated areas in the motor and sensorimotor cortex (figure from www.kateharrisonart.com).

counting it, its actual appearance activates a P300 waveform in the user's EEG, which is mainly located in the parietal areas. This approach does not require training.

The most widely known P300-based BCI is the P300 speller [87]. As depicted in Figure 1.15, it is basically composed of a 6×6 matrix of letters, symbols, numbers or commands [57, 88, 89]. The task consists in looking at the desired target and silently counting how many times this target flashed in the matrix afterwards. The rows and columns are flashed in random order. As the flashing of the target letter is a rare and relevant stimulus (oddball paradigm), it triggers a positive involuntary so-called *P300 potential*, appearing with a time delay of about 300 ms [57]. During each *trial*, each row and each column are flashed, so that the computer was able to determine which letter the subject was looking at, by using the intersection of the detected P300

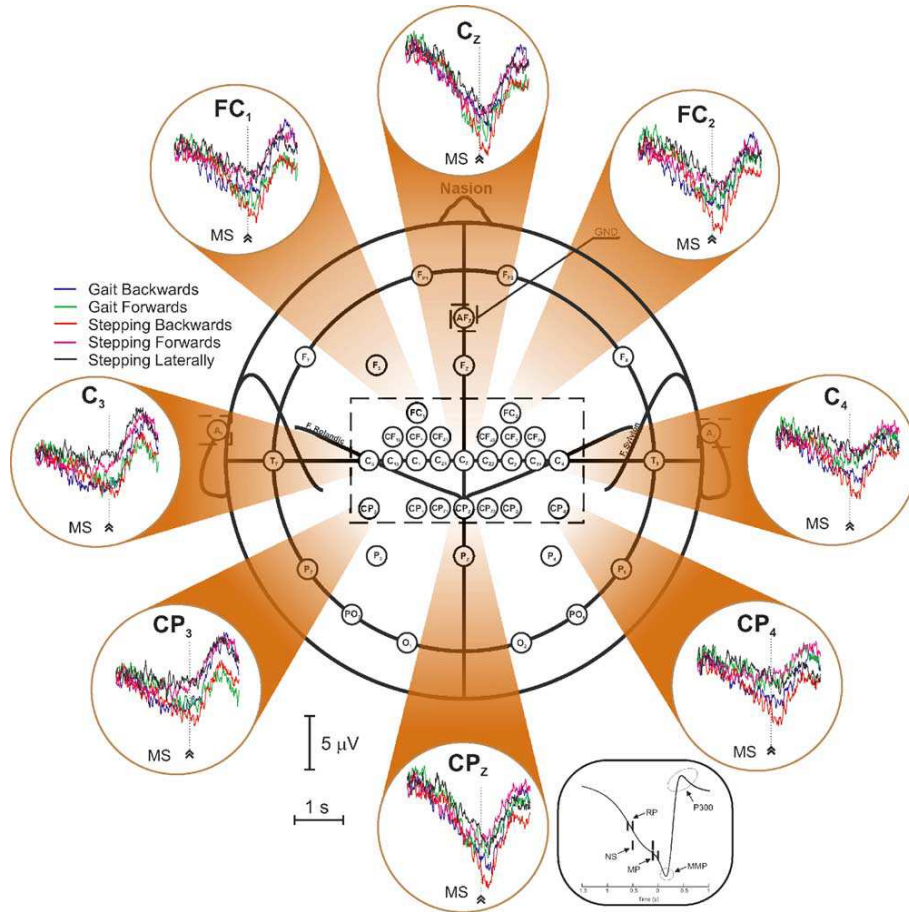


Figure 1.13: It clearly appears that the BP potentials are similar for all the five tasks. A classification between those tasks would be difficult. The potentials are strong over the motor cortex area close to the midline [86].

responses. Due to a very low SNR, good performance can only be achieved by repeating this process several times. This obviously decreases the reactivity of the device. Although most of the applications based on P300 evoked potentials employ visual stimuli, auditory stimuli have been used for people with visual impairment [90].

Sensorimotor Rhythms (μ and β)

As used in Chapter 11, μ (7-13 Hz) and β (13-30 Hz) sensorimotor rhythms, that could be simultaneously located at different electrodes, are the most widely used in BCIs (γ band can also be defined between 30 and 50 Hz). Although independent beta rhythms can be generated, some β rhythms are harmonics of μ . Major BCI groups have used these signals such as Wadsworth [92], Berlin [93], or Graz [67].

Indeed, modifications of sensorimotor rhythms are used: Event-Related Desynchronization (ERD) and Event-Related Synchronization (ERS). Similar modifications are observed between actual

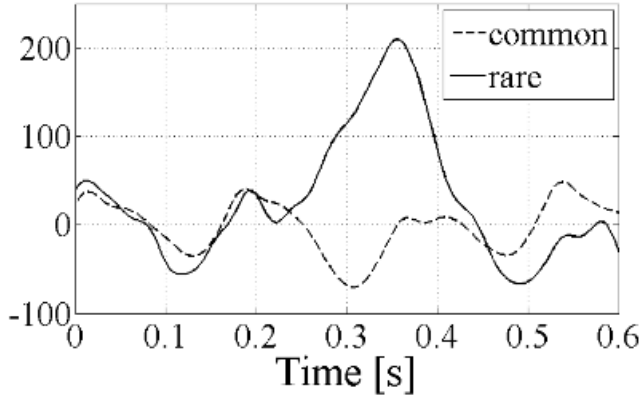


Figure 1.14: The P300 response appears as a positive potential around 300 ms after a relevant and rare stimulus [91].



Figure 1.15: The P300 speller is the most widely known P300 application. It is composed of a 6 x 6 symbol matrix [91].

and imaginary motor movement, which is an essential property to ease transposition from healthy BCI users to patients. While ERD leads to a decreased magnitude, ERS is linked to an enhancement of the rhythms. As shown in Figure 1.16, an actual movement (time 0s) is preceded by a μ ERD starting up to 2.5 s before onset, reaches the maximum little after and recovers to its original level within a few seconds. But, the beta rhythm display a more complex behaviour consisting in a short ERD during the movement initiation and a peaked ERS after movement execution. As depicted in Figure 1.16, gamma rhythms (36-40 Hz) also display specific behaviours.

Because imaginary movements can be performed in a self-paced way, related BCIs can operate in either synchronous or asynchronous mode. Prediction of human movement intent before their onset is possible [95]. One should notice that this result can be achieved without any movements.

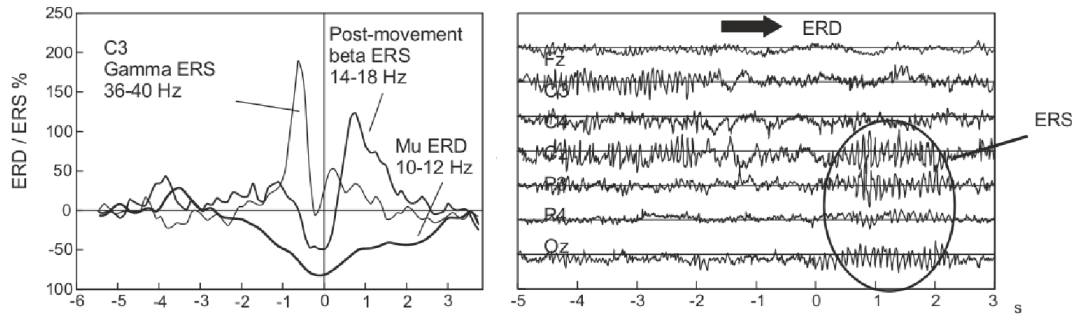


Figure 1.16: Several ERD/ERS can be observed in the μ , β and γ bands [94].

Electrooculographic Signal (EOG)

As used in Chapter 8, severely disabled people are sometimes only able to move their eyes. That is one of the main reasons for looking for interfaces relying on eye movements. Among those interfaces, a common example is a mouse control, which allows the patient to interact with the environment without any limb movement [96, 97]. Additionally, the same researchers showed that specific eye moment sequences could help controlling a wheelchair while getting a good controllability [98, 99]. Finally, in our own research, we have recently proposed to control a lower limb prosthesis in a similar way combined with a central pattern generator-based gait model [100].

The eye can be seen as an electrical dipole [101]. Nerve cells located in the back of the eye provoke a decrease of the electrical potential. This leads to a potential difference between the front and the back of the eye. Therefore, the displacement of the ocular dipoles creates a potential modification by polarizing the electrodes around the eyes. This is the underlying concept of ElectroOculoGraphic (EOG) signal recording. The observed potential differences are 16 μ V and 14 μ V for horizontal and vertical movements, respectively.

Basically, as depicted in Figure 1.17, natural eye movements are characterized by three different types of movements: saccades, fixations and blinks [101]. Saccades appear when a rapid change (up to $400^\circ/\text{s}$) of eye gaze direction occurs. Most of the time, they do not last more than 80 ms and they do not have a magnitude variation higher than 20° . On the other hand, fixations correspond to the time of a fixed eye gaze. Although in theory, the signal should be constant during fixations, human eye is never fixed and small involuntary micro-saccades and noise could be interpreted as voluntary saccades. Blinks correspond to a two-way vertical reflex movement occurring when the eyes quickly close and open. The average blink duration is between 100 ms and 150 ms and the blink rate is between 7 and 50 per minute. Fatigue can significantly increase the blink rate of a subject.

Finally, an intrinsic property of the EOG signal makes the automatic detection task complex: the drift [101]. This drift comes from the slight biological modification of the rest potential with time. To properly deal with saccades and blinks, this drift must be removed such as other noises like electrical power and muscle activity.

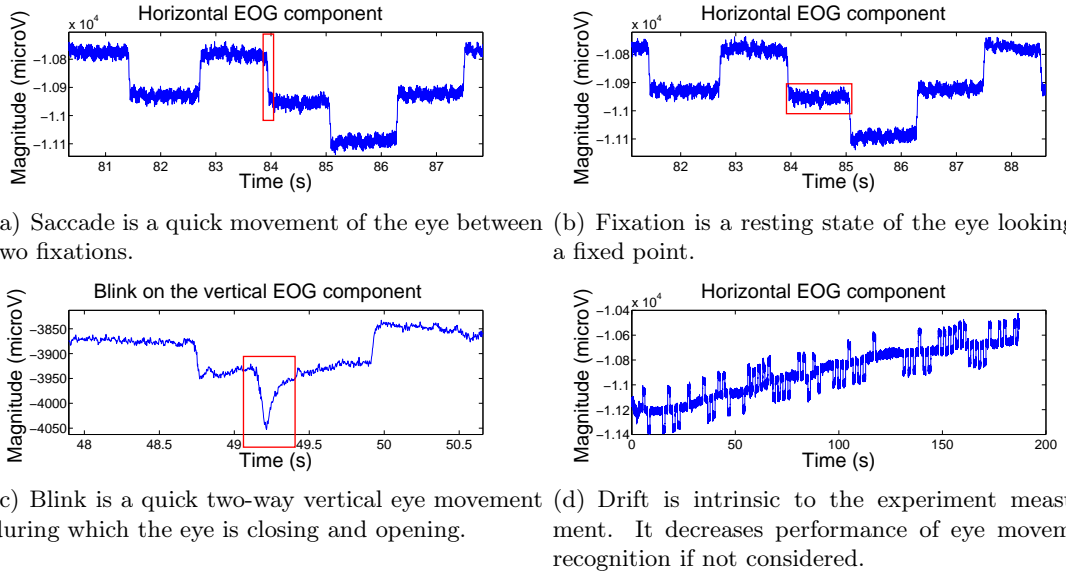


Figure 1.17: Typical EOG events are blinks, saccades and fixations. Furthermore, a drift in the measurement makes the recognition step more difficult.

1.3 Strategies To Integrate The User Intent and Contributions

1.3.1 Strategies

Many ankle foot devices are still not integrating a direct brain user intent. Indeed, by mainly using biomechanical sensors, current active orthoses/prostheses are not considering the direct will of the user. Obviously, such devices could gain in usability if they could anticipate the next move. This could be achieved by measuring brain-related activity. This is what I want to contribute to in this work.

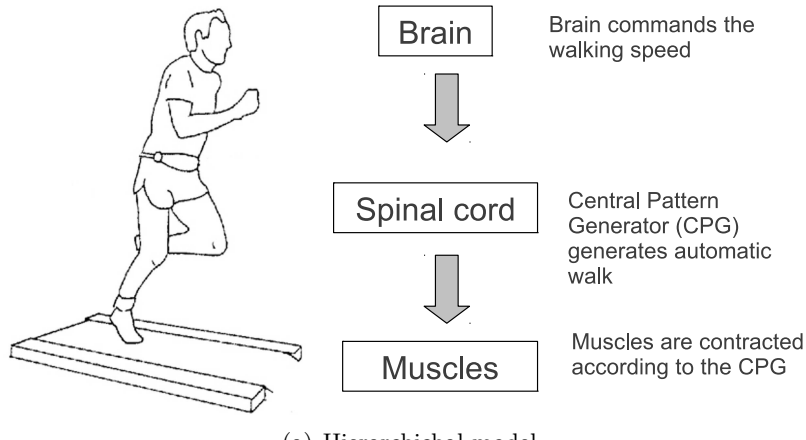
Two main strategies to integrate the user intent in ankle devices are proposed and investigated: 1) Central Pattern Generators-based (CPGs) or 2) brain-based systems.

Following a hierarchical model depicted in Figure 1.18(a), the brain control can be summarized to a stepping frequency management, i.e. a speed gait management [102]. Then, the CPG, which is located in the spinal cord, is able to generate periodic automatic gait patterns adapting to the current speed by converting the brain will. In clear, from the CPG output, the EMG signals from the legs can be derived. As the CPGs are also able to integrate sensory feedbacks, this approach allows to provide a robust and stable control. Indeed, when a perturbation is occurring, i.e. uneven surface, this CPG is able to correct the trajectory. Therefore, the main work will be to provide and assess such gait models as well as interfaces allowing to decide of the current speed. The latter problem is actually not trivial as movement creates artefacts that may corrupt the used interface.

On the other hand, as depicted in Figure 1.18(b), the brain-based control model considers that the brain is the master of locomotion. At each time, it provides inputs that directly control

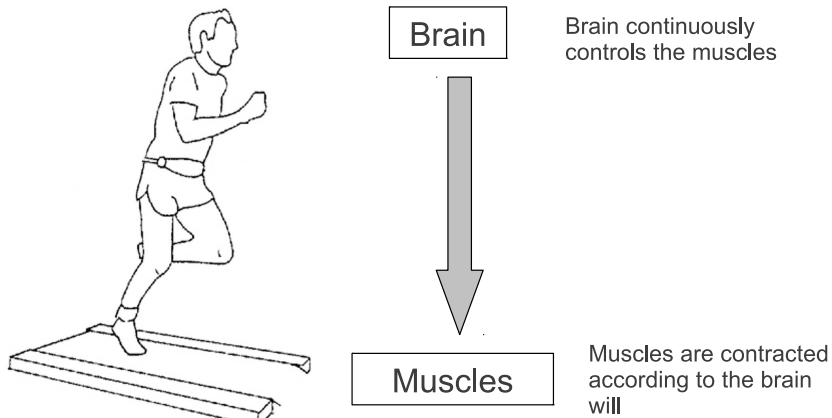
the leg muscles. Thereby, a solution would be to find the corresponding command signal in the brain. Then, a direct decoding or transformation of the gait intent signals will be sufficient to control an ankle device. Here, the main work will be to find the brain control signal among noise and artefacts as well as the most suitable decoding process.

One hierachical model of locomotion



(a) Hierarchical model.

One direct brain control model of locomotion



(b) Direct control model.

Figure 1.18: Two gait models are available: hierarchical and direct controls.

1.3.2 Artefact Problematic

Artefact processing has always been a challenge while dealing with electroencephalographic signal (EEG). Different standard types of artefacts can be observed and corrected: muscular, ocular and mechanical artefacts. Muscular artefacts arise when electrical activities from the muscles pollute the EEG signal through the skin. The contaminated frequency band is usually starting from 10/15 Hz up to high frequencies. The most affected electrodes are often located around the neck but the noise can spread over the whole scalp depending on the signal strength and used reference (common average reference increases the multiple channels contamination). In Figure 1.19, artefact pollution during yawning, chewing and head movements is illustrated. In Figure 1.20, the frequency spread of the neck EMG signals reach above 100 Hz while walking on a treadmill.

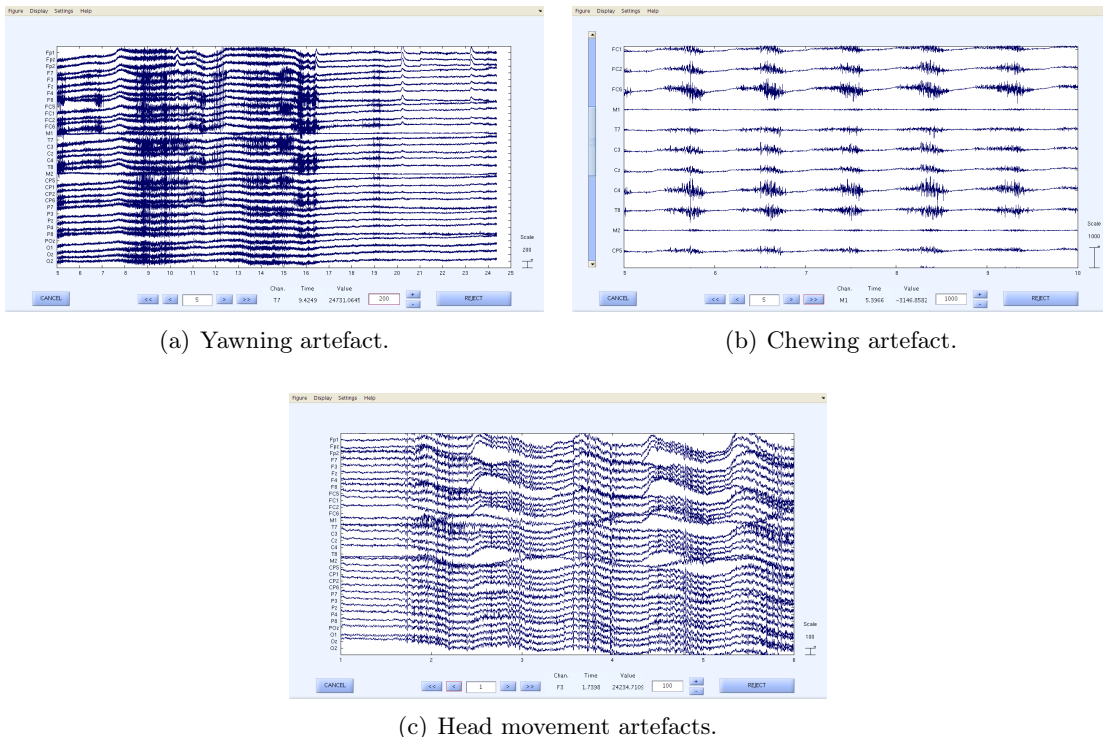


Figure 1.19: Chewing, yawning and head movement artefacts are strongly corrupting the EEG signal.

Ocular artefacts come from the cornea/retina dipole whose movement creates potential variations in the frontal part of the EEG recordings. Most of the spectrum power is detected below 20 Hz, while the most affected electrodes are typically frontal electrodes. As shown in Figure 1.21, blinks and eye movements strongly modify the shape of the signal. This requires dedicated signal processing techniques before further analysis of the brain signal.

Finally, mechanical artefacts are mainly movement dependent. For instance, as depicted in Figure 1.22, under constant-speed walking conditions, quasi-periodic electrode movements create

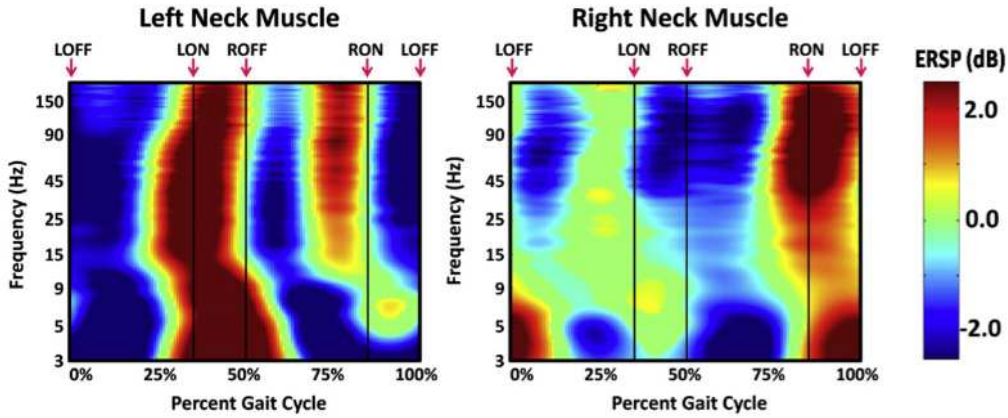


Figure 1.20: The neck muscle artefact has a very large frequency band pollution. It clearly appears that specific care should be taken [103].

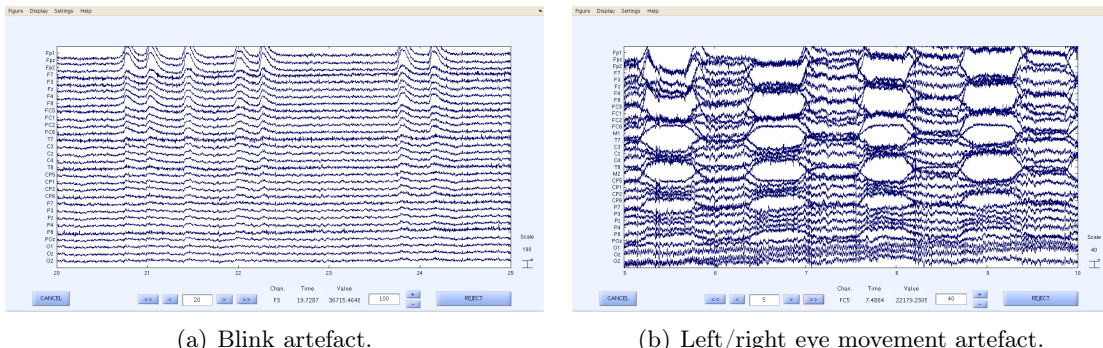


Figure 1.21: Eye movements and blinks may also strongly affect the brain signals.

quasi-synchronized movement artefacts. In this specific case, the affected spectrum fundamentally matches the stepping frequencies and its harmonics. Moreover, as the electrode system is not linear, more complex frequencies are also present making difficult to remove. Because this type of artefact has no clear time-frequency response, standard artefact removal techniques are inefficient, especially in newly studied conditions such as locomotion.

1.3.3 Organization of The Manuscript

To take up the two challenging strategies (continuous brain control and hierarchical control), three major problems have to be addressed in this thesis:

Part I proposes to study gait modelling based on CPGs. In Chapter 2, a programmable CPG, borrowed from robotics, is used to optimally fit elevation angles of human lower limb kinematics. Then, the development of a fully controlled orthosis prototype with this methodology is also detailed. In Chapter 3, another type of model based on a Dynamic Recurrent Neural Network (DRNN) combined with sinusoidal inputs is analysed.

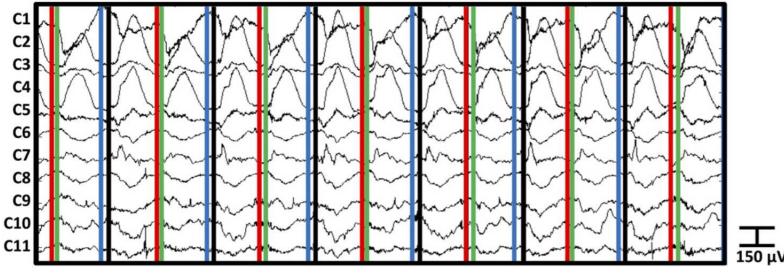


Figure 1.22: During walk, the movement/mechanical artefact can provoke strong magnitude variations that are quasi phase-locked to the gait cycle [103].

Part II investigates the standard BCI/BNCI interfaces under an ambulatory context. Indeed, in order to control the CPG-based gait model, a high-level command has to be emitted to modify the current gait cycle frequency. In this part, I revisit several widely known BCIs under ambulatory conditions such as the P300 and SSVEP. Chapter 4 analyses the impact of gait on the SSVEP SNR response distribution. Chapter 5 deals with the performance assessment of several original gait-related artefact removal techniques on a four-state P300 BCI. Chapter 6 investigates the objective and subjective online performance of the SSVEP and P300 interfaces. In this Chapter, subjects had the opportunity to control the treadmill speed by the BCI. Afterwards, in addition to standard objective performance measures such as classification accuracy, questionnaires and interviews allowed to get an overall opinion about the efficiency of such interfaces. Nevertheless, developing BCI interfaces for disabled people who can not afford them could be highly problematic to spread the technology. Therefore, in Chapter 7, a deep comparative study of a low-cost Emotiv EPOC headset and a medical device is performed. Indeed, this low-cost device could contribute to more widely spread BCI applications. Finally, Chapter 8 proposes a scheme to use EOG signal in an ambulatory interface and a quantitative review of saccade detection.

Part III analyses the fundamentals of gait-related signals. In Chapter 9, a deep review of the current knowledge about spontaneous brain signals that occurs during walk is proposed. In Chapter 10, brain signals while performing gait-like movements sitting on a chair are briefly analysed. In Chapter 11, automatic gait intent detection systems are proposed. The study evaluates how well standard machine learning methods could detect the willingness of subject to start walking from a baseline. A detailed time-frequency analysis and artefact interaction is provided. Then, in Chapter 12, a new hardware system is proposed to estimate this movement artefact. The obtained artefact signal is time-frequency analysed and compared to current gait-related studies. Finally, in Chapter 13, a first artefact analysis is provided. Thanks to an accelerometer, the transmission of stepping frequency harmonics to the EEG data and frequency artefact pollution are illustrated.

Finally, Part IV is devoted to briefly summarized other related research areas I have been focused on during my PhD thesis: attention, BCI in games, overt attention. Abstracts and related publications are shown.

Bibliography

- [1] National Spinal cord Injury Statistical Center. Facts and figures at a glance, 2013.
- [2] National Cancer Institute. Cancer prevalence and cost of care projections, 2013.
- [3] American Heart/Stroke Association. Impact of stroke (stroke statistics), 2013.
- [4] Uustal H and Baerga E. *Physical Medicine and Rehabilitation Board Review*, chapter Gait Analysis. Demos Medical Publishing, New York, 2004.
- [5] H. van Hedel and V. Dietz. Rehabilitation of locomotion after spinal cord injury. *Restorative Neurology and Neuroscience*, 28(1):123 – 134, 2010.
- [6] Inc. Global Industry Analysts. Orthopedic orthotics, a global business strategy report, 2012.
- [7] O& P Business News. New report offers global projections for orthopedic prosthetic and orthotic markets, 2011.
- [8] Thomas Black. Businesses bet on iron man-like exoskeletons, 2013.
- [9] R. Jimenez-Fabian and O. Verlinden. Review of control algorithms for robotic ankle systems in lower-limb orthoses, prostheses, and exoskeletons. *Medical Engineering and Physics*, 34(4):397 – 408, 2012.
- [10] J. Ward. *Dynamic Pace Controller for the Robotic Gait Trainer and Stroke Patient Case Study*. Arizona State University, 2007.
- [11] Joseph Hitt, Thomas Sugar, Matthew Holgate, Ryan Bellman, and Kevin Hollander. Robotic transtibial prosthesis with biomechanical energy regeneration. *Industrial Robot: An International Journal*, 36(5):441–447, 2009.
- [12] M.A. Holgate, A.W. Bohler, and T.G. Sugar. Control algorithms for ankle robots: A reflection on the state-of-the-art and presentation of two novel algorithms. In *Biomedical Robotics and Biomechatronics, 2008. BioRob 2008. 2nd IEEE RAS EMBS International Conference on*, pages 97–102, 2008.
- [13] L.R. Palmer. Sagittal plane characterization of normal human ankle function across a range of walking gait speeds. Master’s thesis, Department of Mechanical Engineering, MIT, 2002.

- [14] J.A. Blaya. Force-controllable ankle foot orthosis (afo) to assist drop foot gait. Master's thesis, Department of Mechanical Engineering, MIT, 2003.
- [15] J.A. Blaya and H. Herr. Adaptive control of a variable-impedance ankle-foot orthosis to assist drop-foot gait. *Neural Systems and Rehabilitation Engineering, IEEE Transactions on*, 12(1):24–31, 2004.
- [16] M.F. Eilenberg, H. Geyer, and H. Herr. Control of a powered ankle foot prosthesis based on a neuromuscular model. *Neural Systems and Rehabilitation Engineering, IEEE Transactions on*, 18(2):164–173, 2010.
- [17] H.A. Varol and M. Goldfarb. Real-time intent recognition for a powered knee and ankle transfemoral prosthesis. In *Rehabilitation Robotics, 2007. ICORR 2007. IEEE 10th International Conference on*, pages 16–23, 2007.
- [18] Ekso bionics Company. The ekso product, 2013.
- [19] Gregory Sawicki and Daniel Ferris. A pneumatically powered knee-ankle-foot orthosis (kafo) with myoelectric activation and inhibition. *Journal of NeuroEngineering and Rehabilitation*, 6(1):23, 2009.
- [20] S.K. Au, P. Bonato, and H. Herr. An emg-position controlled system for an active ankle-foot prosthesis: an initial experimental study. In *Rehabilitation Robotics, 2005. ICORR 2005. 9th International Conference on*, pages 375–379, 2005.
- [21] Warren M. Grill, Sharon E. Norman, and Ravi V. Bellamkonda. Implanted Neural Interfaces: Biochallenges and Engineered Solutions. *Annual Review of Biomedical Engineering*, 11(1):1–24, 2009.
- [22] Hochberg Leigh R., Bacher Daniel, Jarosiewicz Beata, Masse Nicolas Y., Simeral John D., Vogel Joern, Haddadin Sami, Liu Jie, Cash Sydney S., and van der Smagt Patrick. Reach and grasp by people with tetraplegia using a neurally controlled robotic arm. *Nature*, (7398):372?375, 2012.
- [23] RIC. The rehabilitation institute of chicago, 2013.
- [24] Richard B. Buxton, Kamil Uluda, David J. Dubowitz, and Thomas T. Liu. Modeling the hemodynamic response to brain activation. *NeuroImage*, 23, Supplement 1(0):S220 – S233, 2004.
- [25] L.F. Nicolas-Alonso and J. Gomez-Gil. Brain computer interfaces, a review. *Sensors*, 12(2):1211–1279, 2012.
- [26] S. Baillet, J.C. Mosher, and R.M. Leahy. Electromagnetic brain mapping. *Signal Processing Magazine, IEEE*, 18(6):14–30, 2001.
- [27] P.L. Nunez, R. Srinivasan, A.F. Westdorp, R.S. Wijesinghe, D.M. Tucker, R.B. Silberstein, and P.J. Cadusch. Eeg coherency i: Statistics, reference electrode, volume conduction, laplacians, cortical imaging, and interpretation at multiple scales. *Electroencephalography and Clinical Neurophysiology*, 103(5):499–515, 1997.

- [28] H. H. Jasper. The ten twenty electrode system of the international federation. *Electroencephalography and Clinical Neurophysiology*, 10:371–375, 1958.
- [29] B.J. Fisch and R. Spehlmann. *Fisch and Spehlmann's EEG primer: basic principles of digital and analog EEG*. Elsevier, 1999.
- [30] A. Delorme and S. Makeig. EEGLAB: An open source toolbox for analysis of single-trial EEG dynamics including independent component analysis. *Journal of Neuroscience Methods*, 134(1):9–21, 2004.
- [31] F. Campos Viola, J. Thorne, B. Edmonds, T. Schneider, T. Eichele, and S. Debener. Semi-automatic identification of independent components representing EEG artifact. *Clinical Neurophysiology*, 120(5):868–877, 2009.
- [32] R. Ferdousy, A.I. Choudhory, Md.S. Islam, Md.A. Rab, and Md.E.H. Chowdhury. Electrotoculographic and electromyographic artifacts removal from EEG. pages 163–167, 2010.
- [33] H. Nolan, R. Whelan, and R.B. Reilly. Faster: Fully automated statistical thresholding for EEG artifact rejection. *Journal of Neuroscience Methods*, 192(1):152–162, 2010.
- [34] Thierry Castermans, Matthieu Duvinage, Guy Cheron, and Thierry Dutoit. Eeg and human locomotion - descending commands and sensory feedback should be disentangled from artifacts thanks to new experimental protocols position paper. In *BIO SIGNALS*, pages 309–314, 2012.
- [35] T. Castermans, M. Duvinage, M. Petieau, T. Hoellinger, C.D. Saedeleer, K. Seetharaman, A. Bengoetxea, G. Cheron, and T. Dutoit. Optimizing the performances of a p300-based brain-computer interface in ambulatory conditions. *Emerging and Selected Topics in Circuits and Systems, IEEE Journal on*, 1(4):566–577, 2011.
- [36] Trevor Thompson, Tony Steffert, Tomas Ros, Joseph Leach, and John Gruzelier. Eeg applications for sport and performance. *Methods*, 45(4):279 – 288, 2008.
- [37] R.J. Ratcliffe and K.G. Holt. Low frequency shock absorption in human walking. *Gait and Posture*, 5(2):93–100, 1997.
- [38] K.E. Misulis and T.C. Head. *Essentials of clinical neurophysiology*. Number vol. 1. Butterworth-Heinemann, 2003.
- [39] A.C.M. Vanrijn, A. Peper, and C.A. Grimbergen. High-quality recording of bioelectric events .1. Interference reduction, theory and practice. *Medical & biological engineering & computing*, 28(5):389–397, SEP 1990.
- [40] H. De Talhouet and J.G. Webster. The origin of skin-stretch-caused motion artifacts under electrodes. *Physiological Measurement*, 17(2):81–93, 1996.
- [41] Scott E. Kerick, Kelvin S. Oie, and Kaleb McDowell. Assessment of EEG signal quality in motion environments. *Army Research Laboratory Report*, (ARL-TR-4866), 2009.

- [42] K. Gramann, J.T. Gwin, N. Bigdely-Shamlo, D.P. Ferris, and S. Makeig. Visual evoked responses during standing and walking. *Frontiers in Human Neuroscience*, 4, 2010.
- [43] Gareth R. Barnes, Arjan Hillebrand, Ian P. Fawcett, and Krish D. Singh. Realistic spatial sampling for MEG beamformer images. *Human Brain Mapping*, 23(2):120–127, 2004.
- [44] D.J. Krusienski, M. Grosse-Wentrup, F. Galán, D. Coyle, K.J. Miller, E. Forney, and C.W. Anderson. Critical issues in state-of-the-art brain-computer interface signal processing. *Journal of Neural Engineering*, 8(2), 2011.
- [45] Tonio Ball, Markus Kern, Isabella Mutschler, Ad Aertsen, and Andreas Schulze-Bonhage. Signal quality of simultaneously recorded invasive and non-invasive {EEG}. *NeuroImage*, 46(3):708 – 716, 2009.
- [46] Ted G.H. Yuen, William F. Agnew, and Leo A. Bullara. Tissue response to potential neuroprosthetic materials implanted subdurally. *Biomaterials*, 8(2):138 – 141, 1987.
- [47] Zenas C. Chao, Yasuo Nagasaka, and Naotaka Fujii. Long-term asynchronous decoding of arm motion using electrocorticographic signals in monkeys. *Frontiers in neuroengineering*, 3, 2010.
- [48] Stephan Waldert, Tobias Pistohl, Christoph Braun, Tonio Ball, Ad Aertsen, and Carsten Mehring. A review on directional information in neural signals for brain-machine interfaces. *Journal of Physiology-Paris*, 103(3?5):244 – 254, 2009.
- [49] A. Abbott. Neuroprosthetics: In search of the sixth sense. *Nature*, 442(7099):125–127, 2006.
- [50] L. Grand, L. Wittner, S. Herwik, E. Göthelid, P. Ruther, S. Oscarsson, H. Neves, B. Dombovári, R. Csercsa, G. Karmos, and I. Ulbert. Short and long term biocompatibility of NeuroProbes silicon probes. *Journal of Neuroscience Methods*, 189(2):216–229, 2010.
- [51] R.Christopher deCharms, Kalina Christoff, Gary H Glover, John M Pauly, Susan Whitfield, and John D.E Gabrieli. Learned regulation of spatially localized brain activation using real-time fmri. *NeuroImage*, 21(1):436 – 443, 2004.
- [52] R.J. Jaszcak and R.E. Coleman. Single photon emission computed tomography (spect): Principles and instrumentation. *Investigative Radiology*, 20(9):897–910, 1985.
- [53] Michael E. Phelps, Edward J. Hoffman, Nizar A. Mullani, and Michel M. Ter-Pogossian. Application of annihilation coincidence detection to transaxial reconstruction tomography. *Journal of Nuclear Medicine*, 16(3):210–224, 1975.
- [54] Shirley M Coyle, Tomas E Ward, and Charles M Markham. Brain?computer interface using a simplified functional near-infrared spectroscopy system. *Journal of Neural Engineering*, 4(3):219, 2007.

- [55] T. Vaithianathan, I.D.C. Tullis, N. Everdell, T. Leung, J. Meek, and D.T. Delpy. Functional imaging of the brain using a portable NIR instrument. *Proceedings of SPIE - The International Society for Optical Engineering*, 4955:96–102, 2003.
- [56] Shirley Coyle, Tomas Ward, Charles Markham, and Gary McDarby. On the suitability of near-infrared (NIR) systems for next-generation brain-computer interfaces. *Physiological Measurement*, 25(4):815, 2004.
- [57] L.A. Farwell and E. Donchin. Talking off the top of your head: toward a mental prosthesis utilizing event-related brain potentials. *Electroencephalography and Clinical Neurophysiology*, 70(6):510 – 523, 1988.
- [58] Jonathan R. Wolpaw, Niels Birbaumer, Dennis J. McFarland, Gert Pfurtscheller, and Theresa M. Vaughan. Brain-computer interfaces for communication and control. *Clinical Neurophysiology*, 113(6):767 – 791, 2002.
- [59] Robert Leeb, Doron Friedman, Gernot R. Müller-Putz, Reinhold Scherer, Mel Slater, and Gert Pfurtscheller. Self-paced (asynchronous) bci control of a wheelchair in virtual environments: a case study with a tetraplegic. *Intell. Neuroscience*, 2007:7:1–7:12, April 2007.
- [60] Gert Pfurtscheller, Gernot R. Müller, Jörg Pfurtscheller, Hans Jürgen Gerner, and Rüdiger Rupp. ‘Thought’ - control of functional electrical stimulation to restore hand grasp in a patient with tetraplegia. *Neuroscience Letters*, 351(1):33 – 36, 2003.
- [61] Anatole Lécuyer, Fabien Lotte, Richard B. Reilly, Robert Leeb, Michitaka Hirose, and Mel Slater. Brain-computer interfaces, virtual reality, and videogames. *Computer*, 41:66–72, October 2008.
- [62] José del R. Millán, Rüdiger Rupp, Gernot Mueller-Putz, Roderick Murray-Smith, Claudio Giugliemma, Michael Tangermann, Carmen Vidaurre, Febo Cincotti, Andrea Kubler, Robert Leeb, Christa Neuper, Klaus R Mueller, and Donatella Mattia. Combining brain-computer interfaces and assistive technologies: State-of-the-art and challenges. *Frontiers in Neuroscience*, 4(0):12, 2010.
- [63] Nathan Fitzsimmons, Mikhail Lebedev, Ian Peikon, and Miguel A.L Nicolelis. Extracting kinematic parameters for monkey bipedal walking from cortical neuronal ensemble activity. *Frontiers in Integrative Neuroscience*, 3, 2009.
- [64] R. Rao and R. Scherer. Brain-computer interfacing. *IEEE Signal Processing Magazine*, 27(4):152 – 150, July 2010.
- [65] Collectif. *Traitements de la parole (French Edition)*. Presses Polytechniques et Universitaires Romandes (PPUR).
- [66] L.F. Nicolas-Alonso and J. Gomez-Gil. Rehabilitation with poststroke motor recovery: A review with a focus on neural plasticity. *Stroke Research and Treatment*, page 13 pages, 2013.

- [67] G. Pfurtscheller, C. Neuper, G.R. Muller, B. Obermaier, G. Krausz, A. Schlogl, R. Scherer, B. Graimann, C. Keinrath, D. Skliris, M. Wortz, G. Supp, and C. Schrank. Graz-bci: state of the art and clinical applications. *Neural Systems and Rehabilitation Engineering, IEEE Transactions on*, 11(2):1–4, 2003.
- [68] D. Regan. *Human Brain Electrophysiology: Evoked Potentials and Evoked Magnetic Fields in Science and Medicine*. Elsevier, New York, NY, USA, 1989.
- [69] C S Herrmann. Human eeg responses to 1-100 hz flicker: resonance phenomena in visual cortex and their potential correlation to cognitive phenomena. *Exp Brain Res*, 137(3-4):346–53, 2001.
- [70] Jinghai Yin, Derong Jiang, and Jianfeng Hu. Design and application of brain-computer interface web browser based on vep. In *BioMedical Information Engineering, 2009. FBIE 2009. International Conference on Future*, pages 77–80, 2009.
- [71] Yijun Wang, Ruiping Wang, Xiaorong Gao, Bo Hong, and Shangkai Gao. A practical vep-based brain-computer interface. *Neural Systems and Rehabilitation Engineering, IEEE Transactions on*, 14(2):234–240, 2006.
- [72] Ivan Volosyak. Ssvep-based bremen bci interface boosting information transfer rates. *Journal of Neural Engineering*, 8(3):036020, 2011.
- [73] Zhenghua Wu, Yongxiu Lai, Yang Xia, Dan Wu, and Dezhong Yao. Stimulator selection in ssvep-based bci. *Medical Engineering and Physics*, 30(8):1079 – 1088, 2008.
- [74] Sergio Parini, Luca Maggi, Anna C. Turconi, and Giuseppe Andreoni. A robust and self-paced bci system based on a four class ssvep paradigm: algorithms and protocols for a high-transfer-rate direct brain communication. *Intell. Neuroscience*, 2009:2:1–2:11, January 2009.
- [75] P.F. Diez, V.A. Mut, E.M. Avila Perona, and E. Laciar Leber. Asynchronous bci control using high-frequency ssvep. *J Neuroeng Rehabil*, 8, 2011.
- [76] N. Birbaumer, T. Elbert, A. G. Canavan, and B. Rockstroh. Slow potentials of the cerebral cortex and behavior. *Physiological reviews*, 70(1):1–41, January 1990.
- [77] T. Hinterberger, S. Schmidt, N. Neumann, J. Mellinger, B. Blankertz, G. Curio, and N. Birbaumer. Brain-computer communication and slow cortical potentials. *Biomedical Engineering, IEEE Transactions on*, 51(6):1011–1018, 2004.
- [78] Andrea Kübler, Boris Kotchoubey, Thilo Hinterberger, Nimr Ghanayim, Juri Perelmouter, Margarete Schauer, Christoph Fritsch, Edward Taub, and Niels Birbaumer. The Thought Translation Device: A Neurophysiological Approach to Communication in Total Motor Paralysis. *Experimental Brain Research*, 124(2):223–232, January 1999.
- [79] N. Birbaumer, T. Hinterberger, A. Kubler, and N. Neumann. The thought-translation device (ttd): neurobehavioral mechanisms and clinical outcome. *Neural Systems and Rehabilitation Engineering, IEEE Transactions on*, 11(2):120–123, 2003.

- [80] I.H. Iversen, N. Ghanayim, A. Kubler, N. Neumann, N. Birbaumer, and J. Kaiser. A brain?computer interface tool to assess cognitive functions in completely paralyzed patients with amyotrophic lateral sclerosis. *Clinical Neurophysiology*, 119(10):2214 – 2223, 2008.
- [81] HansH. Kornhuber and Lüder Deecke. Hirnpotentialanderungen bei willkurbewegungen und passiven bewegungen des menschen: Bereitschaftspotential und reafferente potentiale. *Pfluger's Archiv fur die gesamte Physiologie des Menschen und der Tiere*, 284(1):1–17, 1965.
- [82] H Shibasaki, G Barrett, and E. Halliday. Components of the movement-related cortical potential and their scalp topography. *Electroencephalography and Clinical Neurophysiology*, 49(3):213–226, 1980.
- [83] Hiroshi Shibasaki and Mark Hallett. What is the bereitschaftspotential? *Clinical Neurophysiology*, 117(11):2341 – 2356, 2006.
- [84] Omar Feix do Nascimento and D. Farina. Movement-related cortical potentials allow discrimination of rate of torque development in imaginary isometric plantar flexion. *Biomedical Engineering, IEEE Transactions on*, 55(11):2675–2678, 2008.
- [85] Toshiaki Wasaka, Hiroki Nakata, Tetsuo Kida, and Ryusuke Kakigi. Gating of seps by contraction of the contralateral homologous muscle during the preparatory period of self-initiated plantar flexion. *Cognitive Brain Research*, 23(2?3):354 – 360, 2005.
- [86] Omar Feix do Nascimento, Kim Dremstrup Nielsen, and Michael Voigt. Influence of directional orientations during gait initiation and stepping on movement-related cortical potentials. *Behavioural Brain Research*, 161(1):141 – 154, 2005.
- [87] N. Birbaumer, N. Ghanayim, T. Hinterberger, I. Iversen, B. Kotchoubey, A. Kubler, J. Perelmouter, E. Taub, and H. Flor. A spelling device for the paralysed. *Nature*, 398(6725):297–8, March 1999.
- [88] K. Tanaka, K. Matsunaga, and H.O. Wang. Electroencephalogram-based control of an electric wheelchair. *Robotics, IEEE Transactions on*, 21(4):762–766, 2005.
- [89] E.M. Mugler, C.A. Ruf, S. Halder, M. Bensch, and A. Kubler. Design and implementation of a p300-based brain-computer interface for controlling an internet browser. *Neural Systems and Rehabilitation Engineering, IEEE Transactions on*, 18(6):599–609, 2010.
- [90] A. Furdea, S. Halder, D.J. Krusienski, D. Bross, F. Nijboer, N. Birbaumer, and A. Kubler. An auditory oddball (p300) spelling system for brain-computer interfaces. *Psychophysiology*, 46(3):617–625, 2009.
- [91] B. Rivet, A. Souloumiac, V. Attina, and G. Gibert. xdawn algorithm to enhance evoked potentials: Application to brain-computer interface. *Biomedical Engineering, IEEE Transactions on*, 56(8):2035–2043, 2009.

- [92] J.R. Wolpaw, D.J. McFarland, T.M. Vaughan, and G. Schalk. The wadsworth center brain-computer interface (bci) research and development program. *Neural Systems and Rehabilitation Engineering, IEEE Transactions on*, 11(2):1–4, 2003.
- [93] B. Blankertz, F. Losch, M. Krauledat, G. Dornhege, G. Curio, and K.-R. Muller. The berlin brain–computer interface: Accurate performance from first-session in bci-naive subjects. *Biomedical Engineering, IEEE Transactions on*, 55(10):2452–2462, 2008.
- [94] G. Pfurtscheller and C. Neuper. Motor imagery and direct brain-computer communication. *Proceedings of the IEEE*, 89(7):1123–1134, 2001.
- [95] Ou Bai, Varun Rathi, Peter Lin, Dandan Huang, Harsha Battapady, Ding-Yu Fei, Logan Schneider, Elise Houdayer, Xuedong Chen, and Mark Hallett. Prediction of human voluntary movement before it occurs. *Clinical Neurophysiology*, 122(2):364 – 372, 2011.
- [96] R. Barea, L. Boquete, M. Mazo, and E. Lopez. Wheelchair guidance strategies using eog. *J. Intell. Robotics Syst.*, 34(3):279–299, 2002.
- [97] Rafael Barea, Luciano Boquete, Jose Manuel Rodriguez-Ascariz, Sergio Ortega, and Elena Lopez. Sensory system for implementing a human?computer interface based on electrooculography. *Sensors*, 11(1):310–328, 2010.
- [98] R Barea, L Boquete, M Mazo, and E Lopez. Wheelchair guidance strategies using eog. *Journal of Intelligent and Robotic Systems*, 34(3):279–299, 2002.
- [99] R. Barea, L. Boquete, S. Ortega, E. Lopez, and J.M. Rodriguez-Ascariz. Eog-based eye movements codification for human computer interaction. *Expert Systems with Applications*, 39(3):2677 – 2683, 2012.
- [100] M. Duvinage, T. Castermans, and T. Dutoit. Control of a lower limb active prosthesis with eye movement sequences. In *Computational Intelligence, Cognitive Algorithms, Mind, and Brain (CCMB), 2011 IEEE Symposium on*, pages 1 –7, april 2011.
- [101] A. Bulling, J.A. Ward, H. Gellersen, and G. Tro? andster. Eye movement analysis for activity recognition using electrooculography. *Pattern Analysis and Machine Intelligence, IEEE Transactions on*, 33(4):741 –753, april 2011.
- [102] M. Duvinage, T. Castermans, T. Hoellinger, G. Cheron, and T. Dutoit. Modeling human walk by pcpg for lower limb neuroprostheses control. In *Neural Engineering (NER), 2011 5th International IEEE/EMBS Conference on*, pages 317–321, 2011.
- [103] Joseph T. Gwin, Klaus Gramann, Scott Makeig, and Daniel P. Ferris. Electrocortical activity is coupled to gait cycle phase during treadmill walking. *NeuroImage*, 54(2):1289 – 1296, 2011.

Part I

Central-Pattern Generator Based Gait Modelling

Chapter 2

Programmable Central Pattern Generator-based Gait Model and Orthosis Implementation

Contents

2.1	Introduction	44
2.2	Gait Model	44
2.2.1	PCPG Description	44
2.2.2	Experimental and methodological approaches	47
2.2.3	Results and discussion	48
2.3	Orthosis Design and Control	50
2.3.1	Orthosis Hardware	50
2.3.2	Gait cycle control strategies	52
2.4	Practical needs	53
2.4.1	Frequency adaptation	53
2.4.2	Phase-resetting	54
2.5	Simulation Results	55
2.6	Conclusion and Future Work	57
2.6.1	Conclusion	57
2.6.2	Future Work	57

Abstract

Central pattern generators (CPGs) are known to play an important role in the generation of rhythmic movements in animal and human gait. The comprehension of their underlying mechanism has led to the development of an important family of algorithms at the basis of autonomous walking robots. In this Chapter, an original and biologically-inspired leg prosthesis control system is proposed to integrate a high-level command from a BCI.

First, we demonstrate that human walk periodic patterns can be modelled by a Programmable Central Pattern Generator (PCPG) algorithm. In this study, we modelled the kinematics of foot angle of elevation of seven subjects walking on a treadmill at 10 different speeds. To best modify the PCPG parameters, we found that a low-level order polynomial interpolation of the PCPG parameters as a function of speed provides good similarity indices between real walk and generated patterns at different speeds. The obtained smooth interpolation suggests that continuous modification of the speed could be performed, e.g. generate patterns at non learned speeds. Additionally, results suggest that walk would be advantageously modelled by two PCPGs for modelling low- and high- speeds.

Second, a foot lifter orthosis prototype driven by this modified PCPG algorithm and based on biomechanical sensors is presented. After a learning phase, the PCPG output is used to drive the orthosis actuator during the swing phase when the foot is in the air, in order to help patients suffering from foot drop. During the stance phase, i.e. when the foot is on the ground, the orthosis just follows the subject movement. In practice, given that human gait is not perfectly periodic, the phase of this control signal needs to be reset with actual movement. Therefore, two phase-resetting procedures were studied: one standard hard phase-resetting leading to discontinuities and one original soft phase-resetting allowing to recover the correct phase in a smooth way. The simulation results and complete design of the orthosis hardware and software are detailed. Overall, although the developed prototype is working as desired, the smooth phase resetting method should be made quicker and tests on disabled people still need to be performed.

This chapter is based upon the following publications:

- M. DUVINAGE, R. JIMENEZ-FABIAN, T. CASTERMANS, O. VERLINDEN, T. DUTOIT, 2011, *An active foot lifter orthosis based on a PCPG algorithm*, Proceedings of the IEEE 12th International Conference on Rehabilitation Robotics (ICORR 2011), ETH Zurich, Switzerland, June 29 - July 1, pp 116-122.
- M. DUVINAGE, T. CASTERMANS, T. HOELLINGER, G. CHERON, T. DUTOIT, 2011, *Modeling Human Walk by PCPG for Lower Limb Neuroprostheses Control*, Proceedings of the 5th International IEEE/EMBS Neural Engineering Conference, Fiesta Americana Grand Coral Beach, Cancun, Mexico, April 27 - May 1, pp. 317-321.

- M. DUVINAGE, T. CASTERMANS, R. JIMENEZ-FABIAN, T. HOELLINGER, M. PETIEAU, O. VERLINDEN, G. CHERON, T. DUTOIT, 2012, *Human Walk Modeled by PCPG to Control a Lower Limb Neuroprosthesis by High-Level Commands*, Journal of Systemics, Cybernetics and Informatics, volume 10, number 3, pp. 70-80.

2.1 Introduction

Because BCIs still lack reliability, they are often managed in a framework of shared control [1]. This principle has extensively been used for controlling a wheelchair [2]. In this approach, a BCI provides high-level commands (*turn right*, *turn left* and *move forward*) and all the low-level problems are solved by the wheelchair feedback system based on several sensors. As a hierarchical gait model is considered, this shared control principle is particularly adapted to integrate brain-based high-level commands in an orthosis. Given a high-level command provided by an ambulatory BCI, the prosthesis will execute all the low-level commands, e.g. generate gait kinematics and manage feedback control, thanks to the CPG.

In this Chapter, the focus is on the Programmable Central Pattern Generator (PCPG). Actually, a lot of research have been performed to model biological CPGs. Up to now, such models have been widely implemented in the field of robotics, particularly in the development of small autonomous walking robots, from multi-legged insect-like robots to humanoids [3] and one active prosthesis based on motion detection [4]. Although many CPG mathematical models have been proposed, e.g. based on mathematical equations or Dynamic Recurrent Neural Network (DRNN) [5], most of them suffer from the lack of controllability. It is indeed not trivial to model a given periodic pattern and explicitly, i.e. easily, modify the pattern frequency in a smooth way. From that point of view, the PCPG has these advantageous properties.

As detailed in Section 2.2, a modification of the PCPG use is proposed to model human locomotion at several speeds and to allow it to be controlled by current Brain-Computer Interface (BCI) techniques [1]. The walk pattern is tuned in frequency and in magnitude to be able to adapt speed continuously and smoothly according to the user's intent. In order to demonstrate the feasibility of such a system, the implementation of the PCPG algorithm on an actual foot lifter orthosis has been performed in Section 2.3. This type of orthosis helps people affected by foot drop problems who are unable to elevate their feet. Thus, the two-step control strategy that aims at mimicking at best the ankle behaviour is particularly well-tailored. Using foot-related angle is not a limitation because it is known to be the most complex signal to model in human locomotion leading to better results in case of other angles. Because gait is not a perfectly periodic pattern, two-phase resetting techniques, which allow to synchronize the PCPG pattern to the actual movement, are presented in Section 2.4. Finally, in Section 2.5, the simulation results to realistic conditions are presented.

2.2 Gait Model

2.2.1 PCPG Description

A PCPG is able to learn a standard gait pattern. This standard gait pattern was obtained by averaging about 50 gait cycles performed on a treadmill, determined and synchronized by a peak detection algorithm able to locate all the relevant maxima in the kinematics recordings. Ideally, the standard pattern could be derived from the subject himself before his accident or, more probably, from a similar subject in terms of his gait parameters such as age, height, etc [4].

As defined in [6], a PCPG is a kind of Fourier series decomposition and is composed of several adaptive oscillators. This algorithm is governed by the following equation system:

$$\dot{x}_i = \gamma(\mu - r_i^2)x_i - \omega_i y_i + \epsilon F(t) + \tau_i \sin(R_i - \phi_i) \quad (2.1)$$

$$\dot{y}_i = \gamma(\mu - r_i^2)y_i + \omega_i x_i \quad (2.2)$$

$$\dot{\omega}_i = -\epsilon F(t) \frac{y_i}{r_i} \quad (2.3)$$

$$\dot{\alpha}_i = \eta x_i F(t) \quad (2.4)$$

$$\dot{\phi}_0 = 0 \quad (2.5)$$

$$\dot{\phi}_i = \sin(R_i - \text{sgn}(x_i) \cos^{-1}(-\frac{y_i}{r_i})) - \phi_i, \forall i \neq 0 \quad (2.6)$$

with

$$R_i = \frac{\omega_i}{\omega_0} \text{sgn}(x_0) \cos^{-1}(-\frac{y_0}{r_0}) \quad (2.7)$$

and

$$F(t) = P_{\text{teach}}(t) - \sum_{i=0}^N \alpha_i x_i \quad (2.8)$$

As depicted in Figure 2.1, oscillators are coupled between each other. The instantaneous phase of the fundamental oscillator R_0 is scaled at the frequency ω_i through R_i and the phase difference with the fundamental oscillator is given by ϕ_i . In the standard approach, the coupling constant τ_i is chosen constant over all oscillators. They are each composed of one adaptive magnitude coefficient α_i and one frequency parameter ω_i . μ has a role of normalization of the learned pattern with respect to $r_i = (x_i^2 + y_i^2)^{\frac{1}{2}}$. The other parameters γ and ϵ aim at accelerating the convergence while limiting stability problems [6]. The $Q_{\text{learned}}(t)$ signal resulting from the sum of oscillator outputs is compared to the $P_{\text{teach}}(t)$ gait pattern target and the error value $F(t)$ is computed. Throughout the learning step consisting in integrating the differential equations by a 4th order Runge-Kutta method with a fixed step size, all the parameters of the PCPG are modified in order to minimize $F(t)$ (the typical learning time is less than five minutes on a standard laptop). When this learning step is finished, $F(t)$ is close to zero and the system is generating the right pattern as depicted in Figure 2.2.

Properties of PCPGs make them suitable for trajectory generation in robotics and also for prosthesis applications. In fact, the pattern learned by a PCPG can be easily controlled in magnitude and in frequency thanks to a simple linear change of the $\vec{\omega}$ and $\vec{\alpha}$ vectors representing the \Re^N PCPG states (N is the number of oscillators). This linearity leads to a smooth change of the global system behavior. For instance, if the $\vec{\omega}$ vector is divided by two, the underlying frequency of the standard temporal pattern is divided by two. The same effect occurs for the $\vec{\alpha}$ vector, which governs the pattern magnitude.

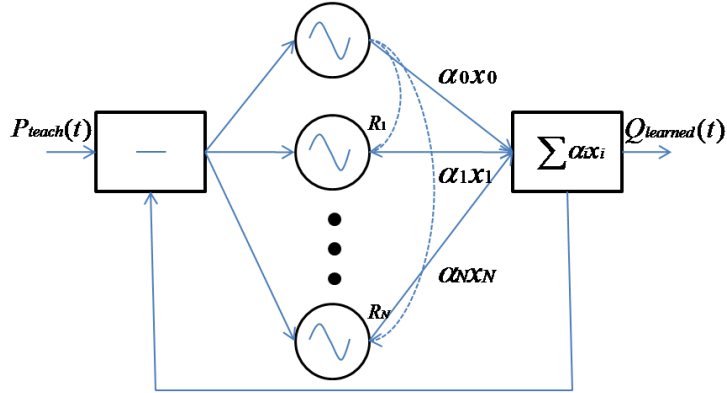


Figure 2.1: The PCPG is able to learn the frequency components of a periodic signal as well as the various phases and magnitudes. The main interest of PCPGs is the possibility to modify a learned pattern in amplitude or frequency in a smooth way. This Figure is inspired from [6].

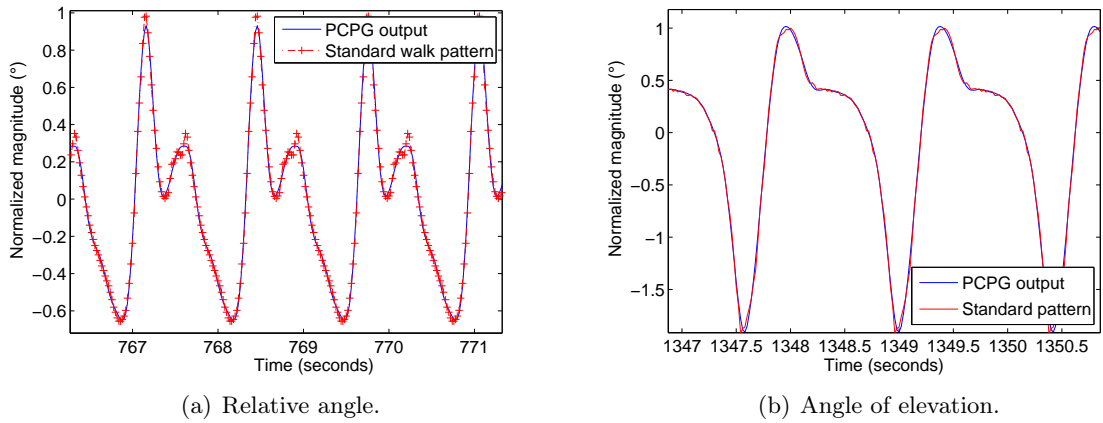


Figure 2.2: The PCPG is able to learn quasi-perfectly an average normalized pattern of foot angle by means of 5 oscillators determined by the frequency complexity of the signal for both absolute and relative angles.

Finally, as proposed in [7], it is possible to couple several PCPGs to model different joint angles. This is performed thanks to equations of coupling between the fundamental oscillators of each PCPG and by learning the phase difference:

$$\begin{cases} \dot{x}_{0,k} = \gamma(\mu - r_{0,k}^2)x_{0,k} - \omega_{0,k}y_{0,k} + \tau \sin(R_{0,k-1} - \phi_{0,k}) \\ \dot{\phi}_{0,k} = \sin(R_{0,k-1} - R_{0,k} - \phi_{0,k}) \end{cases} \quad (2.9)$$

$$(2.10)$$

where $(0, k)$ denotes the first oscillator of the k th PCPG (frequencies of joint angles are the same).

2.2.2 Experimental and methodological approaches

To train the PCPG for each subject, three standard gait patterns were needed. These temporal patterns consist of the angle of elevation of the foot, the shank and the thigh of a healthy subject walking on a treadmill at 3 km/h, a typical medium speed. The elevation angles were computed using the positions of 23 passive markers disposed on the subject and determined by six infrared Bonita Vicon cameras. The kinematics data were recorded during 60 seconds at 100 Hz.

The standard gait patterns were obtained by averaging about 50 walking cycles, determined and synchronized by a peak detection algorithm able to locate all the relevant maxima and minima angle values of the kinematics recordings. Here, the patterns were synchronized by the maxima because of a clearer peak and because they correspond to the heel strike area. Each standard pattern is thus a kind of average pattern along the 60-second recordings. After determining and normalizing these standard patterns, the PCPG was trained using the procedure previously described. Figure 2.2 shows how well the PCPG is able to reproduce the standard pattern of the foot elevation angle using 7 oscillators.

The originality of this approach is to generate gait patterns with the PCPG in a way differing from the bipedal robots described in the literature which consists in walking so far as possible without taking into account the potential patient itself. Indeed, one of the main goals in prosthetics is to provide the user with the most comfortable walk possible. Therefore, at each step, the studied pattern should be adapted in terms of frequency and magnitude, i.e. respectively the stepping frequency and stride-related length between two heel strikes whatever the walking speed. Kinematics data were thus recorded for seven subjects at 10 different speeds, from 1.5 to 6 km/h, by steps of 0.5 km/h. For a specific angle, the normalized and centred pattern learned by the PCPG for the speed of 3 km/h and generated for all the other speeds were automatically calibrated. This calibration was done in frequency by determining the ratio between the fundamental frequencies of the real walk pattern at the studied speed and the PCPG pattern generation at 3 km/h. Similarly, magnitude was computed by the ratio between the average peak-to-peak magnitudes in order to fit the standard gait patterns. Moreover, by this procedure, we wanted to determine if it exists a mathematical link between the PCPG magnitude and frequency parameters (the $\vec{\alpha}$ and $\vec{\omega}$ vectors) as a function of the walking speed. Indeed, this could allow to control the PCPG in a continuous way.

To prove the relevancy of this approach, a Similarity Index (SI) was assessed between the PCPG output $f_1(t)$ and the standard gait pattern $f_2(t)$ at each speed to show the true potential of this method and the result of the mathematical link between PCPG parameters and speed. This index is defined as:

$$SI = \frac{\int_{-\frac{T}{2}}^{\frac{T}{2}} f_1(t)f_2(t) dt}{\left[\int_{-\frac{T}{2}}^{\frac{T}{2}} f_1(t)^2 dt \int_{-\frac{T}{2}}^{\frac{T}{2}} f_2(t)^2 dt \right]^{\frac{1}{2}}} \quad (2.11)$$

where T is the period of the limit cycle, $f_1(t)$ and $f_2(t)$ being synchronized, i.e. the matching between both patterns is based on the maximum of each pattern. Note that if both functions are identical, $SI = 1$.

2.2.3 Results and discussion

In this section, we demonstrate that a mathematical link based on polynomial interpolation is sufficient to control the PCPG parameters along the speed. Moreover, we demonstrate that human walk can be learned by a PCPG and subsequently generated at different walking speeds. Although results are presented for the foot angle of elevation, similar results were obtained for the other angles, i.e. thigh and shank angles of elevation. Related-relative angles would be easily obtained by the same procedure. Therefore, this approach can be easily extended to a full lower limb prosthesis in its principles.

Thank to our methodology, we found a mathematical link between the PCPG magnitude and frequency parameters (the $\vec{\alpha}$ and $\vec{\omega}$ vectors) as a function of the walking speed. Most of the time, this link was established by computing low-level order polynomial interpolation function at the least mean square sense as shown in Table 2.1.

Table 2.1: The orders of the polynomial interpolation are quite low except for subject 2. For this subject, a strange behaviour in frequency was observed, i.e. the frequency first decreases and then increases while speed is increasing.

Order	Magnitude	Frequency
Subject 1	4	3
Subject 2	4	8
Subject 3	4	5
Subject 4	5	3
Subject 5	4	3
Subject 6	4	4
Subject 7	3	3

Figure 2.3 shows results obtained for a specific subject. One can notice that the subject increases his walking speed at first by extending his movement magnitude, and then by increasing his stepping frequency. This confirms results obtained with stride length and stepping frequency in [8] and a similar behavior was obtained on the majority of the subjects. It has to be emphasized that this interpolation can be computed specifically for any subject, increasing therefore the precision and adequacy of the prosthesis control at each step. Unfortunately but logically, no kind of inter-person standard gait patterns was found due to the high variability of walk styles as mentioned in [4].

Moreover, as BCI is far from working perfectly, a confidence level of the command could be derived and integrated in the speed parameter change. Considering that an *accelerate* command increases the actual speed of 0.5 km/h by default, if the decision is uncertain, e.g. reliable at 75 %, 75 % of the speed increase can be actually performed thanks to the parameter interpolation.

To show the relevancy of this approach, Similarity Indices were computed for all subjects with and without interpolation. Globally, SI values without interpolation are very good but show a logical degradation for speeds differing more and more from the PCPG learned speed as shown in Table 2.2. Regarding the interpolation, the impact of the dissimilarity increase is clearly negligible as depicted in Figure 2.4.

An alternative to improve this procedure which relies on a single PCPG could be to manage

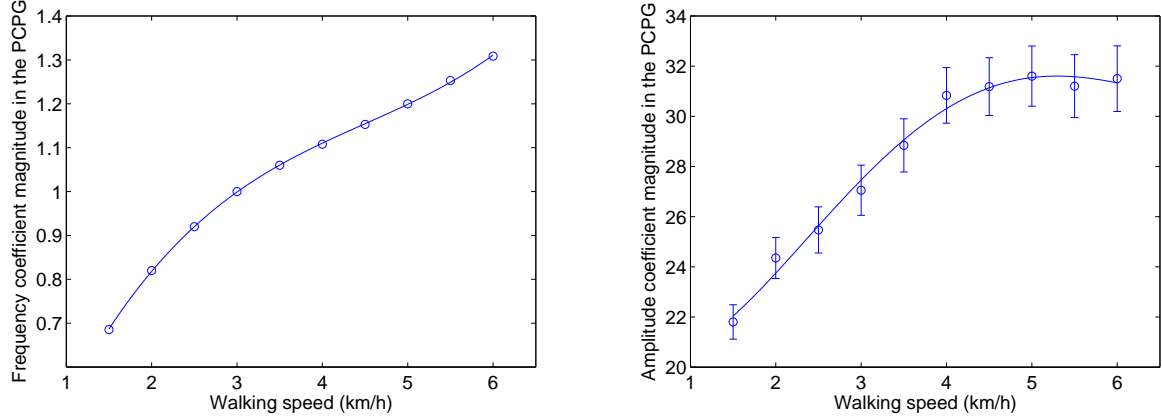


Figure 2.3: Evolutions of the foot pattern frequency (left) and magnitude (right) PCPG parameters as a function of the walking speed. The interpolation is performed for 10 walking speeds with a 4th-order polynomial function. Error bars in magnitude represent the high magnitude variability (standard deviation) of each gait cycle. Similar results are derived from the shank and thigh patterns.

Table 2.2: SI values are quite good over all speeds expressed in km/h except for subject 3. For this subject, the generated patterns at 5.5 and 6 km/h are too different from the learned pattern.

Speed(km/h)	1.5	2	2.5	3	3.5	4	4.5	5	5.5	6
Subject 1	0.97	0.99	0.99	1	1	0.99	0.98	0.95	0.93	0.93
Subject 2	0.92	0.95	0.98	1	1	0.99	0.95	0.93	0.90	0.92
Subject 3	0.92	0.97	0.99	1	0.99	0.95	0.91	0.92	0.86	0.80
Subject 4	0.97	0.99	1	1	0.99	0.99	0.97	0.96	0.93	0.92
Subject 5	0.93	0.96	0.99	1	1	0.98	0.96	0.96	0.95	0.92
Subject 6	0.95	0.97	1	1	1	0.98	0.97	0.95	0.91	0.9
Subject 7	0.99	1	1	1	1	0.98	0.97	0.96	0.95	0.92
Average	0.95	0.98	0.99	1	1	0.98	0.96	0.95	0.92	0.90
Standard Deviation	0.027	0.018	0.005	0.001	0.004	0.016	0.025	0.016	0.034	0.045

a multi-PCPG system at a multi-interpolation level; each PCPG will model a typical range of speeds with its own interpolation, e.g. 0.5-2 km/h where SI are sufficiently high compared to the level of requirements. The merging of those PCPGs would be used to model as perfectly as possible real walk while making the change of PCPG as smoothed as possible.

In order to provide better SI results, a shaping neural network approach was shortly tested without success. Inspired from [9], the PCPG output could be shaped by a fitter such as a Multi-Layer Perceptron or a recurrent neural network. In brief, these systems aim at mapping the PCPG output to the actual kinematics measurement by computing a non-linear function. However, although the learning provides excellent results, the test performed on a non-learned speed does not beat the previously presented method. Therefore, no results are reported but further analysis should be undertaken before concluding of the total failure of the approach.

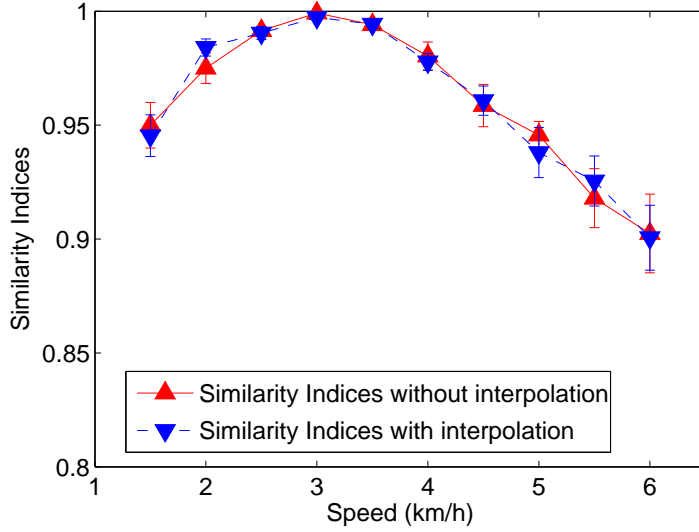


Figure 2.4: The difference between SI values obtained with and without the interpolation is not significant. Error bars are standard errors.

2.3 Orthosis Design and Control

2.3.1 Orthosis Hardware

As shown in Figure 2.5, the orthosis is made of several components: two custom-fit plastic shells, two commercial flexure joints, a linear actuator, a ball-link transmission, a load cell to measure the actuator force, and two force sensors installed in the orthosis sole, under the heel and the toes. The plastic shells were designed using a 3D scan of the right foot and leg of a healthy subject, adding mounting surfaces for the actuator, the flexure joints, and the mechanical transmission. The actuator includes a position control unit based on a PID controller that can be driven by an external analog signal in the range of 0 to 10 V.

However, this first prototype is quite cumbersome. One of the problems that still represent an obstacle in the development of active orthoses is the weight of the commercial actuators. For this preliminary prototype, a commercial actuator including the motor, the transmission, and the control electronics was the first choice to facilitate the construction in the shortest time. The weight of the actuators found in the market that satisfied the mechanical requirements for developing a complete gait cycle was above 3.5 kg. In order to reduce the actuator weight, the selection was done according to an estimate of the root-mean-square torque during the swing phase and the maximum velocity developed by the ankle in one gait cycle, considering the maximum intrinsic ankle stiffness and damping coefficients. The chosen actuator weight is about 1.6 kg and its maximum power is around 117 W, which corresponds to a third of the peak power developed by a healthy ankle [10].

Therefore, in a second prototype shown in Figure 2.6, a lightweight custom-fit actuator with passive energy-storage elements was developed, powerful enough for the stance phase as well. Control strategies specific to an active stance phase are implied by the torque-angle law of a healthy ankle during the heel strike, the flat foot and the toe off. This mainly consists in three different but similar controls mimicking a spring with different parameters.

The control and the PCPG algorithms reside in a DsPIC 30F4013 microcontroller running at 120 MHz. Both algorithms are calculated at each time step at a sampling frequency of 500 Hz but the output of one or the other is chosen according to the orthosis state, as detailed in the next section. The differential equations of the PCPG are solved by a simple explicit Euler integration method. The microcontroller manages three analog (two sole force sensors and one load cell) inputs for the signals coming from the force sensors. The position command is generated using Pulse Width Modulation (PWM) with a 9-mV resolution after amplification. Initialization commands for the actuator are generated using four digital outputs whereas the actuator state (home sequence completion) is monitored using one digital input.

A typical gait cycle for ground-level walking has a fundamental frequency around 1 Hz. To minimize the effects of noise coming from the sensors and to smooth the command signal, the analog inputs and the PWM output are filtered by low-pass first-order filters with a cutoff frequency of 15 Hz, which mainly determines the bandwidth. The microcontroller architecture is shown in Figure 2.7.

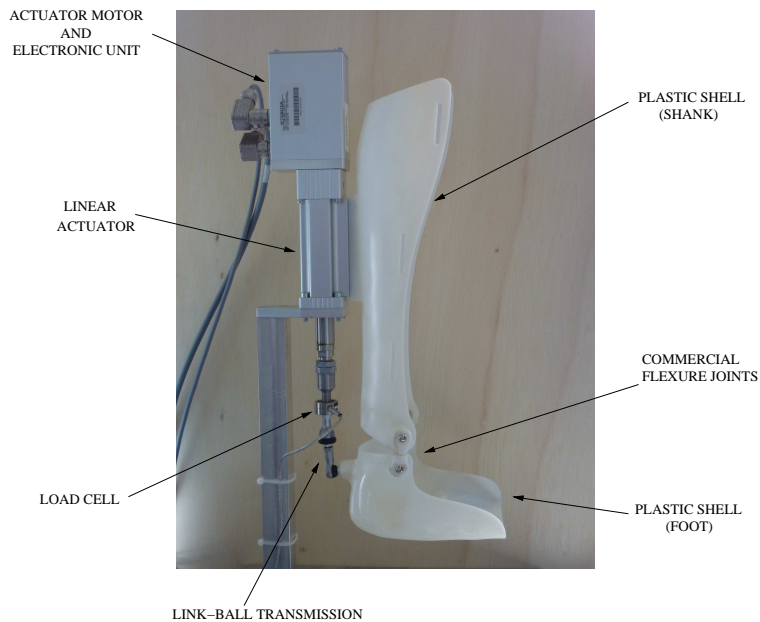


Figure 2.5: The orthosis prototype is made of several important components.

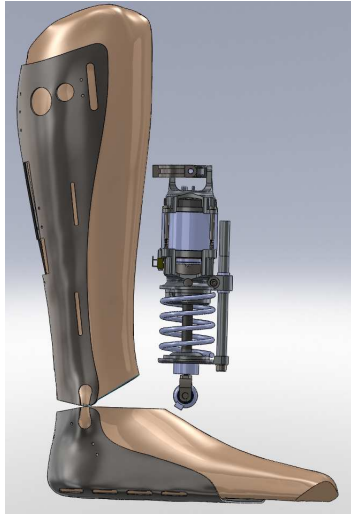


Figure 2.6: The second orthosis prototype is composed of several main components. The spring is used to stock energy during specific gait phases. A homemade ultra-compact actuator of around 3 kg is controlling the orthosis in a way depending on the current gait phase. Moreover, this system is suitable for an active stance phase as well.

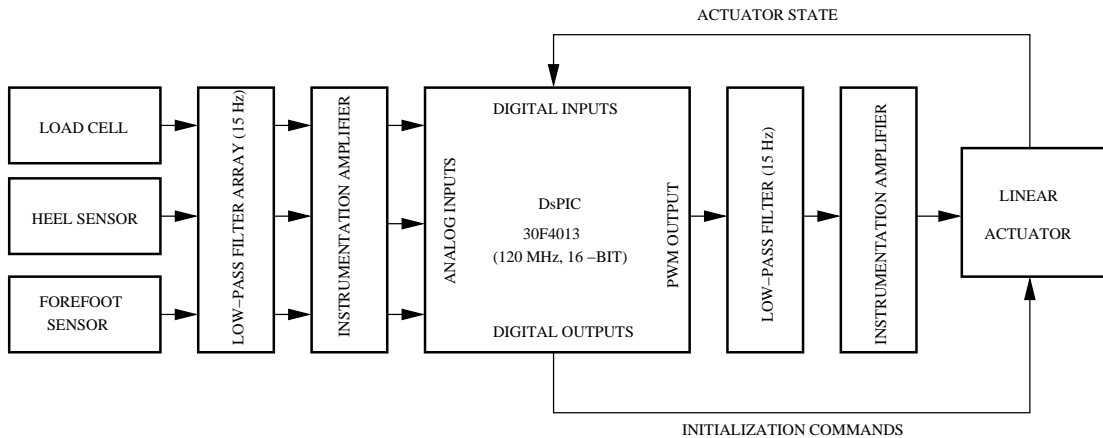


Figure 2.7: The block diagram shows the microcontroller architecture.

2.3.2 Gait cycle control strategies

In gait, there are two main events: the Heel Strike (HS) and the Toe Off (TO) for each foot, which correspond to the time of the initial contact of the heel with the ground and the time of the last contact of the toes respectively. There are also two different phases: the stance phase, i.e. between the HS and the TO, and the swing phase, i.e. between the TO and the HS when the foot is in the air. As a first objective of the orthosis is to help people with foot drop problems, two different control modes are used, one for the stance phase when the subject entirely drives the orthosis and another one for the swing phase when the PCPG output governs the system.

The first mode is active during the stance phase, allowing the free motion of the foot around an equilibrium point (approximately at a foot angle of 90° with respect to the tibia) but, at the same time, providing a certain level of stability through a virtual stiffness element. This part of the control algorithm is based on the following expression

$$\dot{x} = c(f - k(x - x_r)) \quad (2.12)$$

where \dot{x} is the time derivative of the actuator position, denoted by x ; $c = 6.6 \frac{\text{mm}}{\text{Ns}}$ is the proportional gain; f is the actuator force, measured by the load cell; $k = 3.8 \frac{\text{N}}{\text{mm}}$ is the desired virtual stiffness; and $x_r = 39.1$ mm is the desired equilibrium position. The actuator possesses an internal controller that regulates the rod position taking an external analog signal as a reference. In our scheme, x represents this external signal. The internal controller has a relatively fast response considering the time scale in which a normal stride develops so the displacement command x is assumed to be equivalent to the actual actuator displacement. Because of the stable linear system structure, if f remains bounded, the stability at the output x is insured. In the second prototype, the control strategies specific to an active stance phase are implied by the torque-angle law of a healthy ankle during the heel strike, the flat foot and the toe off. This mainly consists in three different but similar controls mimicking a spring with different parameters.

The second mode is associated to the swing phase and is intended to help the patient to achieve enough foot clearance to initiate the next gait cycle. As a preliminary approximation, this part of the algorithm will mainly consist in a trajectory tracking scheme to follow the PCPG position pattern similar to that developed by a healthy foot during the swing phase. This tracking is performed by the internal controller.

2.4 Practical needs

2.4.1 Frequency adaptation

Given that the only available information is the TO and HS events, they have to be used to determine the gait period. In this paper, this period estimation T_{est} is obtained by the time between two successive HS of the same foot. To consider when the subject is stopping walking, if the next HS does not appear after a predetermined time T_{max} , the orthosis switches to the follower mode. Because the PCPG has to be controlled in angular frequency, the estimated angular frequency is given by $\omega_{est} = \frac{2\pi}{T_{est}}$. For easier frequency control purpose, the Normalized Frequency Control (NFC) parameter F_ω is obtained by $F_\omega = \frac{\omega_{est}}{\omega_0}$ where ω_0 is the fundamental angular frequency of the learned standard pattern.

By experiments, it was noticed that the observed frequency at the output of the PCPG F_{obs} and the command frequency F_{com} were not equal, probably due to the integration method (Euler method is known to modify the period of integrated signals). A linear regression was sufficient to perfectly model this frequency shift:

$$F_{obs} = 1.0294 * F_{com} - 0.04 \quad (2.13)$$

This easily leads to:

$$F_\omega = \frac{(\omega_{est} + 0.08 * pi)}{(1.0294(\omega_0))} \quad (2.14)$$

2.4.2 Phase-resetting

Obviously, at constant speed, gait cycles are not perfectly identical [11]. This fact and numerous perturbations can provoke phase mismatch between the perfectly periodic PCPG output and the real gait pattern in addition to change in frequency. If this mismatch is too important, the subject has to compensate for it leading to a non-natural gait. The aim of this phase-resetting is to pave the way to allow the orthosis to adapt to the patient as quickly and smoothly as possible aiming at increasing the subject comfort.

The phase-resetting consists in resynchronizing the PCPG state according to special events. Therefore, the PCPG will be phase reset on the HS to allow the system to recover the correct phase in a smooth way at the time of the TO. Two approaches are available: a *hard* and a *soft* phase-resetting.

The hard phase-resetting relies on a direct modification of the integrated values: in each oscillator i , x_i and y_i are put to standard values corresponding to the HS event. The main advantage of this approach is the quick phase-locking whereas the disadvantages are (1) a more sensitive reaction to noise in the frequency estimation due to small variations in gait cycles at constant speeds or in the measurement itself and (2) important modification of the actuator state leading to a delay of recovery because of the low-pass filter. In the case of a foot lifter orthosis, during the stance phase, the actuator is not commanding the system and thus, the latter disadvantage is mitigated. However, it is a real problem in the case of a complete prosthesis.

In the soft phase-resetting, the original PCPG algorithm was slightly modified. To control the phase of the first PCPG oscillator, a coupling with a reference oscillator at instantaneous phase $R_{0,r}$ was established. This allows to modify the phase difference $\phi_{0,r}$ between the reference oscillator and the first oscillator of the PCPG. Formally, the reference oscillator is as follows:

$$\dot{x}_{0,r} = \gamma(\mu - r_{0,r}^2)x_{0,r} - \omega_{0,r}y_{0,r} + \tau \sin(R_{0,r}) \quad (2.15)$$

whereas the coupling with the PCPG (subscripted by p) is shown in:

$$\dot{x}_{0,p} = \gamma(\mu - r_{0,p}^2)x_{0,p} - \omega_{0,p}y_{0,p} + \tau \sin(R_{0,r}k - \phi_{0,r}) \quad (2.16)$$

where $k = \frac{\omega_{0,p}}{\omega_{0,r}}$. The coupling with the other oscillators of the PCPG is identical to the previous description. Because the phase of higher order oscillators had more difficulties to follow a phase

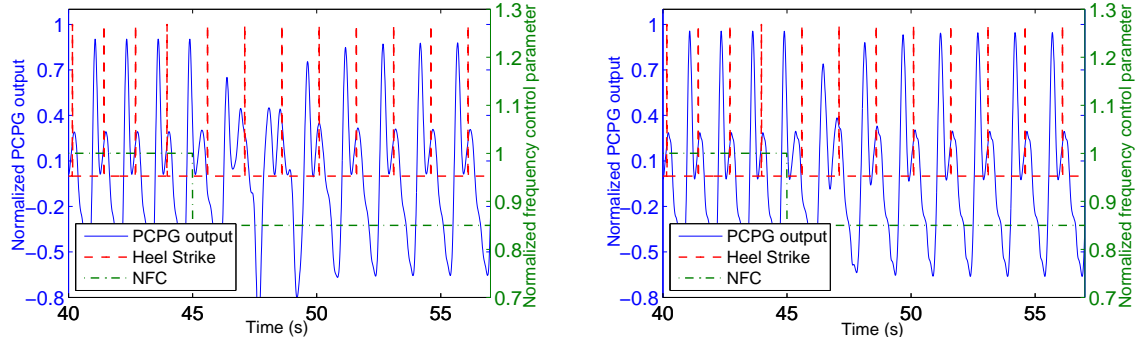


Figure 2.8: On the left: without enhancements, the soft phase-resetting leads to an important and long transient. On the right: this problem is strongly mitigated.

change in experiments, coupling constant was defined as $\tau_i = \tau \frac{\omega_{i,p}}{\omega_{0,p}}$. Figure 2.8 shows how this modification can produce a smooth and robust kinematics output when a phase reset is applied. In our experiments, we chose $k = 1$.

2.5 Simulation Results

In this Section, results about the system response to two realistic perturbations for both phase-resetting techniques are presented. These were obtained using the microcontroller connected to the orthosis (the PCPG output shows the command of the orthosis, not the actual position of it). Gait events were generated by simulation. First, a steep speed change is considered. Then, a speed change according to a chirp function is described in order to expose the behaviour of each technique to a highly changing environment.

To model a rapid change of frequency, i.e. of the subject's speed, the heel strike period is suddenly modified. To be coherent with practical applications, speed is instantaneously decreased by 1 km/h from the speed of 4 km/h (from $F_\omega = 1.13$ to $F_\omega = 1$). As depicted in Figure 2.9, the hard phase-resetting is recovering the correct phase quasi-instantaneously at the price of a non-continuous modification (with a small transient due to the low-pass filtering when connected to the orthosis) whereas the soft phase-resetting takes much more time for recovering (less than two gait cycles) with a very smooth transition. Similar results are obtained when the speed is suddenly increased.

To show the behaviour of both techniques in quasi-continuous speed adaptation, a chirp function was used to decrease the normalized frequency control parameter F_ω . This parameter was decreased from 1.3 to 0.7 by 0.1 step every two heel strikes of the same foot, which corresponds to a deceleration from 6 km/h to 1.5 km/h in 12 gait cycles for the studied subject. As depicted in Figure 2.10, at first, when the frequency is changed, the system can not detect this information and is not adapting leading to a certain phase delay depending on the frequency difference. Then, at the following heel strike, the system detects the correct phase and frequency. Regarding the

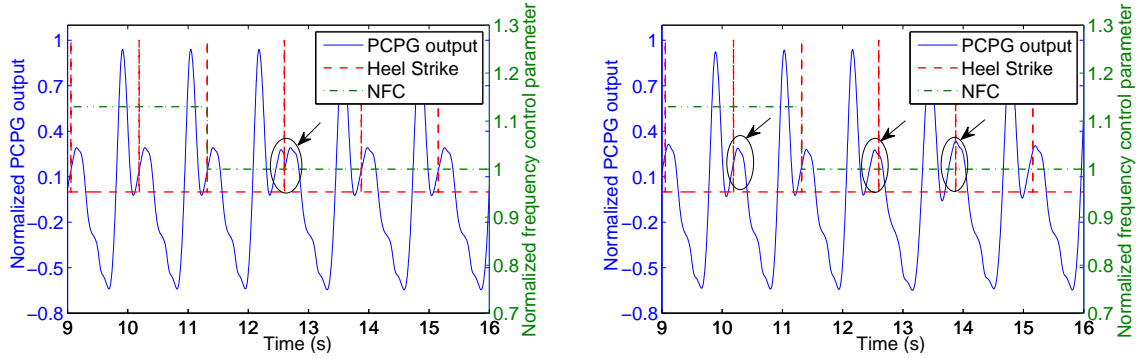


Figure 2.9: On the left: the hard phase-resetting is able to quasi-immediately recover the correct phase at the price of discontinuities shown by the arrow. This clearly leads to be more sensitive to frequency estimation noise. On the right: the soft phase-resetting is recovering the phase quite slowly but in a perfectly continuous way. Indeed, the first arrow on the left is showing the correct place of the HS event. The next ones indicate that there is a decreasing phase offset.

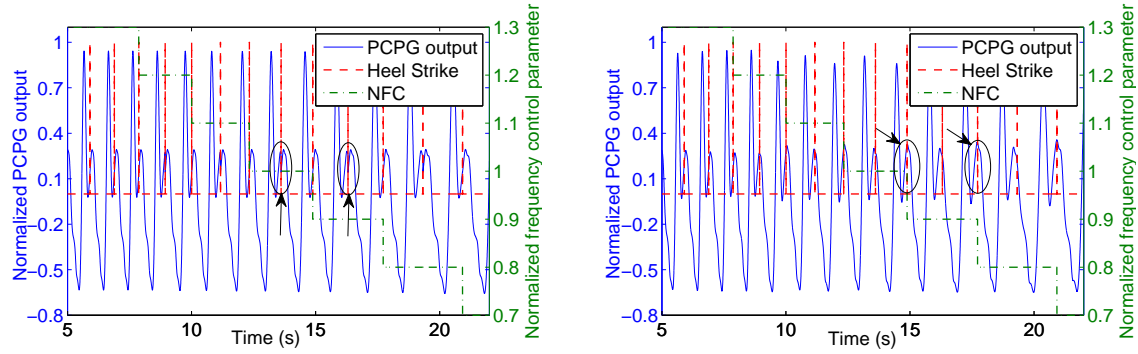


Figure 2.10: On the left: the hard phase-resetting is working as in the steep speed change. On the right: the soft phase-resetting does not totally recover the right phase when a speed change occurs as indicated by the arrows. However, the phase delay is quite small.

hard phase-resetting, the phase adaptation is done quasi-immediately as in the steep speed change whereas the soft resetting method takes more time and does not converge quickly enough to totally recover the phase when the next modification occurs. The same conclusion about the discontinuities can be reported. In a smooth approach, our frequency estimation scheme implies an intrinsic delay, namely the system can not predict the actual speed before the HS. Enhancements could be brought by using for instance additional gait events or sensors.

2.6 Conclusion and Future Work

2.6.1 Conclusion

In this Chapter, a way to model human walk to drive a lower limb prosthesis given a Brain-Computer Interface output is explained. Considering high-level commands provided by the BCI and after learning standard gait patterns (angles of elevation of the different parts of the leg as a function of time), a PCPG provides an adaptive kinematics output able to drive the artificial limb, according to the walking speed desired by the user. To show the feasibility of this approach, an orthosis prototype is composed of three main parts: a PCPG-based model of human locomotion, a sole sensor-based gait control switching strategy and a heel strike-based phase-resetting approach.

It is demonstrated that a PCPG is able to learn almost perfectly standard human walk patterns. Moreover, it is shown that low-level polynomial function can model the evolution of the PCPG parameters as a function of the walking speed. This interpolation enables to drive the prosthesis in a smooth way during accelerations or decelerations, increasing thus the comfort of the patient. This approach also paves the way to integrate a confidence level of the high-level command. If the command is uncertain, a smaller speed gap is actually performed than in the certain case.

A twofold gait control strategy was developed. Sole sensors provide information about gait events such as heel strike and toe-off. During the stance phase, i.e. the foot is on the ground, the follower mode allowing the patient to entirely govern the orthosis is activated. Otherwise, in the swing phase, i.e. when the foot is in the air, the PCPG human model is fed in the orthosis, which aims at mimicking as closely as possible the gait pattern and increasing the patient's comfort.

Two phase-resetting methods are detailed and their advantages and disadvantages are discussed. A hard version consists in directly modifying the values of the PCPG at the heel strike event, which could lead to discontinuities in the pattern. This problem can be mitigated in a foot lifter orthosis because of the specific control strategy (during the stance phase, after a heel strike, the orthosis is in the follower mode) but has to be improved in full prostheses. Therefore, a second and original soft phase-resetting scheme based on a reference oscillator and a harmonic-adaptive coupling constant is described leading to a smooth PCPG output transition. This scheme is obviously more robust to slight frequency estimation variations intrinsic to gait at constant speed. However, when this estimation is based on heel strike events, it is shown that the phase recovery is not quick enough.

2.6.2 Future Work

Future work will be dedicated to enhance the similarity between the gait model and the actually measured kinematics. A first approach could be to use multiple PCPG-based gait modelling with their own interpolation on several speed ranges, e.g. low speeds, middle speeds, high speeds or running speeds. An important verification will be to ensure smooth speed change of the PCPG output. Further investigation on shaping neural networks, i.e. using non-linear mapping, to enhance the PCPG output would be of interest.

Another work will be to refine the metrics used to assess the model. Indeed, depending on the application, each part of the gait cycle has not the same importance. A weighted Similarity Index could be a solution. Additionally, user satisfaction is the most important criteria of a successful device. Hence, more considerations of user feedback in terms of adaptation [12], comfort, *etc.*, should be considered.

As inspired from [9], the periodical signal provided by the PCPG could be used by a shaping neural network leading to EMG signals. When the paralysed muscles still remain innervated in such a way that it can be stimulated by an electric current, the obtained EMG signals could be the input of a Functional Electrical Stimulation device (FES). This FES approach has already been used in a hybrid assistive system combined with a mechanical orthosis [13].

Finally, increasing the speed of recovery in the soft phase resetting method while keeping the smooth aspect is an interesting research area. In addition to parameter optimization, this could be done by using other gait events or sensors in both frequency estimation and phase-resetting. An alternative could be to combine the hard and soft phase-resetting methods to increase reactivity while remaining quite smooth. For instance, heel strikes of the injured foot could be used with hard phase-resetting, while toe off of the injured foot could be used with soft phase-resetting to slowly recover the phase and facilitate the hard phase-resetting work. This procedure would avoid steep magnitude modification just before the injured foot leaves the ground.

Bibliography

- [1] José del R. Millán, Rüdiger Rupp, Gernot Mueller-Putz, Roderick Murray-Smith, Claudio Giugliemma, Michael Tangermann, Carmen Vidaurre, Febo Cincotti, Andrea Kubler, Robert Leeb, Christa Neuper, Klaus R Mueller, and Donatella Mattia. Combining brain-computer interfaces and assistive technologies: State-of-the-art and challenges. *Frontiers in Neuroscience*, 4(0):12, 2010.
- [2] J. del R. Millán, F. Galán, D. Vanhooydonck, E. Lew, J. Philips, and M. Nuttin. Asynchronous Non-Invasive Brain-Actuated Control of an Intelligent Wheelchair. In *31st Annual International Conference of the IEEE Engineering in Medicine and Biology Society*, 2009.
- [3] Auke Jan Ijspeert. Central pattern generators for locomotion control in animals and robots: a review. *Neural Networks*, 21(4):642–653, 2008.
- [4] G. C. Nandi, A. J. Ijspeert, and A. Nandi. Biologically inspired CPG based above knee active prosthesis. In *2008 IEEE/RSJ International Conference on Intelligent Robots and Systems, IROS*, pages 2368–2373, 2008.
- [5] Barak A. Pearlmutter. Gradient calculation for dynamic recurrent neural networks: a survey. *IEEE Transactions on Neural Networks*, 1995.
- [6] L. Righetti, J. Buchli, and A.J. Ijspeert. From dynamic hebbian learning for oscillators to adaptive central pattern generators. In *Proceedings of 3rd International Symposium on Adaptive Motion in Animals and Machines – AMAM 2005*. Verlag ISLE, Ilmenau, 2005.
- [7] L. Righetti and Ijspeert A.J. Programmable central pattern generators: an application to biped locomotion control. In *Proceedings of the 2006 IEEE International Conference on Robotics and Automation*, 2006.
- [8] Eishi Hirasaki, Steven T. Moore, T. Raphan, and Bernard Cohen. Effects of walking velocity on vertical head and body movements during locomotion. *Experimental Brain Research*, 127:117–130, 1999.
- [9] S. D. Prentice, A. E. Patla, and D. A. Stacey. Simple artificial neural network models can generate basic muscle activity patterns for human locomotion at different speeds. *Experimental Brain Research*, 123:474–480, 1998.
- [10] S.K. AU. *Powered Ankle-Foot Prosthesis for the Improvement of Amputee Walking Economy*. PhD thesis, Department of Mechanical Engineering, MIT, 2007.

- [11] Jeffrey M. Hausdorff. Gait dynamics, fractals and falls: Finding meaning in the stride-to-stride fluctuations of human walking. *Human Movement Science*, 26(4):555 – 589, 2007. European Workshop on Movement Science 2007, European Workshop on Movement Science 2007.
- [12] Stephen Cain, Keith Gordon, and Daniel Ferris. Locomotor adaptation to a powered ankle-foot orthosis depends on control method. *Journal of NeuroEngineering and Rehabilitation*, 4(1):48, 2007.
- [13] D. Popovic, R. Tomovic, and L. Schwirtlich. Hybrid assistive system-the motor neuroprosthesis. *Biomedical Engineering, IEEE Transactions on*, 36(7):729–737, 1989.

Chapter 3

Dynamic Recurrent Neural Network Models Physiological Central Pattern Generator

Contents

3.1	Introduction	63
3.2	Background	63
3.3	Methods	65
3.3.1	Experimental Setup	65
3.3.2	Dynamical Recurrent Neuronal Network	66
3.3.3	Experiment 1: Proof of concept	67
3.3.4	Experiment 2: Multiple pattern learning and prediction	69
3.3.5	Neuronal properties and connectivity after learning	70
3.3.6	Statistical analysis	70
3.3.7	Computations	70
3.4	Results	73
3.4.1	Experiment 1: Proof of concept	73
3.4.2	Experiment 2: Prediction of intermediary velocities	73
3.4.3	DRNN structures from experiment 2	76
3.4.4	Neurophysiological similarity	76
3.4.5	Structural Similarities	79
3.5	Conclusion	81

Abstract

The existence of dedicated neuronal modules such as those organized in the cerebral cortex, thalamus, basal ganglia, cerebellum or spinal cord raises the question of how these functional modules are coordinated for appropriate motor behaviour. Study of human locomotion offers an interesting field for addressing this central question. The coordination of the elevation of the 3 leg segments under a planar covariation rule [1] was recently modelled [2] by phase-adjusted simple oscillators shedding new light on the understanding of the central pattern generator processing relevant oscillation signals.

We describe the use of a dynamic recurrent neural network (DRNN) mimicking the natural oscillatory behaviour of human locomotion for reproducing the planar covariation rule in both legs at different walking speeds. Neural network learning was based on sinusoid signals integrating frequency and amplitude features of the first three harmonics of the sagittal elevation angles of the thigh, shank and foot of each lower limb. We verified the biological plausibility of the neural networks.

Best results were obtained with oscillations extracted from the first three harmonics in comparison to oscillations outside the harmonic frequency peaks. Physiological replication steadily increased with the number of neuronal units from 1 to 80, where similarity index reached 0.99. Analysis of synaptic weighting showed that the proportion of inhibitory connections consistently increased with the number of neuronal units in the DRNN. This emerging property in the artificial neural networks resonates with recent advances in neurophysiology of inhibitory neurons that are involved in central nervous system oscillatory activities. The main message of this Chapter is that this type of DRNN may offer a useful model of physiological central pattern generator for gaining insights in basic research and developing clinical applications.

This chapter is based upon the following publication:

- T. HOELLINGER, M. PETIEAU, **M. DUVINAGE**, T. CASTERMANS, K. SEETHARAMAN, A.M. CEBOLLA, A. BENGOETXEA, Y. IVANENKO, B. DAN, G. CHERON, 2013, *Biological oscillations for learning walking coordination: dynamic recurrent neural network functionally models physiological central pattern generator*, Frontiers in Computational Neuroscience, 29 May 2013.

3.1 Introduction

From Chapter 2, we saw that although Programmable Central Pattern Generators (PCPG) provide good results in modelling gait, it does not perfectly fit the kinematics. Indeed, when the generated gait pattern speed is too far from the learned speed, a decrease of similarity index was observed. In order to adapt the pattern, the use of a non-linear filter having properties of generating rhythmic signals was advised.

This is why this Chapter deals with the implementation of a Dynamic Recurrent Neural Network-based (DRNN) CPG. In this approach, a sinusoidal signal is fed to the neural network, which shapes the output kinematics accordingly. This aims at getting a better overall comfort for the patient. In Section 3.2, the background of this approach is detailed. In Section 3.3, the experimental setup, the DRNN model, the description of the experiments, the statistical analysis and the computation details are described. In Section 3.4, the results of both experiments and the structure analysis of the obtained network, the neurophysiology and structural similarities between CPG model and humans/animals are proposed. In Section 3.5, the main finding, the limitations of the current approach are summarized.

3.2 Background

Neuronal modules profoundly influence many aspects of motor behaviour. However, little is currently known about the control mechanisms that allow the coordination of these modular entities. In this theoretical context, human locomotion is a challenging movement because of the numerous neuroanatomical modules implicated in the different aspects of whole body movement, ranging from the cyclic propulsion of the limb to balance control. In spite of these intricate movement components and neuronal modules involved, it has been proposed that the overall control can be realized by reducing the number of degrees of freedom of the system into global variables [3, 4, 5, 6, 7]. The fact that the elevation angles of the three main lower limb segments are coordinated during gait within a covariation plane [1], forming an elliptic loop corroborates the idea that control of locomotion is also submitted to the general law of reducing variables [2]. This general law is also applicable for different walking speeds [8], for forward and backward directions [9], rectilinear or curvilinear walking paths [10], walking with stilts [11, 12], or with a transfemoral prosthesis walk [13], with different levels of body weight unloading [14] and for running [15]. Notably, this inter-segmental coordination is not present in newly walking toddlers [16, 17, 18], but covariation planarity rapidly emerges over the first few days of independent walking experience, while the shape of the loop and plane orientation 'mature' gradually over several years. This evolution indicates that the attractor plane and the shape of the loop are neurophysiologically defined, rather than being imposed by biomechanical constraints (see [19, 20] for discussion). More recently, the developmental study of this complex behaviour in a new born baby [21] has permitted revisiting the concept of locomotor modules coding for the control of movement primitives.

This modular approach raises the question of the dynamic coordination of modules in the context of oscillatory properties of neuronal. Indeed, the dynamical structure of these modules must logically obey a common principle for movement generation: the production of oscillatory

activity. Although this principle is well accepted in case of the rhythmic nature of locomotion [22, 23], the recent study of [24] surprisingly demonstrates that non-periodic movements such as reaching are also generated by neuronal oscillation. This means that there is a strong possibility that the spinal modules organized in a central pattern generator (CPG) could be dynamically controlled by cortical and/or supraspinal oscillations. Interestingly, Barliya et al. [2] recently modelled the time course of elevation angles of the three lower limb segments in terms of simple oscillators coupled with appropriate time shifts reproducing the orientation of the plane and their elliptical shape. The oscillators were obtained by taking, after Fourier transform, the first three harmonics of the elevation angle kinematics. Each of these oscillators could be interpreted in term of oscillatory module acting in such a way that the orientation of the plane and the elliptic shape of the coordination are conserved. It could thus be possible that oscillatory signals derived from these harmonics are used for activating CPG modules.

The existence of CPG in the spinal cord in mammals has been proposed a century ago [25]. In essence, it represents a group of neurons acting as a network to produce coordinated patterns of rhythmic activity. New evidence has shown the presence of CPG in the spinal cord in humans [26, 27]. The characteristics of such CPG modules are their adaptability and robustness that lead to the production of different gait patterns adapted to their current environmental context. For example, young infants (less than 1 year old) are already able to walk over a split-belt treadmill with different types of coupling [28]. Some of them were even able to walk in opposite directions. Mimicking physiology, the robotic and neuroscientific community developed artificial CPGs that are commonly used to animate robots from multi-legged insect-like to humanoids (for a review see [29]). In their pioneering work in the cat, [30] proposed an analytic model of limb locomotor pattern generator based on recorded muscle activity induced by electrical stimulation over the mesencephalic locomotor region in the decerebrate cat. In this model, locomotor like patterns of six muscles resulted from six independent oscillators with dedicated parameters. These oscillators were reduced to simple sine and cosine functions fed by a tonic input. Since then, different methods have been used from coupled non-linear oscillators [31, 32, 33], to highly detailed biophysics of small groups of interconnected neurons [34] and rhythm genesis of larger groups of neurons [35] mainly in animal models. While human locomotion has often been reproduced computationally in the robotic field using equations that are numerically integrated [31, 32, 36, 37, 38], few methods involving neuron modelling for human gait generation have been studied so far. Among them Prentice and coauthors [39, 40] have successfully transformed fundamental timing signals (sine and cosine inputs) into individual muscles activation bursts related to gait locomotion at different speeds using a feedforward neural network. Our group used the electromyographic (EMG) signals of the lower limb muscles as input for a dynamic recurrent neural network (DRNN) producing as output the lower kinematics during locomotion [41, 42]. However, the possibility to produce the motion of the lower limb segments by means of oscillations derived from the three harmonics of the Fourier transform of walking kinematics has not yet been assessed by means of the same DRNN. We show here that after learning based on different walking velocities, the DRNN is able to reproduce the lower limb kinematics of both legs. The DRNN can also generalize to the unlearned walking velocities. The analysis of the required network structure (e.g. number of units, distribution of time constant and synaptic sign) provides a basis for the discussion about the constraints required for the elaboration of a CPG.

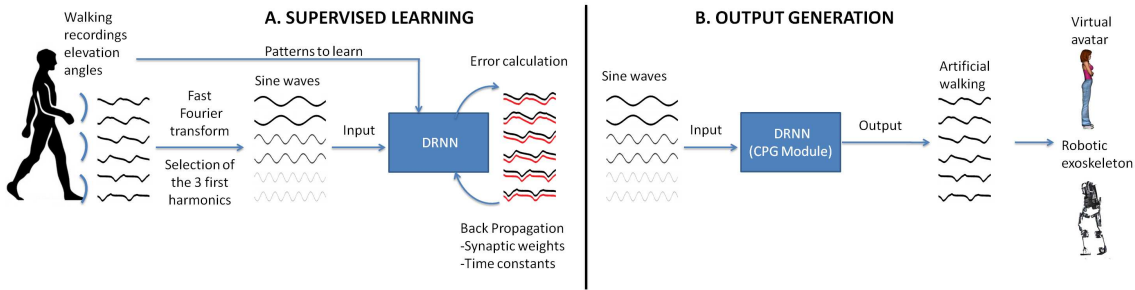


Figure 3.1: Realization of a CPG module based on experimental recordings of human walking. (A). In the first step, the elevation angles of the thigh, shank, foot of the two legs are transformed in the time frequency domain using fast Fourier transform (FFT). Then the signal characteristics are computed for the first three harmonics and back-transformed into temporal space using sine waves formulation. These data are fed as input to the DRNN learning the transformation in kinematic signals (elevation angles). (B). A successful learning will permit the DRNN to predict kinematics based on sine wave inputs only. These output signals can produce biologically plausible walking patterns in a virtual reality avatar or an actual robotic exoskeleton.

3.3 Methods

3.3.1 Experimental Setup

Seven healthy subjects aged from 25 to 35 years (mean age: 28 years) participated in this experiment. The protocol consisted of walking on a treadmill at 11 different velocities (from 1 (0.28 m/s) to 6 km/h (1.67 m/s) stepped by 0.5 km/h (0.14 m/s)) leading to 11 trials per subject (total of 77 trials over all subjects). Whole body kinematics was recorded using Vicon system with six infrared Bonita cameras recording at 100 Hz during 40 seconds for each trial. The tracking consisted of recording 29 markers placed over the whole body. The position of the markers in an orthogonal reference was computed using a custom biomechanical model. From the position of the markers of both legs, the kinematic (elevation) angles relative to the vertical plane of the laboratory have been calculated bilaterally for thighs, shanks and feet. In this study we performed two experiments. The first one, 'proof of concept', was done to ascertain the feasibility of a DRNN to learn elevation angles from pure sine waves. This part only includes supervised learning on a single pattern (Figure 3.1A). The second experiment was performed in order to study the possibility to learn multiple patterns of walking (i.e. velocities) and to predict kinematics from unlearned patterns (Figure 3.1B). After that, the DRNN structures were analysed.

3.3.2 Dynamical Recurrent Neuronal Network

The DRNN is capable of modelling time-varying input-outputs and has varying weights as well as varying time constants for the artificial neurons [43]. The adaptive time constants make it dynamic [44]. The DRNN is governed by the following equations:

$$T_i \frac{dy_i}{dt} = -y_i + F(x_i) + I_i \quad (3.1)$$

where $F(a)$ is the squashing function $F(a) = (1 + e^{-a})^{-1}$, y_i is the state or activation level of unit i , I_i , is an external input (or bias), and x_i is given by:

$$x_i = \sum_j w_{ij} y_j \quad (3.2)$$

which is the propagation equation of the network (x_i is called the total or effective input of the neuron i , w_{ij} is the synaptic weight between units i and j). The time constants T_i will act like a relaxation process. In order to make the temporal behaviour of the network explicit, an error function is defined as:

$$E = \int_{t_0}^{t_1} q(y(t), t) dt \quad (3.3)$$

where t_0 and t_1 give the time interval during which the correction process occurs. The function $q(y(t), t)$ is the cost function at time t which depends on the vector of the neuron activations y and on time. We then introduce new variables p_i (called adjoint variables) that will be determined by the following system of differential equations (to help solving the learning process not detailed here):

$$\frac{dp_i}{dt} = \frac{1}{T_i} p_i - e_i - \sum_j \frac{1}{T_i} w_{ij} F'(x_j) p_j \quad (3.4)$$

with boundary conditions $p_i(t_1) = 0$. After the introduction of these new variables, we can derive the learning equations:

$$\frac{\partial E}{\partial w_{ij}} = \frac{1}{T_i} \int_{t_0}^{t_1} y_i F'(x_j) p_j dt \quad (3.5)$$

$$\frac{\partial E}{\partial T_i} = \frac{1}{T_i} \int_{t_0}^{t_1} p_i \frac{dy_i}{dt} dt \quad (3.6)$$

The sinusoid signals derived from the fast Fourier transform (FFT) kinematic data are sent as input to a DRNN (Figures 3.1 , 3.2 , cf. experiment 1, experiment 2) that has to learn from these data to produce the kinematics specified as elevation angles (Figure 3.1A). Successful trainings were also used to produce kinematic patterns from unknown inputs (Figure 3.1B) aiming to produce walking for multiple purposes, such as virtual avatars or robotic exoskeletons. The training is supervised, involving learning rule adaptations of synaptic weights and time constant of each unit [44, 45]. A specific training procedure using Almeida algorithm was used to optimize learning performance [46]. The DRNN involves a looping mechanism (fully connected

structure) which enables this network to learn and store information (memory). This equips the network with the ability to model complex situations with multiple influences. The DRNN was successfully used to map EMG signals into kinematics during walking [41], for the identification of the triphasic EMG pattern in subjects performing fast elbow flexion movements [47] or to predict specific muscular activity in elite fencers compare to amateurs [46].

3.3.3 Experiment 1: Proof of concept

DRNN computation has been used to prove that simple sine waves with specified temporal characteristics can be used as input to an artificial neural network to be transformed into elevation angles obtained from kinematic recordings during locomotion (Figure 3.3).

Input: construction of sine waves

As the learning phase of the DRNN is a time-consuming process, we had to select appropriate sample from the whole available data as input. Moreover, even if the kinematics during walking is relatively stable, it may vary too much to feed the DRNN during the learning phase. For these reasons, we extracted two consecutive gait cycles from the 40 seconds of experimental data recorded in each trial (Figure 3.2A , black curves). They were chosen so as to be representative in terms of frequency of the whole recording set. Then, to determine the kinematic characteristics of gait, we transformed the data of the lower limb segments elevation angles into the time frequency domain using the Matlab fft function to get the Fast Fourier Transform (FFT) power amplitude and their related frequency values of the first three harmonic peaks (Figure 3.2B). It has been shown previously that the first two Fourier harmonics accounted for approximately 98% of the experimental variance of the thigh, shank and foot angles [8]. We decided to create sine waves based on the characteristics of the first three harmonics to ensure that the signal proposed as learning input to the DRNN contains enough information to match the desired output precisely.

We extracted the values of the three frequencies (f_1, f_2, f_3) corresponding to the maximal amplitudes (a_1, a_2, a_3). It was verified that $f_2 = 2f_1$ and $f_3 = 3f_1$. We then artificially produced six sinusoidal signals using frequency values as parameters (equations 3.7 and 3.8).

$$y_{fi,1} = \sin(2\pi f_i t) \quad (3.7)$$

$$y_{fi,2} = \sin(-(2\pi f_i t)) \quad (3.8)$$

$$\text{For } i = 1, 2, 3$$

These six sine waves thus correspond to the frequency characteristics of the kinematic patterns that will be further used as pattern to be learned. For the sake of clarity we called the set of original inputs set SEA (for set of equations A). Additionally, we produced six new sine waves using the preceding computations (equations 3.7 and 3.8) where $f_1' = f_1 + 0.25$ Hz and six other sine waves where $f_1'' = f_1 - 0.25$ Hz, respectively called SEB (for set of equations B) and SEC (for set of equation C). Please note that in the latter two cases the original relations $f_2 = 2f_1$ and $f_3 = 3f_1$ were respected and hence $f_2' = 2f_1 + 0.50$ Hz; $f_3' = 3f_1 + 0.75$ Hz in the set SEB and $f_2'' = 2f_1 - 0.50$ Hz; $f_3'' = 3f_1 - 0.75$ Hz in the set SEC. Three different input sets (SEA, SEB, SEC) were thus defined for learning.

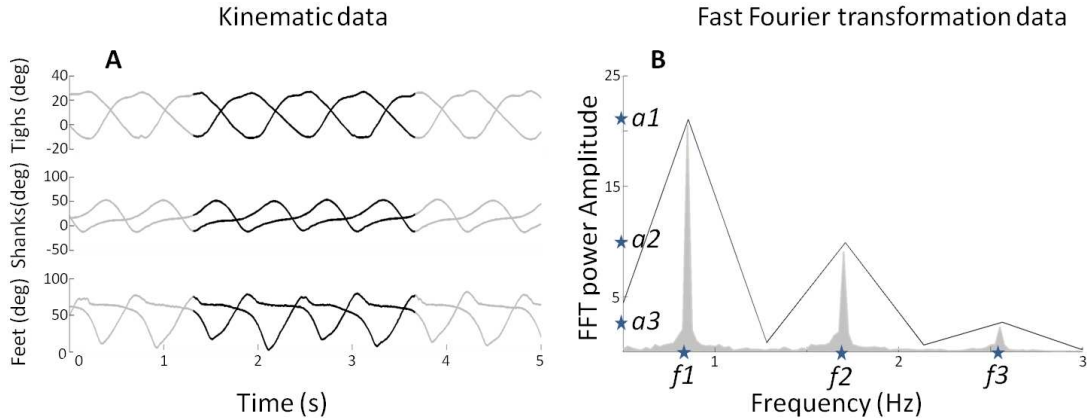


Figure 3.2: (A). Elevation angles (in degree) of the three segments (thigh, shank and foot) for each leg as a function of time for a subject walking at 3 km/h (0.83 m/s). The whole pattern is presented for duration of 5 s. The black lines represent a pattern for two gait cycles used to determine the FFT characteristics. (B). The mean FFT transformation for six joints for 40 s (in grey) and the two gait cycles (in black). Note that the two gait cycle patterns are selected so as to preserve the FFT characteristics in terms of amplitude and frequency (stars) for the overall pattern of 40 s. These characteristics are used as parameters to generate sine waves as input of the DRNN.

Pattern to learn: kinematic data

The pattern to learned corresponds to the elevation angles of the right and left thigh, shank, foot segments in the two gait cycles of a 3 km/h (0.83 m/s) walk, normalized between -1 and 1. The outputs were the same for SEA, SEB and SEC whereas inputs differed.

DRNN learning phase

It was expected that the DRNN would learn how to transform the input to output thanks to its dynamical and recurrent structure of 30 hidden neurons. For each of the seven subjects, the network iterated 10,000 times. This process was repeated 100 times, leading to 100 different networks. At the end of the learning phase, we selected for each subject the network for which the difference between predicted and real kinematics was minimal. This computation was performed by calculating a similarity index (SI) [48] defined by the following equation :

$$SI = \frac{\int_{-\frac{T_c}{2}}^{\frac{T_c}{2}} p_1(t)p_2(t)dt}{[\int_{-\frac{T_c}{2}}^{\frac{T_c}{2}} p_1(t)^2 dt \int_{-\frac{T_c}{2}}^{\frac{T_c}{2}} p_2(t)^2 dt]^{\frac{1}{2}}} \quad (3.9)$$

where T_c is the period of the limit cycle, p_1 and p_2 being synchronized, i.e. the matching between both patterns is based on the maximum of each pattern. Note that if both functions are identical, $SI=1$. SI was calculated with the recorded pattern of elevation angles and the output of the DRNN.

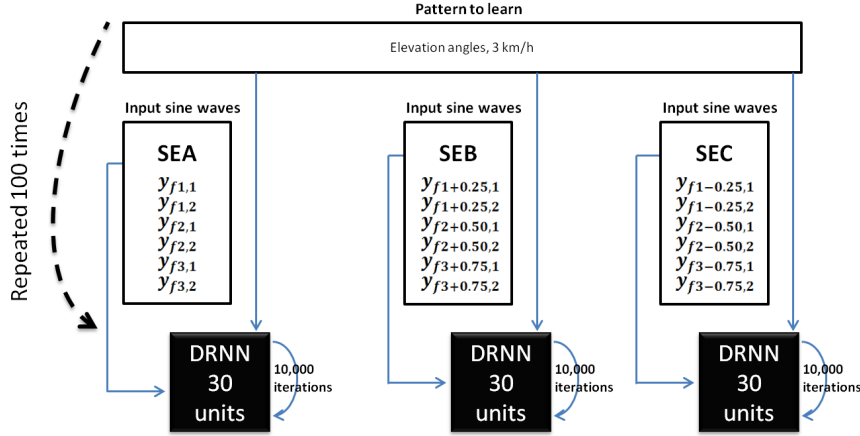


Figure 3.3: DRNN learning method for experiment 1. For each subject, we trained 100 DRNNs to learn a pattern of kinematic (corresponding to a velocity of 3km/h (3.83m/s)) from sine waves (equations 3.7 and 3.8). Three sets of learning were defined as the input differed (SEA, SEB, SEC). The structures of DRNNs were modelled with 30 hidden units for each set of training. Each network iterated 10,000 times to change its synaptic weights and time constants. For each subject and structure we selected the network with the highest SI value. For each condition, the design of the network is then processed with 6 inputs, 30 hidden units and 6 outputs.

3.3.4 Experiment 2: Multiple pattern learning and prediction

In this experiment sine waves were modulated in frequency and amplitude and transformed into kinematic data using multi-pattern training. The prediction of kinematic pattern from unknown sine wave pattern was also tested.

Input

As for the proof of concept methods, we extracted two gait cycles of each trial for multiple velocities (in km/h) ($v=1.5, 2.5, 3.5, 4.5, 5.5$). We transformed the kinematic data into the time-frequency domain to get their frequency (f_1, f_2, f_3) and amplitude (a_1, a_2, a_3) (Figure 3.2B) parameters using the following set of equations (3.10 and 3.11).

$$y_v, f_{i_v}, a_{i_v,1} = a_{i_v}(\sin(2\pi f_{i_v}t)) \quad (3.10)$$

$$y_v, f_{i_v}, a_{i_v,2} = a_{i_v}(\sin(-(2\pi f_{i_v}t))) \quad (3.11)$$

For $i = 1, 2, 3$

Patterns to learn: kinematic data

The patterns to be learned consisted of elevation angles of the right and left thigh, shank and foot segments corresponding to the two gait cycles, normalized between -1 and 1. These patterns were obtained from recordings at multiple velocities (in km/h) ($v=1.5, 2.5, 3.5, 4.5, 5.5$).

DRNN training phase

We used the possibility to train the DRNN in a multi-pattern purpose [49]. For each subject, the DRNN was trained to match the inputs/outputs patterns corresponding to five different velocities within a single DRNN structure. 100 networks were made per subject, each of them iterating 50,000 times. This operation was assigned for 1, 2, 3, 4, 5, 6, 7, 8, 9, 10, 20, 30, 40, 50, 60, 70 and 80 hidden units. When this was completed, we selected the best network for each subject and each number of hidden units using the maximal SI values.

Output Prediction

We built sine waves from intermediary pattern velocities (km/h) ($v=2,3,4,5$) as explained above. We fed the best DRNN structures previously obtained after the training phases with these unlearned inputs sine waves and analysed DRNN behaviour by calculating the predicted output with experimental data using SI values.

3.3.5 Neuronal properties and connectivity after learning

Introduction of timing allows modelling of more complex frequency behaviour, improves the non-linearity effect of the sigmoid function and the memory effect of time delays [45]. The distribution of the time constant and the synaptic weights between units [44] after learning was analysed after multiple pattern learning and prediction. In particular, we recorded the number of positive and negative connections inside DRNN structures of the best networks. Additionally we studied the distribution of neuronal time-constants.

3.3.6 Statistical analysis

Statistical analysis was performed using Statistica software (Statsoft, www.statsoft.com). For each test performed and described in the result section, we firstly verify whether the data were distributed normally using Kolmogorov-Smirnov test. When the data were normally distributed we use ANOVA with repeated measures and *post-hoc* Fisher analyses. When it was not possible to use ANOVA we used non-parametric tests such as Friedman ANOVA or sign tests.

3.3.7 Computations

All DRNN computations were performed in the Hydra computing center hosted in ULB. We allocated 1 node and 10Gb of memory per computation (i.e. per subject per condition in the experiment 1, per subject per structure in the experiment 2). The computations were run in parallel to optimize the learning duration. Afterwards we simulated 5% of the overall experiment in the same conditions to estimate the learning time. The overall duration of the process was obtained by linear interpolation (Figure 3.4).

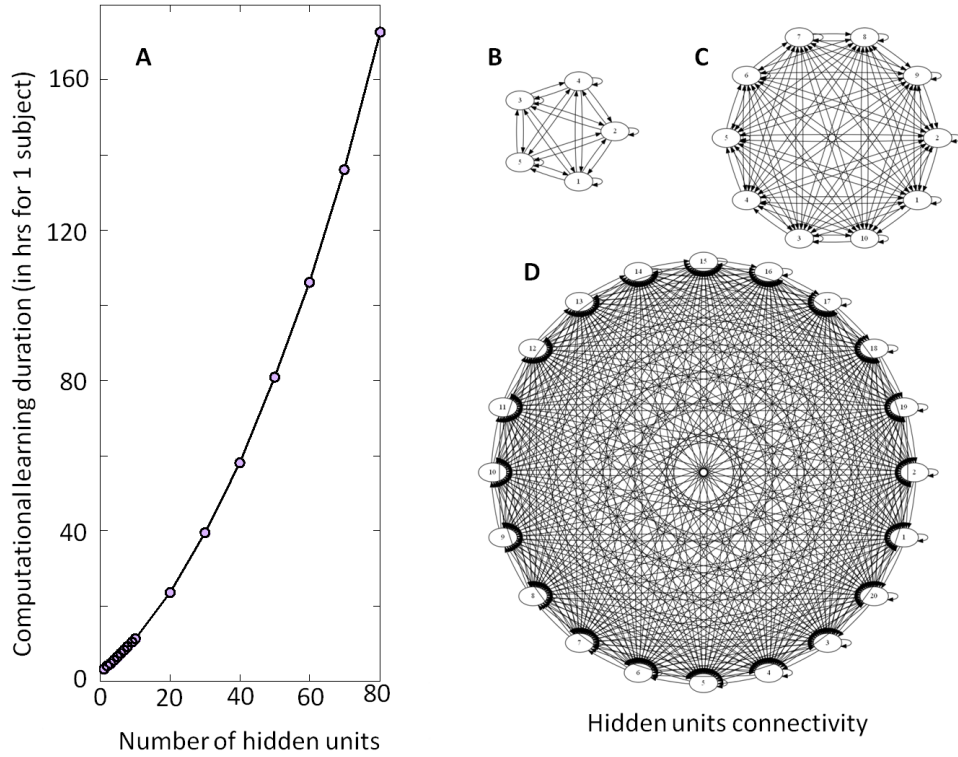


Figure 3.4: Illustration of the DRNN structure and computational time. (A). Computational learning duration for one subject for experiment 2 (in hours). The grey circles represent the estimation of time required per number of hidden units from a recalculation of 5% of the procedure. Please note that the overall process for the seven subjects has taken approximately 200 days to be computed. (B), (C) and (D) represent the connectivity of the hidden layer with 5, 10 and 20 neurons, respectively. As the number of neurons increases, the number of connections increases by a factorial multiplication as well as the time required to adjust connection weight and time constant. Please note that only the units of the hidden layers are represented without input or output neurons.

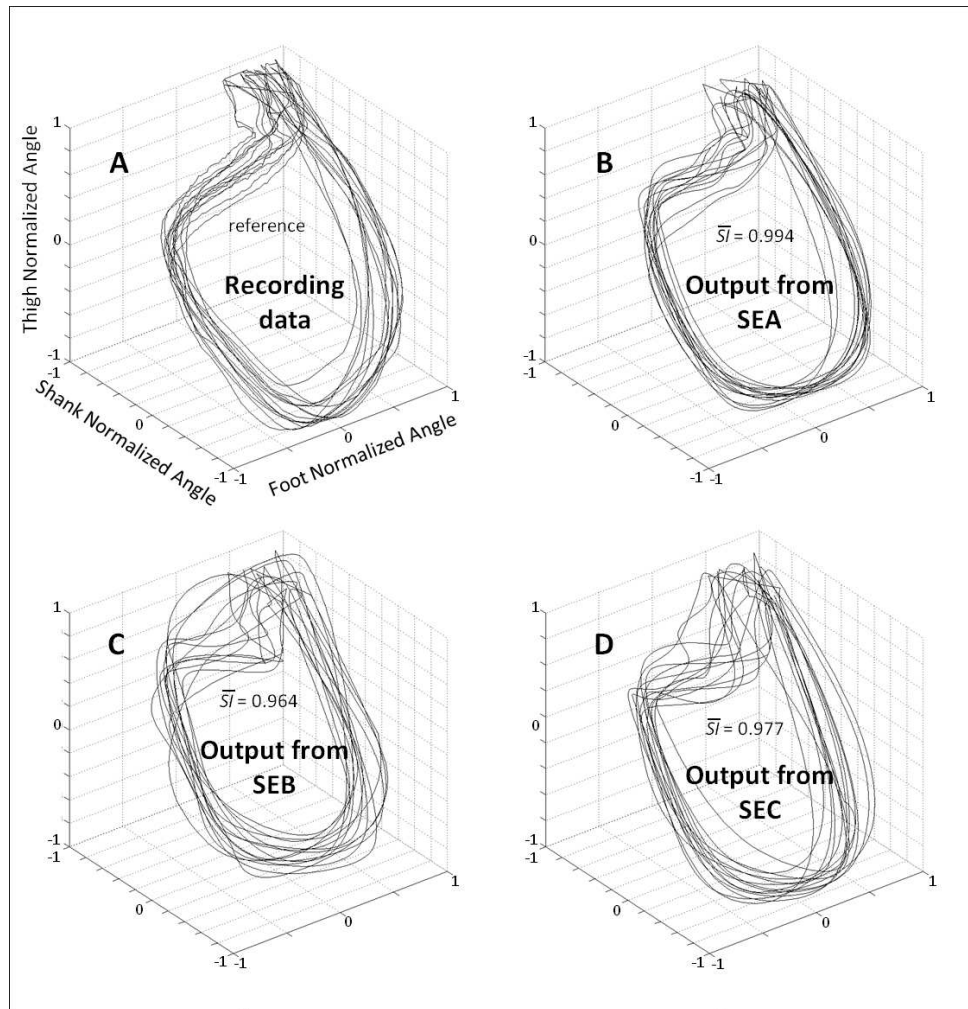


Figure 3.5: Planar covariation between normalized thigh, shank and foot for all participants. (A). Recording data - The patterns correspond to the real kinematics of 2 gait cycles for all participants. Best kinematic patterns predicted by the DRNN for each subject where SEA (B), SEB (C) and SEC (D) were fed as input. \bar{SI} is the average of similarity index value (SI) in each condition for all subjects when compared with the recording data.

3.4 Results

3.4.1 Experiment 1: Proof of concept

A statistical test was designed to compare SI values from different input types (SEA, SEB or SEC) (Figure 3.3 and Figure 4.4). The Kolmogorov-Smirnov did not reject the hypothesis that SI values were normally distributed ($D = 1.4414, p > 0.20$) when analysing together values of the different inputs (SEA, SEB or SEC). We used an ANOVA with repeated measures where dependant variable was SI and the independent variable chosen was the type of input. The analysis showed an effect of the input frequency in the DRNN prediction (SI value) ($H F_{(2,12)} = 38.110, p = 0.00001$). *Post-hoc* analysis confirmed that SI values of original group of unchanged frequency input (SEA) were higher than the 2 modified groups where frequency inputs have changed (SEB and SEC).

3.4.2 Experiment 2: Prediction of intermediary velocities

As we decided to use frequency (f_1, f_2, f_3) and amplitude (a_1, a_2, a_3) characteristics to modulate inputs for multiple learning procedures (equations 3.10 and 3.11), we have verified that there was a statistical significance of these parameters for different velocities. The Kolmogorov-Smirnov test for f_1 ($D = 0.14370, p < 0.1$), f_2 ($D = 0.14370, p < 0.1$) and f_3 ($D = 0.14370, p < 0.1$) was not clear enough to reject the fact their population may follow a normal law. When looking at the distribution, they tend to be normal and it is possible that the significance of the test is due to the weak number of values. According to similar test, the values for parameters a_1 ($D = 0.08476, p > 0.2$), a_2 ($D = 0.08758, p > 0.2$) and a_3 ($D = 0.09035, p > 0.2$) were normally distributed. We then used two ANOVA with repeated measures where the dependent variables were, respectively, the amplitude and frequency values and the within-subject factors were velocity of walking and the specific harmonic (1, 2 or 3).

ANOVA shows significant changes in amplitude ($F_{(10,60)} = 31.351, p < 0.0001$) and frequency ($F_{(10,60)} = 69.276, p < 0.0001$) with an increase in velocity. *Post-hoc* analyses revealed an increase in f_1, f_2, a_1, a_2, a_3 and a decrease of f_3 with an increase in the velocity. These significant differences justified their use for building specific sine waves for different walking velocities (Figure 3.6).

Concerning the performance of the DRNN outputs, we wanted to verify if the SI value applied for the best networks was different for learning and prediction. Additionally we wanted to statistically check if the number of hidden units of the networks increases the *SI* value (Figure 3.7). The Kolmogorov-Smirnov did not verify that the populations of *SI* values among the learning ($D = 0.18467, p < 0.01$) or the prediction ($D = 0.20684, p < 0.01$) were normal. Thus, to compare the *SI* values between learning and prediction process we chose to use a sign test as the structure of the network (weights and time constant) were the same. This test reveals no significant differences in *SI* values between the two populations except when the network contains 1, 2, 4, 5, 6 and 7 neurons. Moreover we use a Friedman test to analyse *SI* values (dependent variable) according to the number of hidden units (independent variables) of the network. There is an effect of the number of hidden units to the *SI* both for learning ($\chi^2_{(16)} = 111.5630, p < 0.0001$) and for prediction ($\chi^2_{(16)} = 109.372, p < 0.0001$).

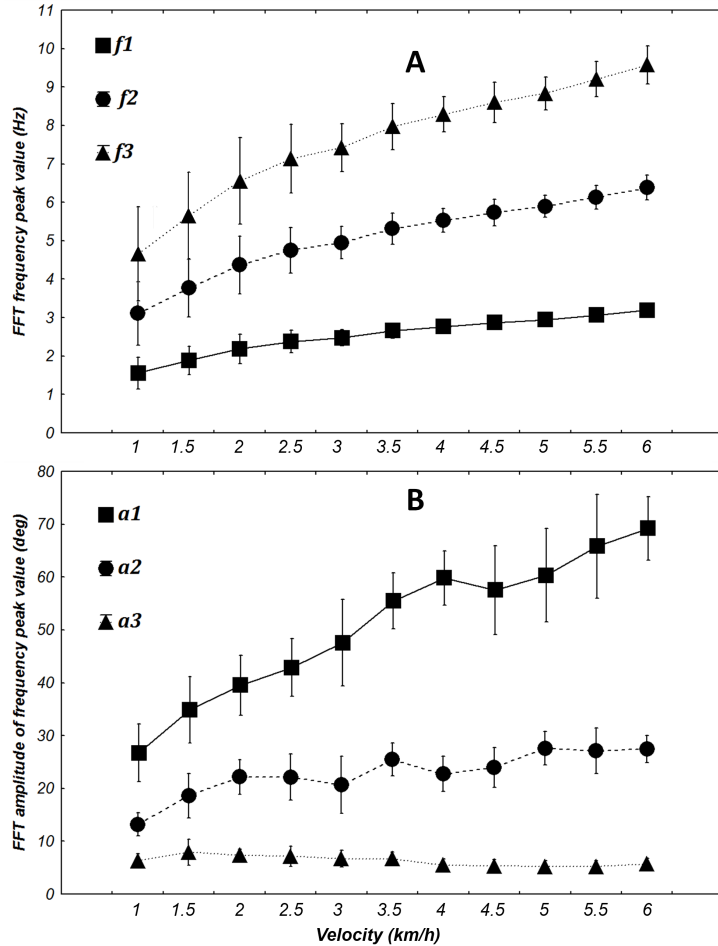


Figure 3.6: Evolution of the frequency (A) and amplitude (B) of the first three harmonics when transforming elevation angles into the time frequency domain (FFT) at different walking velocities (from 1 to 6 km/h (0.28 to 1.67m/s)). The FFT peaks of each angle are averaged for each velocity for both frequency and amplitude. Squares, circles and triangles represent the mean value for 7 subjects and whiskers represent the 95% confidence interval.

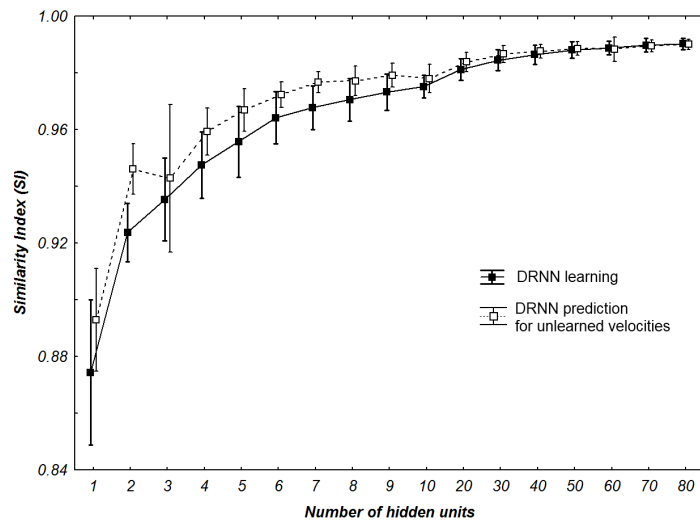


Figure 3.7: SI values of all multi-patterns learning and prediction for all participants with different number of hidden neurons. Whiskers correspond to 95% confidence interval.

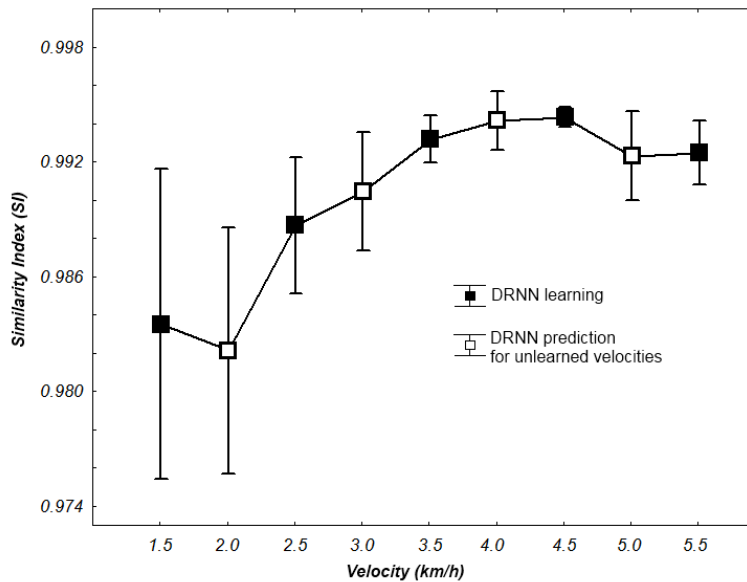


Figure 3.8: SI values for learning and prediction with a 80 hidden units network according to walking velocity. Whiskers correspond to 95% confidence interval.

We also analyse the output of the DRNN for specific velocities where the hidden layer was the biggest with 80 units. A Kolmogorov-Smirnov run together with learning and prediction values did not verify that the populations of *SI* was normal ($D = 0.18342, p < 0.05$). We use a Friedman test to analyse *SI* values (dependent variable) according to the velocity (independent variables) of the network. There is an effect of the velocity to the *SI* ($\chi^2_{(8)} = 30.22, p = 0.00019$). A posthoc analysis at 0.05 significance level reveals that *SI* values of 4.5 km/h were different from 1.5 and 2 km/h. *SI* values of 4km/h were also different from 2km/h.

3.4.3 DRNN structures from experiment 2

Weight distribution analysis

The percentage of positive and negative weights was calculated for each best network per subject per condition. We wanted to verify if the distribution of the positive and negative weights were different (Figure 3.10A). The Kolmogorov-Smirnov test did not verify that the distribution of positive weights were normal ($D = 0.15022, p < 0.01$) nor the distribution of negative weights ($D = 0.15022, p < 0.01$). We then used a non-parametric sign-test to compare the two-distribution as the two samples were dependent. Regardless of the number of hidden units, the test shows a difference between the distributions of the two populations ($Z = 9.482, p < 0.0001$). When the number of units in the test were included, it appears that the population of negative weights is higher than population of positive weights when the network possesses more than 3 hidden units (for 4 hidden units, $Z = 2.268, p = 0.023342$). When the structure of the DRNN reaches 80 hidden neurons, $70.6 \pm 0.84\%$ of the synapses are negative.

Time constant distribution analysis

The distribution of the time constant was represented by the median of neuronal time constants of the best networks per subject and number of hidden units (Figure 3.10B). The Kolmogorov-Smirnov displayed a normal distribution of the time constant median ($D = 0.09110, p > 0.20$). ANOVA with repeated measures was designed with the number of hidden units as independent variable and time constant median as dependent variable. ANOVA analysis shows an interesting effect of the number of hidden neurons ($F_{(16,96)} = 3.6245, p < 0.0001$). Overall, post-hoc analysis revealed that the distribution of the time constants were different when the network was small (less than 5 hidden units). It also reveals that the networks with 80 hidden neurons were differently distributed than medium-sized network (8 to 10 hidden neurons).

3.4.4 Neurophysiological similarity between modeled CPG and CPG in humans and other mammals

The understanding of CPG mechanisms remains central in locomotion study [23, 50, 51]. The CPG is a spinal network of neurons capable of generating a rhythmic pattern of alternate activities between flexor and extensor motoneurons on the same side with reciprocal activation of homologous motoneurons in the contralateral limb. This intrinsic spinal circuitry has been well described in many invertebrate and vertebrate animals, and is highly conserved even in humans, where greater cortical control of spinal modules is required working in conjunction with sensory

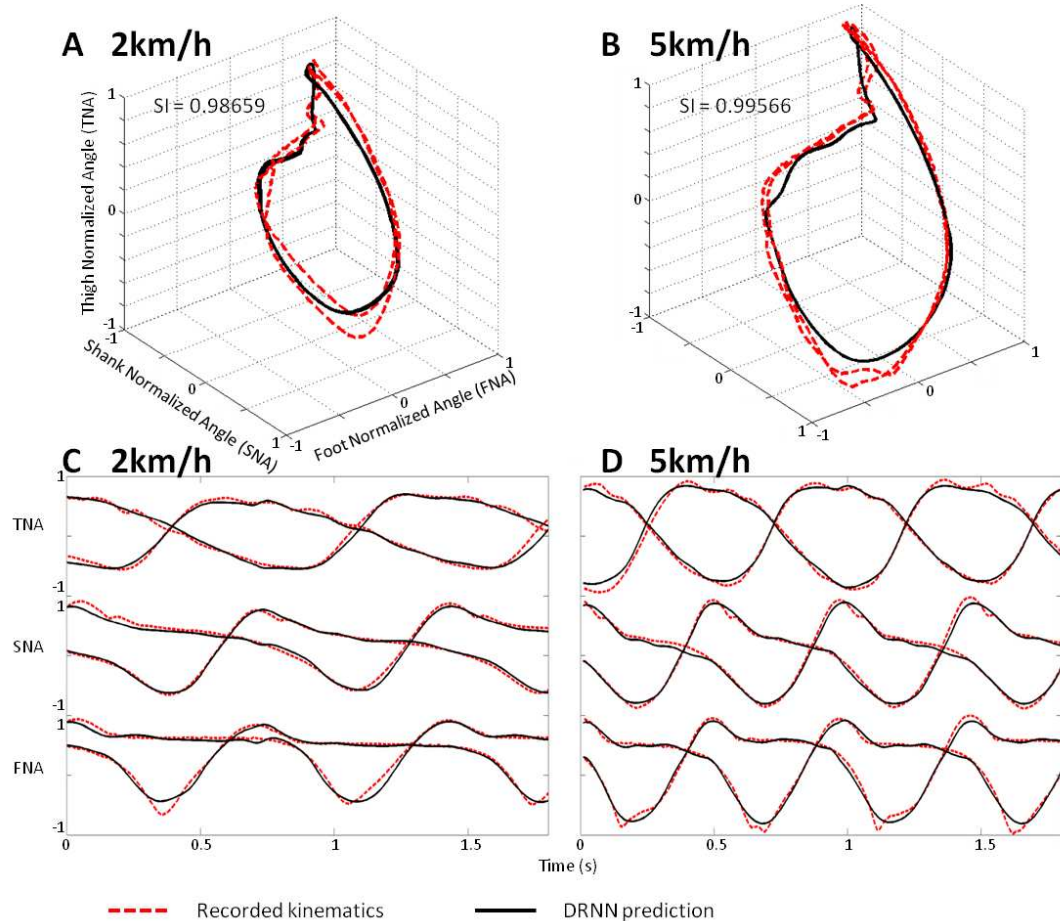


Figure 3.9: Prediction of intermediate velocities in one subject. A. Planar covariation of the normalized thigh, shank and foot for one participant walking at 2 km/h. B. Planar covariation of the normalized thigh, shank and foot for the same participant walking at 5 km/h. C. Kinematics of walking of the normalized thigh, shank and foot for the same participant walking at 2 km/h. D. Kinematics of walking of the normalized thigh, shank and foot for the same participant walking at 5 km/h. In each subplot the red dotted line corresponds to the experimental data whereas black thick line correspond to the output of the DRNN.

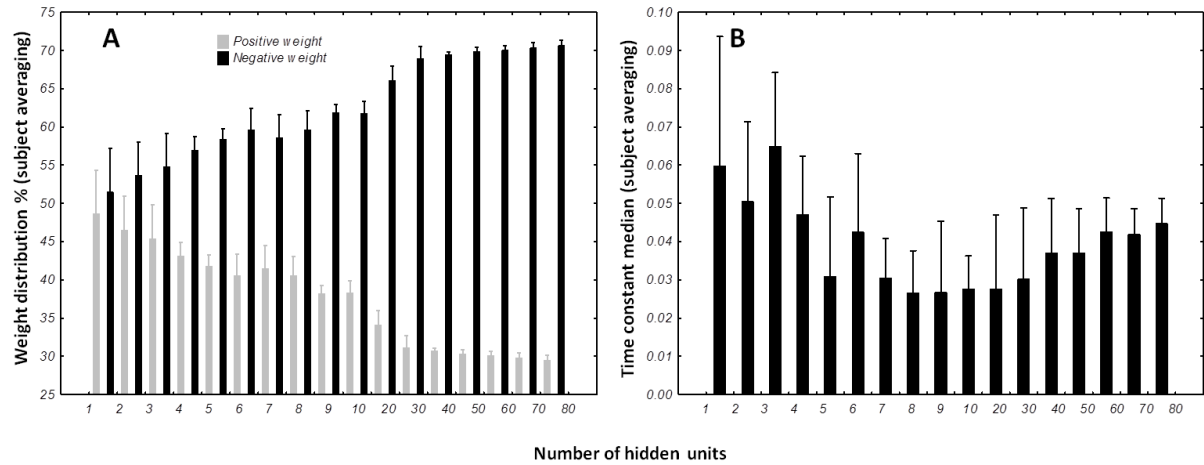


Figure 3.10: Distribution of weights (A) and time constants (B) among the DRNN structures. The horizontal axis represents the number of hidden neurons and vertical the percentage of population. The bars represent the mean distribution among the best DRNN for each subject. Whiskers represent the 95% confidence intervals.

feedback [26, 27, 52, 53, 54]. The unique characteristics of human walking probably reflect a complex neural mechanism responsible for pattern production. It is therefore difficult to directly extend experimental findings obtained in quadruped animals to human walking [55, 56]. The fact that some patients with incomplete spinal injury can move their legs in a rhythmic fashion [57] and that the primary sensorimotor cortex provides oscillatory commands towards the spine during walking [58] motivates new experiments in which different types of oscillatory signals could be used as input to the CPG-like DRNN. In this context, recent studies have shown EEG oscillations in relation to the gait cycle phase including event-related spectral perturbation in the alpha-beta and gamma bands [42, 59, 60, 61]. These results are consistent with a top down control of locomotion [56] and demonstrate the feasibility of extracting EEG signals from the sensorimotor cortex controlling the contralateral foot placement during walking. Although the distinction between the brain signals directly linked to the motor commands and those related to the treatment of multiple sensory signals is a hard task. In this context, [62] have found evidence of synchrony in the frequency domain between the primary motor cortex and the tibialis anterior muscle prior to heel strike during the swing phase of walking signifying that rhythmical cortical activity is transmitted via the corticospinal tract to the active muscles. Additionally Wagner et al. [61], showed a significant difference in the alpha (8-12Hz) and beta (18-21Hz) rhythm recorded over the central midline area between passive and active walking with exoskeleton. The role played by specific oscillations related to the initiation and control of human locomotion coming from supraspinal structure was recently demonstrated by local field potential recordings performed in the pedunculopontine nucleus in parkinsonian patients during rest and unconstrained walking [63]. Alpha oscillation recorded in the caudal part of this nucleus is correlated with gait speed and permits to suppress 'task irrelevant' distraction for improving gait performance. Moreover, these authors showed that gait freezing of parkinsonian patient

was associated with the attenuation of these alpha waves. Consistent with this aspect of gait physiology, in our model, input sine waves are sufficient to predict successful output with the DRNN and offer the possibility to mimic such type of supraspinal oscillatory input. It could be advanced that nonlinear mapping of sinusoidal oscillations to kinematic pattern should be realized by other mathematical functions, such as by a Taylor series, but such multi-dimensional approximation seems to be highly difficult to obtain and does not permit testing different network configurations mimicking biological organization such as the CPG. In the present study, we focused on input oscillation derived from the first three harmonics of kinematic signals, which were slower than the alpha frequency range. However, it could be possible to extract slower oscillation from alpha or beta derived signals (envelope) in order to activate the DRNN in our future work.

3.4.5 Structural Similarities of modelled CPG and neurophysiological CPGs in animals

It has been suggested that the biological CPG is considered to serve two basic functions: rhythm generation (RG) and pattern formation (PF). Initially proposed by Perret and Cabelguen [64], the idea that the biological CPG is composed of a rhythm and a pattern-amplitude generator is now widely accepted [23, 50, 65, 66, 67, 68] and paved the way to more complex models of multi-level CPG [69] (see below). It is well recognized that rhythm generating networks can be realized by means of (1) pacemaker neurons with intrinsic membrane properties such as those described in the stomatogastric ganglion of crustaceans or in the mammalian thalamus [70] or (2) most simplistic neurons without intrinsic pacemaker properties but interacting with inhibitory synapses for producing oscillation as emergent properties of this neuronal population [71]. Both neuronal systems thus present the fundamental ability to oscillate. Firstly described in the tadpole and lamprey CPGs, glutamatergic excitatory neurons distributed along the cord [72] assume the function of rhythmic generator by driving motor neurons and other ipsilateral and commissural inhibitory neurons coordinating the different CPG modules. By blocking the inhibitory networking in the lamprey and also in rodent and cat, many authors [50] have demonstrated that the glutamatergic burst neurons are the generators of the CPG rhythm. In addition to intrinsic rhythm generation properties, the walking CPGs need to integrate the ipsilateral coordination of flexors and extensors across the same or different joints in a limb and perform inter-limbs coordination. It has been proposed [73] that a subpopulation of neuronal CPG that drives extensor activity is tonically active and is regulated via inhibitory interactions with another CPG rhythmic structure responsible for flexors activity in the same hemicord. This assumption may explain why, during experimental recordings on the neonatal mouse isolated spinal cord, spontaneous deletions of extensor activity do not perturb rhythmic flexor activity. Thus, the inhibitory interneurons play a major role in the temporal sculpting and coordination of the CPG units. The interneurons and the Renshaw cells are involved in this function and in the regulation of walking speed. In addition, the left-right coordination is assumed by a complex network of excitatory and inhibitory commissural interneurons acting on both motor neurons and inhibitory interneurons of the contralateral side [50]. Interestingly, we have shown that a great percentage of artificial neurons became inhibitory neurons (negative synaptic weight) when the number of neurons progressively increases in the DRNN structure. In this context, it was recently demonstrated in

awake mice that the spiking activity of inhibitory neurons of the barrel cortex is organized in order to balance excitation and prevent explosive activity in the recurrently connected cortical microcircuit [74]. This physiological mechanism can also be proposed in the present case of the emergent structure of artificial DRNN circuit. Another, not exclusive explanation can reside in the prevalence of inhibitory recurrent connections for producing network oscillation [71, 75]. In their review, [76] have proposed that inhibitory interneurons play a major role in the CPG of rodent spinal cord. The interneurons are likely to control the bursting of motor neurons during locomotion and it appears that the synaptic transmission mediated by glycine and GABA shifts from excitatory to inhibitory during the prenatal period. It was recently demonstrated that in the absence of glutamatergic synaptic transmission, the flexor-extensor alternation appears to be generated by the inhibitory interneurons, mediating reciprocal inhibition from muscle proprioceptors to antagonist motor neurons [68]. The present artificial model does not pretend to mimic the complexity of the CPG structure. Instead, it presents a highly simplified recurrent organization from which CPG-like dynamic function emerges, following appropriate learning. Sinusoidal inputs serve as temporal referent to produce rhythmic angles patterns. This model could correspond to the RG structure described previously as a higher order structure that determines rhythmic output of the system [69] since sine waves are transformed into kinematics. Another, lower order structure responsible for the phasing and intensity coordination [69] could be assumed by another model of DRNN transforming theoretical kinematics into practical muscle orders. We have already studied such relation where EMG signals from walking were used to predict kinematics [41]. To conclude to this point, we propose that the two model driving two specific DRNNs (one for producing elevation angles from sine waves and one producing muscular patterns from elevation angles during walking) could act as a complementary top-down pathway to produce adequate coordinated patterns as it has been proposed to model the locomotion in spinal mouse [73]. The present results can also be discussed in the light of the electrical stimulations performed in the mesencephalic locomotor region (MLR) inducing locomotor behaviour in decerebrate cat [77] or in lamprey [78]. In mice, prolonged rhythmic stimulation on the midline of the caudal hindbrain or the ventral spinal cord (C1-C4) induces a stable locomotor activity [68]. Typically, low-frequency stimulation leads to slow-frequency movements and inversely fast-frequency stimulation leads to fast-frequency movements. Our model is in accordance with this physiological behavior, when amplitude of the artificial sine wave inputs increases, the amplitude of stepping increases as well, leading to a change in walking velocities (Figure 3.6B). In terms of neurological development, there is some evidence for the existence of CPG very early in CNS maturation [21, 79]. Neonatal, so-called 'infant' stepping has been ascribed to similar EMG patterns activity in different directions inducing stereotyped yet non-functional walking patterns [80]. This leads the authors to conclude that the same CPG controls different stepping in human infants in contrast with some studies in adults [9, 81]. Interestingly, we found that DRNN with only four hidden artificial neurons can generate walking pattern, whereas at least 50 hidden neurons are the prerequisite to generate accurate movements (Figure 3.7). Obviously, recruitment and training of such high numbers of neurons requires long computational time. For example, with a 4 hidden units DRNN structure, the learning process lasts about 5 minutes based on our computer performance while 160 minutes are necessary for a DRNN containing 80 units (Figure 3.4)

3.5 Conclusion

In a hierarchical gait model, Central Pattern Generators (CPGs) play an important role. From Chapter 2, it was shown that Programmable Central Pattern Generators (PCPGs) were an interesting option. However, there is still a lack of performance when the generated speed is far from the learned one. Indeed, the shape of the frequency-adjusted human gait pattern is not constant, especially at low speeds. To improve the performance, a non-linear filter approach was suggested. Data from seven healthy subjects were used.

In this Chapter, we show that a fully connected recurrent neural network is able to reproduce human walking pattern based on oscillatory properties of kinematics. Although, this network is a black box model without prewired structure mimicking a physiological CPG, its actual performance allows direct comparison with CPG dedicated structure and related algorithm [32]. Moreover, by the inherent input-output mapping, the DRNN models not only the CPG but also neural feedback pathways and the musculoskeletal system. For simplicity, we consider this neural network as "CPG-like structure" here. We proved that the DRNN is capable of generating the kinematics as elevation angles pattern of walking for both limbs (six degrees of freedom) from simple oscillations corresponding to the three main harmonics of the walking kinematics. Moreover, by modulating those frequencies and tuning them in amplitude as input, the DRNN was able to learn and reliably predict walking kinematics at different velocities. After this appropriate learning the DRNN can thus be considered as a CPG-like structure that would continuously receive oscillation inputs to produce the relevant elevation patterns of the six leg segments. Another interesting result is observed when looking at the structure of best CPGs obtained after learning. Hence, it appears that all of them contain a major part of negative connection weight between units.

However, there are infinite different ways to train the DRNN and this is a strength of this approach. It implies a corollary limitation as not all possibilities could be tested in the present study. For example, in order to better document its generalization ability, the model could be trained for a defined low range of velocities, e.g. from 1 to 4 km/h, and then tested with unlearned oscillation input corresponding to higher velocities. A reverse procedure could also be made, i.e. from faster training to slower predictions. Furthermore, inter-subjects generalization has not been studied in the present investigation. The actual usefulness of performing this would largely depend on the basic or application purposes. Another limitation of the present work is the lack of feedback testing, which necessitates a priori identification of a reliable signal and a new operational strategy for learning. Future work will address these aspects specifically.

For future work, a DRNN can be used to produce gait kinematics in numerous and various applications. For rehabilitation it can be used to train people for recovering a walking pattern corresponding to their physical characteristics by training with an appropriate feedback. Specifically dedicated DRNN based on the proper dynamics of participants could be used for medical applications such as in prosthesis and exoskeleton control [42]. It can also be integrated in BCI applications in which higher order commands can be used, e.g., from steady state visual or somatosensory evoked potentials [42] or P300 [82, 83]. This neuronal avenue might lead to the decoding of higher neuronal commands that govern CPG mechanisms. Since these CPG can

be trained using specific sinusoidal frequency signals, it might be possible to extract this type of signals from specific EEG rhythms. One of the strengths of this approach is that it is not necessary to determine in advance the topology and the timing sequences between the artificial neurons. This contrasts with other CPGs, such as a recently developed ones [31] based on coupled oscillators [38], where adjustment of intrinsic parameters by optimization techniques was necessary.

Additionally, by introducing an informational delay [84] or an artificial distance based on a Gaussian factor modulating the weights between the different neurons [85], it will be possible to analyse the self-tailored organization of the links between neurons and the possible emergence of specific topologies. In this case it will also be possible to select different modular architectures of the DRNN.

Bibliography

- [1] N. A. Borghese, L. Bianchi, and F. Lacquaniti. Kinematic determinants of human locomotion. *The Journal of Physiology*, 494(Pt 3):863–879, August 1996.
- [2] Avi Barliya, Lars Omlor, Martin A Giese, and Tamar Flash. An analytical formulation of the law of intersegmental coordination during human locomotion. *Experimental brain research. Experimentelle Hirnforschung. Expérimentation cérébrale*, 193(3):371–385, March 2009.
- [3] Nikolai Aleksandrovich Bernstein. *The co-ordination and regulation of movements*. Pergamon Press, 1967.
- [4] Tamar Flash and Binyamin Hochner. Motor primitives in vertebrates and invertebrates. *Current opinion in neurobiology*, 15(6):660–666, December 2005.
- [5] F. Lacquaniti, R. Grasso, and M. Zago. Motor Patterns in Walking. *Physiology*, 14(4):168–174, August 1999.
- [6] F Lacquaniti, Y P Ivanenko, and M Zago. Kinematic control of walking. *Archives Italiennes De Biologie*, 140(4):263–272, October 2002.
- [7] Mark L. Latash. *Synergy*. Oxford University Press US, 2008.
- [8] L Bianchi, D Angelini, G P Orani, and F Lacquaniti. Kinematic coordination in human gait: relation to mechanical energy cost. *Journal of neurophysiology*, 79(4):2155–2170, April 1998.
- [9] R Grasso, L Bianchi, and F Lacquaniti. Motor patterns for human gait: backward versus forward locomotion. *Journal of neurophysiology*, 80(4):1868–1885, October 1998.
- [10] Grégoire Courtine and Marco Schieppati. Tuning of a Basic Coordination Pattern Constructs Straight-Ahead and Curved Walking in Humans. *Journal of Neurophysiology*, 91(4):1524–1535, April 2004.
- [11] Nadia Dominici, Elena Daprati, Daniele Nico, Germana Cappellini, Yuri P Ivanenko, and Francesco Lacquaniti. Changes in the limb kinematics and walking-distance estimation after shank elongation: evidence for a locomotor body schema? *Journal of neurophysiology*, 101(3):1419–1429, March 2009.

- [12] Fran oise Leurs, Yuri P Ivanenko, Ana Bengoetxea, Ana-Maria Cebolla, Bernard Dan, Francesco Lacquaniti, and Guy A Cheron. Optimal walking speed following changes in limb geometry. *The Journal of Experimental Biology*, 214(Pt 13):2276–2282, July 2011.
- [13] F Leurs, A Bengoetxea, A M Cebolla, C De Saedeleer, B Dan, and G Cheron. Planar covariation of elevation angles in prosthetic gait. *Gait & posture*, 35(4):647–652, April 2012.
- [14] Y P Ivanenko, R Grasso, V Macellari, and F Lacquaniti. Control of foot trajectory in human locomotion: role of ground contact forces in simulated reduced gravity. *Journal of neurophysiology*, 87(6):3070–3089, June 2002.
- [15] Yuri P. Ivanenko, Germana Cappellini, Nadia Dominici, Richard E. Poppele, and Francesco Lacquaniti. Modular Control of Limb Movements during Human Locomotion. *J. Neurosci.*, 27(41):11149–11161, October 2007.
- [16] G Cheron, A Bengoetxea, E Bouillot, F Lacquaniti, and B Dan. Early emergence of temporal co-ordination of lower limb segments elevation angles in human locomotion. *Neuroscience Letters*, 308(2):123–127, August 2001.
- [17] G Cheron, E Bouillot, B Dan, A Bengoetxea, J P Draye, and F Lacquaniti. Development of a kinematic coordination pattern in toddler locomotion: planar covariation. *Experimental Brain Research. Experimentelle Hirnforschung. Exp rimentation C r brale*, 137(3-4):455–466, April 2001.
- [18] Yuri P Ivanenko, Nadia Dominici, Germana Cappellini, and Francesco Lacquaniti. Kinematics in newly walking toddlers does not depend upon postural stability. *Journal of neurophysiology*, 94(1):754–763, July 2005.
- [19] Halim Hicheur, Alexander V Terekhov, and Alain Berthoz. Intersegmental coordination during human locomotion: does planar covariation of elevation angles reflect central constraints? *Journal of neurophysiology*, 96(3):1406–1419, September 2006.
- [20] Y P Ivanenko, A D’Avella, R E Poppele, and F Lacquaniti. On the origin of planar covariation of elevation angles during human locomotion. *Journal of Neurophysiology*, 99(4):1890–1898, April 2008.
- [21] Nadia Dominici, Yuri P Ivanenko, Germana Cappellini, Andrea D’Avella, Vito Mondi, Marika Cicchese, Adele Fabiano, Tiziana Silei, Ambrogio Di Paolo, Carlo Giannini, Richard E Poppele, and Francesco Lacquaniti. Locomotor primitives in newborn babies and their development. *Science (New York, N.Y.)*, 334(6058):997–999, November 2011.
- [22] A P Georgopoulos and S Grillner. Visuomotor coordination in reaching and locomotion. *Science (New York, N.Y.)*, 245(4923):1209–1210, September 1989.
- [23] Sten Grillner. Biological pattern generation: the cellular and computational logic of networks in motion. *Neuron*, 52(5):751–766, December 2006.

- [24] Mark M Churchland, John P Cunningham, Matthew T Kaufman, Justin D Foster, Paul Nuyujukian, Stephen I Ryu, and Krishna V Shenoy. Neural population dynamics during reaching. *Nature*, 487(7405):51–56, July 2012.
- [25] T. Graham Brown. The Intrinsic Factors in the Act of Progression in the Mammal. *Royal Society of London Proceedings Series B*, 84:308–319, December 1911.
- [26] B Bussel, A Roby-Brami, O R Néris, and A Yakovleff. Evidence for a spinal stepping generator in man. Electrophysiological study. *Acta neurobiologiae experimentalis*, 56(1):465–468, 1996.
- [27] Blair Calancie, Belinda Needham-Shropshire, Patrick Jacobs, Keith Willer, Gregory Zych, and Barth A Green. Involuntary Stepping After Chronic Spinal Cord Injury Evidence for a Central Rhythm Generator for Locomotion in Man. *Brain*, 117(5):1143–1159, October 1994.
- [28] Jaynie F Yang, Erin V Lamont, and Marco Y C Pang. Split-belt treadmill stepping in infants suggests autonomous pattern generators for the left and right leg in humans. *The Journal of neuroscience: the official journal of the Society for Neuroscience*, 25(29):6869–6876, July 2005.
- [29] Auke Jan Ijspeert. Central pattern generators for locomotion control in animals and robots: a review. *Neural Networks: The Official Journal of the International Neural Network Society*, 21(4):642–653, May 2008.
- [30] A E Patla, T W Calvert, and R B Stein. Model of a pattern generator for locomotion in mammals. *The American journal of physiology*, 248(4 Pt 2):R484–494, April 1985.
- [31] M. Duvinage, T. Castermans, T. Hoellinger, G. Cheron, and T. Dutoit. Modeling human walk by PCPG for lower limb neuroprostheses control. *5th International IEEE/EMBS Conference on Neural Engineering (NER)*, pages 317–321, May 2011.
- [32] M. Duvinage, T. Castermans, T. Hoellinger, and J. Reumaux. Human Walk Modeled by PCPG to Control a Lower Limb Neuroprostheses by High-Level Commands. *Journal of Systemics, Cybernetics and Informatics*, 10(3):70–80, 2012.
- [33] Auke Jan Ijspeert, Alessandro Crespi, Dimitri Ryczko, and Jean-Marie Cabelguen. From swimming to walking with a salamander robot driven by a spinal cord model. *Science (New York, N.Y.)*, 315(5817):1416–1420, March 2007.
- [34] J Hellgren, S Grillner, and A Lansner. Computer simulation of the segmental neural network generating locomotion in lamprey by using populations of network interneurons. *Biological cybernetics*, 68(1):1–13, 1992.
- [35] Tom Wadden, Jeanette Hellgren, Anders Lansner, and Sten Grillner. Intersegmental coordination in the lamprey: simulations using a network model without segmental boundaries. *Biological Cybernetics*, 76(1):1–9, 1997.

- [36] Jean-Charles Ceccato, Christine Azevedo-Coste, and Jean-Rene Cazalets. Real time control of a CPG-based model of the human trunk in different walking conditions. *Conference Proceedings: ... Annual International Conference of the IEEE Engineering in Medicine and Biology Society. IEEE Engineering in Medicine and Biology Society. Conference*, 2009:1388–1391, 2009.
- [37] L. Righetti, J. Buchli, and A.J. Ijspeert. From Dynamic Hebbian Learning for Oscillators to Adaptive Central Pattern Generators. *Proceedings of 3rd International Symposium on Adaptive Motion in Animals and Machines*, page 45, 2005.
- [38] L. Righetti and A. J Ijspeert. Programmable central pattern generators: an application to biped locomotion control. *Proceedings 2006 IEEE International Conference on Robotics and Automation, 2006. ICRA 2006*, pages 1585–1590, May 2006.
- [39] S D Prentice, A E Patla, and D A Stacey. Simple artificial neural network models can generate basic muscle activity patterns for human locomotion at different speeds. *Experimental Brain Research. Experimentelle Hirnforschung. Expérimentation Cérébrale*, 123(4):474–480, December 1998.
- [40] S D Prentice, A E Patla, and D A Stacey. Artificial neural network model for the generation of muscle activation patterns for human locomotion. *Journal of Electromyography and Kinesiology: Official Journal of the International Society of Electrophysiological Kinesiology*, 11(1):19–30, February 2001.
- [41] G Cheron, F Leurs, A Bengoetxea, J P Draye, M Destrée, and B Dan. A dynamic recurrent neural network for multiple muscles electromyographic mapping to elevation angles of the lower limb in human locomotion. *Journal of Neuroscience Methods*, 129(2):95–104, October 2003.
- [42] G Cheron, M Duvinage, C De Saedeleer, T Castermans, A Bengoetxea, M Petieau, K Seetharaman, T Hoellinger, B Dan, T Dutoit, F Sylos Labini, F Lacquaniti, and Y Ivanenko. From spinal central pattern generators to cortical network: integrated BCI for walking rehabilitation. *Neural plasticity*, 2012:375148, 2012.
- [43] Barak Pearlmutter. Dynamic recurrent neural networks. *Carnegie Mellon University Repository*, January 1990.
- [44] J.P Draye, D. A Pavicic, G. A Cheron, and G. A Libert. Dynamic recurrent neural networks: a dynamical analysis. *IEEE Transactions on Systems, Man, and Cybernetics, Part B: Cybernetics*, 26(5):692–706, October 1996.
- [45] Jean-Philippe Draye, Davor Pavicic, Guy Cheron, and Gaëtan Libert. Adaptative time constants improve the prediction capability of recurrent neural networks. *Neural Processing Letters*, 2(3):12–16, June 1995.
- [46] G. Cheron, M. Duvinage, T. Castermans, F Leurs, A Cebolla, A Bengoetxea, C De Saedeleer, M. Petieau, T. Hoellinger, K. Seetharaman, J.P Draye, and B. Dan. Toward

- an Integrative Dynamic Recurrent Neural Network for Sensorimotor Coordination Dynamics. In *Recurrent Neural Networks for Temporal Data Processing*, pages 67–80 chap 5. 2011.
- [47] G. Cheron, A.M Cebolla, Ana Bengoetxea, Fran oise Leurs, and Bernard Dan. Recognition of the physiological actions of the triphasic EMG pattern by a dynamic recurrent neural network. *Neuroscience Letters*, 414(2):192–196, March 2007.
- [48] A Bengoetxea, B Dan, F Leurs, A M Cebolla, C De Saedeleer, P Gillis, and G Cheron. Rhythmic muscular activation pattern for fast figure-eight movement. *Clinical Neurophysiology: Official Journal of the International Federation of Clinical Neurophysiology*, 121(5):754–765, May 2010.
- [49] A. Bengoetxea, F. Leurs, A. Cebolla, S. Wellens, J. P. Draye, and G. Cheron. A dynamic recurrent neural network for drawing multi-directional trajectories. *Computer Methods in Biomechanics and Biomedical Engineering*, 8(sup1):29–30, 2005.
- [50] Ole Kiehn. Locomotor circuits in the mammalian spinal cord. *Annual review of neuroscience*, 29:279–306, 2006.
- [51] Serge Rossignol and Alain Frigon. Recovery of locomotion after spinal cord injury: some facts and mechanisms. *Annual review of neuroscience*, 34:413–440, 2011.
- [52] Trevor Drew, Wan Jiang, and Witold Widajewicz. Contributions of the motor cortex to the control of the hindlimbs during locomotion in the cat. *Brain Research Reviews*, 40(1–3):178–191, October 2002.
- [53] J. Duysens and HW. Van de Crommert. Neural control of locomotion; The central pattern generator from cats to humans. *Gait & posture*, 7(2):131–141, March 1998.
- [54] S Rossignol, G Barri re, O Alluin, and A Frigon. Re-expression of locomotor function after partial spinal cord injury. *Physiology (Bethesda, Md.)*, 24:127–139, April 2009.
- [55] Hugues Barbeau, Andr  Pepin, Kathleen E. Norman, Michel Ladouceur, and Alain Leroux. Review : Walking After Spinal Cord Injury: Control and Recovery. *The Neuroscientist*, 4(1):14–24, January 1998.
- [56] Charles Capaday. The special nature of human walking and its neural control. *Trends in Neurosciences*, 25(7):370–376, July 2002.
- [57] V Dietz, G Colombo, L Jensen, and L Baumgartner. Locomotor capacity of spinal cord in paraplegic patients. *Annals of neurology*, 37(5):574–582, May 1995.
- [58] Christian la Foug re, Andreas Zwergal, Axel Rominger, Stefan F rster, Gunther Fesl, Marianne Dieterich, Thomas Brandt, Michael Strupp, Peter Bartenstein, and Klaus Jahn. Real versus imagined locomotion: a [18F]-FDG PET-fMRI comparison. *NeuroImage*, 50(4):1589–1598, May 2010.

- [59] Joseph T Gwin, Klaus Gramann, Scott Makeig, and Daniel P Ferris. Electrocortical activity is coupled to gait cycle phase during treadmill walking. *NeuroImage*, 54(2):1289–1296, January 2011.
- [60] Jenny Haefeli, Stefanie Vögeli, Jan Michel, and Volker Dietz. Preparation and performance of obstacle steps: interaction between brain and spinal neuronal activity. *The European Journal of Neuroscience*, 33(2):338–348, January 2011.
- [61] Johanna Wagner, Teodoro Solis-Escalante, Peter Grieshofer, Christa Neuper, Gernot Müller-Putz, and Reinhold Scherer. Level of participation in robotic-assisted treadmill walking modulates midline sensorimotor EEG rhythms in able-bodied subjects. *NeuroImage*, 63(3):1203–1211, August 2012.
- [62] T H Petersen, M Willerslev-Olsen, B A Conway, and J B Nielsen. The motor cortex drives the muscles during walking in human subjects. *The Journal of physiology*, 590(Pt 10):2443–2452, May 2012.
- [63] Wesley Thevathasan, Alek Pogosyan, Jonathan A Hyam, Ned Jenkinson, Tom Foltyne, Patricia Limousin, Marko Bogdanovic, Ludvic Zrinzo, Alexander L Green, Tipu Z Aziz, and Peter Brown. Alpha oscillations in the pedunculopontine nucleus correlate with gait performance in parkinsonism. *Brain: a journal of neurology*, 135(Pt 1):148–160, January 2012.
- [64] C Perret and J M Cabelguen. Main characteristics of the hindlimb locomotor cycle in the decorticate cat with special reference to bifunctional muscles. *Brain research*, 187(2):333–352, April 1980.
- [65] P Guertin, M J Angel, M C Perreault, and D A McCrea. Ankle extensor group I afferents excite extensors throughout the hindlimb during fictive locomotion in the cat. *The Journal of physiology*, 487 (Pt 1):197–209, August 1995.
- [66] D J Kriellaars, R M Brownstone, B R Noga, and L M Jordan. Mechanical entrainment of fictive locomotion in the decerebrate cat. *Journal of neurophysiology*, 71(6):2074–2086, June 1994.
- [67] M C Perreault, M J Angel, P Guertin, and D A McCrea. Effects of stimulation of hindlimb flexor group II afferents during fictive locomotion in the cat. *The Journal of physiology*, 487 (Pt 1):211–220, August 1995.
- [68] Adolfo E Talpalar, Toshiaki Endo, Peter Löw, Lotta Borgius, Martin Hägglund, Kimberly J Dougherty, Jesper Ryge, Thomas S Hnasko, and Ole Kiehn. Identification of minimal neuronal networks involved in flexor-extensor alternation in the mammalian spinal cord. *Neuron*, 71(6):1071–1084, September 2011.
- [69] David A McCrea and Ilya A Rybak. Organization of mammalian locomotor rhythm and pattern generation. *Brain research reviews*, 57(1):134–146, January 2008.

- [70] M Steriade and R R Llinás. The functional states of the thalamus and the associated neuronal interplay. *Physiological reviews*, 68(3):649–742, July 1988.
- [71] Caroline Geisler, Nicolas Brunel, and Xiao-Jing Wang. Contributions of intrinsic membrane dynamics to fast network oscillations with irregular neuronal discharges. *Journal of neurophysiology*, 94(6):4344–4361, December 2005.
- [72] Sten Grillner. The motor infrastructure: from ion channels to neuronal networks. *Nature reviews. Neuroscience*, 4(7):573–586, July 2003.
- [73] Guisheng Zhong, Natalia A Shevtsova, Ilya A Rybak, and Ronald M Harris-Warrick. Neuronal activity in the isolated mouse spinal cord during spontaneous deletions in fictive locomotion: insights into locomotor central pattern generator organization. *The Journal of physiology*, 590(Pt 19):4735–4759, October 2012.
- [74] Luc J Gentet, Michael Avermann, Ferenc Matyas, Jochen F Staiger, and Carl C H Petersen. Membrane potential dynamics of GABAergic neurons in the barrel cortex of behaving mice. *Neuron*, 65(3):422–435, February 2010.
- [75] Mark Wildie and Murray Shanahan. Establishing Communication between Neuronal Populations through Competitive Entrainment. *Frontiers in computational neuroscience*, 5:62, 2011.
- [76] H Nishimaru and M Kakizaki. The role of inhibitory neurotransmission in locomotor circuits of the developing mammalian spinal cord. *Acta physiologica (Oxford, England)*, 197(2):83–97, October 2009.
- [77] M L Shik, F V Severin, and G N Orlovsky. Control of walking and running by means of electrical stimulation of the mesencephalon. *Electroencephalography and clinical neurophysiology*, 26(5):549, May 1969.
- [78] Andrew D. McClellan and Sten Grillner. Activation of ‘fictive swimming’ by electrical microstimulation of brainstem locomotor regions in an in vitro preparation of the lamprey central nervous system. *Brain Research*, 300(2):357–361, 1984.
- [79] J F Yang, M J Stephens, and R Vishram. Infant stepping: a method to study the sensory control of human walking. *The Journal of physiology*, 507 (Pt 3):927–937, March 1998.
- [80] T Lamb and J F Yang. Could different directions of infant stepping be controlled by the same locomotor central pattern generator? *Journal of neurophysiology*, 83(5):2814–2824, May 2000.
- [81] A Thorstensson. How is the normal locomotor program modified to produce backward walking? *Experimental brain research. Experimentelle Hirnforschung. Expérimentation cérébrale*, 61(3):664–668, 1986.

- [82] Thierry Castermans, Matthieu Duvinage, Mathieu Petieau, Thomas Hoellinger, Caty De Saedeleer, Karthik Seetharaman, Ana Bengoetxea, Guy Cheron, and Thierry Dutoit. Optimizing the performances of a P300-based Brain-Computer Interface in ambulatory conditions. *IEEE Journal of Emerging and Selected Topics in Circuits and Systems (JETCAS)*, 1(4):566 – 577, 2011.
- [83] M. Duvinage, T. Castermans, R. Jimenez-Fabian, M. Petieau, K. Seetharaman, T. Hoellinger, C De Saedeleer, G. Cheron, O. Verlinden, and T. Dutoit. A five-state P300-based foot lifter orthosis: Proof of concept. *The 3rd IEEE Biosignals and Biorobotics conference (ISSNIP)*, pages 1–6, 2012.
- [84] J P Draye, G Cheron, G Libert, and E Godaux. Emergence of clusters in the hidden layer of a dynamic recurrent neural network. *Biological cybernetics*, 76(5):365–374, May 1997.
- [85] Jean-Philippe Draye, Jack M Winters, and Guy Cheron. Self-selected modular recurrent neural networks with postural and inertial subnetworks applied to complex movements. *Biological Cybernetics*, 87(1):27–39, July 2002.

Part II

Brain-Computer Interfaces in An Ambulatory Framework

Chapter 4

SSVEP Response Distribution Under Different Luminosity and Movement Conditions

Contents

4.1	Introduction	95
4.2	Method	95
4.2.1	SSVEP Paradigm	95
4.2.2	Experiment Description	96
4.2.3	Performance Evaluation	96
4.3	Results and Discussion	99
4.4	Conclusions	104

Abstract

Among the huge efforts of researchers to bring Brain-Computer Interfaces (BCI) out of the lab, dealing with artefacts always represents a challenge. Because of these spurious signals, only a decreased performance may be offered to end-users leading to a high abandonment rate.

In order to address some of these potential artefacts, we propose an ambulatory Steady-State Visual Evoked Potential (SSVEP) study using a 32 electrode EEG cap. In this paper, eight healthy subjects had to look at a LED panel whose flickering frequency ranged from 10 Hz to 46 Hz by 2 Hz step. Several conditions were considered: sitting on a chair/walking on a treadmill at 3 km/h and a normal/maximal luminosity of the LED panel. The analysis is mainly based on the Signal-to-Noise Ratio (SNR) distribution.

The average SNR in the occipital area under walking condition is significantly worse than under sitting conditions. Muscle artefacts from the neck strongly affect the SSVEP response in this area. Several unexpected behaviours, which are unlikely linked to artefacts, were also observed.

In conclusion, without any artefact removal techniques, results suggest that gait is not a transparent process for the SSVEP paradigm. However, walking conditions should be able to reach similar performance to sitting conditions using an optimal artefact correction method (still to be designed). Several behaviours that were observed could be helpful for the design of ambulatory BCIs in order to increase the performance of such systems.

This chapter is based upon the following publications:

- M. DUVINAGE, T. CASTERMANS, M. PETIEAU, T. HOELLINGER, K. SEETHARAMAN, G. CHERON, T. DUTOIT, 2013, *A Preliminary Fundamental Study of Ambulatory SSVEP*, Proceedings of the TOBI IV workshop, Sion, Switzerland, January 23-25.
- M. DUVINAGE, T. CASTERMANS, M. PETIEAU, T. HOELLINGER, G. CHERON, T. DUTOIT, 2013, *SSVEP Response Distribution Under Different Luminosity and Movement Conditions*, Journal of NeuroEngineering [Under Review].

4.1 Introduction

Although the Steady State Visual Evoked Potential (SSVEP) is a robust and fast paradigm, it could suffer from gait-related artefacts. Indeed, one study about SSVEP potential with one subject and two frequencies (4 Hz and 6 Hz) showing that no particular impact of gait on SSVEP performance was observed [1]. However, this study does not analyse enough subjects and it does not say anything about Signal-to-Noise Ratio (SNR) distribution modifications of the SSVEP responses under both conditions. Another recent study analysing 11 Hz and 12 Hz SSVEP response while standing and walking has shown that the walking speed does impact on the SSVEP detection accuracy [2]. Nevertheless, a strong lack of this study is to show how SNRs fluctuate over a large frequency range of stimuli. Finally, some current work exists in order to create visual stimulus for real-life applications. For instance, the VUZIX augmented reality eyewears (Vuzix, Rochester, NY, USA) or the famous Google glass could help showing the required stimuli. There are also projects on integrating the stimuli on mobile devices [3, 4].

To get a better picture of the gait impact on the SSVEP response to control an orthosis, we want to study the SSVEP response under several different conditions: luminosity and sitting/walking conditions. This should also help the researcher to design ambulatory SSVEP-based BCI. Luminosity was assessed to detect whether this parameter can influence conclusions. This study, which considers realistic out-of-the-lab conditions, should help researchers designing an ambulatory BCI. In Section 4.2, the SSVEP paradigm, the experiment and the performance measure are described. In Section 11.6, results are summarized and discussed.

4.2 Method

4.2.1 SSVEP Paradigm

As depicted in Figure 1.9, SSVEP is a strong steady state potential that mainly arises in the occipital area, i.e. the O_x electrodes, when a subject is looking at a flickering stimulus whose frequency is usually considered to be higher than 4 Hz, although it is possible to get an SSVEP response in the range 1-100 Hz [5]. This potential is generated at the stimulated frequency and its harmonics. The main advantage of this type of BCI is the relatively high SNR with a clear peak in the FFT occurring at the frequency of interest and some of its harmonics. Moreover, as discussed in [6], the Signal-to-Noise Ratio (SNR) SSVEP response has three main frequency bands with peaks around 15 Hz, 31 Hz and 41 Hz. Logically, this leads to a high potential bitrate that can even reach around 100 bits/min [7].

In this study, LEDs were used as stimulators. Indeed, the flickering stimulus can be either produced by a CRT/LCD screen or by a LED. From previous studies and at the same luminance and modulation depth, it is known that LEDs produce stronger fundamental SSVEP responses than LCD/CRT screens [8]. Given the so short rising and descending edges, the LED flicker spectrum has a strong fundamental, weak harmonics and a global cleaner generated signal compared to other technologies. Obviously, this leads to a cleaner SSVEP response with a stronger fundamental and weaker harmonics in the emitting light.

Moreover, SSVEP response strength is strongly linked to the precision of the generated frequency, i.e. a small jitter can dramatically decrease the performance of such BCIs. This jitter is clearly much smaller with LED than with screens whose control depends on the operating system latency and on the computer hardware. As discussed in [8], LED technology has an intrinsic quicker response and a more stable generated light.

4.2.2 Experiment Description

Basically, the experiment consisted in comparing the SSVEP brain response under different conditions: sitting/walking and normal/high luminosity. During the experiment, the subject had to focus on a 63-LED panel (7×9 cm) depicted in Figure 4.1, whose flickering frequency was increased from 10 to 46 Hz (to avoid low-frequency mechanical gait artefacts) by 2 Hz step (scanning of 19 frequencies, randomly within ascending and descending order). The distance between the LEDs and the subject's eyes was checked during the whole experiment and fixed at 70 cm. For each flickering frequency, two recording sessions were performed while walking on a treadmill at 3 km/h and two others were recorded while sitting on a chair. By modulating the potential supply of the LED panel, these two sessions encompass two luminosity conditions, which were the same for each subject: one that could be used for a daily life application and one that tends to the supportable limit common to every subjects. For each session and for each frequency, a 30-second EEG dataset was recorded leading to a total of 76 recordings per subject. They had the instruction to just look at the center of the panel. In total, eight healthy subjects without any known physical or neurological disorders participated in this experiment (age-range: 26-35 years).

EEG was recorded using a 128-electrode cap (but only 32 electrodes depicted in Figure 4.2 were used in the analysis because no additional conclusions could be made from the full EEG recordings), which was connected to the ANT amplifier system (Advanced Neuro Technology, ANT, Enschede, The Netherlands) digitizing the signals at 512 Hz. Left ear was chosen as reference. Electrode impedance was measured and maintained under $20 \text{ k}\Omega$ for each channel using electrode gel. A common average reference was used as suggested by [9]. Additionally, Electromyographic (EMG) signals of the neck (superior region of the left and right trapezia) were acquired to obtain a measure of muscle artefacts in order to help interpreting the results. EOG signals were also acquired. Finally, a footswitch was placed at the heel of the right foot in order to study gait cycle synchronized artefacts. All procedures were approved by the Université Libre de Bruxelles Internal Review Board and complied with the standards defined in the Declaration of Helsinki.

4.2.3 Performance Evaluation

To detect the SSVEP response across all the channels and scanned frequencies, local Signal-to-Noise Ratios (SNRs) were calculated. SNR gives an indication of how acute is the SSVEP peak spectrum response compared to the background noise in terms of power. Additionally, this measure is directly linked to the bitrate, which is an important performance measure in BCIs.



Figure 4.1: The LED stimulator used in the experiment was the upper one of the four available around the screen. For each condition, the height of the LED panel was adapted to the eye position. The EEG recording device was an ANT system (contrary to the one depicted in the Figure).

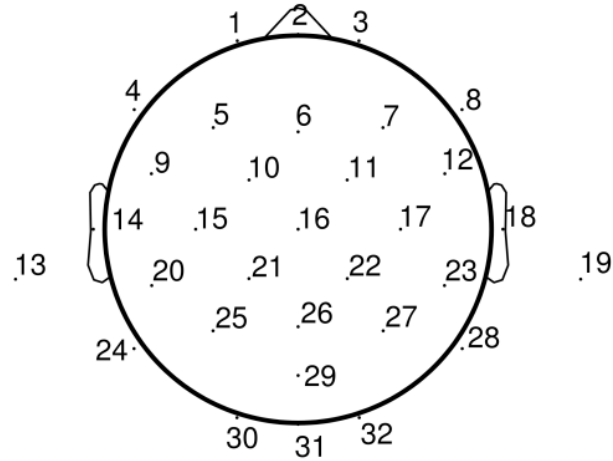


Figure 4.2: Among the 32 used electrodes, two were placed at the ears for potential re-referencing. The other electrodes were chosen on main brain areas like occipital and parietal ones.

As recalled in [9], for each EEG channel m , SSVEP power $P_m(f)$ can be defined as:

$$P_m(f) = 2 \times |F_m(f)|^2 \quad (4.1)$$

where $F_m(f)$ is the maximum of the FFT estimate of the Fourier coefficient in a narrow frequency band centred at the stimulus frequency. The maximum was a much more robust solution to the slight difference between controlled frequency and observed frequency from the LED panel. The

noise power $N_m(f, \delta f_N)$ was estimated in a wide frequency band $f \pm \delta f_N$ centred on the stimulus frequency but excluding the narrow frequency band. The narrow frequency band was set in the [0, 0.1] Hz interval and the wide frequency band was set in the [0.1, 0.5] Hz interval.

Considering the previous definitions, SNR is thus defined as:

$$SNR_m(f) = \frac{P_m(f)}{N_m(f, \delta f_N)} \quad (4.2)$$

In order to depict the results that are not due to statistical fluctuations of noise, a one-tailed 95% distribution threshold was applied based on the non SSVEP responses. Indeed, SNR fluctuations were measured by computing SNRs at non-flickering frequencies, excluding harmonics of the stimulated frequency. The obtained distribution followed a lognormal distribution. By computing the logarithm and fitting a normal curve, the threshold at 95 % can be easily found as shown in Figure 4.3. This procedure allows to only focus on SSVEP SNRs that are unlikely due to noise (in dark blue in figures). For each dual condition (movement type and luminosity), all the SNR results across frequencies and electrodes are depicted in a matrix figure. Rows correspond to a flickering frequency and columns represent the electrodes mentioned in Figure 4.2.

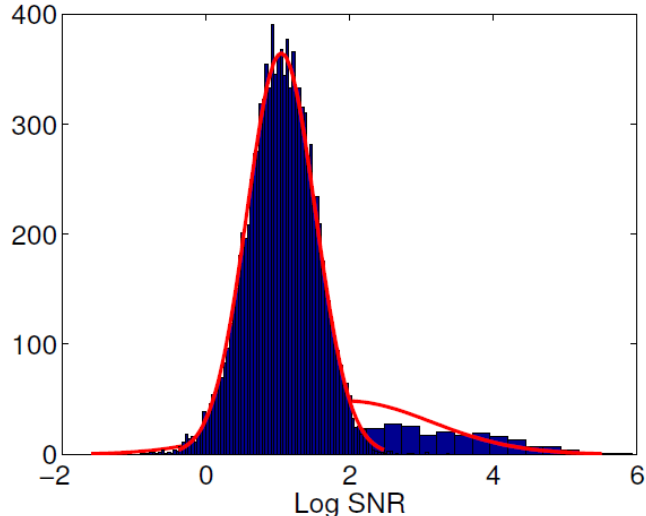


Figure 4.3: The SNR distribution consists in two different parts. The first Gaussian distribution is attributed to the SNR fluctuations of non-SSVEP responses. The second part is related to the elicited SSVEP responses.

4.3 Results and Discussion

In this section, the main results are depicted while discussing both the luminosity and movement parameters. Results are discussed upon SNR measures but a complementary analysis of signal and noise is provided to define some potential reasons of the observed results.

In terms of luminosity, results are somehow expected. As depicted in Figure 4.4, the mean SNR computed with O1, Oz, O2 and POz for each flickering frequency is higher when luminosity is increased. It clearly appears that a higher luminosity improves the contrast between areas with and without SSVEP responses. This phenomenon was observed on all subjects. By analysing the signal component of the SNR computation, we observed that this increase was due to a higher brain response. Logically, when a SSVEP response is insufficient compared to the noise level for a given luminosity, a higher luminosity allows it to be observed. Thereby, the luminosity can have a strong impact on what could be the efficient response frequency range of the stimulus and which areas to consider when designing an SSVEP-based BCI. Otherwise, the common average referencing effect could be observed in frontal part: an increase of the SNR in standard non-responding areas, which is in phase opposition.

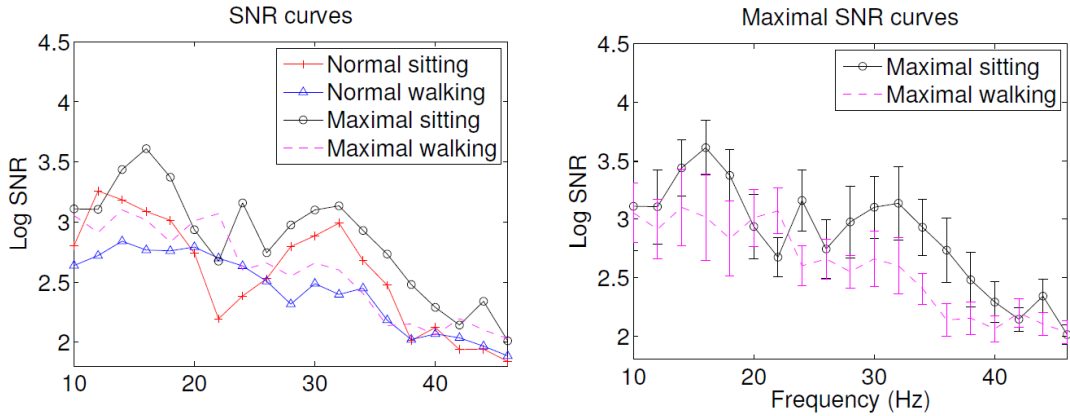


Figure 4.4: Over the eight subjects, the SNR curves for all conditions show that a higher luminosity leads to a curve translation. The sitting curves are similar to the state-of-the-art knowledge whereas the walking curves have diminished resonance peaks due to EMG artefacts. Standard errors report a high variability between subjects.

As shown in Figure 12.1, under sitting conditions, although the results are somehow heterogeneous among the subjects, a fairly standard behaviour is observed. The SSVEP potentials are mainly located in the occipital (8/8, i.e. in 8 out of 8 subjects)/parietal-occipital (8/8)/parietal (6/8) areas as expected. For one subject shown in Figure 4.6, there was a SSVEP response only in the occipital area whatever the conditions. Moreover, some significant -but lower- responses are elicited in the central (5/8)/centro-parietal (6/8) area close to the midline. These results are coherent with previous studies which reported the presence of two global peaks ranging from 5 to 28 Hz and from 28 to 36 Hz [6, 9].

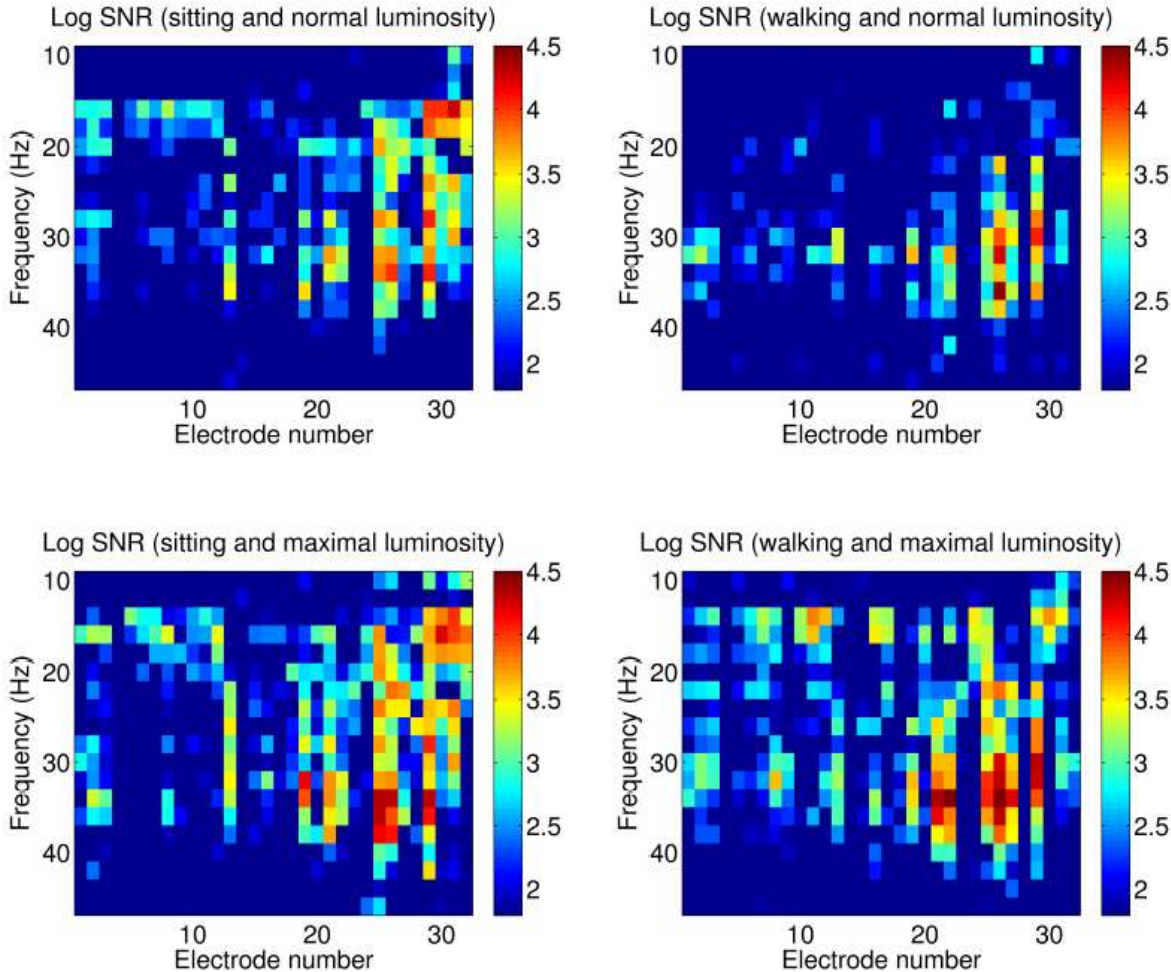


Figure 4.5: The main SSVEP response is located in the occipital/parieto-occipital/parietal areas (dark blue represents non significant SNRs). Obviously, a higher luminosity implies a higher SNR response. Moreover, some SSVEP responses disappear or decrease in some frequency bands while walking. It could be due to mechanical and muscle artefacts or spontaneous brain signal interference. These plots were obtained for one representative subject.

In comparison, for most of the recorded subjects, walking conditions may not be seen as a transparent process for the SSVEP paradigm. First, for most subjects as shown for a representative subject in Figure 4.6, the occipital SNR magnitude appears to decrease (and sometimes vanishes). O1 and O2 electrodes are the most affected sensors while Oz and POz produce robust SNRs. This seems to be due to EMG artefact pollution from the neck. Indeed, as illustrated in Figure 4.7 for one representative subject, Electromyographic (EMG) signals feature a large frequency band activity from 1 Hz to 30/45 Hz, especially in the beta and gamma band. By analysing the signal and the noise components, we obviously observed that the signal is most

of the time slightly increased (due to the addition of EMG signals) while the noise is strongly increased over all the analysed frequencies as illustrated in Figure 4.8. This artefactual origin was also checked with Independent Component Analysis (ICA) on several representative recordings.

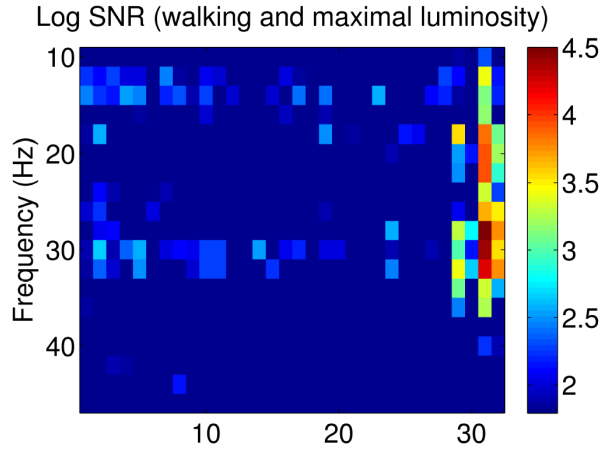


Figure 4.6: For this subject, walking does not modify a lot the SNR distribution. Under both conditions, the SSVEP response is located in the occipital area (electrodes 29 to 32).

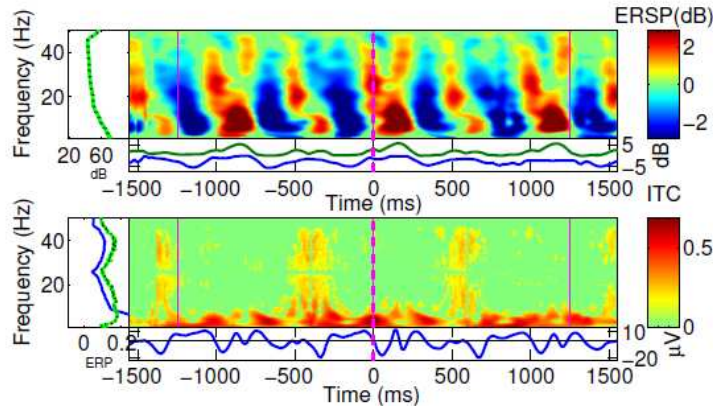


Figure 4.7: For this representative subject, muscular artefacts are present in our frequency range of interest. Also, there is a strong Inter Trial Coherence below 10 Hz suggesting a mechanical artefact. The time 0 represents the right heel strike.

Second, as depicted in Figure 4.9, the SNR magnitude seems to be slightly reinforced for 3 subjects (that had activity in these areas while sitting) in the fronto-central, central and centro-parietal areas close to the midline that could go up to 16-26 Hz depending on the subjects. This may correspond to the feet area on the homunculus over the motor/sensorimotor areas. However, we did not observe a strong decrease in the noise, i.e. a general decrease of the alpha band spectrum, in this frequency band as suggested by [12]. Therefore, this effect should be

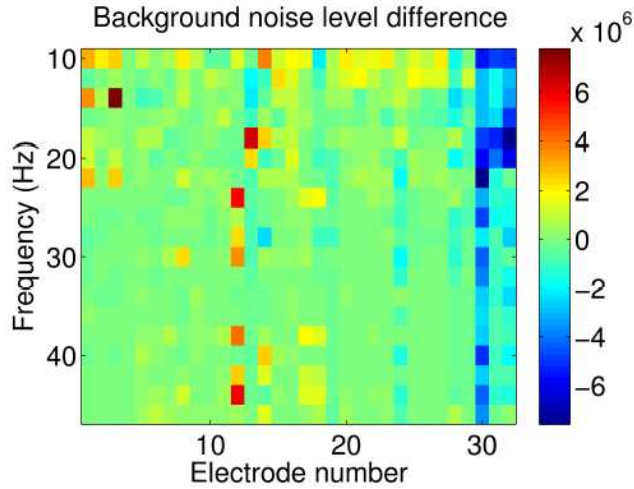


Figure 4.8: For one representative subject, the difference between sitting and walking conditions of background noise level indicates that there is much more noise in the occipital area under walking conditions (blue). The EMG artefacts affect more the O1 and O2 electrodes than the midline occipital Oz and POz electrodes.

mitigated.

The SNR increase was thus mainly due to an increase in the SSVEP brain response to the stimulus. The previous statements should exclude a potential explanation due to EMG artefacts. Actually, these should impact the noise level instead of the signal only. By looking at the raw data, we sometimes observed that stepping frequency harmonics were present at a stimulated frequency. However, this was seldom detected and although this effect should not be discarded, it should be fairly mitigated. Another potential explanation could be an actual shorter distance between the screen and the subject during the walking experiment than in the sitting case despite the recalibration between each frequency session. By checking the signal component, we did not observe a general signal level increase but it looks like a more selective area-based increase. This effect should not be due to common average reference (the increase is not uniform). Finally, an impact of gait on the subject's attention can not be excluded as attention has an impact on the SSVEP response [13]. This could potentially explain the observed results on some subjects. However, this aspect will need a devoted experiment to precisely discover what the effects are.

For one subject, a shift of the activated frequency band was observed as depicted in Figure 4.10. Indeed, under sitting conditions, two frequency bands are mainly responsive: 10-20 Hz and 28-36 Hz whereas under ambulatory conditions, the single main area corresponds to the 18-28 Hz without any explanation. By looking at the signal and noise components, we discovered that the reason of this behaviour is twofold. First, the signal is strongly increased in the 18-28 Hz. Second, the noise is increased due to muscle artefacts making disappear some frequency bands.

Finally, the overall impact of gait on the occipital area SSVEP response is clearly visible on Figure 4.4. Under walking conditions, these peaks are much less strong. This behaviour is mainly explained by a relative constant SSVEP signal concurrently to an increase of noise due

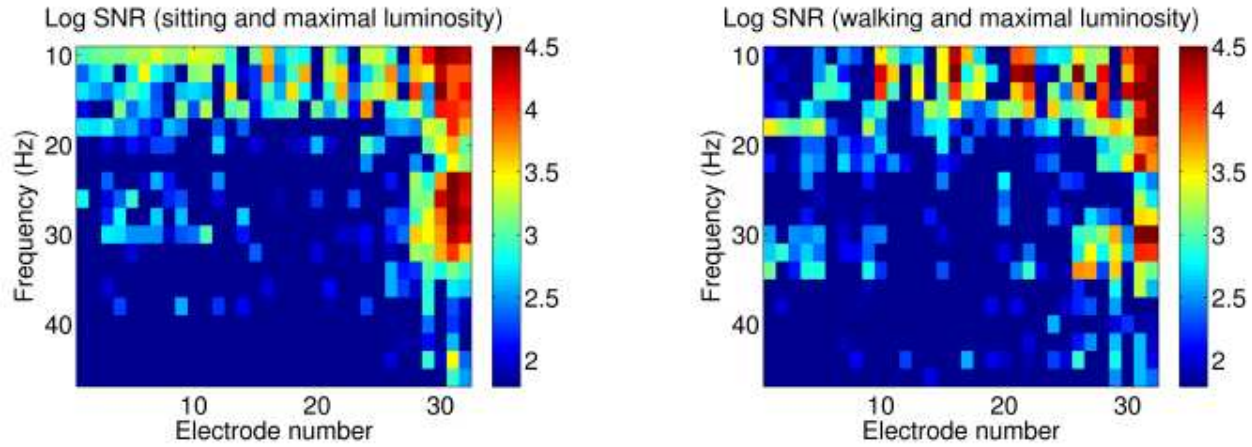


Figure 4.9: For this subject, a reinforcement can be observed in the fronto-central, central and centro-parietal areas close to the midline below 16 Hz while walking. This may correspond to the feet localization on the homunculus over the motor/sensorimotor areas.

to EMG artefact pollution. By computing a two-way repeated measure ANOVA, we detected a significant decrease of the SNR between sitting and waking conditions with a large effect size ($F(1, 7) = 6.19$, $p = 0.042$, partial $\eta^2 = 0.469$). This observation would mean that using sufficient and dedicated gait-related artefact removal method could lead to a similar SNR curve as under sitting conditions. Some leads to remove those artefacts are currently studied by some researchers including Independent Component Analysis, Canonical Correlation, *etc* [2].

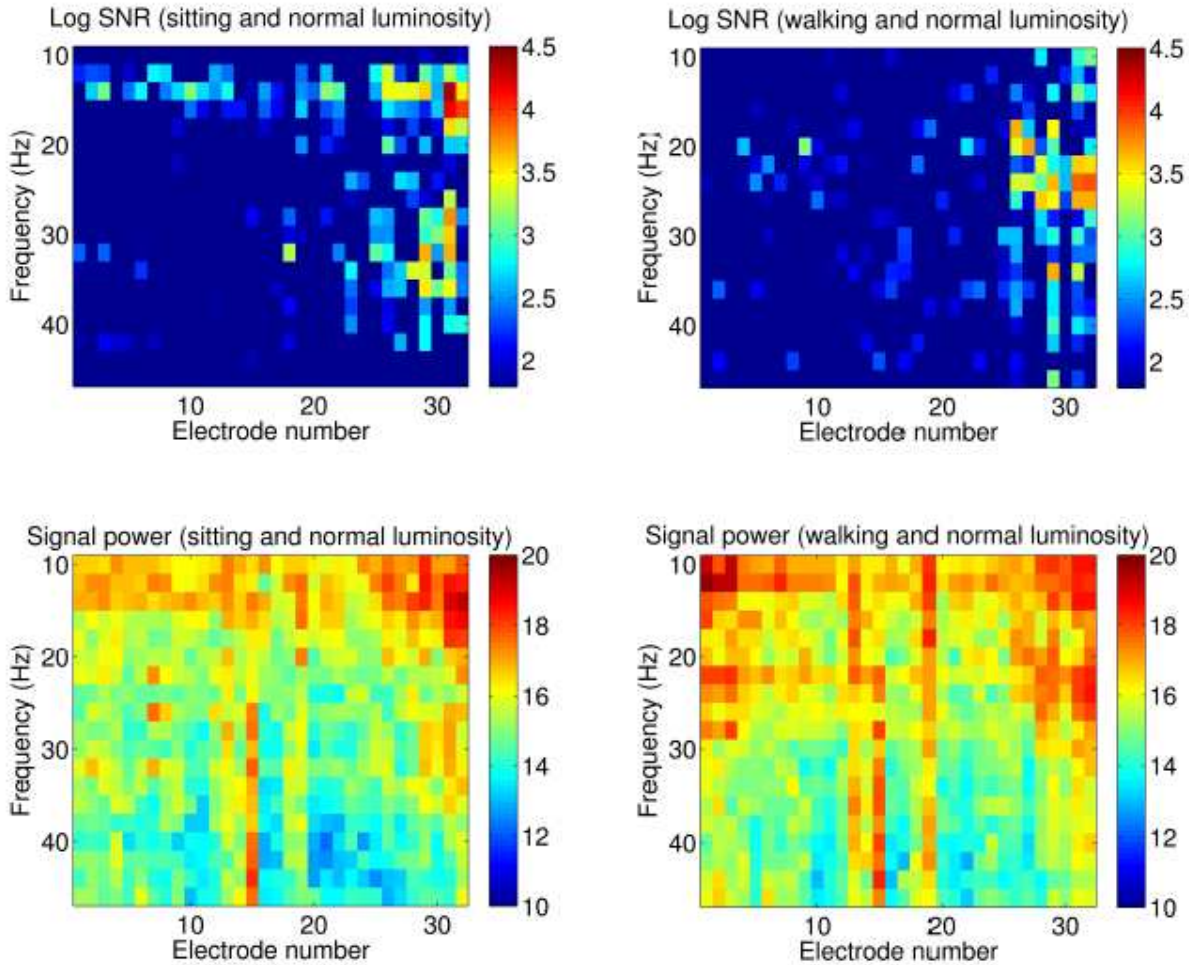


Figure 4.10: With a normal luminosity, most of the responsive frequency bands are disappearing under normal walking conditions while another frequency band is popping up. This is mainly due to a localized increase of the signal combined with a widespread increase of the EMG pollution.

4.4 Conclusions

In this Chapter, the impact of luminosity and movements on the SSVEP response distribution is studied. This aims at giving indications to how adverse movements can affect the SSVEP paradigm. In order to decrease the abandonment rate of BCI patients for out-of-the-lab applications, these hostile conditions could help to better design a potentially more widely spread ambulatory BCI.

In this experiment, the LED-based stimulus frequency ranges from 10 Hz to 46 Hz by 2-Hz step. Normal and maximal luminosity were envisaged. Moreover, sitting and ambulatory conditions were studied. The analysis was based on Signal-to-Noise Ratio (SNR) without any artefact removal techniques. This analysis method aims at showing what an EEG recording sys-

tem would record as differences between walking and sitting conditions and determine if further specific artefact care would be required.

Luminosity has an evident effect: it increases the SNR values. This was observed by a translation of the SNR curve and an increased SSVEP power while keeping a constant background noise.

Under sitting conditions, although somehow heterogeneous between subjects, coherent results with the literature were obtained. SSVEP responses were mainly detected in the occipital, parieto-occipital and parietal areas. Moreover, some significant -but lower- responses are elicited in the central and centro-parietal area close to the midline. In the occipital area, the two frequency response peaks are much weaker (around 15 Hz and 31 Hz).

Under ambulatory conditions, some modifications in the measured responses appear. First, for most subjects, the occipital SNR magnitude appears to decrease (and sometimes vanishes). This is mainly due to EMG artefacts from the neck that affect the background noise. Second, the SNR magnitude seems to be slightly reinforced for 3 subjects in the fronto-central, central and centro-parietal areas close to the midline that could go up to 16-26 Hz depending on the subjects. This reinforcement is mainly due to an increase of the SSVEP signal. However, further and more detailed investigations would be needed to understand this behaviour.

As future work, two aspects could be interesting. First, understanding the reinforcement origins obtained for several subjects would help the design of SSVEP BCIs. Then, the use of optimal dedicated gait-related artefact removal methods would lead to a SNR curve similar to the one observed under sitting conditions. Some leads to remove those artefacts are currently studied including Independent Component Analysis, Canonical Correlation, *etc* [2, 3]. The occipital sitting SNR curve could be used as a target in the learning process of those techniques. Finally, a subjective comparison between an ambulatory SSVEP and other paradigms would benefit the BCI community [14].

Bibliography

- [1] H. Touyama. A study on eeg quality in physical movements with steady-state visual evoked potentials. In *Engineering in Medicine and Biology Society (EMBC), 2010 Annual International Conference of the IEEE*, pages 4217 –4220, 31 2010-sept. 4 2010.
- [2] Yuan-Pin Lin, Yijun Wang, and Tzzy-Ping Jung. A mobile ssvep-based brain-computer interface for freely moving humans; the robustness of canonical correlation analysis to motion artifacts. In *Engineering in Medicine and Biology Society (EMBC), 2013 Annual International Conference of the IEEE*, 2013.
- [3] Yu-Te Wang, Yijun Wang, Chung-Kuan Cheng, and Tzzy-Ping Jung. Developing stimulus presentation on mobile devices for a truly portable ssvep-based bci. In *Engineering in Medicine and Biology Society (EMBC), 2013 Annual International Conference of the IEEE*, 2013.
- [4] Andrew Campbell, Tanzeem Choudhury, Shaohan Hu, Hong Lu, Matthew K. Mukerjee, Mashfiqui Rabbi, and Rajeev D.S. Raizada. Neurophone: brain-mobile phone interface using a wireless EEG headset. In *Proceedings of the second ACM SIGCOMM workshop on Networking, systems, and applications on mobile handhelds*, MobiHeld ’10, pages 3–8, New York, NY, USA, 2010. ACM.
- [5] C S Herrmann. Human eeg responses to 1-100 hz flicker: resonance phenomena in visual cortex and their potential correlation to cognitive phenomena. *Exp Brain Res*, 137(3-4):346–53, 2001.
- [6] Yijun Wang, Ruiping Wang, Xiaorong Gao, Bo Hong, and Shangkai Gao. A practical vep-based brain-computer interface. *Neural Systems and Rehabilitation Engineering, IEEE Transactions on*, 14(2):234–240, 2006.
- [7] Ivan Volosyak. SSVEP-based bremen BCI interface boosting information transfer rates. *Journal of Neural Engineering*, 8(3):036020, 2011.
- [8] Zhenghua Wu, Yongxiu Lai, Yang Xia, Dan Wu, and Dezhong Yao. Stimulator selection in SSVEP-based BCI. *Medical Engineering and Physics*, 30(8):1079 – 1088, 2008.
- [9] Ramesh Srinivasan, F. Alouani Bibi, and Paul L. Nunez. Steady-State Visual Evoked Potentials: Distributed Local Sources and Wave-Like Dynamics Are Sensitive to Flicker Frequency. *Brain Topography*, 18(3):167–187, March 2006.

- [10] Arnaud Delorme and Scott Makeig. Eeglab: an open source toolbox for analysis of single-trial eeg dynamics including independent component analysis. *Journal of Neuroscience Methods*, 134(1):9 – 21, 2004.
- [11] Yann Renard, Fabien Lotte, Guillaume Gibert, Marco Congedo, Emmanuel Maby, Vincent Delannoy, Olivier Bertrand, and Anatole Lécuyer. Openvibe: An open-source software platform to design, test, and use brain–computer interfaces in real and virtual environments. *Presence: Teleoper. Virtual Environ.*, 19(1):35–53, February 2010.
- [12] A. Presacco, R. Goodman, L. Forrester, and J.L. Contreras-Vidal. Neural decoding of treadmill walking from noninvasive electroencephalographic signals. *J Neurophysiol*, 106(4):1875–87, 2011.
- [13] Ding, Jian, Sperling, George, Srinivasan, and Ramesh. Attentional Modulation of SSVEP Power Depends on the Network Tagged by the Flicker Frequency. *Cerebral Cortex*, 16(7):1016–1029, July 2006.
- [14] M. Duvinage, T. Castermans, M. Petieau, K. Seetharaman, T. Hoellinger, G. Cheron, and T. Dutoit. A subjective assessment of a p300 bci system for lower-limb rehabilitation purposes. In *Engineering in Medicine and Biology Society (EMBC), 2012 Annual International Conference of the IEEE*, pages 3845–3849, 2012.

Chapter 5

Effectiveness of Gait-related Artefact Removal Methods on P300 BCI Performance

Contents

5.1	Introduction	111
5.2	BCIs in ambulatory conditions: a state of the art	111
5.2.1	Artefacts present in EEG recordings	111
5.2.2	Artefacts typically related to gait	112
5.2.3	An ambulatory BCI system based on auditory P300 potentials	112
5.2.4	An ambulatory BCI system based on steady-state evoked potentials	113
5.2.5	Proposed methods to remove gait-related artefacts	114
5.3	Experimental procedure and data analysis	116
5.3.1	Data collection	116
5.3.2	Pre-processing	117
5.3.3	Identification and correction of gait artefacts	119
5.3.4	Feature extraction	121
5.3.5	Classification	122
5.4	Results and discussion	122
5.4.1	Efficiency of the methods in terms of EEG signal properties	124
5.4.2	Efficiency of the methods in terms of P300 classification performance	124
5.4.3	Classification performance using spatial filtering	125
5.4.4	Classification Performance Using The Optimal Configuration	126
5.5	Conclusion	128

Abstract

EEG-based Brain-Computer Interfaces (BCI) could enable their users to control a CPG-based lower-limb device. However, the ambulatory performance of a P300-based interface is still widely unknown. Except for some pioneering works, most of the P300 BCI studies have analysed brain signals while strongly limiting artefacts coming from movement: people were explicitly asked to avoid moving and decreasing the EEG quality. Thus, current BCI technology requires that the user sits and performs as little movements as possible. This is of course a strong limitation for use in ordinary life.

In this Chapter, we thoroughly investigate the possibility to develop a P300-based BCI system under ambulatory conditions. The study is based on experimental data recorded with seven subjects performing a visual P300 speller-like discrimination task while simultaneously walking at three different speeds on a treadmill.

It is demonstrated that a P300-based BCI is definitely usable in such conditions. Different artefact correction methods relying on independent component analysis and template subtraction are described and discussed in details. However, none of the methods outperforms the filtered (preprocessed) raw data approach. Additionally, for real-time applications requiring low-complexity, the results suggest to use seven electrodes for a good trade-off between performance and compactedness.

This chapter is based upon the following publication:

- **M. DUVINAGE, T. CASTERMANS, M. PETIEAU, G. CHERON, T. DUTOIT, 2012, "Are current gait-related artifact removal techniques useful for low-complexity BCIs?", IEEE World Congress On Computational Intelligence (IEEE WCCI), Brisbane, Australia, June 10-15.**
- **T. CASTERMANS, M. DUVINAGE, M. PETIEAU, T. HOELLINGER, C. DE SAEDELEER, K. SEETHARAMAN, A. BENGOETXEA, G. CHERON, T. DUTOIT, 2012, "Optimizing the performances of a P300-based Brain-Computer Interface in ambulatory conditions", IEEE Journal on Emerging and Selected Topics in Circuits and Systems, vol. 4, n. 4, December 2011, pp. 566 - 577.**

5.1 Introduction

Due to artefacts, very few studies are found in the literature concerning brain-computer interfacing, and more specifically the P300 potential, outside of the lab, e.g. in ambulatory context. But, as for the SSVEP potential, if we are interested in a daily life BCI that may suffer from adverse conditions, a deeper knowledge of the potential impact on performance of these realistic conditions should be considered [3].

Therefore, this Chapter focuses on a quantitative analysis of the performance of a P300-based BCI system while the user is walking on a treadmill. Then, new artefact correction methods to optimize this kind of BCI have to be proposed and assessed. In Section 5.2 the origin of artefacts present in EEG recordings is described with a particular emphasis on those typically related to gait. First studies of BCI in ambulatory conditions are then reviewed, as well as signal pre-processing techniques proposed in the literature to correct gait artefacts affecting EEG. In Section 5.3 an overview of the methodology used in this analysis is given, the experimental procedure for data collection is described and the proposed pre-processing methods to correct gait artefacts in EEG are explained. Classification performances of the BCI obtained using the different pre-processing methods are then presented and discussed in Section 5.4.

5.2 BCIs in ambulatory conditions: a state of the art

5.2.1 Artefacts present in EEG recordings

EEG artefacts are spurious signals present in recordings and whose origin is not cerebral. They may arise from the patient itself: the eyes, the tongue, the pharyngeal muscle, the scalp muscles, the heart or the sweat glands all produce electrical potentials which can influence the EEG measurement, especially if they are in movement. Skin resistance changes due to sweating may also badly affect the signals. Electrical interference with power line or surrounding electrical apparatus is another source of artefacts which may be induced electrostatically or electromagnetically. Finally, artefacts may also arise from faulty electrodes or the recording equipment itself.

In many cases, artefacts can be immediately identified by visual spatial analysis: high amplitude potentials appearing at only one electrode are not likely due to cerebral activity. Indeed, brain produces potentials that exhibit a physiological distribution characterized by a maximum voltage amplitude gradually decreasing with increasing distance over the scalp. Likewise, rhythmical or repetitive irregular signals appearing simultaneously in non-adjacent brain areas strongly suggest the presence of artefacts [2].

Algorithms designed to detect and correct EEG artefacts integrate these principles and exploit techniques like temporal filtering, spatial filtering, Independent Component Analysis (ICA) [4, 5], blind source search (BSS) [6] or thresholding of meaningful parameters (e.g. channel variance) based on a prior statistical analysis [7].

5.2.2 Artefacts typically related to gait

In addition to “traditional” artefacts explained above, EEG recordings realized in ambulatory conditions present typical artefacts.

Triboelectric noise is generated by movement, friction and flexion of the cable components, resulting in a static or piezoelectric movement transducer effect [8].

Electrode movements are produced by movements of the head, but also by the shocks undergone by the whole body at each step, which – albeit significantly attenuated – are transmitted to the head [9]. These movements modify the magnetic and capacitive coupling of the user and the electrode leads, leading to an alteration of the parasitic current flowing into the leads [10]. A resulting parasitic voltage drop is then produced in the electrode/gel/skin interface which interferes with the EEG signal [11]. Finally, electrode movements can also cause impedance variation which directly affects the electrode voltage offset [12].

Unfortunately, all these *motion artefacts* are not limited to a small spectral band, so they cannot be simply removed by frequency filtering. In a study conducted to assess EEG signal quality in motion environments [13], it is shown that EEG spectra in the walking (or jogging) condition exhibit frequency peaks consistent with the fundamental stride frequency as well as its harmonics. The authors also state that motion artefacts affect signal integrity most prominently at low frequencies (i.e. the delta band) during steady walk. Nevertheless, the study also shows that traditional N1 and P300 event-related potentials (ERP) elicited during a standard *auditory* discrimination task (i.e. “oddball paradigm”) are not dramatically affected by the walking condition, either in amplitude, in topographic distribution or response time (70% of acceptable trials across all participants). This is however not the case for the jogging condition, for which only 14% of trials were accepted.

Analog conclusions are drawn in a more recent study where subjects are standing or walking on a treadmill while performing a *visual* oddball response task [14]. Applying independent component analysis on their data, the authors could extract visual ERP that were quite similar during standing, slow walking and fast walking.

These two studies thus suggest that recording brain activity accompanying cognitive process during whole body movement is feasible.

5.2.3 An ambulatory BCI system based on auditory P300 potentials

In 2009 was published the first study testing the feasibility of an ambulatory BCI system based on *auditory* P300 potentials [15]. This study was performed with five healthy subjects using only three electrodes (Cz, CPz and Pz) in order to minimize the size of the BCI system. Active electrodes were used. Such electrodes are equipped with a pre-amplifier stage magnifying the signal before sending it to the main amplifier. This is known to greatly reduce cable movements artefacts compared to conventional electrodes [16]. The subjects wore headphones in which two different kinds of sound were generated every second, in a random order. The target auditory stimulus was a “Ding Dong” tone, whereas the sound of a buzzer was chosen for the non-target stimulus. The target stimulus appeared less frequently than the other one and had to be counted by the user. Such rare and relevant stimulus thus triggered a P300 potential in the EEG signals. The experiment was reproduced in three different conditions: sitting, standing and walking.

Each subject participated in four sessions composed of 150 auditory stimuli, for each condition.

The authors used the following processing technique to detect the P300 potentials. Epoching was done by selecting a window of 600 ms starting immediately after the stimulus. The signals were band-pass filtered between 1 and 14 Hz and winsorized (i.e. for each time window and each channel, the 5% most extreme values were replaced by the most extreme value from the remaining 95% samples of that window and that channel). Finally, the dimensionality (and thus the complexity) of the subsequent classification problem was reduced by downsampling the signals to 25 Hz. The residual EEG samples were then concatenated into feature vectors, of which a subset was selected using the Sequential Forward Floating Search (SFFS) feature selection algorithm [17]. Selection of this subset of features was optimized by maximizing the area under the ROC curve [18]. Classification of trials in target or non-target categories was done using a Linear Discriminant Analysis (LDA) classifier, using single trial analysis (i.e. without averaging multiple trials to enhance their signal to noise ratio).

For all experimental conditions, the authors obtained area under the ROC curve values higher than for the case of a random classification. These results suggest that developing a P300-based BCI system in walking condition is realistic, even using only three electrodes, and on the basis of a single trial analysis. As expected, results obtained in the walking condition were overall not as good as for the other conditions. But surprisingly, the authors observed that best performances could be obtained, in some cases, in standing or even walking condition (i.e. not during sitting, which was though expected to be the least noisy condition). The motivation of the users is here thought to have played an important role in the results obtained.

5.2.4 An ambulatory BCI system based on steady-state evoked potentials

A similar feasibility study was published in 2010 [19]. In this case, the authors focused on the steady-state visually evoked potentials (SSVEP) instead of the P300 potentials. SSVEP are widely used to realize BCI systems [20] and are known to give the highest information transfer rates [21]. The experiment was conducted with one subject, using a limited number of active electrodes located on the parietal and occipital regions, which cover the visual cortex (P7, PO7, O1, Oz, O2, PO8 and P8). Two visual stimuli flickering respectively at 4 and 6 Hz were simultaneously presented on a computer display (one located at left side and the other one on the right side). The subject was asked to look at one of the two visual stimuli. EEG signals were recorded in two different experimental conditions: in the first condition, the subject was comfortably sitting on a chair and was not allowed to move. In the second condition, the subject was walking in place, to mimic real walk and thus create similar muscle and motion artefacts. For each of the two conditions, six sessions of 30 seconds each were recorded.

To optimize the detection of the SSVEP induced by the flickering stimuli, the authors tested three ways of segmenting the EEG data, by selecting time windows from 1 to 3 seconds. The signals were band-pass filtered between 1 and 30 Hz, in order to reduce high frequency noise (and by the way power line interference) while keeping several harmonics of the visual stimuli. Different spatial filters were also tested in order to reduce the artefacts or environmental noise. Power spectral densities were computed, and a subset of these was selected using principal component analysis (PCA). This technique was used to reduce the dimensionality of the classification problem and to select the subset of features which maximized the classification performance. An

LDA classifier was used to discriminate EEG signals which were characteristic of the stimulus at 4 Hz or at 6 Hz.

This analysis showed evidence of clear SSVEP including their harmonic signals in either experimental conditions, thus even while performing physical movements. Globally, more classification errors were made in the movement conditions. However, using the longest time window (3 s) and a particular combination of EEG electrodes (PO7 + PO8 - 2 Oz), the classification performance could reach 100% in both experimental conditions.

The results of this study suggest thus that SSVEP-based BCI systems can be realized even in the physically moving context. This opens a new research field, i.e. interfacing new applications with a BCI system in ordinary life.

5.2.5 Proposed methods to remove gait-related artefacts

The two latter pilot studies show that standard neurophysiological phenomena (namely P300 and SSVEP potentials) widely used in BCI can be detected satisfactorily even when the subjects are moving. No special technique was used in these studies in order to reject, correct or even detect motion artefacts generated by the subjects. It is an interesting question to wonder to what extent BCI performances can be improved using preprocessing techniques dedicated to the correction of motion artefacts. To our knowledge, two methods have been proposed and discussed in the literature in order to reach this goal. They are described below.

Template subtraction

Artefact template subtraction procedures have been applied successfully for example to correct EEG signals that were strongly corrupted by fMRI gradient artefacts during functional magnetic resonance imaging [22] or generated by the electrical impulses sent to specific parts of the brain during deep brain stimulation [23]. In short, this technique consists in developing an “idealized” template of the artefact by averaging several of its occurrences. Once computed, this average template is then simply subtracted from the individual corrupted signals. Of course, applying this technique may also remove useful information present in the EEG if it is phase-locked with the artefact.

Recently, this technique has inspired researchers aiming at exploring brain dynamics associated to cognitive processes during whole body movements [24]. In their experiment, subjects performed a visual oddball discrimination task while simultaneously walking or running on a treadmill. To correct locomotion-induced motion artefacts, the authors developed a two-step approach.

First, they removed stride phase-locked mechanical artefact using a channel-based template regression procedure based on time warping. Moving time-window averaging of the stride phase-locked data was used to compute an artefact template for each stride and each channel. In practice, the 10 preceding and the 10 following strides were used for computing the template (this procedure was repeated for each stride).

Then, they applied an adaptive independent component analysis (ICA) mixture model algorithm (AMICA) to decompose EEG signals into spatially static, maximally independent compo-

net (IC) processes [25]. The goal of this second step was to further refine the artefact cleaning process. The authors found that, unlike more spatially stationary artefacts like blinks, eye movements or scalp muscles – which can generally be resolved by ICA decomposition in a few different ICs – gait-related movement artefacts remain on many if not most of the independent components. It was thus not possible for them to reject only a small subset of components totally capturing artefacts. Instead, they applied the same template regression procedure as the one applied to the channel data to obtain artefact-reduced independent components and hence [26], a second set of artefact-reduced EEG signals.

To determine the performance of this two-step artefact removal approach, the authors computed the power spectral density of the EEG signals before and after applying artefact removal. They found no evidence of overcorrection of EEG signals. The authors also compared – by visual inspection – the event-related potentials (ERP) of artefact-reduced datasets to uncorrected ERPs recorded while standing. In walking condition, gait-related artefact was not really significant, as ERPs were found to be nearly identical to visual oddball discrimination events obtained while standing. In contrast, for the running condition, stable and meaningful ERPs were only detectable after artefact removal.

The authors thus conclude that high-density EEG can be used to study brain dynamics during whole body movements and that mechanical artefacts from rhythmic gait events may be minimized using a template regression procedure.

Again, it has to be emphasized that the goal of this study was not directly to develop a BCI system during locomotion, and as such, no conclusion about the impact of this method on the performance of the classification results of a BCI system has been given. Such study will be shown in section 5.4 of this Chapter.

Adaptive filtering

The idea to use an independent (and direct) estimation of the artefacts corrupting signals in order to cancel them is widespread in the literature. The technique able to realize such operation is called *adaptive filtering*. Adaptive filtering is a very efficient method for discriminating signal of interest and artefact, in the difficult case where both have overlapping spectra.

Figure 5.1 illustrates the general structure of an adaptive filter used for noise cancelling. The “reference” signal $x(n)$ is entering a linear filter $H(z)$ which produces an output signal $y(n)$. This output is subtracted from the “corrupted” signal $d(n)$ to compute an error $e(n)$. The goal of adaptive filtering is to minimize the error $e(n)$ by adapting the response of the filter in order to produce an output signal $y(n)$ as close as possible to the noise present in the signal to be filtered. Then, the corrupted signal is simply corrected by subtraction.

In this scheme, it is assumed that the corrupted signal $d(n)$ is composed of the signal of interest $s(n)$ and noise $n_0(n)$, which is additive and not correlated with $s(n)$. Likewise, the reference $x(n)$ must be uncorrelated with $s(n)$ and correlated with $n_0(n)$. The reference $x(n)$ feeds the filter to produce an output $y(n)$ that is a close estimate of $n_0(n)$. The corrupted signal is then “cleaned” by a simple subtraction.

The coefficients of the linear filter are changed (adapted) – and hence its frequency response – to generate a signal similar to the noise present in the signal to be filtered. The adaptive

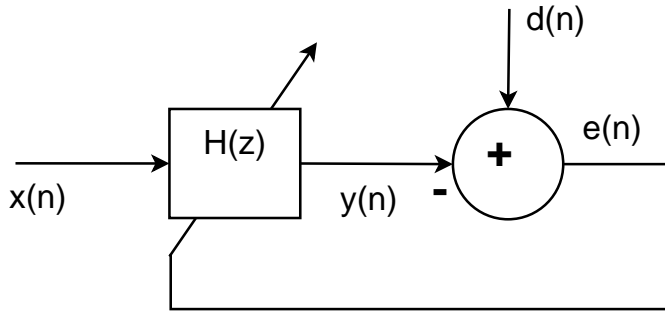


Figure 5.1: Adaptive filter used as a noise canceller. The “reference” signal $x(n)$ is entering a linear filter $H(z)$ producing an output signal $y(n)$, which is subtracted from the “corrupted” signal $d(n)$ to compute an error $e(n)$. This error is minimized by adjusting the coefficients of the filter.

process involves minimization of a cost function, which is used to determine the filter coefficients. Different strategies have been developed to realize the optimization of the filter coefficients, defining different categories of adaptive filters. Examples of well known adaptive filters are the LMS (Least Mean Squares) and RLS (Recursive Least Squares) filters [27].

Applications of this technique in biomedical signals are, for example, removal of maternal electro-cardiogram (ECG) in fetal ECG records [28], detection of ventricular fibrillation and tachycardia [29], and cancellation of heart sound interference in tracheal sounds [30].

In the field of electroencephalography, many papers have been written about cancellation of ECG or ocular artefacts (blinks, eye movements) using adaptive filters. Surprisingly, the technique of adaptive filtering has not been studied to remove motion artefacts. To our knowledge, only a US patent exists [31], describing a technique aimed at correcting both ocular and motion artefacts, on the basis of electrodes placed around the eyes for eye artefact correction, and based on the use of an accelerometer for the motion artefact correction.

In this work, we used adaptive filtering to remove motion artefacts and studied the impact of this technique on the performance of a BCI system based on P300 potentials while walking on a treadmill. Such study, among others, is shown in the next sections of this Chapter.

5.3 Experimental procedure and data analysis

5.3.1 Data collection

Seven healthy volunteers without any known physical or neurological disorders participated in this experiment (age-range: 25-33 years). Each subject realized the P300 experiment walking on a treadmill at 0.42, 0.83 and 1.25 m/s (i.e. 1.5, 3 and 4.5 km/h). A 20-inch computer screen was placed in front of the treadmill, at an approximate distance of 1.5 m of the subject. Figure 5.2 shows the simplified P300-speller interface used in this study. Excepted the reduced number of possible states (4), this interface is quite similar to the traditional P300-speller BCI system using a 6 by 6 matrix [32]. All procedures were approved by the Université Libre de Bruxelles Internal Review Board and complied with the standards defined in the Declaration of Helsinki.

In this experiment, the task of each subject was to look at the green target letter appearing during 3 seconds (not shown on the figure) and count how many times the letter flashed in the matrix afterwards. The rows and columns were flashed in random order. The flashing of the target letter triggered a positive involuntary so-called *P300 potential*, appearing with a time delay of about 300 ms [33]. Strictly speaking, this is not a real oddball paradigm. In fact, given that the target letter is flashed half of the time, the event can not really be considered as rare. However, under ambulatory conditions, specific augmented reality eyewear (Vuzix, Rochester, NY, USA) should be used by displaying stimuli on a semi-transparent module. Obviously, with this kind of system, it is not possible to use a lot of P300 states. Four target letters seem to be a good compromise given that they could be displayed on each corner.

During each *trial*, each row and each column were flashed one time in random order, so that the computer was able to determine which letter the subject was looking at, by using the intersection of the detected P300 responses. In each *trial*, the two lines and the two rows were randomly flashed during 0.2 s with 0.1 s between two flashes. Thus, the subject saw 2 times the target letter highlighted while the two other flashes did not highlight the target letter. Such *trial* was repeated 12 times for the same target letter. Between each *trial* was inserted a 1 s time interval. All this procedure was repeated for 25 target letters. In total, the subject thus saw $2 * 12 * 25 = 600$ times the target letter flashed, and then 600 flashes that did not highlight the target letter. All this procedure was recorded in one *session*, for one subject, at one given walking speed. Actually, there were 2 *sessions* walking at 3 km/h (the first for training the BCI, the second for testing it), one *session* at 1.5 km/h and one at 4.5 km/h (just for testing, as the training was done with the first dataset at 3 km/h). In total, 7 subjects participated in this study. The OPENVIBE software [34] was used to generate the stimuli on the screen and store the EEG signals on disk, as well as the time information of the different visual stimuli.

EEG was recorded using a 32-electrode cap connected to the ANT amplifier system (Advanced Neuro Technology, ANT, Enschede, The Netherlands) digitizing the signals at 512 Hz. Left ear was chosen as reference. Electrode impedance was measured and maintained under $20\text{ k}\Omega$ for each channel using electrode gel. Additionally, a Dytran 3100B piezoelectric accelerometer was plugged into an auxiliary channel of the ANT system. The accelerometer was fixed to a rigid structure strapped on the head of the subjects, as depicted in figure 5.3.

In parallel, the kinematics of the lower limb movements was recorded using a system of six infrared cameras (Bonita, Vicon, Los Angeles, USA) determining at a frequency of 100 Hz the 3D cartesian coordinates (x, y and z) of 23 passive markers disposed on the subjects. Kinematics and EEG data were synchronized using a common trigger signal sent to the two acquisition systems.

5.3.2 Pre-processing

In a first step, the time of important gait events were determined thanks to the kinematics data. Actually, two generic events are defined in human locomotion: the *heel strike*, which is the time of the first contact of the foot with the ground, and the *toe off*, which is the last instant of contact of the foot with the ground. These events are of course defined for both legs, so that 4 typical events follow one another during a gait cycle: the right heel strike (RHS), the left toe off (LTO),



Figure 5.2: Four states are possible in this simplified version of the P300-speller dedicated to send high-level commands (Stop, Low, Medium or High speed), for example, to an active ankle orthosis [3, 35, 36].



Figure 5.3: A piezoelectric accelerometer was placed on the head of the subjects to record acceleration undergone during gait.

the left heel strike (LHS) and finally the right toe off (RTO). During walk on treadmill, the time of these events can be determined as following : the heel strike is defined when the position of the malleolus marker is the most forward (in the treadmill axis direction), while the toe off is defined when the fifth metatarsal marker is in the most backward position [37].

The pre-processing of the EEG signals was inspired from the method described in [24]. After applying a high-pass filter (1 Hz), all the channels presenting a standard deviation above 1000 μ V were rejected. The channels with a kurtosis higher than five standard deviations from the mean were also removed. Finally, uncorrelated neighbor channels (i.e. correlation coefficient with nearby electrodes – distance \leq 3 cm – lower than 0.4 in more than 2 cases) were removed. The channels were then re-referenced to the average of the remaining channels. Generally, one to three channels were discarded by this procedure (in practice, this channel removal procedure did not remove the electrodes we were interested in). The EEGLAB software was used to treat EEG signals [4].

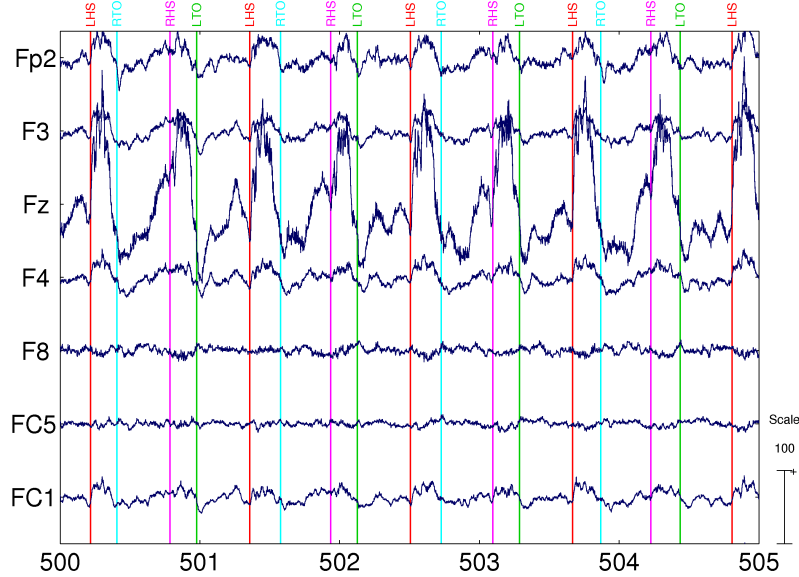


Figure 5.4: EEG recording of a subject walking on a treadmill at moderate speed (3 km/h). The amplitude of the Fz electrode is abnormally high and presents important oscillations directly related to the gait cycle. A similar – although less intense – phenomenon is observed for other electrodes. Heel strike and toe off events are indicated by the vertical lines. The unit of time is the second. Amplitudes of the signals are in μV .

5.3.3 Identification and correction of gait artefacts

After bad channel cleaning, several methods were used to correct, or at least decrease, the motion artefacts linked to gait, illustrated in figure 5.4.

Using a template subtraction method

The following treatment was applied to each channel, as described in [24]. The signals were epoched in gait cycles from one Right Heel Strike (RHS) to the following one. As the gait is a pseudo-periodic movement (the strides are similar but their lengths are different), each epoch was time-warped using EEGLAB toolbox so that the gait events (RHS, LTO, LHS, RTO) happened at the same relative time within each gait cycle. For each time-warped stride, a template artefact was computed by averaging the 10 preceding warped strides and the 10 following ones. Each template artefact was then subtracted from each time-warped stride. Finally, each time-warped stride was reverse time-warped to reconstruct a clean signal in the original time scale. This is the first part of the two-step approach developed in [24] and described in section 5.2.5.

After applying this channel-based artefact removal, the EEG signals were decomposed in independent components using ICA. The same procedure was then applied on the independent components obtained (i.e time-warping according to the gait events, template computing, subtraction and reverse time-warping). Finally, the signals were reconstructed by using the ICA mixing matrix. This is called “subtraction” method in the remainder of this Chapter.

In fact, when applying this method on our datasets, it appeared that ocular or muscular artefacts “polluted” certain artefact templates. Subtraction of such corrupted artefact templates gave rise to overall degradation of the EEG signals by introducing new artefacts that were not present in the original raw data. Therefore, a variant of the original subtraction method was tested, which simply consists in removing eye and muscle artefacts in EEG signals prior to computing the artefact templates. ICA was used to remove these standard well-known artefacts, following the method described in [26]. This variant is called “subtraction + ICA” method in the remainder of this Chapter.

A second drawback was encountered when implementing the original template subtraction method [24]. In fact, this method is based on the hypothesis that the artefacts due to the gait always happen at the same relative time within the gait cycle. In this way, the template built on the time-warped strides is justified and its subtraction is supposed to attenuate artefacts adequately. This is definitely not always the case. In our datasets, the artefacts definitely appeared linked to the gait events but were not always locked on them; the peaks happened *around* the same relative position but not *precisely* on it. This may be explained, for instance, by differing ways of stepping on the ground, sometimes energetically, sometimes very smoothly. Anyway, in these conditions, the fundamental hypothesis of the method is not verified, the template is not representative anymore of the artefacts affecting the signals, and subtracting it from individual waveforms is, in the best case, useless, and in the worst, it generates new spurious artefacts instead of removing them.

Using adaptive filtering

We have seen that the information given by the artefact template is not perfect and cannot always be used directly to clean the EEG corrupted signals by a simple subtraction. Another way of exploiting this information was tested in this study. Instead of simply subtracting the template artefact, we used it as reference signal to feed an adaptive filter used as noise canceller. Here, the hypothesis was that the template artefact is linearly correlated to the motion artefact affecting the EEG signals. The standard LMS and RLS algorithms were used, as implemented in Matlab. For the RLS filter, the exponential memory weighting factor was set equal to 1 (this is sometimes referred to as the growing window RLS algorithm). In the remainder of the Chapter, these two methods are respectively called “RLS templates” and “LMS templates”.

In a second approach, we tested adaptive filtering with the accelerometer signal as the reference. No particular treatment was applied to this signal, excepted a high-pass filtering above 1 Hz. This is called the “RLS accelero” method in the remainder of the Chapter.

Using ICA decomposition of the artefact templates

The idea here was to determine main characteristics of the motion artefacts by decomposing the artefact templates (defined in section 5.3.3) with ICA. This treatment was done in several steps. First, ocular and muscular artefacts were manually cleaned with a first ICA decomposition. Then, the template was created for each channel. Like before, each stride was time-warped and the average was computed for each of them with the ten preceding and the ten following warped strides. Once the time-warped template was obtained for each channel, it was reverse

time-warped to come back in the real time scale taking into account the specificity of each stride.

Afterwards, these template signals were decomposed using ICA, giving rise to the unmixing matrix W_T and the components IC_T :

$$Templates = W_T^{-1} \cdot (IC_T) \quad (5.1)$$

The components that presented a periodicity directly related to the gait were manually considered as being characteristic features of the motion artefact and were thus selected for later rejection.

EEG signals were then decomposed using the same unmixing matrix W_T :

$$W_T \cdot EEG = IC_{EEG} \quad (5.2)$$

The periodic components were removed from the initial EEG signals by putting to zeros the weights of the mixing matrix associated to these components ($W_{T,0}^{-1}$):

$$EEG_{clean} = W_{T,0}^{-1} \cdot (IC_{EEG}) \quad (5.3)$$

This method called “ICA template” is thus different from the others as no subtraction is made here.

5.3.4 Feature extraction

After the pre-processing methods dedicated to gait-related artefacts

In BCI development, feature extraction is the transformation of the EEG signals into a feature vector. This step is necessary to provide the classifier with a reduced number of values describing the most relevant properties of the signals.

Here, the Cz, Pz, POz, O1 and O2 channels were considered because these electrodes are located where the P300 is expected to appear [33]. With the aim of designing a compact BCI system, two configurations of 3 electrodes were selected: Cz O1 O2, on the one hand and Cz Pz POz on the other hand. The signals cleaned by each method described in the previous section were band-pass filtered in 1-16 Hz using a 4th order Butterworth filter. This operation allows to focus on the characteristic frequency band of P300 potentials while removing the undesired slow drift in the measurement and high-frequency noise such as power line interference. Then the signals were down-sampled to 32 Hz to reduce the complexity of the subsequent classification problem. Finally, the signals were epoched thanks to a time-window of 600 ms beginning at the stimulus occurrence.

The special case of spatial filtering

Spatial filtering was also tested in this study. It consisted in using the 32 available raw channels, band-passing them, and down-sampling them as explained in the previous paragraph. Here, no pre-processing method described in section 11.4 was applied. Rather, a spatial filter was designed using the xDawn algorithm [38]. This algorithm consists in linearly combining EEG channels to define a P300 subspace in order to reduce the dimensionality of the classification problem while

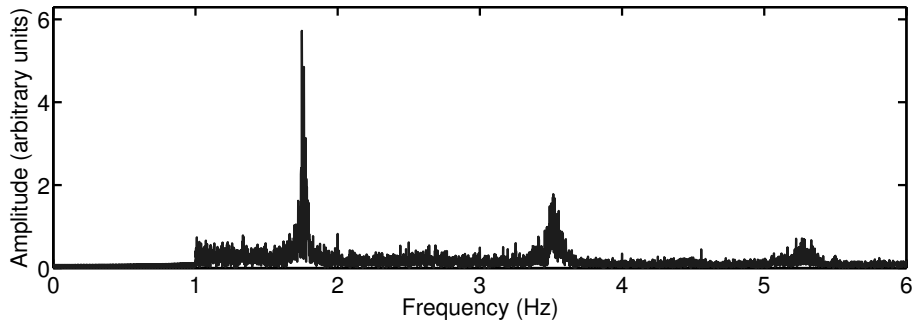


Figure 5.5: EEG spectrum of electrode Oz recorded during gait (3 km/h), after initial standard cleaning and high-pass filtering (“raw” dataset). Three harmonics are clearly visible, which are consistent with the gait fundamental frequency (0.88 Hz).

optimizing the P300 detection. During this optimization, both signal and noise are taken into account, contrarily to a method like PCA which would only consider the signal. Finally, the signals were epoched as previously mentioned.

As an EEG cap with 32 electrodes is difficult to install, cumbersome and not really ergonomic for everyday life use, we decreased the number of input electrodes of the spatial filter and we also tested configurations with 3 (Cz Pz POz), 5 (Cz Pz POz O1 O2), 7 (Cz Pz POz O1 O2 CP1 CP2), and 9 electrodes (Cz Pz POz O1 O2 CP1 CP2 P3 P4), in addition to the 32 electrode configuration. Again, the choice of these electrodes was guided by the natural localisation of the P300 potentials in the parietal and occipital areas of the cortex.

5.3.5 Classification

Before entering the classifier, groups of two epochs corresponding to a specific row/column were averaged. Then, a 12-fold Linear Discriminant Analysis classifier was applied to each two-grouped averaged time windows giving a value which represents the distance to an hyperplane separating at best the target/non-target classes. For a given trial, in a voting classifier, the row/column which has been activated is determined by summing the consecutive LDA outputs and by choosing the maximum value. The choice of a 12-fold LDA classifier was made to ensure a robust training (i.e. limiting overtraining effect).

5.4 Results and discussion

For each subject and each motion artefact correction method, the first dataset recorded at 0.83 m/s was used for the training. Testing was then made on the 3 other datasets, recorded respectively at 0.42, 0.83 and 1.25 m/s. Of course, for testing, all ICA decompositions were directly applied on basis of the trained weights. This section presents and discusses the different results obtained.

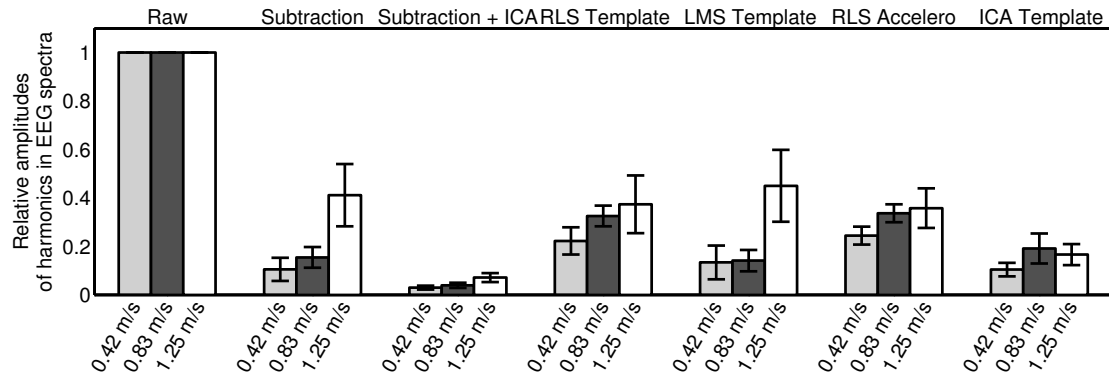


Figure 5.6: Amplitudes of the harmonics found in EEG spectra directly related to the gait, in electrode Oz for preprocessed raw and corrected data. Inter-subject averages are shown. The error bars represent the standard deviation. All the amplitudes are normalized with respect to the raw dataset.

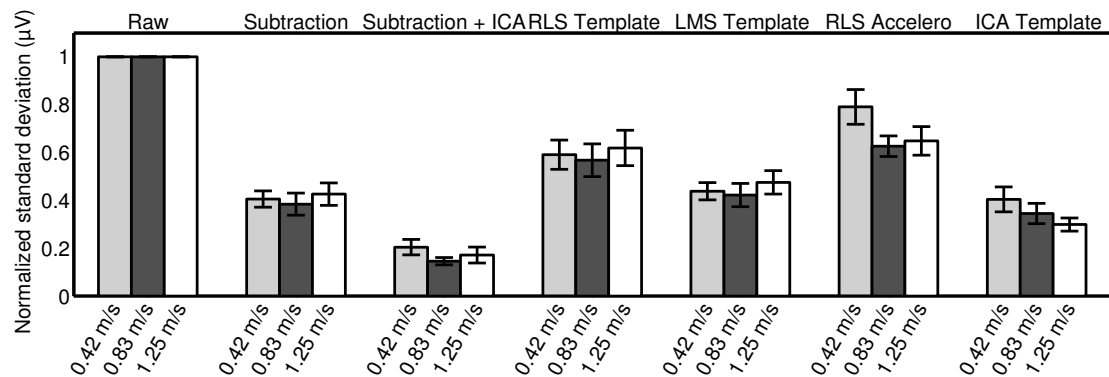


Figure 5.7: Effect of the different artefact correction methods on the standard deviation of the EEG signals recorded on electrode Oz. Inter-subject averages are shown. The error bars represent the standard deviation. Result obtained for preprocessed raw data is given for comparison.

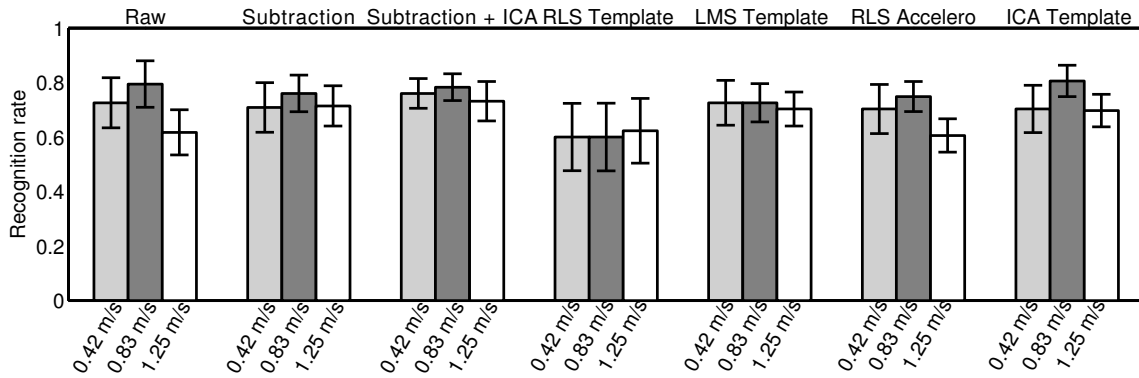


Figure 5.8: Inter-subject averages of the classification rates obtained with Cz O1 O2 (the error bars represent the statistical standard error). On average, the best method on the testing set for the Cz O1 O2 configuration is the subtraction + ICA method. However, no significant difference is found between the different methods.

5.4.1 Efficiency of the methods in terms of EEG signal properties

To evaluate the effect of the different motion artefact correction techniques, we first computed the power spectral density of the resulting signals. As already observed in [13], we found peaks consistent with the gait fundamental frequency in all EEG channels. Figure 5.5 gives an example of such phenomenon for preprocessed raw EEG data (i.e. not corrected by any method described in section 11.4) of one subject walking at 3 km/h. Figure 5.6 shows the amplitudes of the three harmonics after applying the different correction methods, divided by the amplitudes of the same dataset, without any correction. Overall, the amplitudes of the harmonics are drastically reduced (80% on average). Only the two methods using RLS adaptive filtering are less performant (reduction of about 70 % on average). The most efficient method, based on this criterion, is the variant of the template subtraction method (“Subtraction + ICA”), in which ocular and muscular artefacts are first eliminated before computing the templates (see section 5.3.3).

In a second step, standard deviation of the signals was computed in order to assess the different motion artefact correction techniques. As motion artefacts induce higher amplitude signals, it is expected that the standard deviation will be reduced after applying the correction methods. Figure 5.7 shows a comparison of these values both for preprocessed raw and corrected data. Overall, standard deviation is reduced by a factor 2 in the majority of cases. Again, the “subtraction + ICA” method gives the best performance, by reducing standard deviation by a factor 5. We will see in next section if this method gives the most accurate classification results in the framework of a real BCI system.

5.4.2 Efficiency of the methods in terms of P300 classification performance

The third – and most important – way of assessing the quality of motion artefact rejection is to determine the performance of a P300 BCI system in which is injected the same dataset corrected by each of the proposed methods. Inter-subject averages of the classification rates obtained with the two studied electrode configurations and applying the different correction methods on the

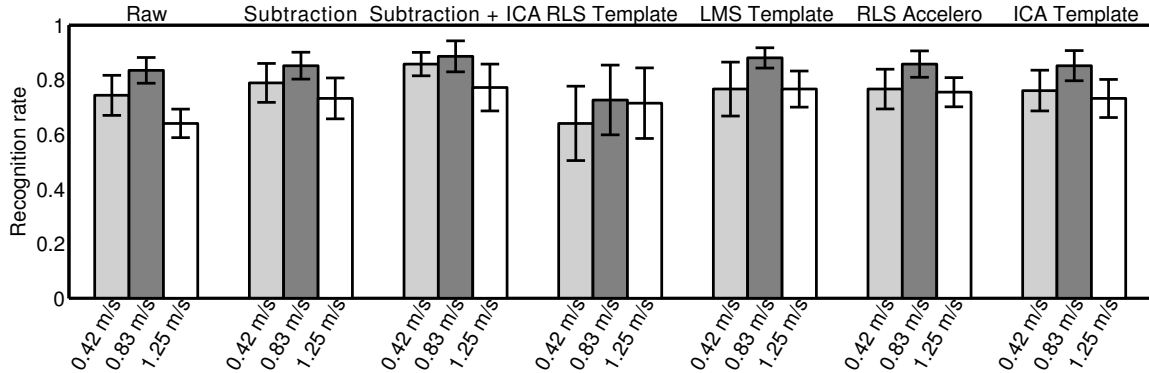


Figure 5.9: Inter-subject averages of the classification rates obtained with Cz Pz POz electrodes (the error bars represent the statistical standard error). The best method on the testing set for the Cz Pz POz configuration is the subtraction + ICA method. However, no significant difference is found between the different methods.

testing datasets are shown in Figures 5.8 and 5.9.

No statistically significant differences were found between the classification rates obtained with the electrode configurations Cz Pz POz and Cz O1 O2 (at best, the p-value is 0.08). Using 3 electrodes, already 70 % of test trials are correctly classified using preprocessed raw data, which is a result significantly better than “chance” (25 % in this case). This confirms the conclusions of several pioneer studies stating that the detection of P300 potentials as well as the development of P300-based BCI systems is feasible in ambulatory conditions (see section 5.2 and [3]).

It has to be reminded that in the latter preliminary studies, no particular treatment was developed to optimize the BCI results in such difficult conditions. Inspecting Figures 5.8 and 5.9, we see that no pre-processing methods proposed in this Chapter allow to improve significantly classification results compared to preprocessed raw data. However, we observed that classification rates are significantly degraded at high speeds using preprocessed raw data. This effect disappears when using any pre-processing method previously described.

It can also be mentioned that the “subtraction + ICA” method, which gives *a priori* the best performance in terms of EEG signal properties, is almost strictly equivalent to preprocessed raw data regarding the P300 classification performance. Also, when increasing the order of the adaptive filter (from 10 to 200) in the RLS template method, we observed a significant degradation of the recognition performance.

Finally, the same conclusions can be drawn for the other electrode configuration considered in this study.

5.4.3 Classification performance using spatial filtering

As presented in section 5.3.4, an additional – and different – approach was also tested in this study: spatial filtering using the xDawn algorithm [38]. Figure 5.10 shows the inter-subject averages of the classification rates obtained using this alternative strategy.

An impressively good result is obtained using 32 electrodes in input: 99 %. Of course,

this figure cannot directly be compared to the classification rates around 80 % obtained with the Cz Pz POz electrode configuration, given that much more information is used in input (32 versus 3 electrodes). As expected, when the number of electrodes is progressively reduced, the performance is degrading. Except with 32 electrodes with a *p*-value of 7 %, no significant differences between the trained speed of 0.83 m/s and the other tested speeds were obtained. Following some statistical tests, our results suggest that the configuration of 7 electrodes, which provides similar results as the 9-electrode configuration with two electrodes less, comprising Cz Pz POz O1 O2 CP1 and CP2, represents the best compromise between compactedness and performance (90 % at 3 km/h).

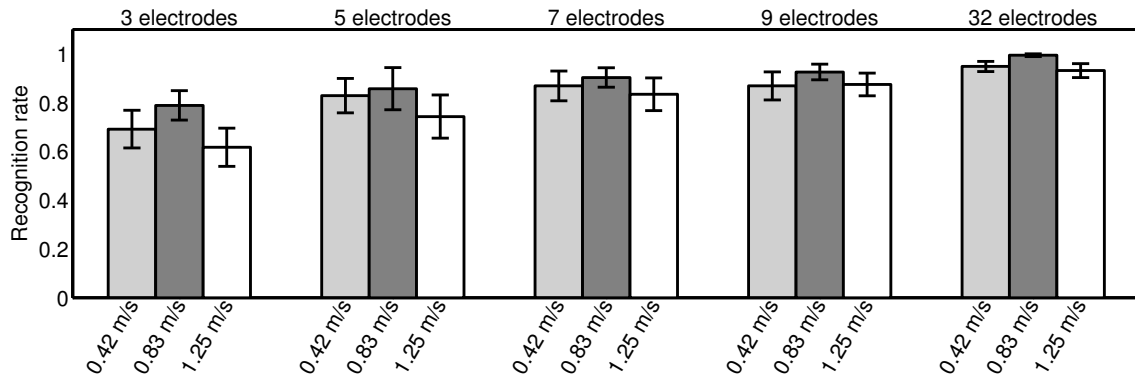


Figure 5.10: Inter-subject averages of the classification rates obtained with the xDawn spatial filter. The xDawn algorithm was tested on several configurations with 3, 5, 7, 9 and 32 electrodes as input. (3 = Cz Pz POz, 5 = Cz Pz POz O1 O2, 7 = Cz Pz POz O1 O2 CP1 CP2, 9 = Cz Pz POz O1 O2 CP1 CP2 P3 P4). The error bars represent the standard errors.

Except with 32 electrodes with a *p*-value of 7 %, no significant differences between the trained speed of 0.83 m/s and the other tested speeds were obtained. Given the statistical tests between the different configurations, the best choices seem to be 7 or 9 electrodes. But, for an overall less complex system, we advise to consider the 7-electrode solution.

5.4.4 Classification Performance Using The Optimal Configuration

Regarding the *k*-fold analysis, a one-way ANOVA (no speed factor) was performed showing that none of artefact removal techniques outperformed the preprocessed raw data. Normality was not violated but the sphericity assumption was not met ($\chi^2(2) = 61.39$, $p = 0.042$) therefore degrees of freedom were corrected using Huynh-Feldt correction estimates of sphericity ($\epsilon = 0.67$). The method factor had a significant effect ($F(6, 36) = 8.73$, $p = 0.001$). However, using post-hoc tests (with a Bonferroni correction), none of the methods significantly outperformed preprocessed raw data. Additionally, as depicted in Figure 5.11 and as already observed in previous studies, results were clearly above the chance level (25%).

On a test set basis, some significant results appeared as depicted in Figure 5.12. Normality assumption was violated and thus, a Friedman's test was computed instead of ANOVA. Each factor was separately considered while removing the effect of the other factor.

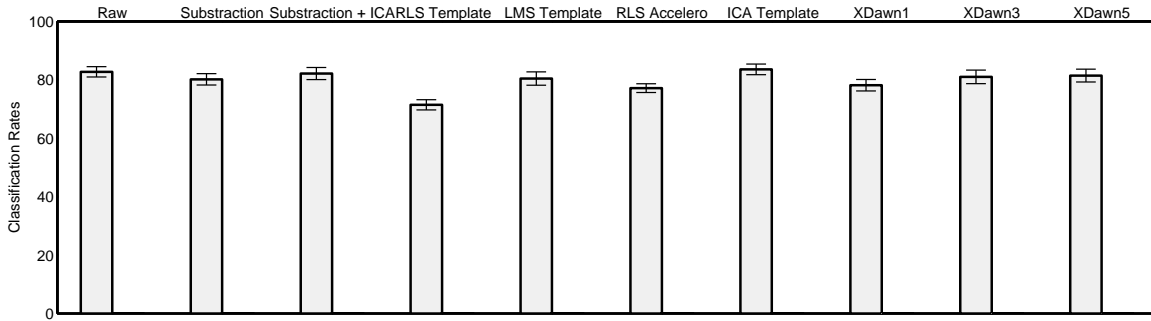


Figure 5.11: This Figure depicts the average results of seven healthy subjects of the k -fold learning. In total, 10 different approaches were studied. None of the artefact removal methods outperformed preprocessed raw data.

Regarding the method factor, a significant effect was pointed out ($\chi^2(9) = 25.29, p = 0.0027, \eta^2 = 0.12$). As post-hoc tests, the same Friedman test was computed removing the “RLS template” and “xDawn (1 output)” techniques, no more significant result were obtained. This shows that none of the methods were likely able to outperform preprocessed raw data even the so-called xDawn spatial filter algorithm. This is consistent with the k -fold approach and with previously analysed data. Although astonishing, this could be explained twofold. Firstly, to be efficient, the xDawn algorithm authors advise to strongly reduce the dimensionality of the P300 subspace (typically, by a factor four). Secondly, the comparison between virtual electrodes and real electrodes could be considered as contraindicated. However, although the number of classified electrodes is different, the xDawn algorithm should summarize the most relevant information in fewer electrodes and lead to better results by magnifying the P300 answer in a simple way that should allow a better estimation of LDA classifier parameters. This can be interpreted as a kind of failure of the xDawn algorithm.

Regarding the speed factor, a significant effect was obtained ($\chi^2(2) = 14.61, p = 0.0007, \eta^2 = 0.0731$). Thus, Wilcoxon Signed-Rank post-hoc tests with a Bonferroni correction of p-values were computed. All the pairwise comparisons were significant with medium effect size (speed 0.42 m/s-0.83 m/s: $Z = -2.86, p = 0.013, r = 0.24$; speed 0.42 m/s-1.25 m/s: $Z = -3.1, p = 0.006, r = 0.26$; speed 0.83 m/s-1.25 m/s: $Z = -5.03, p = 0.0000015, r = 0.42$). This conclusion differs from the 3-electrode configuration. This could be mainly due to the impact of the number of electrodes and/or lack of power in the test.

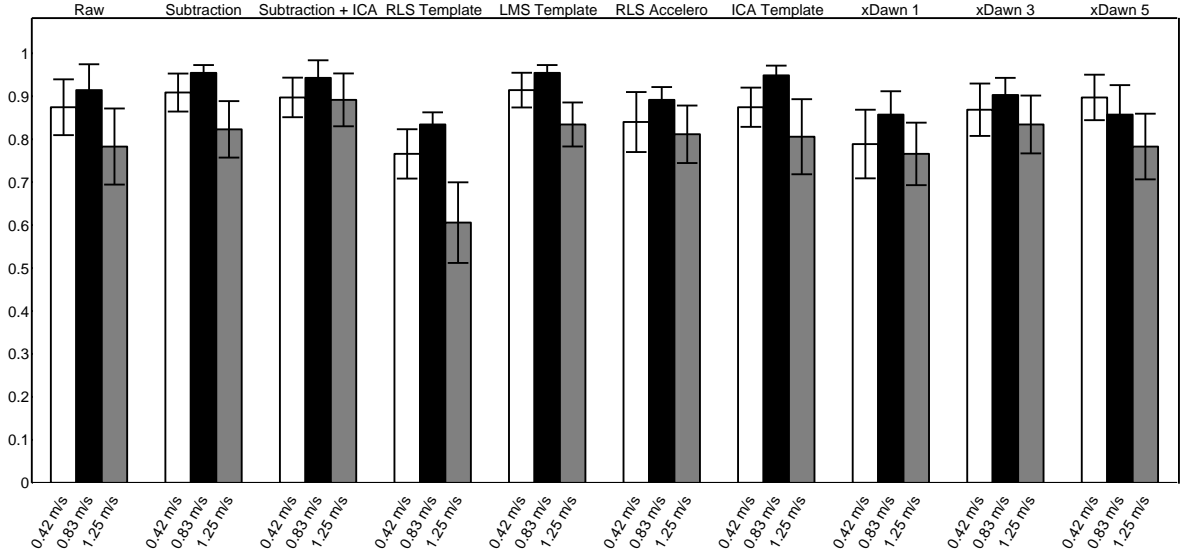


Figure 5.12: This Figure depicts the average classification rates of seven healthy subjects across three different speeds. In total, 10 different approaches were studied. There were again unlikely to outperform preprocessed raw data. Moreover, a medium effect-size impact of speed was observed.

5.5 Conclusion

In this Chapter, we have thoroughly investigated the feasibility of a P300 BCI system in ambulatory conditions. In particular, we have studied the correction of artefacts due to the gait. Seven healthy volunteers participated in a P300 experiment during which they were walking at three different speeds (0.42, 0.83 and 1.25 m/s) on a treadmill.

Several methods have been proposed, implemented and tested to correct (not simply identify the artefacts). These methods were based on template subtraction, Least Mean Squares and Recursive Least Squares adaptive filtering with either a template artefact of the EEG signal or an accelerometer signal as noise reference. Independent Component Analysis and spatial filtering based on the xDawn algorithm were also assessed. The efficiency of these methods was first evaluated in terms of EEG signal properties and then according to the classification performance of a Linear Discriminant Analysis (LDA) classifier. Excepted for the spatial filtering, the different methods were applied on two different configurations of only three electrodes. The choice of a limited number of electrodes was deliberate, with the aim of developing a realistic BCI (in terms of compactedness) for everyday use.

No method proposed in this Chapter could help to significantly increase the performance obtained with the preprocessed raw data (using basic filters and electrode selection). It has to be emphasized that the obtained results were much better than a random classifier. This is in total agreement with preliminary studies found in the literature, investigating the possibility to detect (and develop BCI systems based on) P300 potentials in ambulatory conditions.

We observed that classification rates are significantly degraded at high speeds using preprocessed raw data. However, this effect seems mitigated when using any pre-processing method previously described. This underlines a positive effect of the pre-processing methods.

The alternative approach consisting in applying the xDawn spatial filtering gave very good classification results (99 %) with 32 electrodes in input. As this electrode configuration is too large for a convenient use in everyday life, intermediate electrode configurations were tested. Our results suggest that 7 electrodes (Cz Pz POz O1 O2 CP1 CP2) give the best compromise between compactedness and classification performance (90 %). This is definitely the approach that would be recommended for developing a real-time application.

In this seven electrode configuration, results are not enthusiastic regarding the speed and method factors. Contrary to the three electrode configuration, a medium-size effect of speed is likely to exist. This difference could be mainly due to the impact of the number of electrodes and/or lack of statistical power. Moreover, a significant impact of methods was found in the test and k -fold classifications. However, this was only due to the underperformance of the “RLS template” and “xDawn” (1 output) methods. In other words, none of the artefact removal methods was likely to outperform the preprocessed raw data using seven electrodes under ambulatory conditions.

Thanks to this study, we can conclude that BCI in ambulatory conditions is definitely feasible. On average, motion artefacts do not seem to affect P300 potentials in a dramatic way. This is presumably due to the fact that, on long recordings, they are randomly distributed along the gait cycle. Nevertheless, it is possible to somewhat improve the performance of a P300-based BCI system used in such adverse conditions (high-speeds) thanks to particular methods of artefact correction. In a very-low complexity framework, the recommendation for such a system would be to use preprocessed raw data without any specific gait-related artefact methods. If allowed, a simple spatial filter like xDawn, which gives the best compromise between portability and performance, is a good tradeoff.

Bibliography

- [1] P.L. Nunez, R. Srinivasan, A.F. Westdorp, R.S. Wijesinghe, D.M. Tucker, R.B. Silberstein, and P.J. Cadusch. EEG coherency i: Statistics, reference electrode, volume conduction, laplacians, cortical imaging, and interpretation at multiple scales. *Electroencephalography and Clinical Neurophysiology*, 103(5):499–515, 1997.
- [2] B.J. Fisch and R. Spehlmann. *Fisch and Spehlmann's EEG primer: basic principles of digital and analog EEG*. Elsevier, 1999. ISBN 9780444821485.
- [3] M. Duvinage, T. Castermans, R. Jiménez-Fabián, M. Petieau, K. Seetharaman, T. Hoellinger, C. De Saedeleer, G. Cheron, O. Verlinden, and T. Dutoit. A five-state P300-based foot lifter orthosis: Proof of concept [accepted]. In *The 3rd IEEE Biosignals and Biorobotics conference (ISSNIP), Manaus, Brazil*, 2012.
- [4] A. Delorme and S. Makeig. EEGLAB: An open source toolbox for analysis of single-trial EEG dynamics including independent component analysis. *Journal of Neuroscience Methods*, 134(1):9–21, 2004.
- [5] F. Campos Viola, J. Thorne, B. Edmonds, T. Schneider, T. Eichele, and S. Debener. Semi-automatic identification of independent components representing EEG artifact. *Clinical Neurophysiology*, 120(5):868–877, 2009.
- [6] R. Ferdousy, A.I. Choudhory, Md.S. Islam, Md.A. Rab, and Md.E.H. Chowdhory. Electrooculographic and electromyographic artifacts removal from EEG. pages 163–167, 2010.
- [7] H. Nolan, R. Whelan, and R.B. Reilly. Faster: Fully automated statistical thresholding for EEG artifact rejection. *Journal of Neuroscience Methods*, 192(1):152–162, 2010.
- [8] Trevor Thompson, Tony Steffert, Tomas Ros, Joseph Leach, and John Gruzelier. EEG applications for sport and performance. *Methods*, 45(4):279 – 288, 2008. ISSN 1046-2023. doi: DOI:10.1016/jymeth.2008.07.006.
- [9] R.J. Ratcliffe and K.G. Holt. Low frequency shock absorption in human walking. *Gait and Posture*, 5(2):93–100, 1997.
- [10] K.E. Misulis and T.C. Head. *Essentials of clinical neurophysiology*. Number vol. 1. Butterworth-Heinemann, 2003. ISBN 9780750674416.

- [11] A.C.M. Vanrijn, A. Peper, and C.A. Grimbergen. High-quality recording of bioelectric events .1. Interference reduction, theory and practice. *Medical & biological engineering & computing*, 28(5):389–397, SEP 1990. ISSN 0140-0118.
- [12] H. De Talhouet and J.G. Webster. The origin of skin-stretch-caused motion artifacts under electrodes. *Physiological Measurement*, 17(2):81–93, 1996.
- [13] Scott E. Kerick, Kelvin S. Oie, and Kaleb McDowell. Assessment of EEG signal quality in motion environments. *Army Research Laboratory Report*, (ARL-TR-4866), 2009.
- [14] K. Gramann, J.T. Gwin, N. Bigdely-Shamlo, D.P. Ferris, and S. Makeig. Visual evoked responses during standing and walking. *Frontiers in Human Neuroscience*, 4, 2010.
- [15] F. Lotte, J. Fujisawa, H. Touyama, R. Ito, M. Hirose, and A. Lécuyer. Towards ambulatory brain-computer interfaces: A pilot study with P300 signals. In *ACM International Conference Proceeding Series*, pages 336–339, 2009.
- [16] B Hagemann, G Luhede, and H Luczak. Improved "active" electrodes for recording bioelectric signals in work physiology. *Eur J Appl Physiol Occup Physiol*, 54(1):95–98, 1985.
- [17] P. Pudil, F.J. Ferri, J. Novovicova, and J. Kittler. Floating search methods for feature selection with nonmonotonic criterion functions. In *Pattern Recognition, 1994. Vol. 2 - Conference B: Computer Vision Image Processing., Proceedings of the 12th IAPR International Conference on*, volume 2, pages 279 –283 vol.2, oct 1994. doi: 10.1109/ICPR.1994.576920.
- [18] Tom Fawcett. An introduction to ROC analysis. *Pattern Recognition Letters*, 27(8):861 – 874, 2006. ISSN 0167-8655. doi: DOI:10.1016/j.patrec.2005.10.010.
- [19] H. Touyama. A study on EEG quality in physical movements with steady-state visual evoked potentials. In *Engineering in Medicine and Biology Society (EMBC), 2010 Annual International Conference of the IEEE*, pages 4217 –4220, aug. 31-sept. 4 2010. doi: 10.1109/IEMBS.2010.5627375.
- [20] J. J. Vidal. Toward Direct Brain-Computer Communication. *Annual Review of Biophysics and Bioengineering*, 2(1):157–180, 1973. doi: 10.1146/annurev.bb.02.060173.001105.
- [21] Rolando Grave de Peralta Menendez, Jorge Manuel Miranda Dias, José Augusto Soares Prado, Hadi Aliakbarpour, and Sara Gonzalez Andino. Multiclass brain-computer interface based on visual attention. In *ESANN'2009 proceedings, European Symposium on Artificial Neural Networks - Advances in Computational Intelligence and Learning*, pages 437–442, 22-24 April 2009 2009. ISBN 2-930307-09-9. doi: 10.1109/IEMBS.2010.5627375.
- [22] Philip J. Allen, Oliver Josephs, and Robert Turner. A method for removing imaging artifact from continuous EEG recorded during functional MRI. *NeuroImage*, 12(2):230 – 239, 2000. ISSN 1053-8119. doi: DOI:10.1006/nimg.2000.0599.
- [23] Takao Hashimoto, Christopher M. Elder, and Jerrold L. Vitek. A template subtraction method for stimulus artifact removal in high-frequency deep brain stimulation. *Journal*

- of Neuroscience Methods*, 113(2):181 – 186, 2002. ISSN 0165-0270. doi: DOI:10.1016/S0165-0270(01)00491-5.
- [24] J.T. Gwin, K. Gramann, S. Makeig, and D.P. Ferris. Removal of movement artifact from high-density EEG recorded during walking and running. *Journal of Neurophysiology*, 103(6):3526–3534, 2010.
- [25] J.A. Palmer, S. Makeig, K.K. Delgado, and B.D. Rao. Newton method for the ICA mixture model. In *Acoustics, Speech and Signal Processing, 2008. ICASSP 2008. IEEE International Conference on*, pages 1805 –1808, 31 2008-april 4 2008. doi: 10.1109/ICASSP.2008.4517982.
- [26] Scott Makeig, Tzyy Ping Jung, Anthony J. Bell, and Terrence J. Sejnowski. Independent component analysis of electroencephalographic data. *Adv. Neural Inform. Process. Syst.*, pages 145–151, 1996.
- [27] S.S. Haykin. *Adaptive filter theory*. Prentice-Hall information and system sciences series. Prentice Hall, 2002. ISBN 9780130901262.
- [28] A. Kam and A. Cohen. Maternal ECG elimination and foetal ECG detection-comparison of several algorithms. In *Engineering in Medicine and Biology Society, 1998. Proceedings of the 20th Annual International Conference of the IEEE*, pages 174 –177 vol.1, oct-1 nov 1998. doi: 10.1109/IEMBS.1998.745866.
- [29] N.V. Thakor and Y.-S. Zhu. Applications of adaptive filtering to ECG analysis: noise cancellation and arrhythmia detection. *Biomedical Engineering, IEEE Transactions on*, 38(8):785 –794, aug. 1991. ISSN 0018-9294. doi: 10.1109/10.83591.
- [30] S. Cortes, R. Jane, A. Torres, J.A. Fiz, and J. Morera. Detection and adaptive cancellation of heart sound interference in tracheal sounds. In *Engineering in Medicine and Biology Society, 2006. EMBS '06. 28th Annual International Conference of the IEEE*, pages 2860 –2863, 30 2006-sept. 3 2006. doi: 10.1109/IEMBS.2006.260727.
- [31] Alan S. Gevins, Weixiu Du, and Harrison Leong. Adaptive interference canceler for EEG movement and eye artifacts. *US Patent 5 513 649*, 1996.
- [32] N. Birbaumer, N. Ghanayim, T. Hinterberger, I. Iversen, B. Kotchoubey, A. Kubler, J. Perelmouter, E. Taub, and H. Flor. A spelling device for the paralysed. *Nature*, 398(6725):297–8, March 1999.
- [33] L.A. Farwell and E. Donchin. Talking off the top of your head: toward a mental prosthesis utilizing event-related brain potentials. *Electroencephalography and Clinical Neurophysiology*, 70(6):510 – 523, 1988. ISSN 0013-4694. doi: DOI:10.1016/0013-4694(88)90149-6.
- [34] Yann Renard, Fabien Lotte, Guillaume Gibert, Marco Congedo, Emmanuel Maby, Vincent Delannoy, Olivier Bertrand, and Anatole Lécuyer. Openvibe: An open-source software platform to design, test, and use brain–computer interfaces in real and virtual environments. *Presence: Teleoper. Virtual Environ.*, 19:35–53. ISSN 1054-7460.

- [35] M. Duvinage, T. Castermans, T. Hoellinger, G. Cheron, and Thierry Dutoit. Modeling human walk by PCPG for lower limb neuroprostheses control. In *5th International IEEE EMBS Conference on Neural Engineering*, 2011.
- [36] M. Duvinage, R. Jiménez-Fabián, T. Castermans, O. Verlinden, and Thierry Dutoit. An active foot lifter orthosis based on a PCPG algorithm. In *12th International IEEE Conference on Rehabilitation Robotics*, 2011.
- [37] J.A. Zeni, J.G. Richards, and J.S. Higginson. Two simple methods for determining gait events during treadmill and overground walking using kinematic data. *Gait and Posture*, 27 (4):710 – 714, 2008. ISSN 0966-6362. doi: DOI:10.1016/j.gaitpost.2007.07.007.
- [38] Bertrand Rivet, Antoine Souloumiac, Virginie Attina, and Guillaume Gibert. xDAWN algorithm to enhance evoked potentials: application to brain-computer interface. *IEEE Transactions on Biomedical Engineering*, 56(8):2035–43, August 2009. doi: 10.1109/TBME.2009.2012869.

Chapter 6

Objective and Subjective Assessment of P300 and SSVEP BCIs for Lower Limb Rehabilitation Applications

Contents

6.1	Introduction	137
6.2	SSVEP System	138
6.2.1	SSVEP Approach	138
6.2.2	SSVEP Pipeline	139
6.2.3	Experiment Description	141
6.3	Performance Measures	142
6.3.1	Subjective Feedback Measures	142
6.3.2	Objective Performance Measures	143
6.4	Discussion	143
6.5	Conclusions and Future Work	147

Abstract

Recent research is focussing on bringing out-of-the-lab Brain-Computer Interface (BCI) technologies. It has been recently shown that the P300 and SSVEP responses can be used while walking with a relatively low decreased performance. Additionally, lower limb rehabilitation/prostheses applications are gaining in interest in the neuroscience and BCI communities.

Therefore, this paper aims at comparing a four-state SSVEP BCI plus a non-control state for lower-limb rehabilitation purposes to a similar P300 interface. The comparison relies on the subjective and objective performances assessed by usability and workload. After performing a real-time treadmill speed control, the System Usability Scale and the NASA Task Load Index questionnaires were administered to five healthy subjects.

Results show that the SSVEP BCI has better attributes than its P300 counterpart. Major contributors to this increased performance are the higher reactivity, the asynchronous interface and the felt less cognitive load for command generation. Additionally, there is room for further improvements by using more advanced signal processing techniques and gait-related artefact removal methods.

This chapter is based upon the following publications:

- **M. DUVINAGE, T. CASTERMANS, M. PETIEAU, K. SEETHARAMAN, T. HOELLINGER, G. CHERON, T. DUTOIT, 2012, "A Subjective Assessment of a P300 BCI System for Lower-Limb Rehabilitation Purposes", Proceedings of the 34th Annual International Conference of the IEEE Engineering in Medicine and Biology Society (EMBC 2012), San Diego, USA, August 28 - September 1.**
- **M. DUVINAGE, T. CASTERMANS, M. PETIEAU, T. HOELLINGER, G. CHERON, T. DUTOIT, 2014, *Comparative Objective and Subjective Assessment of Ambulatory SSVEP and P300 Treadmill Control* [Submitted]**

6.1 Introduction

Since its beginning, Brain-Computer Interface (BCI) research has focused on increasing performance without really considering the patient himself [1]. Actually, classification accuracy or information transfer rates have often been used to show the superiority of one paradigm or one method against another. For a long time, new world records were emphasized and some of them were presented as a revolution for heavily disabled patients or for potential gamers that could use BCI as an additional input. However, although information transfer rate and classification accuracy are important, they only represent a part of a reality. As a proof of that, BCI applications are known for having a very high abandonment rate [1], i.e. users quickly give up using the system. As a proposition towards a better acceptance rate, an improved performance and increase enjoyment, some subject-based feedback questionnaires were suggested. The most famous ones are the System Usability Scale (SUS), the NASA Task Load Index (NASA-TLX) which measure the usability and the cognitive load respectively [1]. They are designed for quick and simple administration while giving a fair picture of the analysed features.

In order to bring BCI research outcomes out of the lab, some current work exists in order to create visual stimulus for real-life applications. For instance, the VUZIX augmented reality eyewears (Vuzix, Rochester, NY, USA) or the famous Google glass could help showing the required stimuli in ambulatory BCI applications. There are also some projects on integrating the stimuli on mobile devices, which could lead to autonomous applications [2, 3].

But, although ambulatory BCIs have been shown feasible, few applications have been developed up to now. After a pilot study demonstrating above chance potential performance of auditory P300 interface under free walk conditions [4], additional research has provided more advanced results. In [5], a fundamental study removing the estimated gait-related artefacts indicate that the average P300 potential is not that much affected at normal gait speeds. In [6], coherent results were obtained following a classification approach. By comparing the performance of several artefact removal techniques on a four state visual P300 BCI, the authors discovered that none of these techniques appear to outperform raw data. This is at least partly due to the averaging process in P300 potential detection, which allows to average gait artefacts at different P300 potential times. Regarding the steady state visual evoked, few results have been presented in an ambulatory framework. In [7], no particular impact of gait on SSVEP performance was observed. However, this study only focuses one subject and two frequencies (4 Hz and 6 Hz), which is clearly insufficient. Another recent study analysing 11 Hz and 12 Hz SSVEP response while standing and walking has shown that the walking speed does impact on the SSVEP detection accuracy and the Canonical Correlation Analysis (CCA) has an interest [8] but no feedback was studied. In [9], the SSVEP Signal-to-Noise Ratio (SNR) distribution has been investigated under both sitting and walking conditions. The main conclusion is that the SSVEP response is affected by artefacts but, by proper artefact correction techniques, it should be able to reach sitting condition performance. Additionally, subjects that have most of the response in the occipital area and in the gamma band suffer the most of muscular artefacts.

Another interest of ambulatory BCIs is the possibility to use it as part of a rehabilitation device. For instance, as firstly proposed in [10] and followed by [11], a high-level command can

drive an external rehabilitation/prosthetic device by using a Central Pattern Generator (CPG) as shared control [12]. In other words, the CPG mathematical model will convert the high-level speed command into all the low-level operations required to control the complex device. An interesting contribution in that direction is the development of a knee exoskeleton based on 12 flickering LEDs SSVEP interface [13]. In their paper, the authors propose to follow 2 different strategies: 1) a shared control approach with high level commands and 2) a continuous control of the knee angle. Both strategies were successful on the tested subject while sitting on a chair.

Here, a five state (4 commands plus non-control) P300 and SSVEP BCI were implemented. The subject had the opportunity to control the treadmill speed on which they were walking on. This simulates the control patients could get from P300 and SSVEP-based lower-limb devices such as fitness, rehabilitation and prostheses. In this paper, Section 2 describes the SSVEP approach (the P300 pipeline was already described in a previous Chapter), the pipeline and the experiment description. Section 3 details the subjective and objective performance measures. Section 4 presents and discusses the results.

6.2 SSVEP System

This section first details the SSVEP approach. Then, the acquisition system and the pipeline are explained. Finally, the experiment and its purpose are presented.

6.2.1 SSVEP Approach

SSVEP is known to have a higher reactivity than P300-based interfaces that could even reach around 100 bits/min [14]. Indeed, SSVEP is a strong steady state potential that mainly arises in the occipital area, i.e. the O_x electrodes, at the same frequency and harmonics of the looked flickering stimulus [15].

In this study, LED panels were used as stimulators as depicted in Figure 6.1. From previous studies and at the same luminance and modulation depth, it is known that LEDs produce stronger fundamental SSVEP responses than LCD/CRT screens: LEDs have stronger fundamental and weaker harmonics thanks to a very small jitter [16]. To obtain the best results, we opted for manually controlled pulse stimulations.

To allow comparison with our previous P300 treadmill control system, we are again developing a four-speed BCI managing a non-control state (when no decision is requested by the subject) [10]. As shown in Figure 6.1, the interface is composed of four LED panels disposed at the extremities of a computed screen. Each LED panel corresponds to a desired speed (0, 1.5, 3 or 4.5 km/h). For future implementation, this arrangement could mimic the corner of the Vuzix eyewear.

The main difference with the P300 interface is the asynchronous control. This means that the subject has not to wait for a signal before concentrating on the requested task to change the command. This obviously makes the non-control state, i.e. when the subject is not looking at a LED panel, even more important to detect.



Figure 6.1: Four LED panels were placed around a screen. Each of them was driven by a different frequency by an external stimulator.

6.2.2 SSVEP Pipeline

EEG was recorded using a 32-electrode cap connected to the ANT acquisition system (Advanced Neuro Technology, ANT, Enschede, The Netherlands) digitizing the signals at 512 Hz. Left ear was chosen as reference. Mastoid was not used because of possible pollution from EMG signals of the neck while walking. Electrode impedance was measured and maintained under $20\text{ k}\Omega$ for each channel using electrode gel. Most of the mentioned parameters were chosen based on trial and errors.

The pipeline was composed of several main components: channel and frequency selection, temporal band-pass filter, a Common Spatial Pattern filter, a windowing and a Linear Discriminant Analysis (LDA) classifier using a voting rule for the final decision sent to a Virtual Reality Peripheral Network (VRPN) server [17].

First, relying on our previous results in ambulatory SSVEP [9], the most responsive electrodes were chosen for each subject as detailed in Table 6.1. The most important contributions were mainly from the occipital and parietal areas. The same process was applied to detect the most adequate frequencies also displayed in Table 6.1. There were mainly located around 15 Hz and 30 Hz, i.e. the known peaks of SSVEP response [9, 15].

Then, each frequency of interest was band-passed filter with through a 4th order Butterworth filter. The tolerance was 0.2 Hz at each side. It also allows to remove the undesired slow drift in the measurement and high-frequency noise such as power line interference [18].

Afterwards, a Common Pattern Spatial Filter (CSP) was designed to weight on the different electrodes [19]. By linearly combining EEG channels, the goal is to improve the discrimination of two types of signals by increasing the variance of the first group while decreasing the variance of the second group. This enhances the detection of the desired SSVEP response.

Then, the resulting signal was windowed. Depending on the subject performance, a window of 2 or 3 seconds was used as reported in Table 6.1. This size was decided upon a Receiver

Operator Curve (ROC) analysis. To properly recognize non-control and command states by a simple threshold, the four ROC curves should be similar to those illustrated in Figure 6.2. Then, a 66 % overlap was used for the following window.

Table 6.1: The SSVEP interface was specifically designed for each subject by adapting the used frequencies and electrodes (from Chapter 4, the CSP dimension, the window size and shift were chosen to maximize the performance by trial and errors).

Subjects	Frequencies (Hz)				Used Electrodes	CSP dimension	Windowing/ shift (s)		Experiment Duration (min)
CC	27,7	29,4	33,33	35,71	25;26;27;28;29;30;31;32	3	3	1	18
MD	29,4	31,3	33,33	35,71	21;22;25;26;29;30;31;32	4	2	0,7	15
MP	10,87	11,9	12,82	13,89	21;22;15;16;17;29;30;31;32	25	3	1	20
TC	11,1	12,2	13,16	29,41	29;30;31;32	3	2	0,7	16
TH	12,82	31,3	33,34	35,68	25;26;27;28;29;30;31;32	5	2	0,7	15

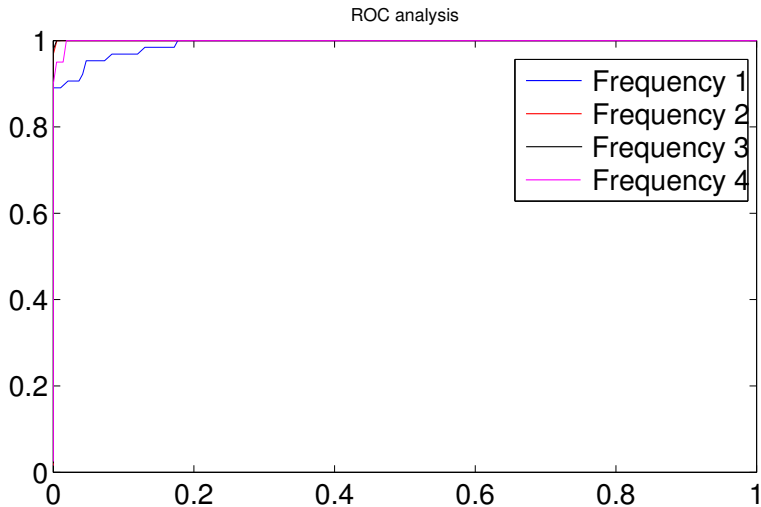


Figure 6.2: With this kind of ROC analysis, it is possible to determine a threshold with a high TPR and a very low FPR. But, when one classifier has an underperforming curve, it becomes challenging (see Frequency 1).

Finally, a different 12-fold LDA classifier was applied to each frequency of interest vs all the remaining ones including non-control. After each classification, a value which represents the distance to a hyperplane separating at best the target/non-target classes was obtained. The decision was sent to a VRPN server for post-processing.

In this post-processing, a dwell-time and a refractory-time were introduced [17]. The dwell-time consists in a number of consecutive identical decisions before finally controlling the treadmill speed and emitting a feedback sound stating the current decision. The refractory-time corresponds to the number of windows for which no decision is considered. Indeed, after a decision is taken, there is a time duration before the feedback is recognized by the subject who stops

looking at the LED panel. Additionally, even when the subject stops looking, some data containing the observed frequency are still in the pipeline due to the window size. In the end, this refractory-time allows to remove redundant decisions. When the device was again ready for the next command, a beep was emitted. These time values were set at 4 and 5 respectively.

6.2.3 Experiment Description

In the SSVEP approach, the experiment was twofold: a two-step offline training session (around 16 min) and an online test session. Because it was shown that gait-related artefacts could affect the measured SNRs, two 30 trial (including non-control) sessions were recorded while sitting and walking at 3 km/h. By concatenating both datasets, the CSP spatial filter was able to learn how to extract at best the SSVEP response during those 60 trials. Each session lasted around 8 minutes. Then, the best threshold was computed to obtain a low False Positive Rate (FPR). When a decision is below this threshold, it is considered as a non-control state. A practical application should not make mistakes while the subject is not looking at the screen given that this state has a higher probability of occurrence (except in city center for prosthesis applications). Moreover, this kind of mistakes would force the subject to frequently re-adjust the current speed due to misclassification of non-control states and would destabilize him due to unexpected speed modifications. In other words, FPR, i.e. the number of non-target elements classified as target ones divided by the total number of non-target, should be as low as possible. In the ROC analysis, the threshold was set between 1% and 3% depending on the shape of the ROC curves.

Following the same procedure, the P300 was again twofold. The first part of the training session consisted of 25 trials of random letters (around 12 minutes). Then, a session of 10 trials of non-control state was recorded while the subject was not looking at the screen. This aimed at determining a threshold (by a Receiver Operating Characteristic (ROC) analysis) from which the voting rule result was significant. Here, the threshold was set around FPR=1%.

Then, the online session aimed at managing the overall system to mimic realistic situations. For the SSVEP (P300) experiment, 100 (60) trials were performed during this session whose duration varies between 15 and 20 (30) minutes. The given instruction was twofold: 1) the subject has to alternate between commands (uniformly distributed) and declare it before each trial and non-control state and 2) when there was an error, the subject had to focus on the same command until success. Additionally, a uniform distribution of commands was requested and checked during the experiment.

Five male healthy subjects (with age between 26 and 35 years old) participated in this experiment (except Subject 3, they were the same in both P300 and SSVEP studies). Subjects did not have any known locomotion-related or SSVEP disturbing diseases or handicaps. After the experiment, each subject was administered SUS and NASA-TLX questionnaires described here below (they were familiarized with them before doing the experiment). Finally, an interview about the answers was performed to identify the system strengths and weaknesses.

6.3 Performance Measures

In this section, the measures of performance are described. First, following [20], the main focus is on subjective feedback measures including SUS and NASA-TLX questionnaires. Then, objective measures, composed of classification rate, non-decision rate and error rate, are introduced.

6.3.1 Subjective Feedback Measures

The System Usability Scale (SUS) questionnaire was invented to meet several major requirements [21]. First, assessing usability is often context-dependent: The employed methodology has to adapt to the specificities of the studied application. Therefore, to allow fair comparison between types of applications/interfaces, the SUS questionnaire should provide a normalised and context-independent value. Second, because the user point of view is of major interest for industry, the evaluation questionnaire has to be cost effective and efficient, i.e. reliable, quick to administrate and understandable both by top managers and programmers, who are not human factor professionals [22].

In its final version, the SUS questionnaire is composed of ten items using a Likert scale, which is quick to answer. Each item corresponds to a statement and the respondent has to indicate the degree of agreement or disagreement on a 5 point scale. After properly scoring and weighting the different ten statements, a SUS score can be derived between 0 and 100. The higher the SUS value, the better the system is [21]. On top of that, a global single item evaluation was asked as proposed in [22, 23]. As shown in Figure 6.3, this item is graded from the worst imaginable (0) to the best imaginable (6) through OK (3).

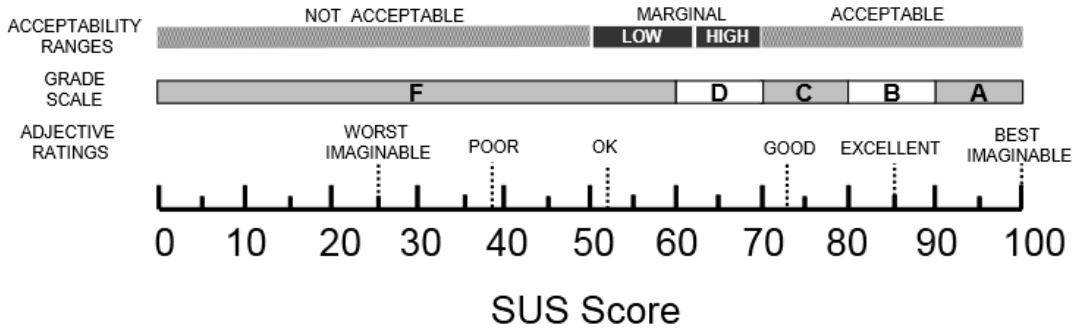


Figure 6.3: The distribution of the SUS scores show that the passable threshold is around 70.

Indeed, several studies about the SUS score has been proposed showing that this scale fulfil the requirements of such questionnaires. In [22, 23], this score has been proven reliable, correlated to other usability questionnaires and genre independent. Moreover, thanks to a huge SUS history, it is possible to compare it with other surveys. In some papers, it was also shown that the ten items can actually be divided into 2 groups: learnability and usability [24]. This could provide an additional point of view for the result interpretation.

Another widely used questionnaire is the NASA Task Load Index (NASA-TLX) [25]. This is a brief and powerful questionnaire for workload evaluation.

This questionnaire follows a two-step procedure. First, subjects have to rate six different item subscales which assess mental demand, physical demand, temporal demand, effort, frustration and performance. Each item is rated using a 20-temporal step bipolar scale resulting in a score between 0 and 100. In addition to detailed instructions, a pair of words are written at each extremity of the scale to help subjects. Given that there are two very different tasks (control and non-control), the evaluation was done 1) on a global basis and 2) focused on control commands.

The second step aims at determining the source of loads. By performing pair-wise comparisons based on the most contributive load item, the subject can determine the weight of each item in the overall workload. By computing the weighted average, a NASA-TLX score is obtained. But, in this study, this weighting was not used.

Some questions are really dependent on the application. Thus, subjects were asked to separately consider fitness and rehabilitation on a treadmill (which are quite close to the experiment considerations). They were also asked to consider the case of a prosthesis in a general context. Obviously, given that this latter application is quite different from the actual experiment, subjective results are less reliable but can give an indication. Of course, in case of small handicaps that are not considered for this latter application, very efficient techniques based on purely mechanical systems are available (for instance, for ankle prostheses [26]).

6.3.2 Objective Performance Measures

As defined in [10], given the specific design of the system, three objective measures were used. The classification accuracy is defined as the ratio between the number of correctly recognized targets and the total number of targets.

The non-decision rate is computed as the ratio between the number of non-control states and the number of trials when a command control (speed modification) is supposed to be emitted. It means that this measures the delay of a non-decision of the system when a person wants to modify the speed.

The error rate is defined as the resulting rate when a command control is emitted.

Because P300 was synchronous contrary to the SSVEP, the used metrics slightly differ depending on the paradigm. Indeed, defining a non-decision rate with the SSVEP is less obvious as there is a smoothing window that prevents a direct decision. During the experiment, no global non-decision was obtained when a command control was required. Therefore, we only measured the errors and the delay resulting of a non-decision is assessed through the subjective study.

6.4 Discussion

In this section, results are firstly discussed relying on objective measures. Then, subjective measures and results of interviews are exposed.

Considering objective measures, results indicate a desired functioning. Indeed, as depicted in Table 6.2, few errors occurred during the experiment (0% for P300 and around 2% for SSVEP). As explained in [27], the price to pay for this "reliability" is a non-zero non-decision rate, which means a delayed decision. In practice, in the P300 approach, this rate sometimes nearly reached

10% (no difference was observed by subjects while speaking during the test). This indicates that decreasing the number of repetitions to speed up the system is quite risky. To obtain the same behaviour of providing commands when the system is quite certain, this would require a higher non-decision rate. On the other hand, being less conservative in the ROC analysis would provoke more unwanted speed modifications that could force the user to re-adjust his current speed more frequently, which could discourage him. In an end-user application, a trade-off should be made depending on the subject profile/feelings. However, all the subjects said that they preferred the conservative approach, which gives the impression of a sufficiently reliable system (even if they did not strictly test another approach). Moreover, it avoids some fears of suddenly modifying the speed when the subject was not prepared to.

Regarding the SSVEP paradigm, this leads to a longer window analysis and longer dwell time before a decision can be made. Moreover, contrary to the P300 paradigm, the four different classifiers make the threshold determination much more complicated as ROC curves are not necessarily close to each other. This explains why there are slightly more errors in both control and non-control states compared to the P300 interface. Moreover, it was observed for the SSVEP approach that subjects, whose main frequency response was located in the gamma band and in the occipital area, could suffer from muscular artefact contamination. This interfere with the SSVEP response by either masking it or by simulating it. By being relax, few problems occur but an out-of-the-lab application would benefit from the design of a specific artefact correction as proposed in [8] or from using a SNR measure as feature.

Table 6.2: The objective measures show that the P300 and SSVEP interfaces are working as desired. The SSVEP non-control classification rate is slightly underperforming. This is due to the more challenging way to determine the threshold. Subject 3 is different from the P300 study.

	P300			SSVEP		
	Classification rate	Non-decision rate	Non-control classification rate	Classification rate	Error rate	Non-control classification rate
Subject 1	93,5	6,5	100	98	2	98
Subject 2	90,6	9,4	100	94	6	96
Subject 3 ^b	90,6	9,4	100	100	0	94
Subject 4	96,8	3,2	100	100	0	100
Subject 5	100	0	100	96	4	92
Mean	94,3	5,7	100	97,6	2,4	96
STD	4,1	4,1	0	2,6	2,6	3,16

Considering questionnaires completed by the five subjects, results depicted in Table 6.3 are roughly just passable in terms of usability but subjects need a relatively low cognitive load. Based on SUS questionnaires, for fitness and rehabilitation, the system passes the *acceptable*

threshold of 70 as defined in [23]. Consistently with the one-item global SUS score, the system can be defined as *good*. On the other hand, such a P300-based prosthesis system is on the edge of reaching this *acceptable* usability but can only be defined as *marginal (high)*.

Considering questionnaires completed by the five subjects, the results depicted in Table 6.3 and Table 6.4 indicate fair performance in terms of usability and subjects require a relatively low cognitive load. Based on SUS questionnaires, all the potential applications based on SSVEP are considered as *acceptable* (above the 70 threshold) as defined in [23]. Based on the one-item global SUS score, the system is considered between *good* and *excellent* in average.

In comparison to the P300 interface, the SSVEP approach was much more appreciated. Both the aggregate and global SUS scores depict improved usability feedback measures. Additionally, the subjects who take part to both experiments consider the SSVEP approach as much more efficient, which gives them a higher confidence. As suggested in the P300 interface study, the higher reactivity is obviously an important feature especially for the orthosis/prosthesis application. Given the specific framework of daily use, and, as stressed on by several subjects, the slow reactivity and the risk of non-recognition in case of emergency stop are highly damaging. Additionally, this is not really adapted for crowded places, i.e. typically a place where many speed modifications have to be done. However, some subjects indicated that this approach could be suited for leisurely walk in large areas. According to them, this could be a way for heavily disabled people to walk outside again. More interestingly, all subjects agreed that, excluding those drawbacks, the global approach is a nice way to control. This suggests that if the system can be increased in reactivity, it would be more broadly accepted. For instance, the SSVEP version allows to a more realistic control in crowded places in city center, i.e. typically a place where many speed modifications have to be done. They also consider that the paradigm itself is easier to manage using an SSVEP, which explains why the cognitive load is higher in the command control for a P300 interaction.

Regarding NASA-TLX values, although the global P300 and SSVEP application are considered as roughly similar in cognitive load, the SSVEP appears less demanding during command control generation. When considering the entire system, the workload remains low. This means that subjects do not consider the P300 and SSVEP interfaces as strongly demanding. In contrast, the NASA-TLX results reveal that the control commands is felt as much more challenging for the P300 approach than the SSVEP interface. This may also explain why usability is improved by the latter mode of interaction. For a prosthesis application, a more important frustration is noticed because of the context that increases risks and the need for reactivity and reliability. However, the increase of this component is lower than in the P300 system still indicating a higher confidence in the SSVEP interface.

In the P300 approach, several subjects pointed out some weak points that could be enhanced to significantly increase the usability. Firstly, a technical support is generally desired, at least, at the beginning. This could be highly improved by using a user-friendly EEG cap with dry electrodes if similar performances are provided. This will also contribute to getting a less cumbersome device. Secondly, the loss of control is one fear of subjects. In addition to a recognition error in risky situations, the stress can provoke another error, etc, until a crash/an abandonment. Thirdly, as expected, the synchronous functioning is quite penalizing and an asynchronous system

would be more appreciated. Fourthly, one subject proposed a system with acceleration/deceleration command instead of fixed speeds in order to avoid too important unwanted speed variations and to provide a more flexible system.

In addition to the reactivity, several other drawbacks were solved in the SSVEP interface. The asynchronous interface is obviously a key point in user experience as it provides a more intuitive interaction and reinforce the reactivity. Furthermore, as reactivity was highly increased, the proposition to integrate acceleration/deceleration command instead of fixed speeds in order to avoid too important unwanted speed variations did not hold anymore. Additionally, stress was attenuated in the SSVEP paradigm because it increases confidence compared to the P300 interface.

Table 6.3: Comparing SUS and Global SUS scores, results are consistent with [23]. Moreover, it indicates that this P300 approach seems to be more suitable for fitness and rehabilitation than prosthesis mainly due to the lack of reactivity. Considering the overall workload, it appears to be quite small in average and the overload peaks reached during control states are smaller than [28].

	SUS (Global SUS)			NASA-TLX Global (Command)		
	Fitness	Rehabilitation	Prostheses	Fitness	Rehabilitation	Prostheses
Subject 1	87.5 (4)	87.5 (4)	77.5 (4)	20 (39.16)	20 (39.16)	25 (44.16)
Subject 2	57.5 (2)	67.5 (4)	62.5 (3)	10 (43)	10 (41.6)	10 (42.16)
Subject 3	80 (5)	75 (5)	70 (5)	25.8 (46.6)	25.83 (46.33)	27.5 (48.33)
Subject 4	77.5 (4)	75 (4)	67.5 (2)	20.8 (33.3)	24.16 (36.6)	27.5 (42.5)
Subject 5	77.5 (4)	72.5 (3)	67.5 (3)	14.16 (26.66)	18.33 (30.83)	21.66 (34.16)
Mean	76 (3.8)	75.4 (4)	69 (3.4)	18.15 (37.7)	19.66 (39)	22.33 (42.262)
STD	11.1 (1.1)	7.43 (0.71)	5.47 (1.14)	6.15 (7.9)	6.19 (5.85)	7.3 (5.15)

Table 6.4: Regarding the SSVEP paradigm, the SUS scores indicate that it could be considered for every applications. The NASA-TLX scores show the global workload is similar to the P300 values. However, the command generation is considered as less demanding in the SSVEP approach.

	SUS (Global SUS)			NASA-TLX (Command)		
	Fitness	Rehabilitation	Prostheses	Fitness	Rehabilitation	Prostheses
Subjet 1	87.5 (6)	87.5 (6)	87.5 (6)	13.3 (19.16)	13.3 (19.16)	13.3 (19.16)
Subject 2	75 (4)	75 (5)	70 (3)	22.5 (21.6)	22.5 (21.6)	23.3 (22.5)
Subject 3	80 (4)	72.5 (4)	70 (4)	13.3 (15)	17.5 (19.17)	21.66 (23.33)
Subject 4	87.5 (5)	87.5 (5)	80 (4)	23.3 (30)	23.33 (30)	29.16 (35.83)
Subject 5	80 (3)	77.5 (3)	75 (3)	30.83 (35)	32.5 (35)	35 (43.33)
Mean	82 (4.4)	80 (4.6)	76.5 (4)	20.64 (24.15)	21.82 (25)	24.49 (28.83)
STD	5.42 (1.14)	7.07 (1.14)	7.41 (1.22)	7.45 (8.17)	7.21 (7.15)	8.17 (10.28)

6.5 Conclusions and Future Work

In this paper, a comparative study of the subjective performance between P300 and SSVEP BCI interfaces for lower-limb rehabilitation purposes, e.g. prosthesis, rehabilitation or fitness control, is provided. In this experiment, the treadmill speed was used as a feedback. Performances were assessed on an objective basis (classification, error and non-decision rates) and on a subjective basis (SUS and NASA-TLX questionnaires). Five healthy subjects participated in this experiment.

Regarding objective measures, the SSVEP system is working as designed. Although more errors were observed in the SSVEP interface, their numbers remain very low (around 2%). Whereas in the P300 approach, this design leads to a non-zero non decision rate, in the SSVEP approach, it delays the command decision by requiring a longer window size and dwell time. Generally, this specific working allowing not to detect a command state when information appears to be too uncertain was well appreciated. Even if they did not test another approach during the experiment, subjects found the tested approach rather reliable. Although they could feel uncomfortable with the non-decision rate, they prefer avoiding an unexpected speed modification.

Regarding subjective measures, enhanced indicators suggest the SSVEP interface has a better interest for such applications. Although subjects expressed reserves about the prosthesis/orthosis application, they all consider that the SSVEP-based interaction appears acceptable while providing an overall assessment between *good* and *excellent* according to the SUS scale. The higher reactivity and asynchronous interface were two of the corner stones for this increased felt performance. Another important contribution to this score is the less demanding cognitive load during command generation compared to the P300 interface. Indeed, the P300 approach could suit fitness and rehabilitation but not really prostheses. More precisely, subjects consider that such a prosthesis control system could be used in large areas, e.g. for promenades, but not in crowded and risky areas, e.g. city center. This is mainly due to the lack of reactivity and to the non-decision rate at critical time.

One main future work will be devoted to use the more advanced signal processing to decrease the overall decision time. For instance, in the Geneva BCI [29], a SSVEP decision is provided every 0.5 s is provided. While keeping a very high classification rate, this quicker decision would still largely enhance the reactivity and thus, the user experience. Another important future work will be to increase the current effort to generate the required stimuli under an ambulatory context [2, 3]. The device would also benefit from artefact correction, especially for selected frequencies in the gamma band and over the occipital area. Finally, other several Brain Neuronal Computer Interfaces (BNCIs) could be investigated. Typically, EOG-based eye movements interfaces will be assessed as it may still increase reactivity [30]. Moreover, when a better understanding of spontaneous cortical gait signals will be available, this assumed more natural but less stable interface becomes also be considered [31].

Bibliography

- [1] Hayrettin Gürkök, Gido Hakvoort, and Mannes Poel. Evaluating user experience in a selection based brain-computer interface game: A comparative study. In Junia Coutinho Anacleto, Sidney Fels, Nicholas Graham, Bill Kapralos, Magy Saif El-Nasr, and Kevin Stanley, editors, *Entertainment Computing - ICEC 2011*, volume 6972 of *Lecture Notes in Computer Science*, pages 77–88, Berlin, Germany, October 2011. Springer Verlag.
- [2] Yu-Te Wang, Yijun Wang, Chung-Kuan Cheng, and Tzzy-Ping Jung. Developing stimulus presentation on mobile devices for a truly portable ssvep-based bci. In *Engineering in Medicine and Biology Society (EMBC), 2013 Annual International Conference of the IEEE*, 2013.
- [3] Andrew Campbell, Tanzeem Choudhury, Shaohan Hu, Hong Lu, Matthew K. Mukerjee, Mashfiqui Rabbi, and Rajeev D.S. Raizada. Neurophone: brain-mobile phone interface using a wireless EEG headset. In *Proceedings of the second ACM SIGCOMM workshop on Networking, systems, and applications on mobile handhelds*, MobiHeld ’10, pages 3–8, New York, NY, USA, 2010. ACM.
- [4] Fabien Lotte, Junya Fujisawa, Hideaki Touyama, Rika Ito, Michitaka Hirose, and Anatole Lécuyer. Towards ambulatory brain-computer interfaces: A pilot study with p300 signals. In *Proceedings of the International Conference on Advances in Computer Entertainment Technology*, ACE ’09, pages 336–339, New York, NY, USA, 2009. ACM.
- [5] Klaus Gramann, Joseph T Gwin, Nima Bigdely-Shamlo, Daniel P Ferris, and Scott Makeig. Visual evoked responses during standing and walking. *Frontiers in Human Neuroscience*, 4(00202), 2010.
- [6] T. Castermans, M. Duvinage, M. Petieau, T. Hoellinger, C.D. Saedeleer, K. Seetharaman, A. Bengoetxea, G. Cheron, and T. Dutoit. Optimizing the performances of a p300-based brain-computer interface in ambulatory conditions. *Emerging and Selected Topics in Circuits and Systems, IEEE Journal on*, 1(4):566 –577, dec. 2011.
- [7] H. Touyama. A study on eeg quality in physical movements with steady-state visual evoked potentials. In *Engineering in Medicine and Biology Society (EMBC), 2010 Annual International Conference of the IEEE*, pages 4217 –4220, 31 2010-sept. 4 2010.
- [8] Yuan-Pin Lin, Yijun Wang, and Tzzy-Ping Jung. A mobile ssvep-based brain-computer interface for freely moving humans; the robustness of canonical correlation analysis to motion

- artifacts. In *Engineering in Medicine and Biology Society (EMBC), 2013 Annual International Conference of the IEEE*, 2013.
- [9] Matthieu Duvinage, Thierry Castermans, Mathieu Petieau, Thomas Hoellinger, Guy Cheron, and Thierry Dutoit. Ssvep response distribution under different luminosity and movement conditions. *Journal of Neuroengineering and Rehabilitation [Submitted]*, 2014.
- [10] M. Duvinage, T. Castermans, M. Petieau, K. Seetharaman, T. Hoellinger, G. Cheron, and T. Dutoit. A subjective assessment of a p300 bci system for lower-limb rehabilitation purposes. In *Engineering in Medicine and Biology Society (EMBC), 2012 Annual International Conference of the IEEE*, pages 3845–3849, 2012.
- [11] Dingguo Zhang, Lin Yao, Ying Wang, and Xiangyang Zhu. Functional interface between brain and central pattern generator for application in human-machine system. In *Robotics and Biomimetics (ROBIO), 2011 IEEE International Conference on*, pages 1873–1877, 2011.
- [12] José del R. Millán, Rüdiger Rupp, Gernot Mueller-Putz, Roderick Murray-Smith, Claudio Giugliemma, Michael Tangermann, Carmen Vidaurre, Febo Cincotti, Andrea Kubler, Robert Leeb, Christa Neuper, Klaus R Mueller, and Donatella Mattia. Combining brain-computer interfaces and assistive technologies: State-of-the-art and challenges. *Frontiers in Neuroscience*, 4(0):12, 2010.
- [13] A.J. McDaid, Song Xing, and S.Q. Xie. Brain controlled robotic exoskeleton for neurorehabilitation. In *Advanced Intelligent Mechatronics (AIM), 2013 IEEE/ASME International Conference on*, pages 1039–1044, 2013.
- [14] Ivan Volosyak. Ssvep-based bremen-bci interface—boosting information transfer rates. *Journal of Neural Engineering*, 8(3):036020, 2011.
- [15] Yijun Wang, Ruiping Wang, Xiaorong Gao, Bo Hong, and Shangkai Gao. A practical vep-based brain-computer interface. *Neural Systems and Rehabilitation Engineering, IEEE Transactions on*, 14(2):234–240, 2006.
- [16] Zhenghua Wu, Yongxiu Lai, Yang Xia, Dan Wu, and Dezhong Yao. Stimulator selection in ssvep-based bci. *Medical Engineering and Physics*, 30(8):1079 – 1088, 2008.
- [17] Russell, Thomas C. Hudson, Adam Seeger, Hans Weber, Jeffrey Juliano, and Aron T. Helser. VRPN: a device-independent, network-transparent VR peripheral system. In *VRST '01: Proceedings of the ACM symposium on Virtual reality software and technology*, pages 55–61, New York, NY, USA, 2001. ACM.
- [18] Ulrich Hoffmann, Jean-Marc Vesin, Touradj Ebrahimi, and Karin Diserens. An Efficient P300-based Brain–Computer Interface for Disabled Subjects. *Journal of neuroscience methods*, 167(1):115–125, January 2008.
- [19] F. Lotte and Cuntai Guan. Regularizing common spatial patterns to improve bci designs: Unified theory and new algorithms. *Biomedical Engineering, IEEE Transactions on*, 58(2):355–362, 2011.

- [20] Pasqualotto Emanuele, Simonetta Alessandro, Gnisci Veronica, Federici Stefano, , and Bellardinelli Marta Olivetti. Toward a usability evaluation of bcis. *International Journal of Bioelectromagnetism*, 13:121–122, 2011.
- [21] J. Brooke. SUS: A quick and dirty usability scale. In P. W. Jordan, B. Weerdmeester, A. Thomas, and I. L. Mclelland, editors, *Usability evaluation in industry*. Taylor and Francis, London, 1996.
- [22] Aaron Bangor, Philip T. Kortum, and James T. Miller. An empirical evaluation of the system usability scale. *Int. J. Hum. Comput. Interaction*, pages 574–594, 2008.
- [23] Aaron Bangor, Technical Staff, Philip Kortum, and James Miller. Determining What Individual SUS Scores Mean : Adding an Adjective Rating Scale. *Journal of Usability Studies*, 4(3):114–123, 2009.
- [24] James R. Lewis and Jeff Sauro. The factor structure of the system usability scale. In *Proceedings of the 1st International Conference on Human Centered Design: Held as Part of HCI International 2009*, HCD 09, pages 94–103, Berlin, Heidelberg, 2009. Springer-Verlag.
- [25] S. G. Hart and L. E. Stavenland. Development of NASA-TLX (Task Load Index): Results of empirical and theoretical research. In P. A. Hancock and N. Meshkati, editors, *Human Mental Workload*, chapter 7, pages 139–183. Elsevier, 1988.
- [26] R. Jiménez-Fabiàn and O. Verlinden. Review of control algorithms for robotic ankle systems in lower-limb orthoses, prostheses, and exoskeletons. *Medical Engineering and Physics*, (0):–, 2011.
- [27] Matthieu Duvinage, Thierry Castermans, René Jiménez-Fabiàn, Thomas Hoellinger, Caty De Saedeleer, Mathieu Petieau, Karthik Seetharaman, Guy Cheron, Olivier Verlinden, and Thierry Dutoit. A five-state p300-based foot lifter orthosis: Proof of concept. In *3rd IEEE Biosignals and Biorobotics conference*, 2012.
- [28] A Riccio, F Leotta, L Bianchi, F Aloise, C Zickler, E-J Hoogerwerf, A Kübler, D Mattia, and F Cincotti. Workload measurement in a communication application operated through a P300-based brain–computer interface. *J. of Neural Eng.*, 8(2):025028, 2011.
- [29] Rolando Grave de Peralta Menendez, Jorge Dias, José Augusto Prado, Hadi Aliakbarpour, and Sara González Andino. Multiclass brain computer interface based on visual attention. In *ESANN*, 2009.
- [30] M. Duvinage, T. Castermans, and T. Dutoit. Control of a lower limb active prosthesis with eye movement sequences. In *Computational Intelligence, Cognitive Algorithms, Mind, and Brain (CCMB), 2011 IEEE Symposium on*, pages 1 –7, april 2011.
- [31] G. Cheron, M. Duvinage, C. De Saedeleer, T. Castermans, A. Bengoetxea, M. Petieau, K. Seetharaman, T. Hoellinger, B. Dan, T. Dutoit, F. Sylos Labini, F. Lacquaniti, and Y. Ivanenko. From Spinal Central Pattern Generators to Cortical Network: Integrated BCI for Walking Rehabilitation. *Neural Plasticity*, 2012:1–13, 2012.

Chapter 7

Performance of the Emotiv Epoch Headset for P300-based Applications

Contents

7.1	Introduction	155
7.2	Previous Studies	155
7.3	Acquisition systems	156
7.3.1	ANT	156
7.3.2	Emotiv EPOC	157
7.4	BCI system	157
7.4.1	P300-based approach	157
7.4.2	P300 pipeline	160
7.5	Performance evaluation	162
7.5.1	Performance measures	162
7.6	Experiment description	162
7.7	Statistical analysis	162
7.8	Results and Discussion	163
7.8.1	P300 Results	163
7.8.2	Other material considerations	165
7.9	Conclusions	167

Abstract

For two decades, EEG-based Brain-Computer Interface (BCI) systems have been widely studied in research labs. Now, researchers want to consider out-of-the-lab applications and make this technology available to everybody. However, medical-grade EEG recording devices are still much too expensive for end-users, especially disabled people. Therefore, several low-cost alternatives have appeared on the market. The Emotiv EpoC headset is one of them. Although some previous work showed this device could suit the customer's needs in terms of performance, no quantitative classification-based assessments compared to a medical system are available.

This paper aims at statistically comparing a medical-grade system, the ANT device, and the Emotiv EpoC headset by determining their respective performances in a P300 BCI using the same electrodes. On top of that, a review of previous Emotiv studies and a discussion on practical considerations regarding both systems are proposed. Nine healthy subjects participated in this experiment during which the ANT and the Emotiv systems are used in two different conditions: sitting on a chair and walking on a treadmill at constant speed.

The Emotiv headset performs significantly worse than the medical device; observed effect sizes vary from medium to large. The Emotiv headset also has higher relative operational and maintenance costs than its medical-grade competitor.

Although this low-cost headset is able to record EEG data in a satisfying manner, it should only be chosen for non critical applications such as games, communication systems, etc. For rehabilitation or prosthesis control, this lack of reliability may lead to serious consequences. For research purposes, the medical system should be chosen except if a lot of trials are available or when the Signal-to-Noise Ratio is high. This also suggests that the design of a specific low-cost EEG recording system for critical applications and research is still required.

This chapter is based upon the following publications:

- M. DUVINAGE, T. CASTERMANS, M. PETIEAU, T. HOELLINGER, G. CHERON, T. DUTOIT, 2013, *Performance of the Emotiv EpoC headset for P300-based applications*, BioMedical Engineering OnLine, Volume 12:56, Published: 25 June 2013, doi:10.1186/1475-925X-12-56.
- M. DUVINAGE, T. CASTERMANS, M. PETIEAU, T. HOELLINGER, C. DE SAEDELEER, K. SEETHARAMAN, G. CHERON, T. DUTOIT, 2012, *A P300-Based Quantitative Comparison Between the Emotiv EpoC Headset and a Medical EEG Device*, Proceedings of the 9th IASTED International Conference on Biomedical Engineering.

7.1 Introduction

Since its beginning, Electroencephalography (EEG)-based non-invasive Brain-Computer Interfaces (BCI) have mainly targeted disabled people [1]. Communication and control are some of the developed applications, notably by allowing to control a mouse, to use a web browser or to spell words just by thought. Other main research areas are the study of motor substitution or motor rehabilitation whose main applications are hand grasping [2] and wheelchair control [3]. Finally, for healthy end-users, BCIs have also been used to augment interactivity in games by using multimodality from the EEG signals and the standard control [4, 5].

Although EEG recording devices are much less expensive and portable than other brain activity recording techniques, they are still much too expensive for a daily use according to a customer point of view, especially for disabled people. As a reminder, the disability leads to an average loss of wages, benefits, *etc.* in such a way that they can not afford these systems. In order to promote more widely spread applications, plenty of commercial EEG devices have been proposed such as Neurosky, Mindflex, Emotiv Epoc, etc [6]. According to [6], the best low-cost EEG device in terms of usability is the Emotiv Epoc headset.

However, to our knowledge, no deep scientific quantitative classification-based comparison of this headset with a medical system has been done. Thus, in order to properly study the Emotiv Epoc headset performance compared to a medical device and assess the relevancy of this low-cost headset contested by several major BCI researchers [7], this Chapter investigates the P300 paradigm in terms of recognition performance under walking and sitting conditions to detect whether conclusions remain the same or not in such different situations. After a short review of current knowledge and a description of the used acquisition devices in Sections 7.2 and 7.3, it also provides a description of the used BCI system in Section 7.4. In Section 7.5, a statistical comparative performance under walking and sitting conditions to detect whether those recording devices are resistant to movement artefacts. Finally, results and some other practical considerations are also detailed in Section 13.3.

7.2 Previous Studies

In previous studies, three main paradigms have been tested with the Emotiv Epoc headset: P300, SSVEP and mental tasks. However, most of them suffer from a non scientific approach or a lack of comparative baseline. Based on a P300/*odd-ball* BCI, the NeuroPhone smartphone application [8] processes EEG signals collected in realtime by the Emotiv Epoc headset. In their paper, the authors present strongly above chance results showing that this device is a good low-cost alternative. However, a comparison of the performance obtained with another EEG acquisition system is not available. Under indoor and outdoor ambulatory conditions, the same conclusion arises for a recent study combining the Emotiv electrodes and an EEG cap in order to get a precise positioning [9]. They did not give the hardware comparative results and the difference with sitting conditions. Furthermore, this way of proceeding could be criticized due to the potential damage to the hardware device. In [10], the authors show that P300 response averaged over around 600 stimuli is similar between the Emotiv system and the Neuroscan system with an

inter-class correlation in the [0.7–0.8] range. The mismatch negativity potentials they obtain also show a strong similarity except for noisy potentials (half of the subjects). Basically, it confirms a previous study [11]: data provided by both systems are alike in general, but the signal has a better Signal-to-Noise Ratio (SNR) in the medical system (g.tec device).

Based on a SSVEP BCI in [12], the researchers showed that the Emotiv Epoch headset provides decreased performance compared to an ActiCap system with 8 channels located over the occipital area under sitting conditions. Given the advantage of placing all the electrodes around the region of interest for the SSVEP paradigm, the conclusion of underperformance is misleading as far as this experiment can not show the true potential of the headset. Indeed, the previous experiment mostly compares the ability of the devices to record EEG at the right place for a given BCI paradigm instead of their intrinsic performance. One should keep in mind that electrodes could be reorganized according to the final goal as performed in [9]. However, it gives an indication that the Emotiv Epoch headset is not dedicated to all the available BCI paradigms. In [13], a comparative study with a g.tec device was initiated also showing worse results for the Emotiv Epoch headset. On four sitting subjects, they obtained an underperformance of around 10%. However, only four common electrodes were used and four subjects were evaluated without considering motion and real life applications.

Finally, in [14], based on mental tasks (relaxation and imaging of two types of pictures), it was reported that an ActiCap medical system was much better than the Emotiv Epoch. However, the authors did not compare the performance of both systems in the same experimental conditions. The electrode number and their location were significantly different. Consequently, the conclusions of this study are possibly misleading when assessing the actual Emotiv headset performance.

7.3 Acquisition systems

7.3.1 ANT

The ANT acquisition system (Advanced Neuro Technology, Enschede, The Netherlands) is composed of a high-density WaveGuard cap system and the corresponding full-band DC amplifier that can reach a sampling rate of 2048 Hz. As shown in Figure 7.1, the WaveGuard cap has 128 Ag/AgCl electrodes covering all the major brain cortical areas (based on the International 10–20 system) with shielded wires in order to be less influenced by exterior noise. Moreover, three different cap sizes are available to adapt as well as possible to the subject's head specificities.

In our experiment, electrode impedance was measured and maintained under $20\text{ k}\Omega$ for each channel using electrode gel and signals were visually checked before recording. The studied electrode positions are the same as provided by the Emotiv Epoch headset. The hardware and software overall cost is around 30,000–50,000\$.

The ANT device is provided with the ASA software. It is composed of several main tools: pre-processing, Event-Related Potential analysis (ERP), source reconstruction using inverse models and time-frequency analysis. All these aspects allow more advanced users, typically researchers/physicians to deeply study the brain signals.



Figure 7.1: The cables and the electrodes are well fixed in order to decrease motion artefacts. The cables are shielded to avoid interference.

7.3.2 Emotiv EPOC

As announced on the Emotiv website, the Emotiv Epoc headset and its Software Development Kit for research mainly includes 14 channels (plus CMS/DRL references, P3/P4 locations) each based on saline sensors. Available channels (also based on the International 10–20 locations) are depicted in Figure 7.2. This headset has not the ability to cope with all the BCI paradigms with the same success without modifying the hardware. For instance, the motor imagery paradigm, which requires central electrodes, should provide bad performance. As shown in Figure 7.3, the headset is completely wireless and has a large Lithium-based battery autonomy of 12 hours. The sampling rate can reach 128 Hz. Additionally, gyroscope generates optimal positional information for cursor and camera controls.

In our experiment, all the standard available electrodes of the Emotiv Epoc headset were used. Electrode impedance was decreased by using saline liquid until the level required by the software was reached (in the $10\text{--}20\text{ }k\Omega$ range) and was checked along the experiment. For the research edition, the total cost is 750\$.

The Emotiv headset is provided with three different detection software: Expressiv, Affectiv and Cognitiv suites. The Expressiv suite aims at interpreting the user's facial expressions in real-time. The Affectiv suite aims at monitoring the user's emotional states in real-time. The Cognitiv suite aims at performing standard BCI-like control.

7.4 BCI system

7.4.1 P300-based approach

As illustrated in Figure 7.4, the P300 evoked potential is an involuntary positive potential that arises around 300 ms after the user has perceived a relevant and rare stimulus [15]. This is

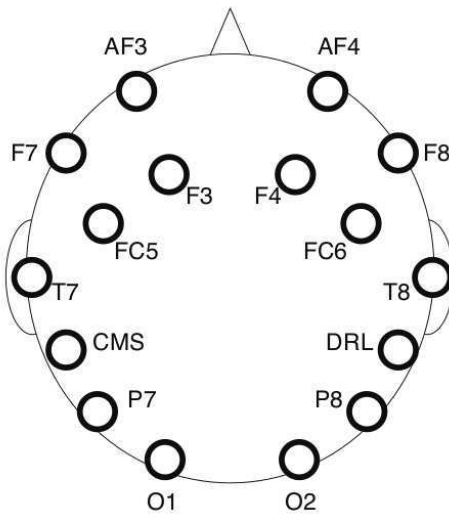


Figure 7.2: The Emotiv Epoch headset is composed of 14 different electrodes in addition to two references (picture attributed to Emotiv and Emotiv EPOC neuroheadset).



Figure 7.3: The Emotiv Epoch headset is handy to place and wireless.

commonly used in an odd-ball paradigm, in which the user is requested to attend to a random sequence composed of two kind of stimuli with one stimulus much less frequent than the other one. If the infrequent stimulus is relevant to the user who is putting his attention on it (e.g. silently counting it), its actual appearance activates a P300 waveform in the user's EEG, which is mainly located in the parietal areas [16].

Following previous work [17] and inspired from the 6×6 matrix P300-speller text editor [18], we are interested in a four-state BCI as depicted in Figure 7.5. Indeed, if mobile applications have to be considered (e.g. control of a prosthesis or augmented interaction in daily life), one can not afford using a lot of states.

The recognition of a given state is quite simple. At the beginning of one trial, one of the four

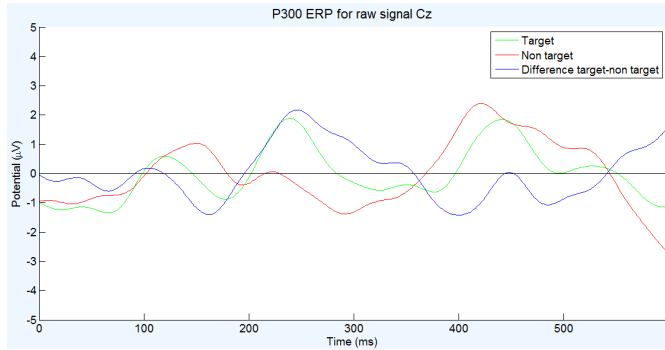


Figure 7.4: When a rare and relevant stimulus appears, a P300 potential is elicited around 250 ms after the stimulus (Target). Otherwise, no particular brain response is observed (Non target). Here, due to our pipeline, another P300 response is elicited. Because the flashes are not strictly rare, the magnitude of the P300 is quite low. Finally, the difference between both conditions is depicted for information. The relatively small magnitude of the P300 peak is likely due to the non-rare occurrence of the target.



Figure 7.5: P300 visualization is divided into four states. After the target the subject has to look at is highlighted in green, the rows/columns are randomly flashed. By detecting the P300 responses, the system is able to recognize the looked target.

letters is highlighted in green. Then, the subject has to look at this letter when each row/column is flashed 12 times to increase the low SNR due to disturbances of other brain, muscular and ocular activities. At the intersection of the detected P300 responses, the computer is able to determine which letter/symbol the subject was looking at.

Obviously, in this approach, the interface is not strictly an odd-ball paradigm. Actually, each letter is flashed 50% of the time, which is not really a rare event. However, previous work showed that this approach provides good results and was thus used in this Chapter [17].

For out-of-the-lab applications, the requirement of an external screen to activate stimuli used in this experiment could be problematic. However, thanks to specific emerging and well-designed VUZIX augmented reality eyewears (Vuzix, Rochester, NY, USA), this problem could be circumvented. As shown in Figure 7.6, by displaying stimuli on a semi-transparent module containing all the key hardware elements, the device should allow ambulatory P300 applications.

Again, the tradeoff of four different states represented by a letter at the four corners of the semi-transparent glasses appears to be a more realistic solution.

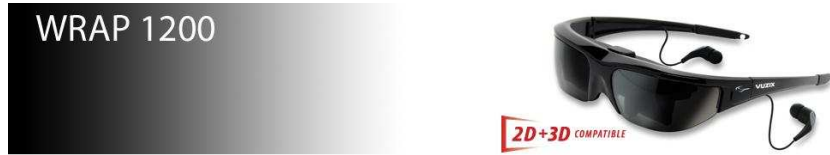


Figure 7.6: The Vuzix eyewear should allow ambulatory P300-based BCI.

7.4.2 P300 pipeline

Considering the Emotiv electrodes on the ANT device (using a common average reference for both devices), the pipeline of the approach (shown in Figure 7.7) includes different main parts: a temporal high-pass filter, an xDAWN-based spatial filter, an epoch averaging and a Linear Discriminant Analysis (LDA) classifier using a voting rule for the final decision. In order to provide more precise coherent comparison results, this is the same pipeline as developed in [19]. As discussed in [19], gait-related artefact removal techniques do not bring significant better performance and are thus not used in this pipeline. Ocular and muscular artefacts are basically not linked to the P300 task (except the first gaze to the letter) leading to a strongly mitigated effect by the averaging. This procedure was implemented in the open source OpenVibe software [20].

In order to obtain a better performance, the EEG signal is high-pass filtered at 1 Hz using a 4th order Butterworth filter. By trial and error, we observed that downsampling (an anti-aliasing filter to avoid adding noise was used in the OpenVibe downsampling box) the data at 32 Hz allows a better behaviour of the LDA classifier while decreasing observed noise. Indeed, the P300 potential is mainly located below 16 Hz whereas an undesired slow biological drift can interfere with the pipeline [21]. This also removes high-frequency noise such as power line interference.

Afterwards, a spatial filter is designed thanks to the xDAWN algorithm [22]. This algorithm aims at magnifying the P300 response by considering both signal and noise contrary to a common principal component analysis. Target/non-target epochs have to be separately fed in the algorithm. By linearly combining EEG channels, this algorithm defines P300 and noise subspaces. When projecting EEG signals into these subspaces, P300 detection is enhanced. In this Chapter, three projection components were retained as the authors basically advise to divide the number of channels by four.

Then, as proposed in the Openvibe software, we use a 600 ms time window epoch. The beginning of the epoch is synchronized with the flashed target. In order to obtain a better SNR, groups of two epochs corresponding to a specific row/column are averaged. The flash, no flash and inter-repetition duration are respectively 0.2 s, 0.1 s and 1 s.

Finally, a 12-fold Linear Discriminant Analysis classifier (LDA) is used to detect whether a P300 was elicited in the brain. In the k -fold approach, the training set is splitted into k uniform groups. Then, $k - 1$ groups are used for training the LDA classifier and the test is performed on the remaining group. After performing this k times, the classifier obtaining the

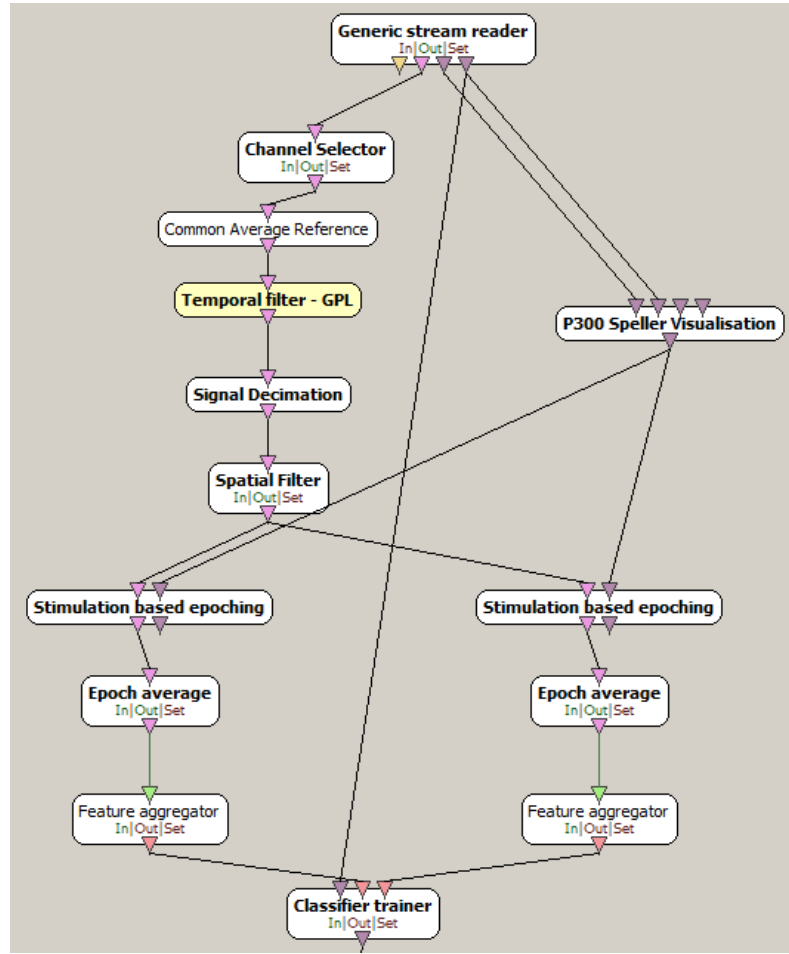


Figure 7.7: The pipeline includes a channel selection, a common average referencing, a high pass filtering, a downsampling, an xDawn spatial filtering, a two-epoch averaging and a LDA classifier (pink flows). To elicit the P300 potential, a rigorous stimulation management (purple flows) has to be done for synchronizing the P300 averaging.

best results is chosen. The reported k -fold value is the average of the k training performance (there is no k -fold on the spatial filter but if there is a bias induced by this choice, it should be the same for each result in average). For each two-grouped time window, the output value of the classifier represents the distance to a hyperplane separating at best the target/non-target P300 classes. This value could also be considered as a confident measure. For a given trial, in a voting classifier, the row/column which has been activated is determined by summing six consecutive LDA outputs (12 repetitions) and by choosing the most probable target.

7.5 Performance evaluation

7.5.1 Performance measures

In this Chapter, two performance measures are assessed: k -fold classification and test set classification rates. The former measure is the single two-grouped epoch classification accuracy, i.e. without any *temporal* averaging. This measure is obtained only on the training set. This helps to assess the difficulties to learn data due to a different hardware device and could be interpreted as an indirect measure of the SNR by their intrinsic correlation. Indeed, if the SNR is increased, the classification task is made easier leading to enhanced performance. Because a specific care for the Emotiv Epoch electrode positioning was performed, the effect of misalignment should be highly mitigated. Furthermore, the P300 response has an inter-subject distribution variability and thus, the effect should be averaged across subjects.

The test set classification rate introduces an averaging in the decision process. In the P300 pipeline, this is performed by a voting classifier on six consecutive repetitions. This measure thus assesses the overall system performance and may be considered as an indication of the perceived usability, although it is incomplete [23].

7.6 Experiment description

In order to compare both devices, two different experiment conditions were tested: sitting on a chair and walking at 3 km/h on a treadmill, which is a convenient speed for subjects. The ambulatory condition was considered to detect whether the devices have similar relative performances when realistic movement artefacts are produced. It also assesses if the recording systems are fixed enough. To train classifiers and to assess the entire system for each condition separately, each session was composed of one training set and one test set of 25 randomly chosen trials (around 12 minutes for each session). The total duration of the experiment per device was around one hour and a quarter (including breaks and data checking). Recordings were performed on different days for a given subject in a random order.

Eight healthy male and one healthy female subjects participated in this experiment with age between 24 and 34 years old. During the experiment, a 20-inch screen (refreshing rate = 60 Hz) in both conditions was placed at about 1.5 meter in front of the subject for the P300 experiment. Subjects were healthy and did not have any known locomotion-related or P300 disturbing diseases or handicap. All procedures were approved by the Université Libre de Bruxelles Internal Review Board and complied with the standards defined in the Declaration of Helsinki.

7.7 Statistical analysis

In order to detect whether the Emotiv Epoch headset is competitive with respect to the medical device, our statistical assessment is only focusing on comparisons between both devices under each condition excluding cross condition analysis. Indeed, the null hypothesis H_0 assumes that the Emotiv headset is the best device or is equivalent. Then, we are looking for evidence of rejecting it meaning that it is likely to be outperformed.

As applied in [24], although our design follows a repeated measure analysis of variance (ANOVA) for each performance measure [25, 26], the omnibus F test was not performed. Actually, the omnibus ANOVA F test is not a necessary condition to control family-wise error rate (FWER) whatever the applied *post-hoc* tests [26, 27]. In this case, the degrees of freedom are spent for somehow useless statistical tests, i.e. tests that do not really correspond to the research question. Furthermore, omnibus F test might show no significance while some of the underlying t -tests are significant leading to a decrease of power and an overall more conservative test. The important information to remind is that researchers can not continue running different statistical analyses until they obtain the results they desire as FWER quickly inflates.

Instead of the widely used procedure, we thus defined only a limited amount of *a priori* comparisons by applying the prescription of [24, 26, 27]. First, we defined all the pairwise comparisons. Thereby, we performed the standard paired t -tests, whose single assumption is data normality, with a standard alpha level of 5%. Given that those comparisons equal the degrees of freedom, we make sure to control FWER inflation without any further adjustments, which leads to a much more powerful test.

However, obtaining significant results is not enough and effect-size is at least as important [24, 26, 28]. Significance only assesses if there is enough evidence to determine whether there is a likely effect between two or more groups. It does not provide information about the size of this effect. If the difference is significant but trivial, the best method is not really outperforming the other ones. The normalized unbiased Hedge'g* effect-size measure somehow tackles this problem by standardly evaluating this effect and by providing some rules of thumb of how big the effect-size is. For instance, absolute Hedge'g* values around 0.1 (≤ 0.16), 0.2 (0.17–0.32), 0.5 (0.33–0.55) or 0.8 (0.56–1.2) respectively mean a trivial, small, medium or a large effect according to [29, 30].

Furthermore, a single value effect size is not sufficient and a 95% interval should be studied. This helps to provide information about how the current effect-size is a good estimation of the underlying one. Obviously, if more data are used, a more precise interval is provided allowing more reliable conclusions (Matlab and a neuroscience toolbox were used [28]).

7.8 Results and Discussion

7.8.1 P300 Results

Globally, as shown in Figure 7.8, the Emotiv Epoch results are not bad at all for such a low-cost system. In fact, the performance is far above the chance level of 25% for each subject, which is consistent with previous studies and responds to old criticisms that this system mainly records muscular and ocular artefacts. Indeed, in this experiment, the elicited P300 response is not synchronized with the gait cycle and thus, the produced Electromyography (EMG) artefacts.

However, as depicted in Figure 7.8 and in Table 7.1, the Emotiv headset appears to underperform the ANT system. On a k -fold based comparison, p -values under sitting and walking conditions are respectively significant at 1.36% and 1.67% with a large effect size indicating relatively large differences in performance. This would mean that the SNR is worse for the Emotiv headset than for the ANT system, which is consistent with [11]. On the test set, both conditions lead to significant results. However, a medium effect is detected under sitting conditions

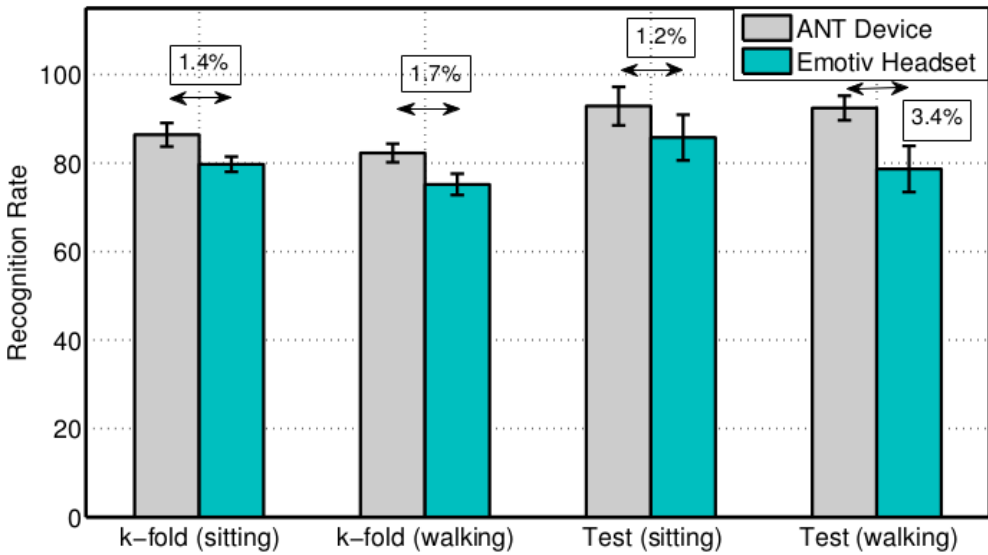


Figure 7.8: This Figure reports average and standard error values of classification rates under sitting/walking conditions for both EEG recording devices as well as p -values.

($p = 1.2\%$) whereas a large effect is again observed under walking conditions ($p = 3.4\%$). Given that effect size intervals are large, the actual value of effect size should be more precisely assessed with a much larger population. Overall, the decrease of performance is coherent with [13] in another context.

Table 7.1: Hedge g results

Hedge g^*	Lower bound	Mean estimate	Upper bound
K-fold (sitting)	0.28	0.95	2.76
K-fold (walking)	0.33	1.00	2.21
Test (sitting)	0.19	0.47	1.81
Test (walking)	0.3	1.05	1.98

Globally, the Emotiv Epoch headset is underperforming the medical device with a medium to large effect size. Confidence intervals were computed by bootstrap as mostly used by the toolbox's authors [28].

Finally, although the Emotiv Epoch performance is quite creditable especially regarding games, several main points have to be considered. First, the offered performance of the Emotiv headset is lower than the medical-grade system one. For non-critical applications such as games, this low-cost device should suit the customer's needs. However, in health-related applications or in research, this underperformance could lead to badly performing system that does not work as designed [31]. On the other hand, if researchers are trying to study new potentials in the brain, the lower SNR could make this discovery more difficult [10]. The previous discussion

suggests that the design of a new low-cost EEG headset device that disabled people can afford and dedicated to applications needing a highly reliable interface, such as rehabilitation systems, is somehow indispensable.

On the other hand, the presented results were obtained looking at a screen on a treadmill. Although treadmill walking is not that different from free walking, the latter one could lead to a more artefactual environment. It could thus be interesting to investigate whether the differences might modify the conclusions. The Vuzix system or the so-called Google Glass as a substitute of the screen may not be that simple. Indeed, potential interferences between the screen device and the EEG recording system may arise decreasing the overall performance. This should not modify the conclusions as the medical-grade system has already considered this issue. Another aspect would be to study the effect of these devices on the P300 response itself.

7.8.2 Other material considerations

The Emotiv EPOC headset and the ANT device can additionally be compared on other aspects: usability, robustness, cleaning, price, comfort, intrusiveness. In terms of usability, the Emotiv EPOC headset provides a much more user-friendly framework. First, the software user interface is handy and does not require a strong learning. This is much more adapted for end-users than the ANT environment, which was basically designed for researchers and physicians. Then, the headset is easy to place and it can be performed without any exterior assistance whereas the ANT device requires more training and some help at the beginning. However, the positioning of the Emotiv EPOC is somehow imprecise if a specific care is not taken, which is typically the case for end-users. This could lead to potential decrease of performance. Although not perfect, this drawback is mitigated in the medical device by the EEG cap.

Robustness is a major concern about the Emotiv headset. Indeed, the hardware is basically made of plastics and low-cost components, which results in a fragile headset whereas the ANT device is made of robust textile and cables and the electrodes cupules are made of high quality plastic. In the Emotiv headset, the plastic-based screw thread can easily break up if a particular attention is not brought during each experiment. In case makeshift repairs are not possible, a new headset has to be bought. Moreover, the electrode metallic parts are quickly oxidized even if cleaned at the end of each experiment as shown in Figure 7.9. After a while, they appear to produce less good signals (during this experiment, all the Emotiv headset electrodes were non oxidized). Moreover, the moss part of all the electrodes is degrading with time and has to be considered as a consumable. All these problems do not happen with the ANT device, which obviously leads to a higher lifespan for the latter system. Thus, the Emotiv headset also requires higher relative operating and maintenance costs.

Regarding the cleaning issues, the ANT system has a strong disadvantage. Due to the gel used to decrease the electrode impedance, the subject needs to wash his hair after the experiment. This is not required with the low-cost system as electrode impedance is lowered by a saline liquid. Price is obviously the strongest commercial argument of the Emotiv device. This headset is able to reach satisfying results for an at least 40 times less expensive solution than a medical device. In terms of comfort, people usually reports feeling some pain after one hour of wearing, which is undoubtedly not the case for medical devices. On average, the ANT cap was considered as much more comfortable.

Finally, in terms of intrusiveness, the Emotiv Epoch headset was much more broadly accepted. Subjects particularly like the wireless connection (although connection losses may arise especially in closed area) and the design of the low-cost device. However, the ANT device was not designed for ambulatory applications; this latter argument should disappear if a specific ambulatory design were available.



Figure 7.9: The oxidation of the electrode is clearly visible in green. On the back, the non-oxidized electrode has a gold color.

7.9 Conclusions

In conclusion, in this Chapter, a quantitative comparison of the low-cost Emotiv Epoc headset and the ANT medical/research EEG device is performed based on a standard P300 Brain-Computer Interface. This aims at contributing to get a better picture of how relevant the Emotiv Epoc is [7] and at giving enough information to researchers/end-users who would like to decide in which device they should invest. When comparing two devices, researchers have to master most of the variables of interest, which depends on what they want to show. In some previous work, the conclusion of the Emotiv Epoc headset underperformance was mainly due to different electrode location and numbers. They could not disentangle this effect from those related to the electrode/amplifier performance. Furthermore, the same process has to be applied on both systems. Given that the reference electrodes are different, a re-referencing after selecting the same electrode locations would give a better picture of their relative performance (in practice, we did not see differences; this could be due to the linear aspect of re-referencing, which computes linear combinations of electrodes, that can be obtained by both the spatial filtering and the LDA classifier).

In terms of performance, contrary to some BCI leader criticisms but coherently with previous Emotiv studies, the Emotiv Epoc headset performance is above random and not due to muscular or ocular artefacts. This was supported by far above chance classification rates. While comparing both systems, a large underperformance of the Emotiv device has to be emphasized. On a k -fold based comparison, p -values under sitting and walking conditions are significant with a large effect size indicating a lower SNR of the Emotiv headset. On the test set, a medium significant effect is detected under sitting conditions whereas a large significant effect is observed under walking conditions. According to these results, the Emotiv Epoc headset is undoubtedly an interesting option. It could be used for non-critical applications such as multimodal games for healthy people or communication and mouse control for disabled users. However, the medium to large underperformance suggests that for critical applications, only a medical-grade EEG recording device should be used. In case researchers can afford having a lot of trials (ERP analysis), it was shown that the Emotiv system may be suitable [10].

In terms of usability, the Emotiv headset has some advantages and disadvantages. It is handy to use, it does only require saline and the investment cost is extremely low compared to a medical-grade system, which is one of the requirements to be widely spread within the disabled people community. On the other hand, subjects are required to learn how to correctly put the headset, connection losses are not infrequent in closed areas, the operating and maintenance costs are relatively higher than in the ANT cap headset and generally, the ANT cap was considered by subjects as more comfortable.

For future work, four main axes can be explored: a larger number of subjects, other BCI paradigms, result durability and the design of a new low-cost EEG headset.

1) The precise assessment of the effect size requires much more subjects (around 100 people). Although the observed effect size is coherent with [13], this could help researchers to precisely know what is the relative value of the Emotiv headset.

2) This study focuses on the P300 speller-like system, i.e. inspired from the so-called P300 speller. However, other standard BCI paradigms exist and could be studied to confirm the results

presented in this Chapter. Spontaneous brain signals, e.g. emotion detection and event-related experiments, could be recorded to detect whether similar results can be observed with both devices.

3) Assessing the durability of the Emotiv headset would benefit the scientific community. Indeed, by experience, we know that the saline liquid is evaporating quicker than the ANT gel. This could lead to a drop of performance for applications used on a full-day basis.

4) Given the needs for a higher reliability in critical applications such as rehabilitation or even orthosis/prosthesis control, the design of a new low-cost EEG headset is required. Ideally, this headset should be light, have a large autonomy, have performance closer to a medical system and be relatively cheap.

Bibliography

- [1] José Del R. Millán, Rüdiger Rupp, Gernot Mueller-Putz, Roderick Murray-Smith, Claudio Giugliemma, Michael Tangermann, Carmen Vidaurre, Febo Cincotti, Andrea Kubler, Robert Leeb, Christa Neuper, Klaus R Müller, and Donatella Mattia. Combining brain-computer interfaces and assistive technologies: State-of-the-art and challenges. *Frontiers in Neuroscience*, 4(0):12, 2010.
- [2] Gert Pfurtscheller, Gernot R. Müller, Jörg Pfurtscheller, Hans Jürgen Gerner, and Rüdiger Rupp. ‘Thought’ - control of functional electrical stimulation to restore hand grasp in a patient with tetraplegia. *Neuroscience Letters*, 351(1):33 – 36, 2003.
- [3] B. Rebsamen, Cuntai Guan, Haihong Zhang, Chuanchu Wang, Cheeleong Teo, M.H. Ang, and E. Burdet. A brain controlled wheelchair to navigate in familiar environments. *Neural Systems and Rehabilitation Engineering, IEEE Transactions on*, 18(6):590–598, 2010.
- [4] Anton Nijholt, Danny Plass-Oude Bos, and Boris Reuderink. Turning shortcomings into challenges: Brain-computer interfaces for games. *Entertainment Computing*, 1(2):85 – 94, 2009.
- [5] Christian Mühl, Hayrettin Gürkök, Danny Plass-Oude Bos, Marieke Thurlings, Lasse Scherfig, Matthieu Duvinage, Alexandra Elbakyan, SungWook Kang, Mannes Poel, and Dirk Heylen. Bacteria hunt. *Journal on Multimodal User Interfaces*, 4:11–25, 2010.
- [6] Kenyon Stamps and Yskandar Hamam. Towards inexpensive BCI control for wheelchair navigation in the enabled environment - a hardware survey. In *Proceedings of the 2010 international conference on Brain informatics*, BI’10, pages 336–345, Berlin, Heidelberg, 2010. Springer-Verlag.
- [7] IEEE review. IEEE Spectrum. IEEE Press Piscataway, NJ, USA, January 2009.
- [8] Andrew Campbell, Tanzeem Choudhury, Shaohan Hu, Hong Lu, Matthew K. Mukerjee, Mashfiqui Rabbi, and Rajeev D.S. Raizada. Neurophone: brain-mobile phone interface using a wireless EEG headset. In *Proceedings of the second ACM SIGCOMM workshop on Networking, systems, and applications on mobile handhelds*, MobiHeld ’10, pages 3–8, New York, NY, USA, 2010. ACM.
- [9] Stefan Debener, Falk Minow, Reiner Emkes, Katharina Gandras, and Maarten de Vos. How about taking a low-cost, small, and wireless eeg for a walk? *Psychophysiology*, 49(11):1617–1621, 2012.

- [10] Nicholas Allan Badcock, Betty Mousikou, Yatin Mahajan, Peter de Lissa, Johnson Thie, and Genevieve McArthur. Emotiv versus neuroscan: Validating a gaming eeg system for research quality erp measurement. *Frontiers in Human Neuroscience*, (122).
- [11] Kirill Stytsenko, Evaldas Jablonskis, and Cosima Prahm. Evaluation of consumer EEG device emotiv epoch. In *MEi:CogSci Conference*, 2011.
- [12] M. Van Vliet, A. Robben, N. Chumerin, N.V. Manyakov, A. Combaz, and M.M. Van Hulle. Designing a brain-computer interface controlled video-game using consumer grade eeg hardware. In *Biosignals and Biorobotics Conference (BRC), 2012 ISSNIP*, pages 1 –6, jan. 2012.
- [13] Yue Liu, Xiao Jiang, Teng Cao, Feng Wan, Peng Un Mak, Pui-In Mak, and Mang I Vai. Implementation of ssvep based bci with emotiv epoch. In *Virtual Environments Human-Computer Interfaces and Measurement Systems (VECIMS), 2012 IEEE International Conference on*, pages 34 –37, july 2012.
- [14] Pavel Bobrov, Alexander Frolov, Charles Cantor, Irina Fedulova, Mikhail Bakhnyan, and Alexander Zhavoronkov. Brain-computer interface based on generation of visual images. *PLoS ONE*, 6(6):e20674, 06 2011.
- [15] L.A. Farwell and E. Donchin. Talking off the top of your head: toward a mental prosthesis utilizing event-related brain potentials. *Electroencephalography and Clinical Neurophysiology*, 70(6):510 – 523, 1988.
- [16] W. Peng, L. Hu, Z. Zhang, and Y. Hu. Causality in the association between p300 and alpha event-related desynchronization. *PLoS One*, 7(4):e34163, 2012.
- [17] M. Duvinage, T. Castermans, M. Petieau, K. Seetharaman, T. Hoellinger, G. Cheron, and T. Dutoit. A subjective assessment of a p300 bci system for lower-limb rehabilitation purposes. In *Engineering in Medicine and Biology Society (EMBC), 2012 Annual International Conference of the IEEE*, pages 3845 –3849, 28 2012-sept. 1 2012.
- [18] Brendan Z. Allison, Elizabeth Winter W. Wolpaw, and Jonathan R. Wolpaw. Brain-computer interface systems: progress and prospects. *Expert review of medical devices*, 4(4):463–474, July 2007.
- [19] T. Castermans, M. Duvinage, M. Petieau, T. Hoellinger, C.D. Saedeleer, K. Seetharaman, A. Bengoetxea, G. Cheron, and T. Dutoit. Optimizing the performances of a p300-based brain computer interface in ambulatory conditions. *Emerging and Selected Topics in Circuits and Systems, IEEE Journal on*, 1(4):566–577, 2011.
- [20] Yann Renard, Fabien Lotte, Guillaume Gibert, Marco Congedo, Emmanuel Maby, Vincent Delannoy, Olivier Bertrand, and Anatole Lécuyer. Openvibe: An open-source software platform to design, test, and use brain–computer interfaces in real and virtual environments. *Presence: Teleoper. Virtual Environ.*, 19(1):35–53, February 2010.
- [21] Ulrich Hoffmann, Jean-Marc Vesin, Touradj Ebrahimi, and Karin Diserens. An Efficient P300-based Brain Computer Interface for Disabled Subjects. *Journal of neuroscience methods*, 167(1):115–125, January 2008.

- [22] B. Rivet, A. Souloumiac, V. Attina, and G. Gibert. xDAWN Algorithm to Enhance Evoked Potentials: Application to Brain Computer Interface. *Biomedical Engineering, IEEE Transactions on*, 56(8):2035 –2043, 2009.
- [23] M. Duvinage, T. Castermans, M. Petieau, K. Seetharaman, T. Hoellinger, G. Cheron, and T. Dutoit. A subjective assessment of a p300 bci system for lower-limb rehabilitation purposes. In *Engineering in Medicine and Biology Society (EMBC), 2012 Annual International Conference of the IEEE*, pages 3845 –3849, 28 2012-sept. 1 2012.
- [24] Nicolas Riche, Matei Mancas, Matthieu Duvinage, Makiese Mibulumukini, Bernard Gosselin, and Thierry Dutoit. Rare2012: A multi-scale rarity-based saliency detection with its comparative statistical analysis. *Signal Processing: Image Communication*, 28(6):642 – 658, 2013.
- [25] Sawyer Steven F. Analysis of variance: The fundamental concepts. *The Journal of Manual and Manipulative Therapy*, 2009.
- [26] David C. Howell. *Statistical Methods for Psychology (Psy 613 Qualitative Research and Analysis in Psychology)*. Wadsworth Publishing, 2012.
- [27] Barbara G. Tabachnick and Linda S. Fidell. *Using Multivariate Statistics (6th Edition)*. Prentice Hall, 2012.
- [28] H. Hentschke and M. C. Stüttgen. Computation of measures of effect size for neuroscience data sets. *European Journal of Neuroscience*, 2011.
- [29] Jacob Cohen. *Statistical Power Analysis for the Behavioral Sciences (2nd Edition)*. Routledge Academic, 1988.
- [30] Mark W. Lipsey. *Design Sensitivity: Statistical Power for Experimental Research (Applied Social Research Methods)*. Sage Publications, Inc, 1989.
- [31] M. Duvinage, T. Castermans, R. Jimenez-Fabian, T. Hoellinger, C. De Saedeleer, M. Petieau, K. Seetharaman, G. Cheron, O. Verlinden, and T. Dutoit. A five-state p300-based foot lifter orthosis: Proof of concept. In *Biosignals and Biorobotics Conference (BRC), 2012 ISSNIP*, pages 1 –6, jan. 2012.

Chapter 8

EOG-based Eye Movement Detection: A Quantitative Review For Controlling A Lower-Limb Orthosis

Contents

8.1	Introduction	175
8.2	EOG Eye Movements	175
8.2.1	EOG Measurements	175
8.2.2	Eye Movement Features	176
8.3	Whole schematic control	177
8.4	Experiment Description	178
8.4.1	Experimental Design	178
8.4.2	Evaluation Metrics	179
8.5	Saccade, Blink and Wink	180
8.5.1	R. Barea (RB)'s Work	181
8.5.2	A. Bulling (AB)'s Work	183
8.5.3	Enhancement Propositions	184
8.5.4	Wink Detection: A. Brandão's approach	186
8.5.5	Others Methods	187
8.6	Results	188
8.6.1	R. Barea (RB)'s Results	188
8.6.2	A. Bulling's results	188
8.6.3	Interface Comparison	189
8.7	Conclusion and Future work	190

Abstract

Heavily disabled people can sometimes only control their eye movements. Therefore, researchers have focused for a long time on using eyes as a communication tools.

In this Chapter, we propose an original and biologically-inspired leg prosthesis control scheme consisting of: an EOG-based eye tracker and a Programmable Central Pattern Generator (PCPG). Additionally, although ElectroOculoGraphic (EOG) signals have been intensively used for human-machine interfaces, none of the available eye movement recognition techniques have been objectively compared to each other. Here, we propose to compare two widely known techniques (the standard R. Barea (RB) and A. Bulling (AB)'s works). We also suggest several potential improvements and the implementation of a method inspired from speech-recognition that were all assessed according to the F1-score. Additionally, we investigate 3 different target configurations on the screen: 3x3, 3x5 and 5x5. This aims at detecting which configuration can reach the best bitrate. Finally, double blink and wink detectors are F1-score evaluated to estimate their relevancy as a mouse click.

In this 8-healthy-subject experiment, we observed that both RB and AB methods provide fairly similar results. According to the bitrate analysis while considering complexity, the 3x3 is the most suitable interface. Among the different potential enhancements, none of the methods seems to outperform the fixed grid. The speech tool-based method provides unexpected good results. Regarding the eye mouse click detectors, their performance should be high enough to be used in a reliable interface.

This chapter is based upon the following publications:

- M. DUVINAGE, J. CUBETA, T. CASTERMANS, M. PETIEAU, T. HOELLINGER, G. CHERON, T. DUTOIT, 2013, *A Quantitative Comparison of the Most Sophisticated EOG-based Eye Movement Recognition Techniques*, Proceedings of the IEEE SSCI series, Singapore, April 16-19.
- M. DUVINAGE, T. CASTERMANS, T. DUTOIT, 2011, *Control of a lower limb active prosthesis with eye movement sequences*, Proceedings of the IEEE Symposium on Computational Intelligence, Cognitive Algorithms, Mind, and Brain (CCMB), Paris, France, April 11-15, pp. 136-142.

8.1 Introduction

Severely disabled people are sometimes only able to move their eyes. That is one of the main reasons for looking for interfaces relying on eye movements. Among those interfaces, a common example is a mouse control, which allows the patient to interact with the environment without any limb movement [2]. Additionally, the same researchers showed that specific eye moment sequences could help controlling a wheelchair while getting a good controllability [2, 3]. Finally, we proposed to control a lower limb prosthesis in a similar way combined with a central pattern generator-based gait model.

Additionally, for two decades, a lot of different eye movement EOG-based recognition techniques have been proposed. But, as explained in [4], none of them have been compared to each other. This strong lack does not allow researchers to assess what their new method brings to the literature. Among them, mainly two different but similar well-known techniques show a deep study for a complete saccade detection system: R. Barea (RB) and A. Bulling's (AB) works [4, 5]. Their main idea is that they both calculate derivative-related information to locate saccades and blinks and to get their magnitude.

To get a complete interface, a kind of mouse click has to be implemented. This can be advantageously achieved by blinks and winks. Thereby, a double blink detector was proposed by R. Barea. On the other hand, as suggested by A. Brandão, a right/left wink detector could also be handy and quite reliable to quickly activate commands [6].

In this framework, this Chapter proposes an innovative scheme to combine current knowledge to achieve the control of a lower limb prosthesis/orthosis as simple and comfortable as possible. Then, a comparison for EOG-based eye movement recognition techniques is proposed, which is quite impossible in the literature given the variety of the used performance measures and frameworks. In Section 8.2, the eye movement measurements and features are explained. In Section 8.3, the whole schematic control is detailed. In Section 8.4, the experiment design and evaluation metrics are described. In Section 8.5, the compared saccade detection methods as well as two activation techniques using double blinks and winks are summarized. We also propose several potential enhancements. In Section 13.3, the results are shown and discussed. We also compute the bitrate for three different target configurations on the screen: 3x3, 3x5 and 5x5.

8.2 EOG Eye Movements

8.2.1 EOG Measurements

In the case of severely disabled people, eye movements are often one of the last means of communication. This is why researchers have tried to interpret eye movements in order to interact with a computer, namely a Human-Computer Interface (HCI). Among the different methods existing to track the eye movements such as special contact lenses, infrared light reflections measured with video cameras, electrooculography (EOG) with simple electrodes around the eyes is the most portable technology.

The electrodes measure the resting potential that is generated by the positive cornea (front of the eye) and negative retina (back of the eye). When the eye rotates, the dipole rotates as well. By

positioning pairs of electrodes around the eyes as shown in Figure 8.1, it is possible to decompose the eye movements on the horizontal and vertical axes. This technique has the advantages of a very high SNR while being easily portable and cheap [5].

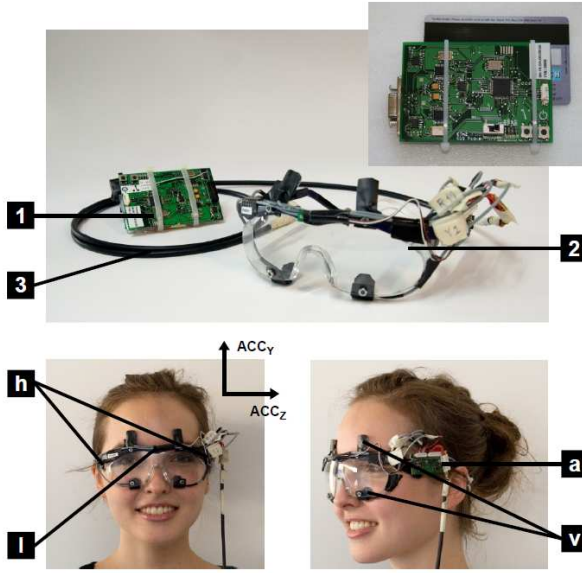


Figure 8.1: There are several components in the EOG-based wearable eye tracker: the DSP (1), the Goggles (2) and the shielded core cable (3). The pictures at the bottom show the Goggles worn by a person with the positions of the two horizontal (h) and vertical (v) dry electrodes, the light sensor (l) and the accelerometer (a) with direction of its axes (ACC _ Y, ACC _ Z). [5]

Given the huge interest of such EOG-based assistive technologies, some hardware solutions have been proposed. Figure 8.1 shows the current most close to market hardware system in terms of its design and its portability, detailed in [5]. This self-contained wearable device consists of goggles with dry electrodes integrated into the frame and a small pocket-worn component with a DSP for real-time EOG signal processing. It has two accelerometers and one light sensor for compensating EOG signal artefacts caused by physical activity and changes in ambient light. It can stream processed EOG signals to a remote device over Bluetooth to command other systems.

8.2.2 Eye Movement Features

The eye can be seen as an electrical dipole [5]. Nerve cells located in the back of the eye provoke a decrease of the electrical potential. This leads to a potential difference between the front and the back of the eye. Therefore, the displacement of the ocular dipoles creates a potential modification by polarizing the electrodes around the eyes. This is the underlying concept of ElectroOculoGraphic (EOG) signal recording. The observed potential differences are 16 μ V and 14 μ V for horizontal and vertical movements, respectively.

Basically, as depicted in Figure 8.2, natural eye movements are characterized by three different types of movements: saccades, fixations and blinks [5]. Saccades appear when a rapid (up to $400^{\circ}/\text{s}$) eye gaze direction occurs. Most of the time, they do not last more than 80 ms and they do not have a magnitude variation higher than 20° . On the other hand, fixations correspond to the time of a fixed eye gaze. Although in theory, the signal should be constant during fixations, human eye is never fixed and small involuntary micro-saccades and noise could be interpreted as voluntary saccades. Blinks correspond to a two-way vertical reflex movement occurring when the eyes quickly close and open. The average blink duration is between 100 ms and 150 ms and the blink rate is between 7 and 50 per minute. Fatigue can significantly increase the blink rate of a subject.

Finally, an intrinsic property of the EOG signal makes the automatic detection task complex: the drift [5]. This drift comes from the slight biological modification of the rest potential with time. To properly deal with saccades and blinks, this drift must be removed such as other noises like electrical power and muscle activity.

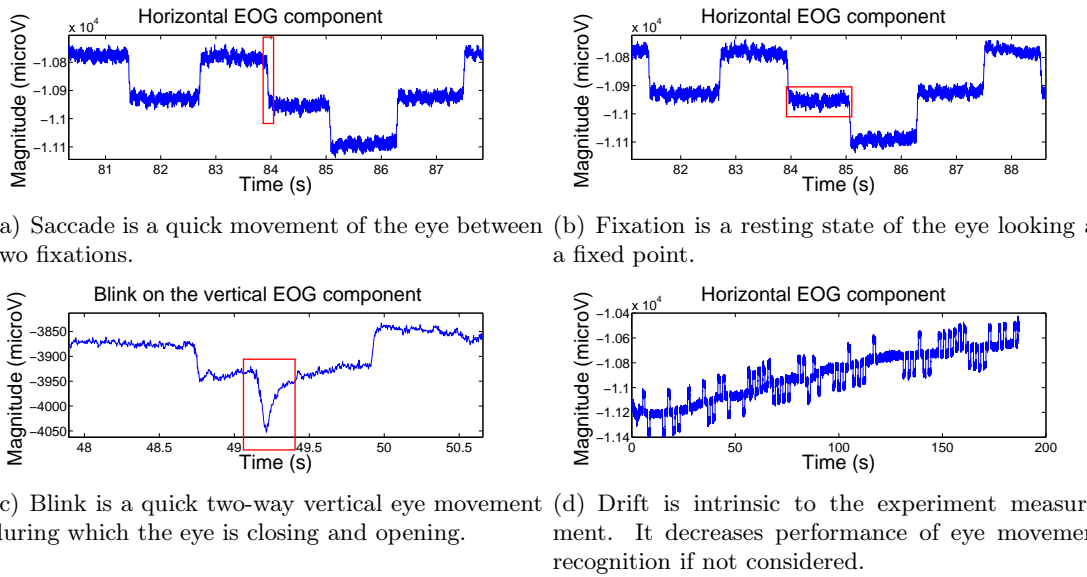


Figure 8.2: Typical eye events are blinks, saccades and fixations. Furthermore, a drift in the measurement makes the recognition step more difficult.

8.3 Whole schematic control

One of the originality presented in this Chapter is the biologically inspired scheme to control a lower limb prosthesis/orthosis by eye movements. This process is composed of a high-level command system based on EOG signals and a PCPG pattern generation to control this prosthesis.

Although not natural, utilizing the EOG output to command systems presents a double interest. First, eye gaze detection can provide the precise direction of eye movements in real time. These movements can thus be labelled as left, right, up or down. Specific eye movement

sequences executed by the user can then be associated to high-level commands sent to the prosthesis actuator. In [5], a study was carried out in order to determine the most efficient eye movement sequences to be used in such context, as well as the best algorithms to detect them. It appears that a simple and quite effective mean to determine eye movement sequences is to use the edit (or Levenshtein) distance. The Levenshtein distance between two given strings is defined as the number of deletions, insertions and substitutions required to transform one of them into the other one. In this case, the string is built by the concatenation of each labelled state of the eyes (e.g. the string associated to a left-right movement would be LR).

The second interest of EOG signals resides in the high speed of eye movements. The user can thus very quickly activate or deactivate a high-level command generation environment. This aims at decreasing the subject attention load to actually command the prosthesis. For example, when the patient wants to change the speed, he enters in this environment by means of a certain sequence of blinks and executes the correct eye sequence to really change the speed. In case of emergency, the patient could of course stop the prosthesis using a specific high-level command (a sequence of winks for example) recognizable without entering in the environment mode. From a practical point of view, it has to be mentioned that an adaptive filter has been developed to remove artefacts due to walk limiting therefore the error rate in eye movement sequences detection [5].

8.4 Experiment Description

In this section, the full experimental setup is described. First, some considerations about the eye movement features are given. Then, the experimental design is explained. Finally, the performance metrics in this framework are detailed.

8.4.1 Experimental Design

As depicted in Figure 8.3, to measure eye movement activity, Ag/AgCl electrodes were vertically and horizontally aligned on the iris. A reference electrode was placed on the back of the hand. All the data were acquired by the Advanced Neuro Technology (ANT, Enschede, The Netherlands) amplifier at a 512 Hz sampling rate.

Using the OpenVibe software and, as depicted in Figure 8.4, three different interfaces were considered by dividing a 27 cm x 37.5 cm screen at 50 cm in front of the subject into equally distributed areas corresponding each to a potential action: 3x3, 3x5 and 5x5. This aimed at detecting whether a more complex interface could lead to a better bitrate. Obviously, by increasing the number of states, the recognition rate could eventually collapse annihilating the potential gain of enhanced command capabilities.

During the experiment, the eighth healthy subjects (as shown in Table 8.1) had to follow the cross, which alternatively appeared at the center or in a random (except center) area each second. For each configuration, each position on the screen was looked at thirteen times. By generating a specific event synchronized with the cross appearance, the algorithm is able to detect the corresponding saccade useful for the learning step and the performance metric computation. Two datasets per configuration were recorded for separately training and testing the methods.

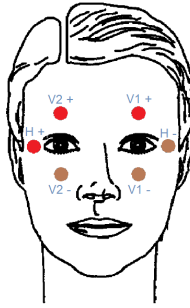
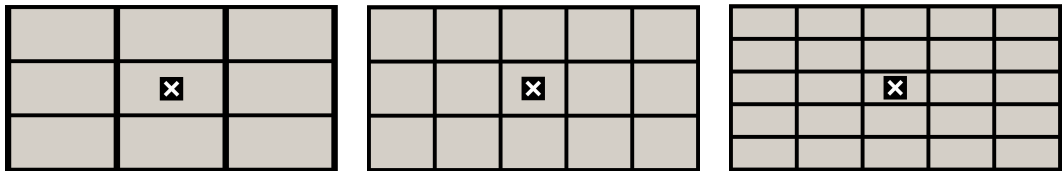


Figure 8.3: Three electrode pairs were vertically and horizontally aligned with the iris. A reference electrode was positioned on the back of the hand.



(a) The 3x3 configuration is able to emit 8 commands.
(b) The 3x5 configuration aims at taking advantage of a better horizontal separability.
(c) The 5x5 configuration tests the most complex conceivable interface.

Figure 8.4: The subject has to look at the cross at each time. This cross alternatively moves between the center and any other positions.

Furthermore, several additional databases were recorded by training-testing pairs. These include 50 trials of voluntary blinks (pseudo-natural blinks), double blinks, right winks, left winks. Two complementary baseline recordings with closed eye and opened eyes were performed to automatically estimate a noise level and get natural blinks. This was obtained by asking the subject to keep his eyes closed.

8.4.2 Evaluation Metrics

To assess the performance of EOG detection techniques, researchers have mainly focused on binary classification theory [5]. In case of a two-class prediction problem, in which the data are labelled either positive (p) or negative (n), four different outcomes can occur as depicted in Table 8.2. Whether a positive class is positively or negatively attributed, the system is facing a True Positive (TP) or a False Negative (FN), respectively. On the other hand, if the actual class is negative, a positive decision yields a False Positive (FP) outcome whereas for the opposite decision, a True Negative (TN) is counted.

Because saccade detection is not a binary decision problem, a slight modification has to be brought [5]. Considering the correct saccade as a positive event, FP is a detected event without matching a saccade and FN is an undetected or badly classified saccade event. TNs are not considered here given our focus on saccades.

From these decisions, three direct performance measures can be obtained: the recall, the

Table 8.1: Eight subjects were enrolled in this preliminary study.

Subject	Genre	Age	Glasses	Lenses
1	m	25	yes	no
2	m	23	no	no
3	m	35	no	no
4	m	30	no	no
5	f	21	no	no
6	m	30	no	no
7	m	20	no	no
8	m	21	yes	no

Table 8.2: ROC-based analysis is essential to get a complete idea of a binary system performance. This can be extended to several class issues.

	Relevant label	Not relevant label
Recognized as relevant	True Positive (TP)	False Positive (FP)
Recognized as not relevant	False Negative (FN)	True Negative (TN)

precision and the classification accuracy. Recall, which is defined as $\frac{TP}{TP+FN}$, gives an information about how correctly classified the positive samples are. On the other hand, precision is computed as $\frac{TP}{TP+FP}$. This characterizes the system capability to detect the truly positive samples. Finally, in this framework, classification accuracy is calculated by $\frac{TP}{TP+FN+FP}$.

Other widely used global measures can be derived from the previous individual indicators: the bitrate and the F1-score. As inspired from the Shannon information transfer rate, under the assumptions of equiprobability of N saccade events with each having a similar accuracy P , bitrate is obtained by $R = \log_2 N + P \log_2 P + (1 - P) \log \frac{1-P}{N-1}$ [7]. Although the required assumptions are not totally met, it was shown that the Wolpaw formula is a robust estimation. On the other hand, the F1-score is a combination of recall and precision rates to consider their intrinsic trade-off. This is computed as $2 \frac{\text{precision} * \text{recall}}{\text{precision} + \text{recall}}$.

To compute all these metrics, saccade events, which correspond to movements from the center to a target and vice versa, have to be associated to targets. This is performed thanks to a window of 1.3 s (starting 0.4 second before the target). The target is attributed to the closest event. A target associated event is removed to avoid overlap with other windows.

8.5 Saccade, Blink and Wink Detection Techniques

In this section, saccade, blink and wink widely known detection techniques are detailed. First, the R. Barea's method is described. Second, the A. Bulling's approach is shown. Third, some potential improvements based on our observations are suggested. Fourth, A. Brandão's approach is described. All the required thresholds were manually chosen and consistent over subjects and methods.

8.5.1 R. Barea (RB)'s Work

As depicted in Figure 8.5, the pipeline of the R. Barea's approach consists of six main steps: preprocessing, Continuous Wavelet Transform (CWT), saccade linear model, artificial neural network, blink detection and ocular movement detection [4]. First, the preprocessing aims at focusing in the frequency band of interest. Thus, a band pass filter is applied in the 0.05-35 Hz frequency band. This allows to remove the slow biological drift as well as high frequency noise such as electric power interference.

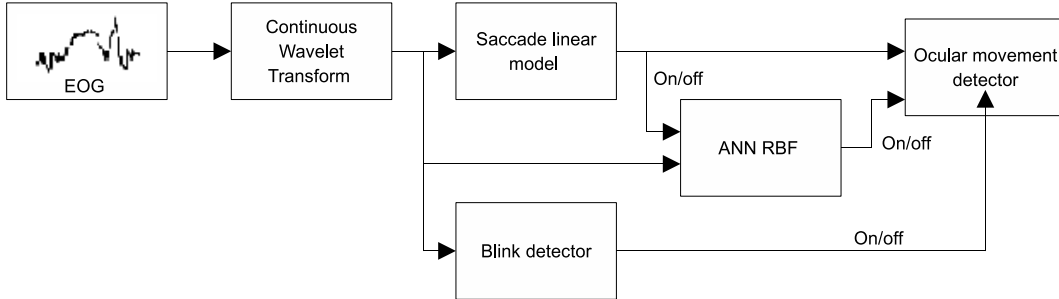


Figure 8.5: The pipeline of the RB method consists of six main steps: preprocessing, Continuous Wavelet Transform (CWT), saccade linear model, artificial neural network, blink detection and ocular movement detection.

Second, the CWT is considered to obtain the derivative while providing a better SNR. This allows to detect quick variations that correspond to saccades and blinks. The CWT coefficients $g(a, \tau)$ belonging to the ψ family are defined by:

$$g(a, \tau) = \int_{-\infty}^{+\infty} f(t) \psi_{a,\tau}^*(t) dt \quad (8.1)$$

with $\psi_{a,\tau}^*(t)$ being the wavelet conjugate of $\psi_{a,\tau}(t)$ defined as:

$$\psi_{a,\tau}(t) = \frac{1}{\sqrt{a}} \psi\left(\frac{t - \tau}{a}\right) \quad (8.2)$$

where a represents the scale factor and τ the translation factor. In this context, the 1-Daubechies mother wavelet (also called Haar function) was chosen. The best scale factor was found at 60 [4]. As shown in Figure 8.6, the SNR is much better using CWT than standard derivative.

Third, to detect whether the CWT output corresponds to a saccade and determines its magnitude, a linear ocular model is utilized by computing a linear regression. Indeed, the underlying assumption is that EOG signal variations are proportional to eye movement magnitudes. In order to avoid false alarms, a threshold on the CWT allows to remove noise and involuntary micro-saccades as shown in Figure 8.7. This threshold is manually determined by a trial-and-error approach.

Fourth, a radial function-based artificial neural network aims at confirming the ocular movements. After a saccade detection from previous steps, a 0.5-s centred window, which introduces a potential delay of 250 ms, is fed to the neural network. This network checks whether it is a

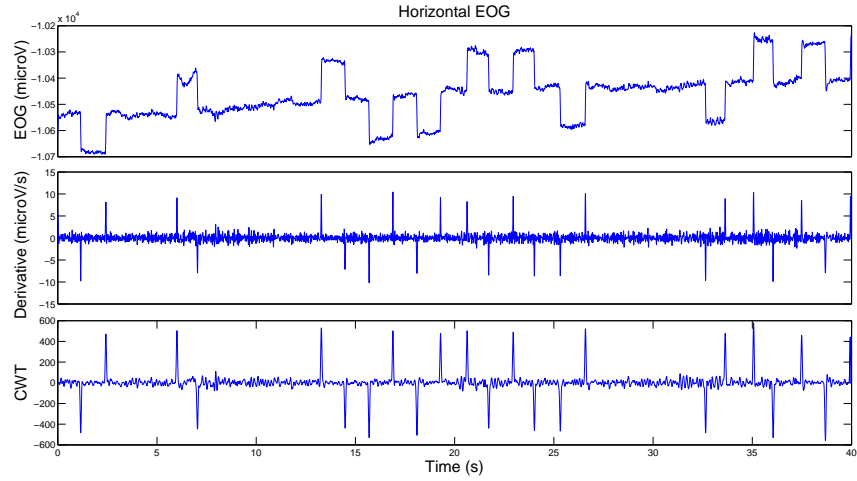


Figure 8.6: The CWT has the same effect than the derivative while getting a much better $\frac{S}{N}$.

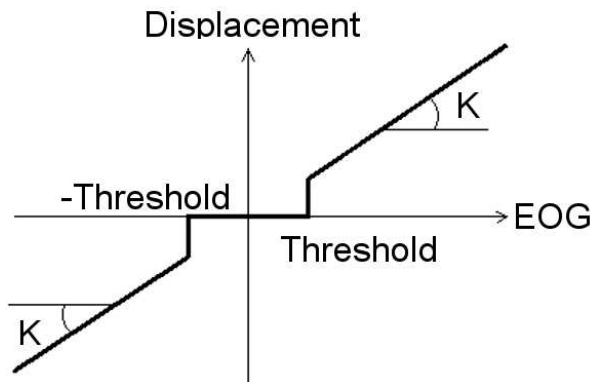


Figure 8.7: A thresholded linear model is used to get an estimation of the eye movement magnitudes.

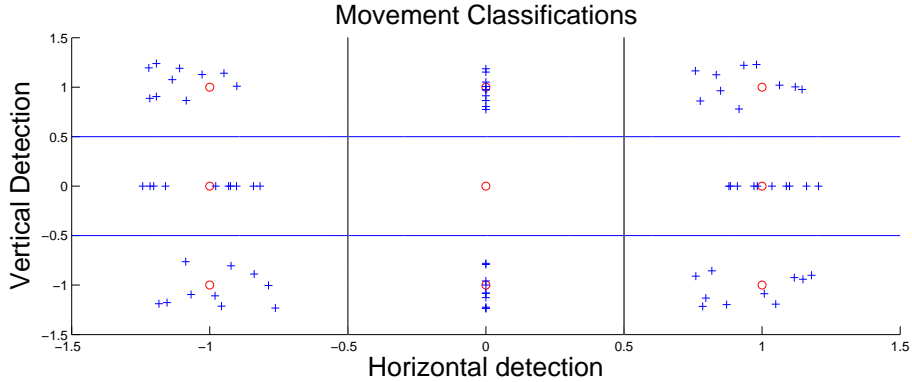


Figure 8.8: EOG events are classified depending on their closest reference targets.

true saccade as learned in the training procedure. The training data consists in fixations and saccades. As reported in [4], this method is really needed when subjects are feeling fatigue using the system. This feed-forward network is composed of one single hidden layer and the learning process is achieved by the Extreme Learning Machine (ELM) algorithm [8]. This algorithm shows good overall performance and is extremely quick.

Fifth, a double-blink detector is incorporated to mimic a mouse click [4]. To generate a double blink, the subject has to blink twice in less than 500 ms. When a potential blink is found by the CWT, a correlation between a blink model and a window centred on this potential blink is performed. Above a certain threshold, a blink is recognized and the algorithm looks for a second similar blink within a 500 ms window by the same procedure. The threshold is found by using a mixed database of double blink, winks, saccades, natural blinks and pseudo-natural blinks.

Sixth, the ocular movement detector summarizes all the information coming from the blink detector and the saccade checking network. Additionally, a nearest neighbourhood classification method is performed. When diagonal movements occur, it may happen that vertical and horizontal movements are not perfectly aligned. To overcome this problem, vertical and horizontal saccades within 0.06 s from each other are considered as one single movement. Finally, saccades are attributed to the euclidean-based nearest neighbour target obtained in the learning process as depicted in Figure 8.8.

8.5.2 A. Bulling (AB)'s Work

As depicted in Figure 8.9, the pipeline of the AB approach is somehow similar to the RB one and consists of six main steps: preprocessing, CWT, blink detection, blink removal, linear saccade model and nearest neighbour classification [5]. First, to remove as much noise as possible, a moving average filter (150 ms) was used. Second, the CWT component is the same as previously described except the scale factor of 20.

Third, the blink detector here aims at determining where natural blinks, which can be recognized as vertical saccades, are located. The detection relies on the particular blink shape of the derivative: a positive peak quickly followed by a negative one. Therefore, the algorithm has simply to detect two consecutive peaks by thresholding the CWT within 0.5 second. Indeed, two

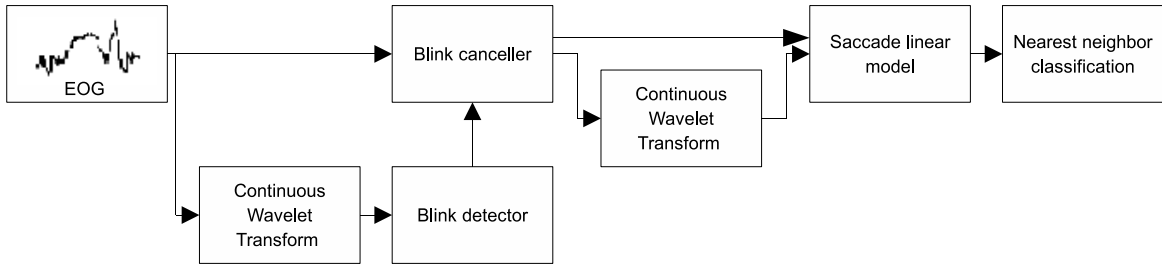


Figure 8.9: The pipeline of the AB method is not that different from the RB one. Again, six main steps are needed: preprocessing, CWT, blink detection, blink removal, linear saccade model and nearest neighbour classification.

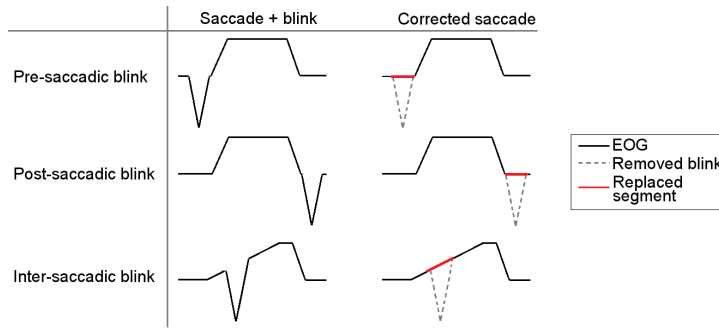


Figure 8.10: Blink removal depends on the configuration: pre-, post- and inter- saccadic.

other modifications were assessed but lead to worse results: a MLP with the same feature and the same method as the double blink detector of R. Barea.

Fourth, as depicted in Figure 8.10, blink removal is performed depending on their configurations: pre-saccadic, post-saccadic and inter-saccadic. Pre-saccadic and post-saccadic are sharing the last peak or the first peak with a saccade; the blink is replaced by the EOG after and before it, respectively. For inter-saccadic blinks, a linear interpolation is computed.

Fifth, the linear model relies on a function whose values are +1, -1 and 0 when the CWT is above a positive threshold, below a negative threshold and in between. Then, succession of +1 and -1 whose duration is below 0.02 s and above 0.2 s are removed. Eye movement magnitude is computed by subtracting EOG value before and after the saccade followed by a linear adjustment by a K factor (determined by linear regression in the learning process).

Sixth, the nearest neighbour classification is applied the same way as described for the RB method.

8.5.3 Enhancement Propositions

From a preliminary assessment, we observed some major issues: lower SNR on vertical channels, misalignment of learned targets, bad diagonal movement classification, inadequately chosen threshold, bad saccade step representation and two-step saccades. First, because of a lower vertical maximum magnitude and of blink pollution, vertical eye movement detection is more

challenging (this is why the 3x5 interface was considered). To mitigate this problem, a moving-window-size moving-average filter was proposed. This allows to decrease the noise during fixations while keeping saccade sharpness by dividing the window size by 10 to 0.02 s around saccade events. As shown in Figure 8.11, this yields a higher CWT SNR.

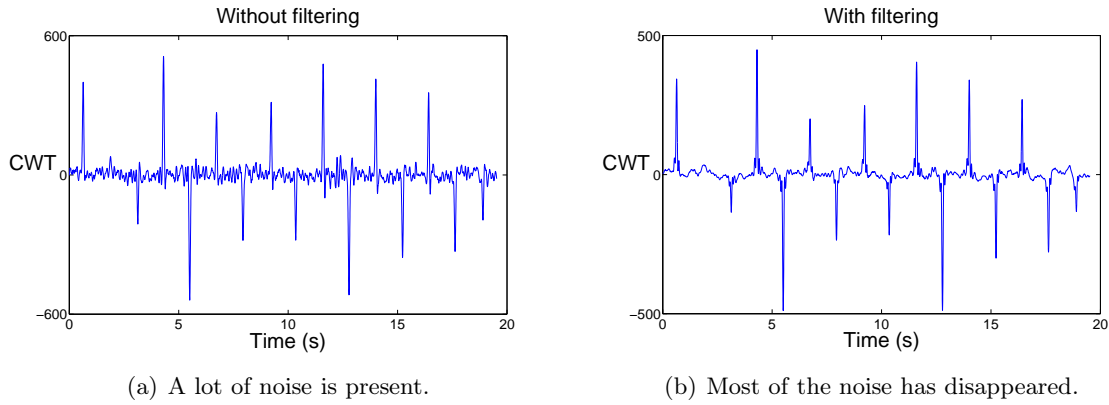


Figure 8.11: The moving-window-size moving-average filter mitigates the noise during fixations while keeping the saccade sharpness. It results in a better SNR.

Second, the target grid computed during the learning process does not always work as desired. As illustrated in Figure 8.12 for the worst subject, the alignments of mean targets is not perfect. There is a kind of linear drift for upside vertical movements and an upside curvature for negative vertical saccades. Potential explanations could be misalignment of electrodes with the iris, not perfectly symmetrically positioned electrodes and the eye mobility limitations. Thus, we propose to offset this inconvenience by creating a customized target grid. Indeed, the mean targets are computed as centroids during the training. This allows to get a more adequate target grid for each person.

Third, given that the vertical movements have a smaller magnitude, some diagonal centroids were too close to horizontal ones leading to misclassification. A simple Vertical Booster (VB) transformation was used to correct that problem: a gap increase between problematic centroids by an overall vertical translation above and below rest position. Thus, an equally-distributed grid is obtained implying better performance.

Fourth, contrary to the standard fixed threshold on the derivative, one alternative is to compute an adaptive thresholding on the EOG acceleration signal [9]. For each new sample, the new threshold is calculated at $N*\sigma$ except when a saccade is detected during which the threshold is fixed. σ is the standard deviation of the 1.2-s sliding window, whose size was determined by trial and error and N is a fixed number to obtain a given percentage of the population, e.g. $N = 3.4$, as chosen in this paper, leads to 99.93 % samples of the distribution. As we obtained better results with speed instead of acceleration, only results based on this approach using speed are reported.

Fifth, as proposed in [10], we assessed the saccade step magnitude by computing the total EOG derivative impulsion. To calculate this overall impulsion, they suggest to consider the integration of the derivative above threshold. Roughly, this is quite equivalent to the EOG step

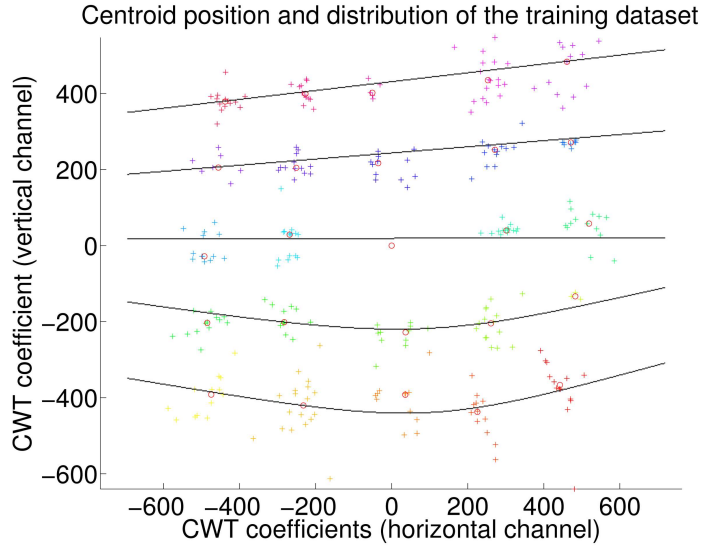


Figure 8.12: For the worst subject, centroids are not perfectly aligned. There are different tendencies that could be explained by misalignment of electrodes with the iris, not perfectly symmetrically positioned electrodes and the eye mobility limitations.

as used in the AB method.

Sixth, some saccades are performed in two steps. For these events, when a saccade was detected, all the saccades present in a 0.55 s window were summed and considered as a single saccade. This was used for every method.

8.5.4 Wink Detection: A. Brandão's approach

As illustrated in Figure 8.13, the A. Brandão's method to detect wink is composed of three main components: a peak detection, a thresholding and a neural network [6].

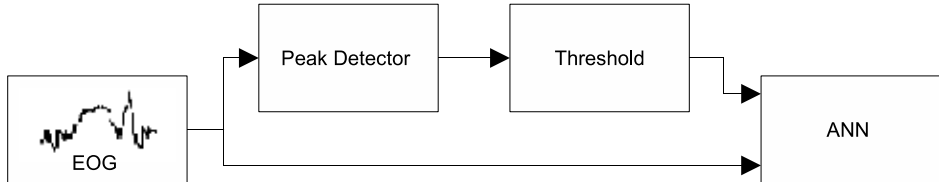


Figure 8.13: The A. Brandão's method aims at detecting right and left winks and natural blinks.

First, the peak detection aims at determining events that correspond to sharp and high-magnitude variations. After a moving average normalisation, a Pan-Tompkins derivative is applied to the signal [11]. Then, the resulting signal is squared before a moving average smoothing.

Second, the thresholding is performed on the peak detector output to prevent considering artefacts. Then, samples below the maximum calibration value are equalled to zero.

Third, the neural network allows to classify right and left winks and natural blinks, which are

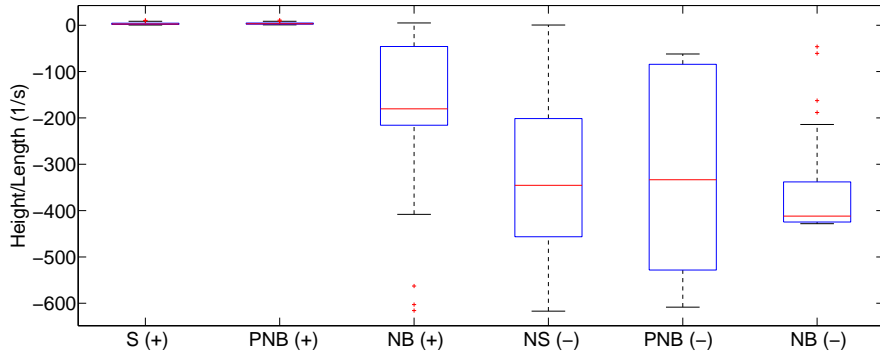


Figure 8.14: A distinction between saccades, blinks and pseudo-natural blinks may not be obvious using height/duration ratio of the CWT peaks (S for saccades, PNB for pseudo-natural blinks and B for blinks).

considered here as noise. A peak-centred 0.4 s EOG signal window is fed to a one hidden layer Multi-Layer-Perceptron (MLP). At the MLP output, all the events are labelled accordingly.

8.5.5 Others Methods

One additional type of method is the one based on speech processing methods consisting of: preprocessing, feature extraction and Dynamic Time Warping pattern recognition [12]. In this method, an endpoint detection is first applied to focus on relevant EOG fragments. Because standard short-time energy is badly performing in noisy EOG signals, spectral entropy was proposed in [13]. Indeed, the entropy of EOG signals is fairly constant what regards noise and the considered EOG segment. This obviously facilitates the recognition. Then, a bandpass filter is applied to the EOG data between 0.5-10 Hz. After a windowing, Linear Predictive Coding Cepstrum (LPCC) coefficients are computed [14]. These coefficients have been found useful in speech recognition. Finally, a Dynamic Time Warping (DTW) pattern recognition system is performed to determine what types of eye-movements are in the data.

With the 3x3 configuration, the obtained performance was around 88 %. This is an unexpected good performance for a completely different approach. The endpoint detection was obviously working quite well and it could be used to enhance saccade detection in other methods.

Another method is based on original features to classify blinks and saccades: ratio between height and duration [15]. If this ratio is smaller than 0.1, a blink is detected. Although interesting, we observed on our data that the distribution of such values are seldom fairly distinguishable. As can be seen on Figure 8.14 for one representative subject, there is a high overlap between positive and negative edges of saccades, natural blinks and voluntary blinks.

8.6 Results

In this section, all the results using the F1-score are exposed for the three interface configurations. First, the R. Barea's methods are exposed. Second, the Bulling's methods are shown. Finally, the three configurations are compared to each other on the basis of their bitrate.

8.6.1 R. Barea (RB)'s Results

As depicted in Figure 8.15, several conclusions can be outlined. First, the F1-scores obtained with the 5x5 configuration are generally far away from the other ones and much more variable when not bad. Obviously, this configuration does not seem adequate for a safe and reliable interface. Indeed, the average F1-score often reaches 50 %, which is insufficient.

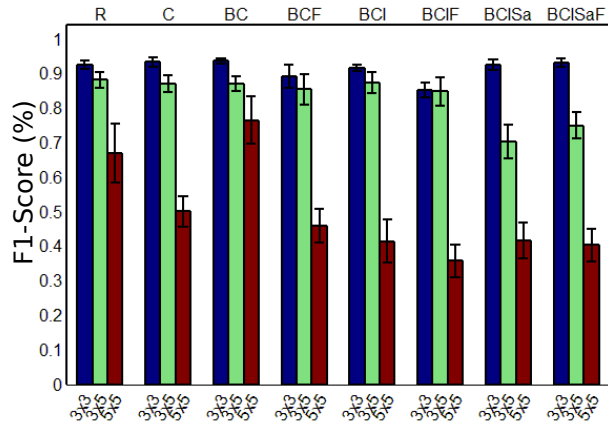


Figure 8.15: Several variants of the RB approach are assessed according to the F1-score: *R* for linear regression, *C* for clustering, *B* for Vertical_Booster, *F* for moving-window-size moving average filter, *I* for CWT integration and *Sa* for adaptive thresholding. The clustering approach seems to be the best method. The vertical booster could bring an added value for the 3x5 configuration.

Second, no clear outperformance of the modified methods can be observed. Indeed, it appears that the clustering approaches roughly provide the same results as the original linear regression method (just a small increase was observed). However, with this approach, the clustering approach also allows to quickly find the correct location of targets contrary to a standard grid decomposition.

8.6.2 A. Bulling's results

An improvement of the AB standard method thanks to the cluster-based alternative is observed for the 3x3 as indicated in Figure 8.16. On the opposite, other configurations do not benefit from this. This is explained by more instability in the cluster positions when a higher number of states is used.

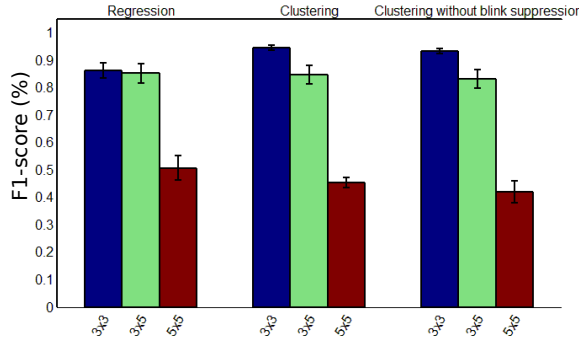


Figure 8.16: The performance plot of AB variants again indicates that the clustering approach is one interesting improvement. Furthermore, blink removal does not seem really useful in terms of F1-score enhancement.

The blink removal step does not seem to bring an added value. Given the low improvement in performance, an embedded solution could afford deleting this component. But, this behaviour could be due to our implementation: when a potential saccade is found, other peaks are summed over a 0.55 s window.

Finally, the clustering-based A. Bulling method offers a performance quite similar to its R. Barea counterpart. As a result, we can not really decide which approach is the best one. But, although the RB method introduces a delay, it appears as a more robust method for an intensive use as required for a daily life application.

8.6.3 Interface Comparison

Using the best of RB methods, at first sight, the 5x5 configuration is obviously not adequate whereas the 3x3 and 3x5 configurations appear relevant. The drop in performance and the high variability make the 5x5 configuration unusable for a reliable interface. Additionally, when sufficiently good, the variability among subjects is very strong making difficult to spread it. On the other hand, the 3x3 and 3x5 configurations have an overall good behaviour. Although the 3x3 configuration has a better performance, it has to be put in perspective with the extended command emission capabilities of other configurations. An objective assessment can be performed thanks to the bitrate evaluation (on the best condition for the 5x5).

As depicted in Figure 8.17, the 3x5 configuration has the best average bitrate. However, this outperformance is rather small and it does not compensate for complexity. As reported in [4], patients are known to prefer simple interfaces such as the 3x3 configuration, especially, for such a low bitrate improvement. Therefore, we would recommend using the 3x3 configuration.

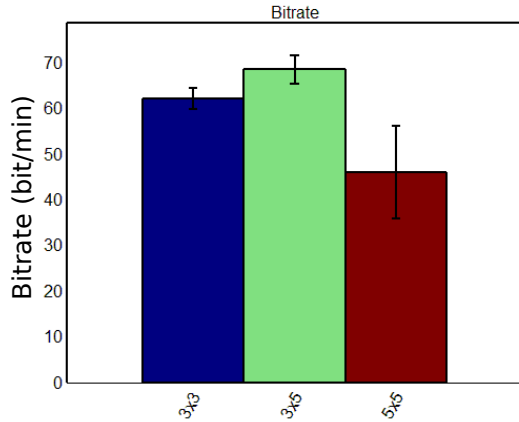


Figure 8.17: A bitrate-based comparison indicates that the 3x5 interface has a slightly better average performance. However, this difference is not significant contrary to the underperformance of the 5x5 interface.

8.7 Conclusion and Future work

In this Chapter, an innovative method to drive a lower limb prosthesis on the basis of EOG signals is explained. Then, a deep comparative study of two widely known EOG-based eye movement detection techniques with a strong historical support in the literature is proposed: the A. Bulling (AB) and R. Barea (RB)'s methods. Different potential enhancements are suggested relying on our preliminary observations. A method based on speech recognition tools has also been tested. All the comparisons are made based on F1-score. Additionally, three different configurations were considered with the aim of achieving the best bitrate: 3x3, 3x5 and 5x5. All the experiments were performed on six healthy subjects.

First, the control scheme is composed of two main steps. At first, an EOG-based eye tracking system generates high-level commands (faster, slower, stop ...) on the basis of specific eye movement sequences executed by the user. After learning average gait patterns (angles of elevation of the different parts of the leg as a function of time), a PCPG provides an adaptive kinematics output to drive the artificial limb, according to the walking speed desired by the user. Unlike current sophisticated active prostheses, the user's intent is fully taken into account.

Inspired from our observations and previous work with EOG signals, we proposed to test some potential improvements. These include adaptive thresholding, impulsion integration, target clustering instead of a fixed grid for correcting distortion of the CWT space and a vertical booster to compensate for asymmetry in the EOG signal between vertical and horizontal movements. Amongst them, none seems to clearly outperform the standard methods. Furthermore, we can not conclude which approach is the best one. Actually, results provided by the enhanced RB and AB approaches are fairly similar. Although the RB method appears more complex and introduces a slight delay, it seems more robust for an intensive use, which is required for daily life applications. Finally, the speech recognition based method shows an overall good behaviour.

The used end-point detection method could be a starting point to enhance the saccade detection in other methods.

Considering the different configurations, we conclude that the 3x3 interface is the most appropriate approach. Indeed, the slight increase of bitrate resulting from a 3x5 interface is not balanced by the huge increase of complexity in the subject's point of view. Patients really prefer simple interfaces except a huge increase of performance is provided. The 5x5 results sharply decrease showing the limitations of the EOG-based interface. Therefore, we recommend the 3x3 interface.

In terms of blink and wink detection, results are pretty satisfying. Indeed, both methods reach around 90 % F1-score, which could lead to a reliable interface. However, the wink detector provides a lower variability.

Bibliography

- [1] R. Barea, L. Boquete, M. Mazo, and E. López. Wheelchair guidance strategies using EOG. *J. Intell. Robotics Syst.*, 34(3):279–299, 2002.
- [2] R Barea, L Boquete, M Mazo, and E López. Wheelchair guidance strategies using EOG. *Journal of Intelligent and Robotic Systems*, 34(3):279–299, 2002.
- [3] R. Barea, L. Boquete, S. Ortega, E. López, and J.M. Rodríguez-Ascariz. Eog-based eye movements codification for human computer interaction. *Expert Systems with Applications*, 39(3):2677 – 2683, 2012.
- [4] Rafael Barea, Luciano Boquete, Jose Manuel Rodriguez-Ascariz, Sergio Ortega, and Elena López. Sensory system for implementing a human computer interface based on electrooculography. *Sensors*, 11(1):310–328, 2010.
- [5] Andreas Bulling. *Eye Movement Analysis for Context Inference and Cognitive-Awareness: Wearable Sensing and Activity Recognition Using Electrooculography*. PhD thesis, ETH Zurich, 2010.
- [6] Santos Brandao Alexandre, Felix Leonardo Bonato, Cavalieri Daniel Cruz, de Sa Antonio Mauricio Ferreira Leite Miranda, Bastos-Filho Teodiano Freire, and Sarcinelli-Filho Mario. Controlling devices using biological signals. *International Journal of Advanced Robotic Systems*, 2011.
- [7] Julien Kronegg, Svyatoslav Voloshynovskiy, and Thierry Pun. Analysis of bit-rate definitions for brain-computer interfaces. In *Conf. on Human-Computer Interaction (HCI'05), Las Vegas*, 2005.
- [8] Guang-Bin Huang and Chee-Kheong Siew. Extreme learning machine: RBF network case. In *Control, Automation, Robotics and Vision Conference, 2004. ICARCV 2004 8th*, volume 2, pages 1029 – 1036 Vol. 2, dec. 2004.
- [9] F. Behrens, M. MacKeben, and W. Schröder-Preikschat. An improved algorithm for automatic detection of saccades in eye movement data and for calculating saccade parameters. *Behavior Research Methods*, 42:701–708, 2010.
- [10] A new method for calculating eye movement displacement from AC coupled electro-oculographic signals in head mounted eye-gaze input interfaces. *Biomedical Signal Processing and Control*, 5(2):142 – 146, 2010.

- [11] Jonathon Mueller. *The effect of differentiation technique utilized in continuous noninvasive blood pressure measurement*. PhD thesis, University of Akron, 2006.
- [12] Zhao Lv, Xiao pei Wu, Mi Li, and Dexiang Zhang. A novel eye movement detection algorithm for EOG driven human computer interface. *Pattern Recognition Letters*, 31(9):1041 – 1047, 2010.
- [13] Jia-Lin Shen, Jeih-Weih Hung, and Lin-Shan Lee. Robust entropy-based endpoint detection for speech recognition in noisy environments. In *ICSLP*. ISCA, 1998.
- [14] Sadaoki Furui. *Digital Speech Processing: Synthesis, and Recognition, Second Edition, (Signal Processing and Communications)*. CRC Press, 2000.
- [15] Yingxi Chen and W.S. Newman. A human-robot interface based on electrooculography. In *Robotics and Automation, 2004. Proceedings. ICRA '04. 2004 IEEE International Conference on*, volume 1, pages 243 – 248 Vol.1, april-1 may 2004.

Part III

Spontaneous Brain Gait Signal Analysis

Chapter 9

Towards Effective Non-Invasive Brain-Computer Interfaces Dedicated to Walk Rehabilitation Systems

Contents

9.1	Introduction	199
9.2	Deciphering Human Locomotion Control	199
9.2.1	Arguments in Favour of a Human CPG	199
9.2.2	Sensory Feedback Regulates the Stepping Patterns	201
9.2.3	Evidence of a Supra-spinal Control	202
9.2.4	An Overview of the Human Locomotion Machinery	203
9.3	Supra-spinal Control of Human Locomotion	205
9.3.1	Spatial Organization of Supra-spinal Control	205
9.3.2	Temporal Characteristics of Supra-spinal Control	210
9.3.3	Results from Invasive Studies	217
9.4	A BCI-based rehabilitation system	219
9.4.1	General Considerations about BCIs	219
9.4.2	Detecting the User Intent	219
9.4.3	Developing a Direct Brain Signals to Limb Kinematics Decoding	222
9.4.4	Producing a Gait/Stepping Movement in a Step by Step Approach	223
9.5	Discussion and Future Works	226

Abstract

In the last few years, significant progress has been made in the field of walk rehabilitation. Motor cortex signals in bipedal monkeys have been interpreted to predict walk kinematics. Epidural electrical stimulation in rats and in one young paraplegic has been realized to partially restore motor control after spinal cord injury. However, these experimental trials are far from being applicable to all patients suffering from motor impairments. Therefore, it is thought that more simple rehabilitation systems are desirable in the meanwhile.

The goal of this Chapter is to describe and summarize the progress made in the development of non-invasive brain-computer interfaces dedicated to motor rehabilitation systems. In a first part, the main principles of human locomotion control are presented. The paper then focuses on the control mechanisms of supra-spinal centres active during gait, including results from electroencephalography, functional brain imaging technologies (NIRS, fMRI, PET, SPECT) and invasive studies. The first BCI applications to gait rehabilitation are then presented, with a discussion about the different strategies developed in the field. The challenges to raise for future systems are identified and commented. Finally, we present some proposals to address these challenges, in order to contribute to the improvement of BCI for gait rehabilitation.

This chapter is based upon the following publication:

- T. CASTERMANS, M. DUVINAGE, G. CHERON, T. DUTOIT, 2014, *Towards effective non-invasive brain-computer interfaces dedicated to walk rehabilitation systems*, Brain Sciences, 2014; 4(1):1-48.

9.1 Introduction

Lower-limb rehabilitation and prosthesis control can obviously gain from a direct brain connexion. By reinforcing the required concentration and coupling it to the actual action, recovery time may be reduced. This is particularly true for more spontaneous BCIs as the activated brain area directly corresponds to the movement action. Furthermore, compared to previously studied standard BCIs, this natural control may lead to a much more widely spread device among the injured population. However, the underlying locomotion mechanism is still not sufficiently understood while the current knowledge is also sparse across a lot of different recording technologies.

Therefore, this Chapter aims at summarizing the current understanding of lower-limb control by combining all the available evidence from different technologies. Additionally, it emphasizes the challenges that researchers are still facing. Finally, it also provides some future research directions to circumvent them. Section 9.2 summarizes the main mechanisms involved in human locomotion control. Section 9.3 focuses on the description of supra-spinal control of locomotion by summarizing the knowledge acquired to date thanks to multiple methods of measuring neuronal activity. Section 9.4 discusses different strategies developed to produce walk rehabilitation systems driven by non-invasive brain-computer interfaces.

9.2 Deciphering Human Locomotion Control

Accumulating evidence suggests that human locomotion is actually based on a very complex hierarchical system which includes several control networks located both at spinal and supra-spinal levels. Basically, high-level motor commands are sent by the brain to a spinal network composed of central pattern generators (CPG) and, at the same time, each level of motor control receives and transmits peripheral sensory information (sensory feedback) which is used to modify the motor output at that level. This section is first devoted to the description of each level of locomotor control, including arguments supporting the existence of a CPG network and, simultaneously, the permanent action of a supra-spinal control. Then, the focus is on the spatial organization of the supra-spinal control and its temporal characteristics.

9.2.1 Production of the Basic Locomotor Patterns: Arguments in Favour of a Human CPG Network

The rhythmic movements of the legs during stepping require a complex sequence of muscle contractions to be executed by the lower limbs. The timing and level of activity of the numerous muscles involved differ widely, as illustrated in Figure 9.1. The complex sequence of muscle contractions is called the motor pattern for stepping. These patterns vary as a function of walking speed, the largest differences occurring between 2.0 and 2.5 km/h for most muscles. A growing body of evidence suggests that the patterns for stepping in mammals are produced at the spinal level by the central pattern generators network [1].

The spinal central pattern generators network consists in coupled antagonist oscillators specifically dedicated to extensor or flexor muscles acting at the different joints. This network generates the rhythm and shapes the pattern of the motor bursts of motoneurons [3, 4]. Their mechanism

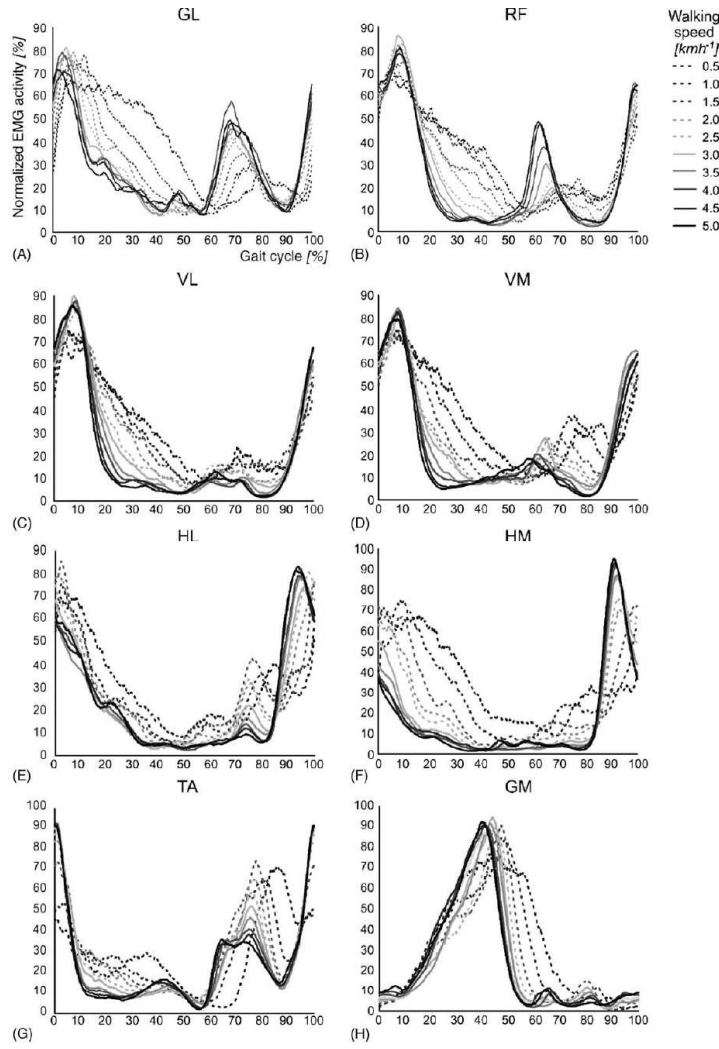


Figure 9.1: Influence of walking speed on EMG activity patterns. EMG activity patterns during different walking speeds of the (A) gluteus maximus (GL), (B) rectus femoris (RF), (C) vastus lateralis (VL), (D) vastus medialis (VM), (E) lateral hamstrings (HL), (F) medial hamstrings (HM), (G) tibialis anterior (TA) and (H) gastrocnemius medialis (GM) muscles. EMG signals were normalized for each subject and each condition by setting the difference between the lowest and highest EMG amplitude at 100% and normalizing the curve according to this value (figure from [2]).

allows to produce simple and coordinated rhythmic movements such as those involved in steady walk. Numerous experiments with spinal cats (i.e. with complete transection of the spinal cord) have demonstrated the presence of such CPG in lower mammals [4] and a similar conclusion has been reached for primates [5]. Regarding humans, the evidence is only indirect [6, 7].

A first argument is the fact that human infants exhibit a stepping behaviour from birth [8] and even before birth, as seen from ultrasound [9] or imaging recordings [10], although the brain has weak influence on the lower limbs movements at this early stage of development. Similar patterns are seen in a variety of other immature mammals [11, 12, 13].

Furthermore, studies with young infants stepping on a split-belt treadmill have shown that the stepping patterns in the two legs could be independent but always remained coordinated (only one leg entering the swing phase at a time), resulting in an integer relationship between the steps on each side. This finding is in favour of the CPG hypothesis because a stepping movement that would be due to a reflex mechanism (e.g. such as the stretch reflex, a muscle contraction in response to stretching in the muscle) would not exhibit such precise coordination. Other studies with babies have also shown that their stepping mechanism responds to different perturbations the same way as the one of lower mammals, for which the existence of CPG is almost certain [14]. Recently, this analogy has been verified on the basis of experimental results consistent with the hypothesis that, despite substantial phylogenetic distances and morphological differences, locomotion in several animal species is built starting from common primitives, perhaps related to a common ancestral neural network [15].

Another argument supporting the theory of a human CPG comes from patients exhibiting involuntary rhythmic spontaneous leg movements after both clinically complete [16, 17] and incomplete [18] spinal cord injury (SCI), thus with minimal influence of cortical signals. Similarly, sleep-related periodic leg movements have been reported. These stereotyped, periodic, repetitive movements involve one or both lower limbs. They consist of dorsiflexion of the ankle and toes and flexion of the hip and knee while the subject is lying down or asleep [19, 20]. The spinal origin of such movements is supported by their presence in patients with complete spinal lesion.

A final evidence that CPG at the basis of our rhythmic locomotor activity can be located in the spinal cord comes from experiments in which specific sites of the spinal cord were electrically stimulated. Indeed, it was shown that tonic electrical stimulation of the dorsal side of the spinal cord could induce locomotor activity in intact, decerebrated and low spinalized cats [21, 22, 23, 24]. A similar spinal cord stimulation applied to persons with a complete spinal lesion elicited a stepping activity with reciprocal organized EMG activity of symmetric muscles [6]. This suggests that a comparable neural network (CPG) to that seen in the cat is present in humans.

9.2.2 Sensory Feedback Regulates the Stepping Patterns

Normal walking is generally considered as an automatic movement. However, it is not necessarily stereotyped. We constantly use sensory input to adjust stepping patterns to variations of the terrain or to unexpected events. Three different types of sensory information are integrated to regulate our way of stepping: somatosensory input from the receptors of muscles and skin, input from the vestibular apparatus (balance control), and visual input [1].

Sensory feedback, elicited during gait, acts directly on the CPG and plays a major role in the phase transitions during the step cycle [25]. In particular, it was shown that limb loading and hip position are powerful signals for regulating the stepping pattern in human infants [26].

Cutaneous reflexes are also known to contribute to the correct execution of leg movements during locomotion. They are largely under the control of the CPG. In this way, it is ensured that reflex activations of given muscles occur at the appropriate times in the step cycle and are

suppressed at other times [27], as illustrated on Figure 9.2. This reflex activity, which regulates the timing and amplitude of the stepping patterns [1, 28, 29], takes place at very specific moments in the gait cycle. In other phases of locomotion, the motor cortex seems to become especially active. In particular, during normal walking, the tibialis anterior (TA) shows two activity periods, one at the end of stance and one at the end of swing. It has been suggested that the first burst is primarily due to output of a spinal CPG whereas the second is more of cortical origin [30]. Indeed, clinical observations on stroke patients clearly show that especially the second burst (end swing) is affected after damage to the motor cortex. Additionally, the transcranial magnetic stimulation studies during gait have also pointed toward a strong involvement of the motor cortex in the generation of this activity [31].

In other contexts than normal locomotion, sensory input from the skin also allows stepping to adjust to unexpected obstacles [1]. The reflex mechanism, by its own, can give rise to a bipedal locomotion system which is stable, reproduces human walking dynamics and leg kinematics, tolerates ground disturbances, and adapts to slopes without parameter interventions, as modelled in [32]. However, arguments exposed hereafter indicate that human locomotion comprises more than a CPG network modulated by reflexes.

9.2.3 Evidence of a Supra-spinal Control

Although the existence of a CPG system modulated by sensory information becomes broadly accepted, many findings indicate that the cortex also plays a role of primary importance in human walking [7]. Indeed, when lesions occur in the supra-spinal region of the central nervous system, recovery of walking is extremely difficult and generally incomplete. This means that intact supra-spinal centres are necessary for functional walking in humans.

Experiments with mammals also provide strong arguments in favour of a supra-spinal control. For instance, after transection of their spinal cord, most cats are not able to generate locomotor movements. This observation suggests that commands for the initiation of locomotor activity must be given at certain level above the lesion. By varying the level of transection, it was shown that the regions for initiation of locomotion are located in the brain stem, i.e. at supra-spinal level [33]. Furthermore, in paralyzed decerebrated cats, the initiation of 'fictive' locomotion (i.e. in absence of movement related afferent feedback) can be realized with electrical stimulation of the mesencephalic locomotor (MLR) region [34]. Such MLR regions have also been described in different vertebrate species, including primates [35].

Another kind of evidence for supra-spinal control of locomotion is provided by the effects of substances mimicking the action of descending pathways. Many studies have shown that a walking pattern can be elicited in acute spinalized cats put on treadmill after intravenous injection of such substances [36, 37, 38]. Furthermore, it is even possible to modify the walking pattern and modulate the step cycle duration and step length by varying the nature of the injected drugs [39, 40].

Also, studies of direct stimulation of neurons in the motor cortex through transcranial magnetic stimulation have shown that the motor cortex likely plays a role in activating the dorsiflexors and plantarflexors during walking in humans [41]. Additionally, significant changes in motor and cognitive demands (i.e. spatial attention) have been observed in the context of bipedal walking in unknown or cluttered dynamic environments [42]. Functional neuroimaging studies have shown

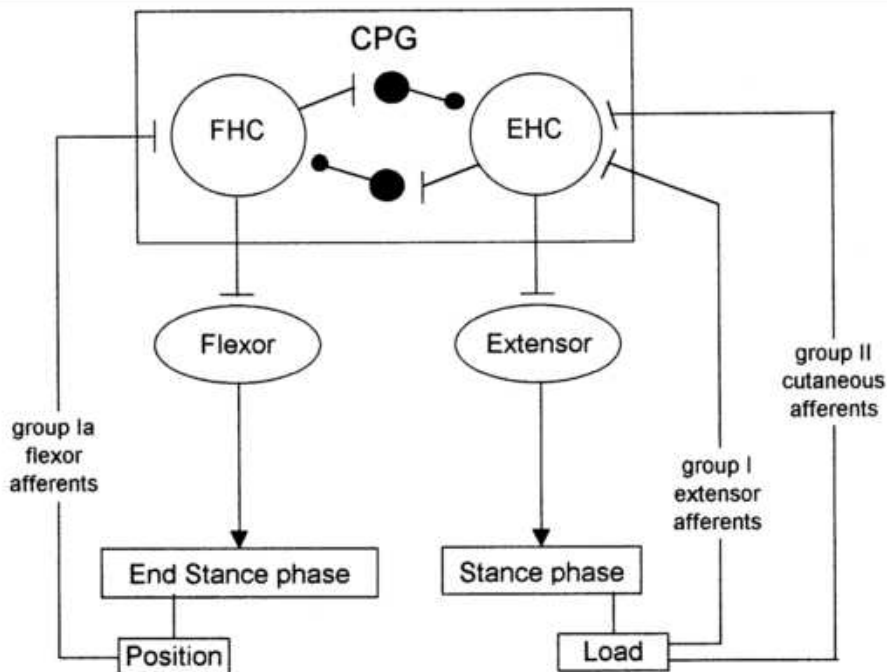


Figure 9.2: Model of the different pathways indicating how afferents can act on the CPG during the stance phase of locomotion. The CPG contains a mutually inhibiting extensor and flexor half-center (EHC and FHC, respectively). During the stance phase, load of the lower limb is detected by group I extensor muscle afferents and group II (low threshold) cutaneous afferents which activate the EHC. In this way, extensor activity is reinforced during the loading period of the stance phase. At the end of the stance phase, group Ia afferents of flexor muscles excite the FHC (which inhibits the EHC) and thereby initiate the onset of the swing phase (adapted from [27]).

that the primary motor cortex is recruited during rhythmic foot or leg movements [43]. Moreover, the technique of functional near-infrared spectroscopy (fNIRS) has allowed to detect involvement of the frontal, premotor and supplementary motor areas during walking [44]. Electrophysiological studies have also provided valuable information concerning the possible cortical origin of the intramuscular and intermuscular electromyographic (EMG) synchronization (coherence) observed in lower limbs during walking [45].

Finally, numerous studies have revealed strong arguments supporting the idea that motor centres in the brain play an important and greater role in human walking compared with quadrupeds, as reviewed in [5, 46, 47].

9.2.4 An Overview of the Human Locomotion Machinery

Figure 9.3 gives a global picture of the human locomotion control process and summarizes the different points discussed so far. Initiation of the movements, rhythm modulation and stopping

come from the superior central nervous system (i.e. the brain). Brain signals are sent to the spinal cord where the complex spinal circuitry manages to decode them (along with the feedback afferent signals coming from the peripheral nervous system). The CPG network produces rhythmic patterns of neural signals. The resulting command signals, called efferent impulses, are emitted by the α motoneurons and transmitted through the motor nerves to the muscles. By contracting in response to the nervous solicitations, muscles produce active forces which are transmitted to the skeleton through the tendons. The forces generate the movements of the limbs. The feet interact with the ground and external forces push the body forward. The balance of the body is ensured by feedback thanks to the proprioceptive organs that respond to mechanical stimuli by generating electrical impulses (action potentials). These action potentials are sent back to the spinal cord through the afferent sensory nerves. The muscle spindles determine the muscle fibre lengths and velocities while the Golgi tendon organs provide information about the muscle forces. Specific cutaneous mechanoreceptors located in the skin are able to detect tension, changes in texture, rapid vibrations, sustained touch, pressure and stretches. Additional mechanoreceptors are also found in the joints.

All this feedback information is integrated in the spinal cord in order to automatically stabilize the walking, by means of reflexes (i.e. without intervention of the brain). This mechanism is valid for limited perturbations and, in case of important perturbations, the superior central nervous system and the vestibulo-oculomotor system have to intervene so as to prevent the fall.

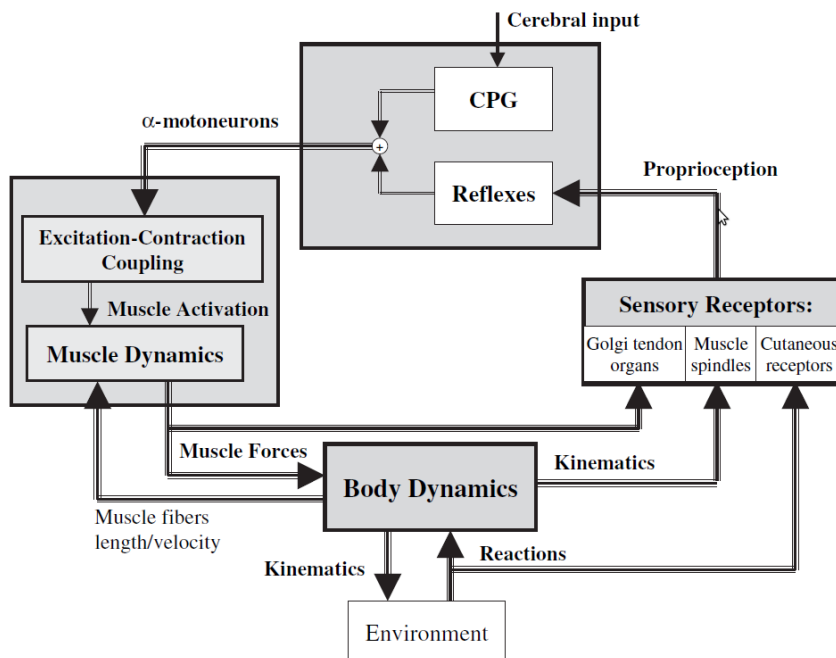


Figure 9.3: Global view of the human locomotion machinery (figure from [48] – see text for details).

9.3 Supra-spinal Control of Human Locomotion

In this section, we focus on the role of the brain in human locomotion control. Spatial organization and temporal characteristics of supra-spinal control are described, with an emphasis on the information that can be detected in a non-invasive way. These aspects are particularly important for the discussion conducted in section 9.4, which concerns the development of non-invasive BCI dedicated to walk rehabilitation systems.

9.3.1 Spatial Organization of Supra-spinal Control

Neuroimaging of gait is not straightforward and practical problems are posed, since the majority of imaging techniques (like PET, fMRI and EEG) require that subjects do not move their head during the experiments. Moreover, functional brain imagery of subjects walking on a treadmill does not allow to discriminate whether the evoked activity is due to sensory input or motor input. Consequently, alternative neuroimaging techniques have to be employed like, for instance, recording cerebral activity during motor planning of walking prior to walking initiation, using tasks that share some cerebral processes with gait, without the need to engage in actual gait (like motor imagery of gait, or repetitive foot movements). The results obtained using these different strategies are detailed below and summarized in Table 9.1.

Publication	Neuroimaging method	Experimental approach	Key findings
Fukuyama et al., 1997 [49]	SPECT	Real gait (on ground)	During gait, increased activity in the supplementary motor area (SMA), medial primary sensorimotor area, striatum, cerebellar vermis and visual cortex
Hanakawa et al., 1999 [50]	SPECT	Real gait (on treadmill)	Cerebral activity during walking also observed in the dorsal brainstem
Miyai et al., 2001 [51]	NIRS	Real gait (on treadmill)	Walking increases cerebral activity bilaterally in the medial primary sensorimotor cortices and the SMA
Suzuki et al., 2004 [52]	NIRS	Real gait at different speeds (on treadmill)	Increase of cerebral activity in the pre-frontal cortex and premotor cortex as locomotor speed increases ; cerebral activity in the medial sensorimotor cortex not influenced by locomotor speed
Malouin et al., 2003 [53]	PET	Motor imagery of standing, gait initiation, real walking, walking with obstacles	Motor imagery of walking increases activity in the pre-SMA (compared to imagined standing); in the left visual cortex and caudate nucleus (compared to imagery of gait initiation)
Jahn et al., 2004 [54]	fMRI	Motor imagery of standing, walking and running	Cerebellar activation increased during motor imagery of running, not during motor imagery of walking and standing; vestibular and somatosensory cortex were deactivated during running but not during walking

Miyai et al., 2001 [51]	NIRS / fMRI	Repetitive foot movements	Foot-extension flexion movements generate a similar brain activation pattern to that associated with walking
Sahyoun et al., 2004 [55]	fMRI	Active vs passive foot movements	During active movements, increase of cerebral activity in the somatosensory cortex, SMA, cingulate motor area, secondary somatosensory cortex, insular cortices, putamen, thalamus and cerebellum
de Jong et al., 2002 [56]	PET	Antiphase flexion and extension movements	Cerebral activations distributed over the right anterior parietal and right dorsal premotor cortex
Christensen et al., 2000 [57]	PET	Bicycle movements	Both passive and active bicycling increase cerebral activity bilaterally in primary sensorimotor cortices, SMA, and the anterior part of the cerebellum.
La Fougère et al., 2010 [58]	PET / fMRI	Real versus imagined locomotion	During real and imagined locomotion: activations in the frontal cortex, cerebellum, pontomesencephalic tegmentum, parahippocampal, fusiform and occipital gyri; deactivations in the multisensory vestibular cortices (superior temporal gyrus, inferior parietal lobule). Real steady-state locomotion seems to use a direct pathway via the primary motor cortex, whereas imagined modulatory locomotion an indirect pathway via a supplementary motor cortex and basal ganglia loop.

Table 9.1: An overview of the results obtained by different functional neuroimaging studies of gait in healthy subjects.

Execution of Real Gait

Despite the experimental difficulties mentioned above, a few techniques allow to assess cerebral activity during actual gait.

Both SPECT and PET scans may be used to study brain activity during actual gait. These techniques allow to separate in time task performance from image acquisition. When radioactive substances are injected intravenously during gait, they are rapidly distributed in the brain proportionally to local cerebral blood flow and, most importantly, remain in the brain for hours. Therefore, the spatial distribution of radionuclides at the time of PET or SPECT scanning reflects the pattern of cerebral perfusion at the time of injection. Using this approach, a significant increase in cerebral activity was found during gait in the supplementary motor area (SMA), medial primary sensorimotor area, striatum, cerebellar vermis and visual cortex [49]. This was the first study to show changes in cortical activity during walking in human subjects, compared to the resting state. Later on, the same group demonstrated that a significant cerebral activity during walking is also observed in the dorsal brainstem [50]. This finding is important, because it is one of the few observations suggesting the presence of brainstem locomotor centers in humans.

Cerebral activity can also be monitored while subjects are walking on a treadmill thanks to NIRS. This technique allows the comparison of several experimental conditions. In [59], the cerebral activities evoked during gait, alternating foot movements, arm swing, and motor imagery of gait were compared. Results of this study indicated that the gait-related responses along the central sulcus were medial and caudal to the activity associated with arm swing. This is quite in agreement with the known somatotopic organization of the motor cortex. Crucially, these authors showed that walking increased cerebral activity bilaterally in the medial primary sensorimotor cortices and the SMA, and to a greater extent than the alternation of foot movements.

In another NIRS study, the effect of different walking speeds on cerebral activity was examined. It was demonstrated that cerebral activity in the prefrontal cortex and premotor cortex tend to increase as locomotor speed increases, whereas cerebral activity in the medial sensorimotor cortex is not influenced by locomotor speed [52].

Gait Initiation

As already mentioned in this review, EEG recording during walking is particularly challenging due to motion artefacts. However, some researchers have published EEG studies prior to and/or during gait initiation [60, 61]. This experimental approach offers two advantages. First, it provides a high temporal resolution analysis of the electrical brain activity in an action where changes in sensory input are minimal. Second, motion artefacts are drastically reduced, because the recording is realized before the onset of any movement. In these studies, stronger event-related potentials were found in the medial central region (Cz) when comparing EEG activity preceding externally-cued gait initiation with activity preceding foot dorsiflexion. This EEG difference indicates that the medial frontal cortex, above its role in initiating a simple foot movement, supports the initiation of gait [62].

Motor Imagery of Gait

Another strategy to assess the cerebral bases of true gait control consists in investigating motor imagery of gait, i.e. the mental simulation of gait without actual execution. This approach presents the advantage to be totally compatible with techniques like fMRI and PET, which provide relatively high spatial resolution and whole-brain coverage. Numerous studies have been published on the subject. Cerebral activity evoked during motor imagery of standing, initiating gait, walking, and walking with obstacles was analysed in [53]. The authors report that motor imagery of walking increased cerebral activity in the pre-SMA when compared to imagined standing, and in the left visual cortex and caudate nucleus when compared to imagery of gait initiation. Comparing motor imagery of walking with or without obstacles increased cerebral activity in the precuneus bilaterally, the left SMA, the right parietal inferior cortex and the left parahippocampal gyrus. This illustrates that the neuronal circuitry of gait can extend beyond motor cortex and it can be modulated by the difficulty of the imagined locomotor task.

In another study, based on fMRI, motor imagery of standing, walking and running was studied [54]. Results obtained indicate an increase in the activation of the cerebellum during motor imagery of running but not during motor imagery of walking and standing. Additionally, vestibular and somatosensory cortex were deactivated during running but not during walking. As

summarized in [62], these findings suggest that speed of gait is under the control of a cerebellar locomotor center, and that cortical processing of vestibular and somatosensory information is particularly important during walking.

Repetitive Leg or Foot Movements

A last approach to assess the supra-spinal control of human locomotion is to study repetitive leg or foot movements. Indeed, it is thought that these movements rely partly on the same neural processes as those used during actual gait. In a combined NIRS and fMRI study, it was shown that foot extension-flexion movements indeed generate a similar brain activation pattern to that associated with walking [51]. Like motor imagery of gait, study of leg or foot movements presents practical advantages like reduction of motion artifacts and possibility to use cumbersome brain imagery techniques. Of course, one does not study real gait in this case, since this motor task additionally requires the coordination of a large number of body parts and includes integration of balance control information.

Using fMRI to compare active versus passive unilateral foot extension-flexion movements, it was found that during active compared to passive foot movements cerebral activity increased in the somatosensory cortex, SMA, cingulate motor area, secondary somatosensory cortex, insular cortices, putamen, thalamus and cerebellum [55]. This suggests that both cortical and subcortical structures are involved in the motor control of rhythmic foot movements.

In a PET study, cerebral activity during antiphase flexion and extension movements of the two upper and the two lower limbs was examined [56]. For both the arms and legs, cerebral activations related to antiphase movements were distributed over the right anterior parietal and right dorsal premotor cortex, suggesting that these structures support the sensorimotor integration required for antiphase movements.

Inter-limb coordination study was assessed with bicycle movements in [57]. Results obtained in this analysis showed that both passive and active bicycling increase cerebral activity bilaterally in primary sensorimotor cortices, SMA, and the anterior part of the cerebellum. After subtraction of passive from active bicycling, significant activation was found in the leg area of the primary motor cortex and the precuneus. This suggests that a significant cerebral control is involved in the production of rhythmic movements such as bicycling.

Summary

Thanks to the numerous neuroimaging studies of gait (or assimilated motor tasks), the supra-spinal control of human locomotion has been identified as lying in different centres in the brain-stem, cerebellum and cortex (cf. Figure 9.4). This cerebral network is believed to modulate locomotion (e.g., gait initiation, termination, velocity, direction, and spatial orientation) and to control balance and gait by integration of multi-sensory information [63]. The most important regions are the cerebellar locomotor region (CLR), the mesencephalic locomotor region (MLR), and the subthalamic locomotor region (SLR).

Remarkable similarities exist between the real and imagined locomotion networks [58]. The first one is the activation of the midline cerebellar area, which controls body and trunk balance, and the cerebellar locomotor region, which is thought to regulate speed and gives rhythmical im-

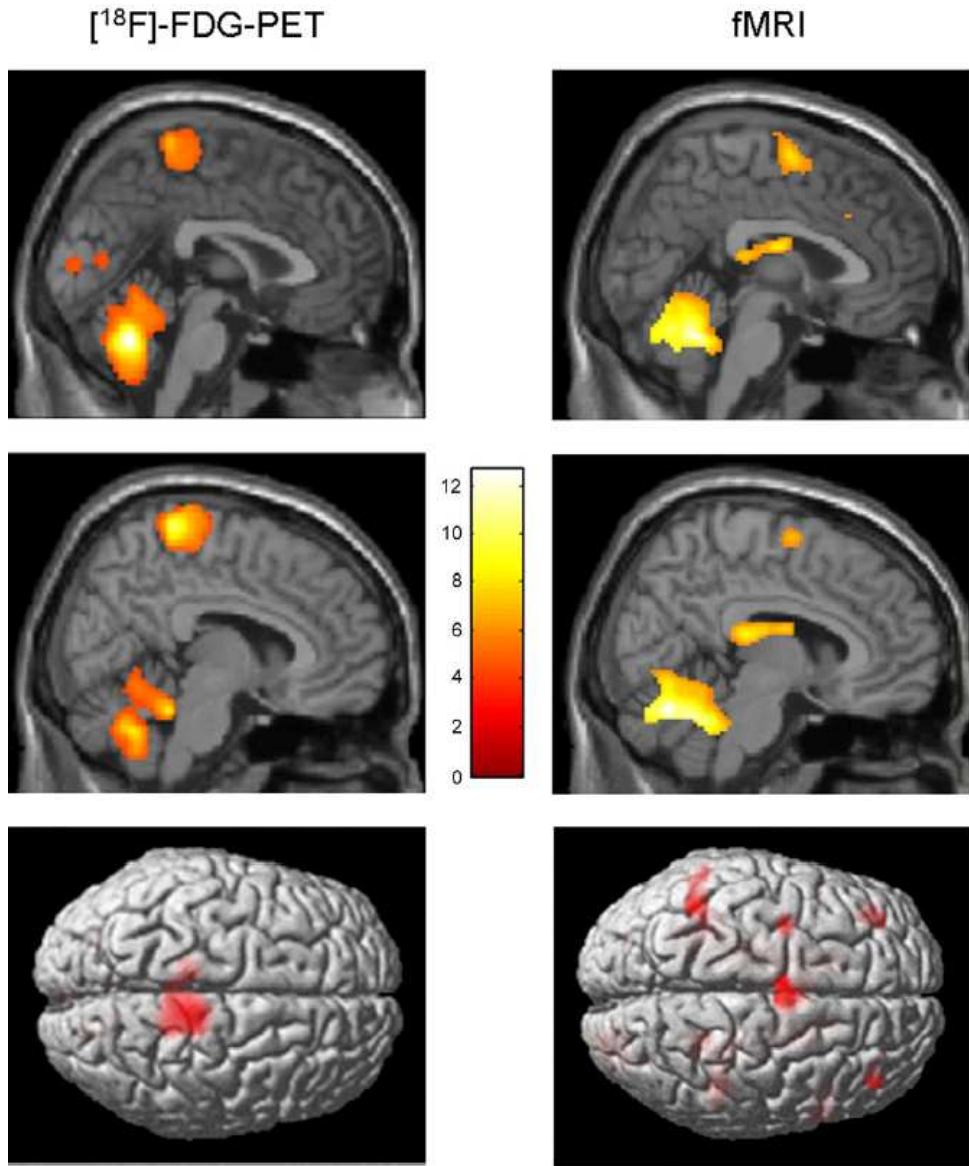


Figure 9.4: Comparison of real (PET) and imagined locomotion (fMRI) brain activations (figure from [58]). Sagittal midline and render views are shown. It can be seen that during real locomotion the primary motorsensory cortices (pre- and postcentral gyri) are active (left) as compared to the supplementary motor areas (superior and medial frontal gyri) in mental imagery of locomotion (right). Furthermore during imagined locomotion the basal ganglia (caudate nucleus, putamen) are active, which is not the case for real locomotion.

pulses to the brainstem and spinal cord [54]. The second remarkable similarity in both paradigms is the activation of occipital visual cortices, which are related to visual processing.

Significant differences between real and imagined locomotion networks have also been found [58]. Whereas the primary motor cortex is activated (in the functional region of the leg) during real locomotion, supplementary motor areas (superior and medial frontal cortex, dorsolateral prefrontal cortex), and basal ganglia (caudate nucleus, putamen) are activated during mental imagery. The most acceptable explanation suggested for this is that the premotor and basal ganglia activations in imagined locomotion could reflect an indirect pathway of locomotion that is responsible for the modulation of locomotion, whereas the primary motor activations in real continuous walking utilize a direct pathway for a steady-state of locomotion (cf. Figure 9.5).

9.3.2 Temporal Characteristics of Supra-spinal Control

The functional brain imaging techniques have brought a lot of useful information to localize the cerebral centres involved in human locomotion control. The weak point of these techniques, however, reside in the poor temporal resolution they offer. In that regard, electroencephalography (EEG) represents an interesting complementary technique for investigating neural processes governing walk and particularly the dynamics of the brain.

Detailed biophysical studies have revealed that single neurons are characterized by a complex dynamics, with the ability to resonate and oscillate at multiple frequencies. Precise timing of their activity within neuronal networks encode information and synchronous activity of oscillating networks is thought to link the single neuron activity to global behaviour [64]. The control of precise actions like locomotion, for instance, requires integration of multiple information and thus, synchrony of different convergent inputs. One of the roles of oscillatory activities in the brain is to operate this synchrony. Indeed, oscillation-based synchrony is the most energy-efficient physical mechanism for temporal coordination [64]. In that regard, it is fundamental to analyse brain dynamics to understand the mechanisms involved in the supra-spinal centres during locomotion.

However, electrophysiological investigation of the cerebral activity elicited during walk is highly challenging. Indeed, head and body movements constitute an important source of mechanical artefacts strongly affecting the EEG signals quality.

Consequently, the main strategy generally used to overcome these experimental difficulties consists in focusing on simplified foot or leg movements which imply common cerebral processes with gait. In these experimental protocols, subjects are mainly static and produce only limited lower limb movements. A strong advantage of this approach is of course that motion artefacts are drastically limited. In this case, however, the full neural activity related to walk is not available and, for instance, cerebral processes involved in posture and balance control are missing. Recording EEG signals of subjects walking on a treadmill include of course all these aspects but then requires a powerful analysis technique to discriminate the different artefact contributions from the real cortical signal. Analysis results of these two approaches, *static* on the one hand and *dynamic* on the other hand, are reviewed hereinafter.

Electrocortical Potentials Related to Lower Limb Activation in Static Condition

The cortical activity associated to bilateral anti-phase and in-phase rhythmic foot movements produced by subjects sitting on a chair was investigated in [65]. In this study, the authors found

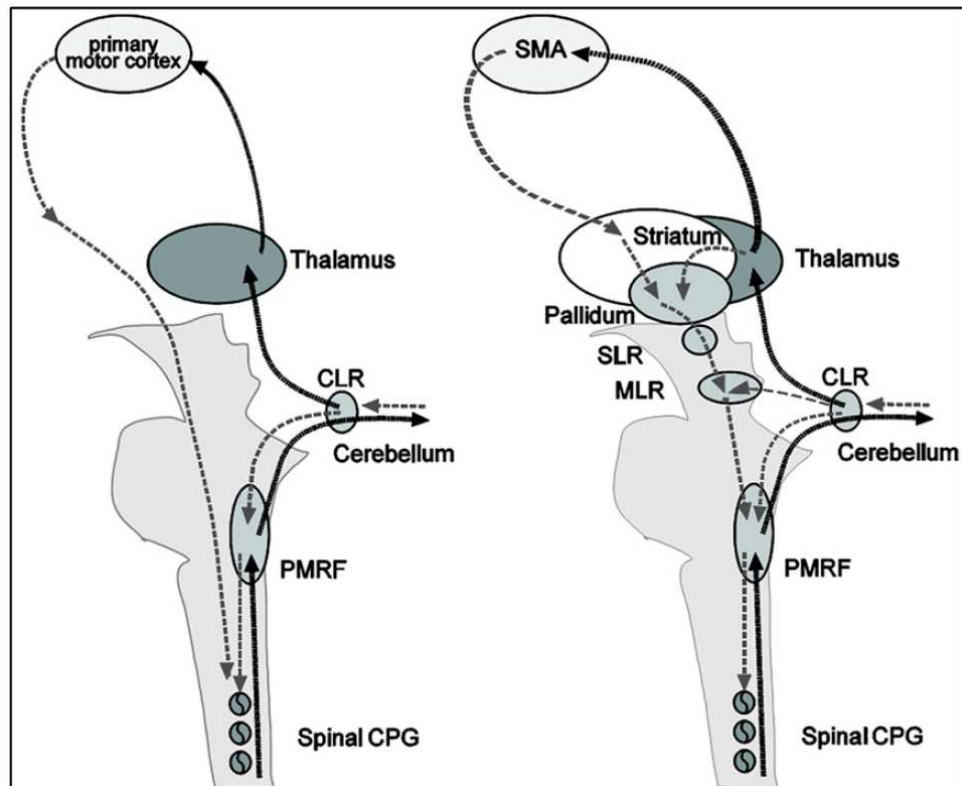


Figure 9.5: Illustration of the executive and planning networks of locomotion, as suggested in [58]. Execution of locomotion in a non-modulatory steady state (left side) goes from the primary motor cortex areas directly to the spinal central pattern generators (CPG), thereby bypassing the basal ganglia and the brainstem locomotor centers. A feedback loop runs from the spinal cord to the cerebellum and thereby via the thalamus to the cortex. For planning and modulation of locomotion (right side) cortical locomotor signals originate in the prefrontal supplementary motor areas and are transmitted through the basal ganglia via disinhibition of the subthalamic locomotor region (SLR) and mesencephalic locomotor region (MLR) where they converge with cerebellar signals from the cerebellar locomotor region (CLR). The MLR functionally represents a crosspoint for motor information from basal ganglia and cerebellar loops. Descending anatomical projections are directed to the medullary and pontine reticular formations (PMRF) and the spinal cord, ascending projections are in the main part concentrated on the basal ganglia and the non-specific nuclei of the thalamus (not shown for sake of clarity). The CLR also projects via the thalamus back to the cortex. Cortical signals are furthermore modulated via a thalamo-cortical-basal ganglia circuit. The schematic drawing shows a hypothetical concept of a direct pathway of steady-state locomotion (left) and an indirect pathway of modulatory locomotion (right).

significant corticomuscular coherence between EEG signals and the anterior tibial muscles, at the stepping frequencies in the central midline region, extending further to the frontal mesial area. During isometric co-contraction of the calf muscles, coherence appeared between 15 and

30 Hz, concentrated on the central midline area (Cz-CPz electrodes). This is the first study demonstrating that there exists a representation of rhythmic foot motor patterns in the cortex, transmitted to the muscles and fed back to the cortex with delays compatible with fast corticospinal transmission, which may be important for gait control.

Assisted lower limb movements have also been investigated using electroencephalography [66]. In this study, subjects performed standardized, assisted stepping movements (i.e. mimicking walk) in an upright position, while being secured to a tilt table. Electrocortical sources associated to the movement-related potential were localized in the primary motor cortex, the premotor cortex, the supplementary motor cortex, the cingulate cortex, the primary somatosensory cortex and the somatosensory association cortex (i.e. in accordance with the findings of functional brain imagery). The authors demonstrated that a clear succession of activations and deactivations was present in the movement-related potential, in direct relationship with specific phases of the gait-like leg movements. In particular, it was shown that cortical activity was the greatest during transition between flexion and extension of the legs and vice versa.

In [67], a non-invasive EEG-based BCI governing a functional electrical stimulation (FES) system for ankle movement is presented. In this application, healthy subjects perform repetitive foot dorsiflexions. EEG patterns underlying this action are detected in real time, and this information is subsequently used to trigger the FES of the tibialis anterior of the contralateral foot so as to achieve its dorsiflexion. In fact, the trigger (or non-trigger) information is given by a linear Bayesian classifier trained using a vector of spatio-spectral features which optimally discriminate the idling and dorsiflexion states. The authors state that analysis of subject-specific prediction models demonstrated that the EEG power changes in the μ , β and low γ bands observed over mid-central areas (i.e. electrode Cz) were the most informative features for classification. This likely corresponds to activity within the primary motor cortex foot representation area and/or supplementary motor area (which is not surprising from a brain anatomy standpoint) and is in perfect agreement with prior studies [68, 69].

Electrocortical Potentials Related to Walk

The first analysis of EEG during walk on treadmill was published by Gwin and co-workers [87]. By using a method based on independent component analysis (ICA) combined with an inverse modelling approach, the authors claimed they could discriminate electrocortical sources, muscle sources and other artefacts from the raw EEG signals. They found that cortical activity in the anterior cingulate, posterior parietal and sensorimotor cortex exhibited significant and smooth intra-stride changes in spectral power. More precisely, alpha and beta band spectral powers increased in or near the left/right sensorimotor and dorsal anterior cingulate cortex at the end of each stance phase (i.e. as the leading foot was contacting the ground and the trailing foot was pushing off). According to this study, power increases in the left/right sensorimotor cortex were more important for contralateral limb push-off (ipsilateral heel strike) than for ipsilateral limb push-off (contralateral heel strike). Finally, the authors reported evidence of intrastride high-gamma spectral power changes in anterior cingulate, posterior parietal and sensorimotor cortex.

In parallel, Presacco and co-workers [71] showed for the first time that the kinematics of the ankle, knee and hip joints during human treadmill walking can be inferred from EEG signals.

Successful decoding of these signals was done basically by filtering them (0.1 – 2 Hz) and passing them through a linear autoregressive model. According to this study, gait trajectories were inferred with accuracies comparable to those from neural decoders based on multiple single-unit activity recorded in non-human primates [72]. The results of this study indicate a high involvement of a fronto-posterior cortical network in the control of walking and suggest that EEG signals can be used to study in real time the cortical dynamics of walking and to develop brain-machine interfaces aimed at restoring human gait function.

Spatio-frequential Characteristics of the Detected Potentials

From the spatial point of view, all the studies found activations of the brain globally compatible with the primary motor cortex's foot representation area and/or supplementary motor area, except one (cf. Table 9.2). Indeed, Presacco and co-workers [71] report the activation of a complex, distributed and sparse cortical network, in which scalp areas over anterior, right lateral and right anterior-occipital scalp areas seem to equally contribute (at least to their decoding of the kinematics of the right leg, for subjects walking on a treadmill). The same results were published in [73].

From the frequential point of view, spectral power variations were generally found from alpha to gamma bands but, astonishingly, a successful neural decoding of treadmill walk was realized by Presacco and co-workers [71] using EEG signals band-pass filtered between 0.1 and 2 Hz. This is particularly surprising, because it was shown in two other studies, conducted to assess EEG signal quality in motion environments [74, 75], that EEG spectra in the walking (or jogging) condition exhibit frequency peaks consistent with the fundamental stride frequency as well as its harmonics. The authors in [74] also state that motion artefacts affect signal integrity most prominently at low frequencies (i.e. the delta band) during steady walk. In their analysis protocol, Presacco and co-workers [71] do not mention any pre-processing method aiming at either correcting or discriminating these motion artefacts from the real cortical signals. The only way for them to make the choice of this frequency band legitimate is the fact that good results are obtained and, moreover, other studies exploited the same portion of the EEG spectrum to decode upper limb movements. We strongly emphasize the fact that, in the latter studies, no motion artefact due to gait is produced. Consequently, this might suggest that the decoding of kinematics of walk – *periodical* movement – on the basis of the EEG signals is done by Presacco and co-workers [71] with a linear autoregressive model exploiting the *periodical* motion artefacts present in the EEG recordings. This option is furthermore supported by the fact that no spectral information is given under 3 Hz in the study of Gwin [76].

This last point is corroborated by a recent paper from Antelis and co-workers [77]. These authors have focused on several publications in which are reported successful reconstructions of different limb kinematics from EEG using the low frequency activity of the EEG and linear regression models [78, 79, 80]. Antelis and co-workers [77] showed that the mathematical properties of the linear regression model and of the correlation metric used in these studies could explain the good results reported. Moreover, they demonstrated that correlation results obtained with real EEG signals, shuffled or random EEG data were not statistically different. This means that the linear models developed in [78, 79, 80] are able to provide the same results irrespectively of the presence or absence of limb velocity information in EEG signals.

Other recent studies dedicated to EEG analysis during a locomotion task may be added to this discussion. Severens and co-workers [81] investigated the possibility of measuring event-related desynchronizations (ERD) [82] and event-related spectral perturbations (ERSPs) during walking on treadmill. After cleaning EMG artifacts using canonical correlation analysis (CCA), they found an ERD in the mu band above the central motor cortex (electrode Cz) and in the beta band above the lateral motor cortex (electrodes C3 and C4). In addition, they found that ERSPs in mu and beta bands were coupled to the gait cycle with significant differences between left swing, right swing and double support phase of the gait cycle. They did not report any signal of cortical origin at low frequency. Indeed, as the low frequency modulations they found in the ERSPs were also visible in the occipital channels, the authors explained these were very unlikely related to brain activity and probably due to remaining artefacts.

Wagner and co-workers [83] also showed that mu and beta rhythms are suppressed during active walking in the Lokomat, a robotic gait orthosis. They also provided evidence of modulations of the lower gamma band (25 to 40 Hz), localized in central midline areas and related to the phases of the gait cycle. For different reasons, the authors speculate that these activations and deactivations might be related to sensorimotor processing of the lower limbs in the complex motor pattern of human locomotion. Although their ERSPs plots exhibit ERD and ERS around and below 5 Hz, they neither comment them nor claim that these originate from cortical activity.

About the Origin of the Detected Signals

Among all the works described in previous paragraph, only [65] tried to determine the origin of the information flux contained in the studied signals (descending commands from the brain or sensory feedback sent to the brain). This is done by computing time delays between EEG time series and electromyographic activity of the involved lower limb muscles by means of the “maximizing coherence method” [84]. Actually, the other studies presented in previous paragraph do not consider this aspect and give no indication on the direction of the brain-muscle interaction (i.e. if it is up-going or down-going). It is therefore unknown, for instance, if the intra-strides spectral power variations found by Gwin[76] are due to voluntary movements or sensory feedback (or a combination of both). The same question arises concerning the EEG decoding presented by Presacco and co-workers [71]. Resolving this ambiguity is particularly crucial, though, for the development of gait rehabilitation systems. Indeed, if the information detected in the EEG signals is purely due to a sensory feedback of the gait-related movements, it would be unusable to drive any device, given that no valid *prediction* of a movement can be done exploiting sensory information *resulting* from it.

Most importantly, studying EEG signals in treadmill walking also requires the need to exclude gait-related artefacts. Too few studies tackle this issue [85]. In particular, [87] used an ICA analysis coupled with an inverse solution approach. These authors claim that they could disentangle muscular contributions and other artifacts from real cortical signals. However, in a previous study, the very same authors [76], using the very same dataset, clearly stated that:

“Unlike more spatially stationary artefacts in EEG signals arising from eye movements, scalp muscles, fMRI gradients, etc., which may be resolved by ICA decomposition into a subspace of one or more independent components, we found that gait-related movement artefact remained in many if not most of the independent components. This prevented us from removing only a

small subset of components capturing the movement artefacts.”

For this reason, they considered the removal of motion artefacts from EEG during walking and running on treadmill using an artefact template subtraction method. Such method allowed to enhance the detection of P300 potentials in ambulatory conditions. Nevertheless, the study of cerebral processes involved in human locomotion is not possible using a subtraction method, as it would undoubtedly remove interesting signal from the EEG recordings. For this reason, the authors used only the ICA approach to clean the EEG signals [87]. In this study, the issue of motion artefacts was completely eluded and no mention was made of any appropriate treatment to reject them. Thus, it can be doubted that the time-frequency analysis plots shown in that paper do not contain any motion artefact contribution. In the discussion conducted in [85], it was shown that a time-frequency analysis of the signal of an accelerometer placed on the head of a subject walking at 1.67 m/s on a treadmill presented periodic power spectral changes over large frequency bands, in a similar way to the results obtained after ICA by [87].

Finally, it should be noted that on the basis of a spectral analysis it is not possible to determine which cortical region is directly involved in the transmission of motor commands to the muscles. In contrast, coherence analysis reveals anatomical coupling between cortical activity and the motor output to the muscles by detecting common rhythmicities in EMG and EEG signals. In the study conducted in [86], the coupling between electroencephalographic (EEG) and electromyographic (EMG) signals from leg muscles during treadmill walking was investigated. The authors report significant coherence between EEG signals recorded over the leg motor area (Cz electrode) and EMG from the tibialis anterior (TA) muscle in the 24 – 40 Hz frequency band before the heel strike, during the swing phase of the gait cycle. The presence of significant imaginary part of the complex coherence indicates that the coupling in the study was not due to non-physiological artefacts. The negative sign of this imaginary part of the coherence suggests that the cortical activity was leading the muscle activity. Time lag estimates between EEG and EMG signals are consistent with the typical cortico-spinal conduction times. This result indicates that rhythmic cortical activity in this particular frequency band is transmitted to the lower limb muscles during walking, at specific moments in the gait cycle. This work thus proves and confirms that the motor cortex directly contributes to the muscle activity involved in human locomotion. On top of this, according to the significant coherence values (24–40 Hz around Cz) found by [86], the multiple ERD-ERS detected by Gwin [87] in the 3–24 and 40–76 Hz bands are obviously not indicative of a direct corticospinal drive, at least, not to the tibialis anterior. Thus, one may think that these signals, if not affected by residual artefacts, would rather reflect the control of sensory afferents (i.e. one of the hypotheses formulated by the authors in [87] themselves). It is interesting to note that the studies by Wagner [83] and Severens [81] do not report multiple ERD-ERS in α , β and γ bands and are in line with the coherence study made by [86].

Publication	Aim of the study	Approach/cleaning method	Activated brain areas	Frequency bands of interest
Raethjen et al., 2008 [65]	Rhythmic foot movements	Static/no cleaning	Central midline region + frontal mesial area	Stepping frequency + β band (15 – 30 Hz)

Wieser et al., 2010 [66]	Assisted lower-limb movements	Static/ no cleaning	M1, PMC, SMA, CC, S1, SA	No frequency analysis. Activations are directly related to specific phases of the gait-like movements
Do et al., 2011 [67]	BCI dedicated to a FES system for ankle movement	Static/ no cleaning	Mid-central areas (electrode Cz)	μ , β and low- γ bands
Gwin et al., 2011 [87]	EEG activity during treadmill walking	Dynamic/ ICA cleaning (AM-ICA)	Anterior cingulate, posterior parietal and sensorimotor cortex	α and β bands + clear evidence of high- γ intra-stride spectral power changes
Presacco et al., 2011 [71]	Neural decoding of treadmill walking from EEG signals	Dynamic/ no cleaning	Involvement of a broad fronto-posterior cortical network	Delta band (0.1 – 2 Hz)
Severens et al., 2012 [81]	Detection of ERD/ERS during walking	Dynamic/ CCA cleaning	ERD found in the μ band above the electrode Cz and in the β band above the lateral motor cortex (electrodes C3 and C4).	ERSPs in μ and β bands are coupled to the gait cycle with significant differences between left swing, right swing and double support phase of the gait cycle.
Wagner et al., 2012 [83]	Robotic-assisted treadmill walking	Dynamic/ ICA cleaning (Info-max)	Central midline areas	μ and β rhythms suppressed during active walking in the Lokomat; modulations of the lower γ band (25 to 40 Hz) related to the phases of the gait cycle. These might be related to sensorimotor processing of the lower limbs.
Petersen et al., 2012 [86]	Treadmill walking	Dynamic/ coherence analysis	Significant coherence between EEG (Cz) and EMG (Tibialis Anterior) before the heel strike	Coherence between 24 and 40 Hz. Evidence that the coupling is not due to non-physiological artefacts.

Table 9.2: EEG studies of human locomotion: a schematic view of recent results obtained with static and dynamic experimental protocols. M1 is the primary motor cortex, PMC is the premotor cortex, SMA is the supplementary motor cortex, CC is the cingulate cortex, S1 is the primary somatosensory cortex and SA is the somatosensory association cortex.

9.3.3 Results from Invasive Studies

Although this paper is essentially devoted to non-invasive analyses of human locomotion, it may be interesting to report a few important results from invasive studies in order to bring supplementary information to the different elements presented above.

Several invasive studies with mammals report rhythmic cerebral activations in phase with the gait cycle. As mentioned in [88], olfactory neurons, in rats, discharge rhythmically at frequencies closely matching the step cycle [89]. Analogously, in cats, the locomotion activity of more than 90% of neurons of motor cortex are modulated in the rhythm of strides [90]. Moreover, it was shown that the discharge rate means, peaks, and depths of stride-related frequency modulation changed dramatically during accurate stepping as compared with simple walking [91].

In a recent breakthrough [72], bipedal walking patterns could be extracted from the modulations of discharge rates of monkey S1 and M1 neuronal ensembles. In this paper, the activity modulations in hundreds of simultaneously recorded neurons were analysed and it was demonstrated that both M1 and S1 neurons modulated their firing rate in relationship with the gait cycle. Remarkably, the firing rate of each neuron peaked at a particular phase of the stepping cycle. Using a set of linear decoders (Wiener filters), the authors could thus predict locomotion kinematic parameters with a very satisfying accuracy. Large neuronal ensembles were needed for accurate predictions of leg kinematics and the number of units required increased with the task complexity. Also, the authors report a superior performance of neuronal populations drawn from several cortical areas in predicting movement kinematics compared to the performance of populations drawn from a single area. Moreover, results indicated that both M1 and S1 neurons contributed significantly to the prediction of the leg kinematics. As expected, M1 modulations were more useful for predicting future values in the parameters of walking, whereas S1 modulations better predicted the past values. This observation, however, must still be confirmed with more experiments, since accurate predictions of future values of locomotion parameters could be obtained from S1 activity in one of the two monkeys participating in the study. Nevertheless, this work provides the first proof of concept that, in the future, real-time neuroprosthetic systems for restoring bipedal walking in severely paralysed patients could be implemented.

Interesting results were also obtained with electrocorticography. Significant coherence between right sensorimotor cortex and distal left leg muscles was found up to 60 Hz during voluntary induced myoclonic jerks. Additional higher frequency coherence (~ 140 and 190 Hz) was found during sensory-induced myoclonic jerks [92]. Recently, significant decreases (4-7, 8-14 and 15-25 Hz) or increases (26-45 and 65-95 Hz) in power (compared to rest) were reported during spontaneous movement of the hand and/or arm contralateral to electrode grid placement [93]. Furthermore, specific high gamma ECoG responses were also identified during natural expressive speech and natural motor tasks involving upper and lower extremities [94]. Thanks to these

particular features, several research teams have demonstrated that prosthesis control based on ECoG signals is quite feasible [95, 96, 97, 98]. Nevertheless, these promising advances have been made for upper limb applications. It remains to be shown if the same principles can be successfully exploited for developing walk rehabilitation systems.

A last original invasive study which is worth to be mentioned in this review is the first analysis of basal ganglia activity recorded from deep brain stimulation (DBS) electrodes in human subjects during treadmill walking [99]. Recordings were made with patients who has DBS electrodes located in the globus pallidus internum (GPi) for treatment of neck and upper trunk motor impairments, with no gait disturbances. The authors report that local field potentials (LFP) spectra of GPi recordings made during walking showed significantly higher power values in the lower frequency bands (4–12 Hz) and in the gamma band (60–90 Hz) as compared to during sitting or standing. The opposite was seen in the beta band (15–25 Hz) where the power was significantly reduced during walking. According to the authors, these changes may initiate or sustain gait-related activity in locomotor brainstem centres. No significant differences over all frequency bands were observed between the sitting and the standing conditions. Additionally, a modulation of the amplitudes in the theta-alpha (6–11 Hz) range was seen in all subjects. The maximum amplitude variation was located between 6 and 11 Hz during the early stance phase of the left leg in the right hemisphere and symmetrically on the left during the early stance phase of the right leg (cf. Figure 9.6). This modulation seems to indicate that information about individual gait cycles is also present in the basal ganglia.

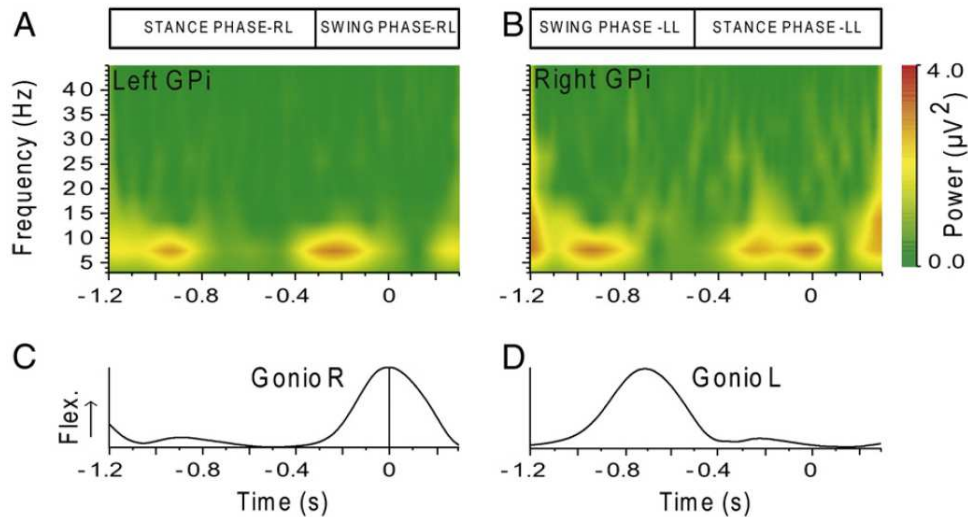


Figure 9.6: Time-frequency plots (wavelet transformation) of LFP oscillations during gait cycle. Upper row (A and B): analysed electrode pair. Right electrode pair is on the right side. C and D: goniometer traces. Modulation of LFPs occurs in the 6–11 Hz frequency range. In this frequency band, amplitudes are up-regulated during the early stance phase and swing phase of the contralateral leg. LL: left leg, RL: right leg, Gonio: goniometer. Flex: flexion. Figure from [99].

9.4 Development of Non-Invasive Brain-Computer Interfaces Dedicated to Rehabilitation Systems

After reviewing the main principles of human locomotion control and, in particular, the spatial and temporal characteristics of the supra-spinal control, the next paragraphs will deal with the development of rehabilitation systems based on non-invasive brain-computer interfaces (BCI). After defining the concept of BCI, different challenges like detecting the movement intention based on EEG signals or translating EEG signals to valuable commands dedicated to rehabilitation systems will be reviewed and discussed.

9.4.1 General Considerations about BCIs

Brain-Computer Interfaces (BCI) include devices or systems which respond to neural or cognitive processes. These systems enable their users – whose neural system may have been destroyed by amputation, trauma or disease – to control a computer or any robotic device by interpreting neurophysiological signals which are recorded and processed following different steps as shown in Figure 9.7. First, the brain signals are pre-processed to clean them as much as possible. Then, some features are extracted and classified so that the computer can determine in which mental state the user was. Finally, the corresponding action is produced by the system. As it is non-invasive, light and relatively cheap, electroencephalography (EEG) is the most used acquisition technique to record cerebral activity of the BCI users.

Thanks to current BCI technology, severely disabled people can communicate [100], control computers [101], or drive robotic [102] or simple prosthetic devices [103] via the power of their brain only, without activating any muscle. Nowadays, BCI applications dedicated to both disabled and healthy users are also being developed in the video game field [104]. Although functional, BCI technology offers information transfer rates that are too limited to control complex systems entirely. Consequently, shared control is used extensively in assistive applications. This means that the BCI user generally sends high-level commands to the system, which is able to operate all the low-level problems [72, 105]. Very interestingly, the benefits of BCI are not limited to the control of simple electric devices. It has been shown that the simple fact of learning to operate a BCI has a positive impact on brain plasticity, with a significant increase in motor cortical excitability and a modification of the brain network topology [106]. As such, BCI could become a viable tool for new post-stroke rehabilitation strategies [107].

In the case of BCI dedicated to walk rehabilitation systems, the first challenge is to detect the user intention (to start walking, to stop, to go faster, to slow down, to turn left or right, ...). Then, the system has to generate a realistic human walk movement, corresponding to the detected user intent. Finally, a feedback should be sent to the user, to help him to control the system. These are the main challenges to raise. They are detailed in the following sections, with an emphasis on existing systems and latest results obtained.

9.4.2 Detecting the User Intent

Detecting the user intent, and particularly predicting the next movement onset, type and direction is of first interest as it could activate rehabilitation devices in a fully natural way. Although

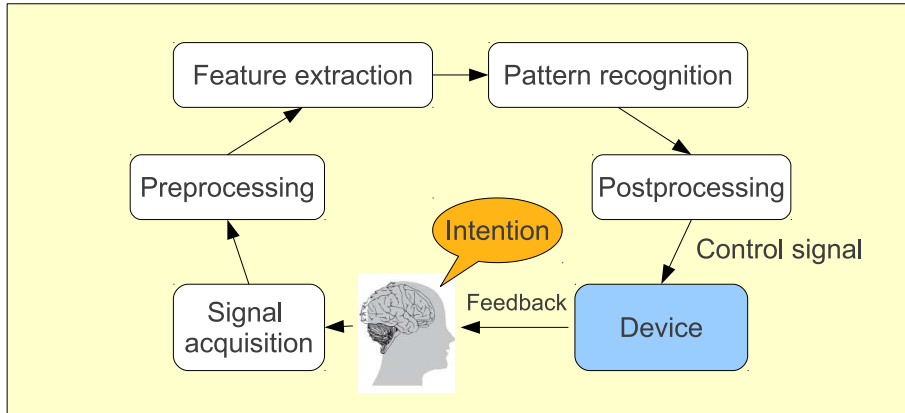


Figure 9.7: General scheme of a classical Brain-Computer Interface (BCI): first of all, the subject performs a specific mental task in order to produce a signal of interest in his brain; then this signal is acquired and generally pre-processed in order to get rid of different artefacts. Afterwards, some discriminating features are extracted and classified (pattern recognition) to determine which specific signal was produced. Finally, the identified signal is associated to a specific action to be performed by a computer or any electronic device.

very few gait intent detection studies have been undertaken [108, 109], predicting the leg movement is of primary importance and would definitely be helpful to adequately control an orthosis/prosthesis. Indeed, from a mechanical point of view, the only interest of using brain signals to control a prosthesis would be to detect early willingness for the next move [110]. Thereby, the whole device could anticipate the movement and adjust as precisely as possible the mechanical system. It has to be underlined that this anticipation is not feasible solely on the basis of physical sensors placed on the rehabilitation system since these detect the movement only once it has been produced.

From a practical point of view, researchers have basically two options to detect the movement intention thanks to EEG signals: look for the emergence of a Bereitschaftspotential (BP) or detect the production of an event-related (de-)synchronization (ERD/ERS) by the brain. The BP, on the one hand, is a slow cortical potential that deepens in negativity about 1.5 s to 1 s before the movement onset. As shown in Figure 1.11, the BP potential can be divided into three different parts. First, in the pre-BP section, the brain signals are not affected by the movement intent yet. Then, in the BP section or *early BP*, the potential slowly decreases about 1.5 s before movement onset and is more prominent in the central-medial areas. Second, the negative slope (NS) or *late BP* corresponds to a steeper slope and starts around 400 ms prior to movement onset. This potential is mainly localized over the primary motor cortex (M1). It was shown that BP potentials are also observed in the brain just before imagination of movements [111]. In a recent study [61], the BP signal was analysed during gait intent. Five different tasks were performed: gait/stepping forward, gait and stepping backward and stepping laterally. As shown in Figure 1.13, the measured potentials vary slightly, depending on the experimental paradigm. The most important potentials and variations occur at the top of the head, around electrode Cz, which corresponds to the leg representation in the motor and sensorimotor cortices.

The event-related desynchronization, on the other hand, manifests itself as a short-lasting decrease of power in some specific frequency bands [108]. This decrease can start as early as 2 s before movement onset. Generally, the ERD occur in μ (8-12 Hz) and β (12-30 Hz) bands, which are directly linked to movement planning and execution. These frequency limits as well as the strength and laterality of the ERD patterns depend on the subject, especially if the patient suffers from stroke impairment [112].

As reviewed in [108], several researchers have succeeded in automatically detecting BP or ERD, in a non invasive way. While most of the studies focus on the upper limb (finger, wrist, arm), only three studies tackle the detection of ankle dorsiflexion movement without cues [67, 113]. The obtained true positive rates range between 82.5% [113] and 100% [67]. Another study evaluated the possibility to classify right-hand, left-hand, tongue or right-foot movements with less success [114]. The single-trial classification of gait and point movement preparation was investigated [109]. Depending on the analysed pair of tasks, the average error rate was 25%.

Finally, motor-imagery was also investigated as an effective BCI paradigm to detect the intention to start walking. It was shown in [115] that paraplegic and tetraplegic patients could trigger a walking simulator by imagining themselves walking or idling. In these two experimental conditions, the EEG power in the 9—13 Hz band in the mid-frontal (FCz), central (Cz) and central-parietal (CPz) areas contained the best discriminant information. Based on these features, classification results estimated offline ranged from about 60 to 90%. This proves that SCI patients have the possibility to operate a robust BCI walking simulator with short training period and satisfying accuracy. This expands the results of a similar analysis that had been undertaken earlier [102]. All these studies are summarized in Table 9.3.

Publication	Acquisition protocol	Brain feature	Key findings
Niazi et al., 2011 [113]	Ankle dorsiflexion movement without cues	BP	Predicted the movement with an average true positive rate of 82.5% around 187 ms before movement onset
Morash et al., 2008 [114]	Perform or imagine right-hand, left-hand, tongue, or right-foot move after a “Go” cue.	ERD/ERS	Predicting which of the four movements/imageries is about to occur is possible (around 40% accuracy)
Velu et al., 2013 [109]	Natural walk from a starting position to a designated ending position, pointing at a designated position from the starting position, or remaining standing at the starting position.	BP	Significant classification achieved for all conditions, with errors for movement vs standing around 25% when averaged across nine subjects.

Do et al., 2011 [67] Do et al., 2012 [116]	Detection of EEG patterns related to repetitive foot dorsiflexions	Activations in Cz electrode	Foot lifter rehabilitation system based on FES (online performance near 100% using FFT based features)
King et al., 2013 [115]	Motor imagery of walking or idling executed by participants with paraplegia or tetraplegia due to SCI	ERD/ERS	The EEG power in the 9–13 Hz band in the mid-frontal (FCz), central (Cz) and central-parietal (CPz) areas were the most different comparing walking and idling imagery. Classification accuracy from 60 to 90%.
Leeb et al., 2007 [102]	One tetraplegic patient imagines movements of his paralysed feet	Detection of β bursts during imagery	Control of a wheelchair in virtual environment (go/stop). Classification results ranging from 90 to 100%

Table 9.3: Several studies of EEG signals preceding lower limb motor tasks are available. The presented results show that it should be feasible to activate a prosthetic/rehabilitation device.

9.4.3 Developing a Direct Brain Signals to Limb Kinematics Decoding

Once the movement intent is detected, the rehabilitation system should produce realistic movements of the lower limbs. Ideally, these movements should be produced according to the patient's needs and/or wishes, in order to render the locomotion process almost instinctive, like in real walk. To this end, direct translation of the brain signals into limb kinematics is desirable. Such results, as previously mentioned, have been obtained with monkeys on the basis of invasive experiments, in the context of bipedal walking [72], direct cortical control of 3D neuroprosthetic devices [117], and cortical control of a prosthetic arm for self-feeding [118]. Several studies analyse this approach as summarized in Table 9.4.

An attempt to reproduce these results with non-invasive signals (EEG) has been made with human subjects [71], as reported earlier in this review, but seems to be unfruitful, according to the arguments developed in [77]. In the same underlying philosophy, robotic assisted gait analysis has shown a difference between active and passive walking around the Pz and Cz electrodes [83]. By automatically detecting these modifications, a monitoring of the brain activation could be performed and determine the best rehabilitation procedure, which could help to quicker recover. For instance, after analysing normal gait with and without a support exoskeleton in [119], the authors suggest that efficient lower limb rehabilitation should be based on actual walk and not staying fixed in one location. Additionally, they reported that it is important for patients to swing their arms during gait training in rehabilitation. Anyway, future investigations will be needed to improve the procedure and verify, after all, if the recorded signals contain or not sufficient

information to control a prosthetic/rehabilitation device permanently. In the meanwhile, other strategies have been developed to achieve a similar goal.

Publication	BCI Paradigm	Rehabilitation Device or Technique	Remarks
Presacco et al., 2011 [71]	EEG to kinematics translation	None	Tries to reproduce results obtained by invasive studies (RMS value between prediction and measurement around 0.68). Highly criticized by [77]
Wagner et al., 2012 [83]	EEG	Lokomat	No control: evaluation of level of participation in robotic-assisted treadmill walking (Fz and Pz difference between active and passive walk)
Tanaka et al., 2013 [119]	NIRS	Exoskeleton	Body motion support type mobile suit. Comparison of the cerebral activity during walking using the suit and normal gait without the suit. Recommendations: most effective for gait training to actually walk and not stay fixed in one location. Important for patients to swing their arms during gait training in rehabilitation.

Table 9.4: Only one study suggests a direct decoding of brain signals into lower limb kinematics. However, it was severely called into question by [77].

9.4.4 Producing a Gait/Stepping Movement in a Step by Step Approach

The alternative strategy to direct translation of EEG signals into walk kinematics signals consists in detecting high level commands from EEG (like accelerate, decelerate, turn left, right, ...), in order to subsequently produce the desired movement using a dedicated algorithm [120, 121]. Generally, this algorithm will drive a functional electrical stimulation (FES) system, a prosthesis, orthosis or exoskeleton [122, 123]. To detect high level commands from brain signals, several BCI paradigms can be exploited using visual stimuli in order to elicit P300 potentials or steady-state visually evoked potentials (SSVEPs) (see [124] for a review on BCI). Tactile stimulation could also be exploited to this aim [125].

To convert high level commands into kinematics, a class of algorithms called programmable central pattern generators (PCPG) is particularly suited for rehabilitation systems dedicated to walk. Inspired by biological CPG, the PCPG algorithm is able to learn practically any periodical pattern (a gait pattern for instance) and automatically reproduce it [126]. Very advantageously, the amplitude and frequency of the patterns produced may be changed on the fly, without producing any abrupt change in the output command signal sent to the exoskeleton actuators. By analysing the gait parameters of healthy subjects walking on a treadmill, our research group showed that adequately combining amplitude and frequency of the PCPG allowed to produce realistic gait kinematic patterns in a range of walking speeds from 1.5 to 6 km/h [120].

Actually, only a few studies were performed under an ambulatory context. After a pilot study investigating the feasibility of mobile auditory P300 detection [127], it was more precisely shown that the P300 potential is not affected that much while walking [75, 76, 128]. Thus, although slow, this approach obtained strongly reliable performance showing the feasibility of the link of a BCI with an external foot lifter orthosis [129]. Based on a SSVEP paradigm, a preliminary study scanning the brain response from 10 Hz to 46 Hz has shown that walking is not a transparent process [130]. In another study using two flickering stimuli, it was shown that ICA and Canonical Correlation Analysis (CCA) were able to extract SSVEP response while walking [131].

When considering studies in the context of lower-limb rehabilitation, some other papers are available. Using a SSVEP paradigm, it was shown that a lower limb exoskeleton could be controlled by both a step by step approach and in a continuous way [132]. In [133], a walk rehabilitation system which recognizes five types of intention is proposed and a 80% accuracy is claimed. In [134], motor imagery-based BCI allows the subject to make a humanoid robot turning right, turning left and walking forward. The most important results are summarized in Table 9.5.

Publication	BCI Paradigm	Rehabilitation Device or Technique	Remarks
Cheron et al., 2012 [121]	EEG (BCI)	Exoskeleton (LOPES)/foot lifter orthosis	Results from the Mindwalker and Biofact projects
Mc Daid et al., 2013 [132]	EEG (SSVEP)	Control of a lower limb exoskeleton. Studies motion intent detection and continuous control by the BCI	The control appears feasible
Duvinage et al., 2013 [130]	EEG (SSVEP)	Scanning of the brain response from 10 Hz to 46 Hz	Gait influences SSVEP brain response
Duvinage et al., 2012 [129]	EEG (P300) + PCPG	Foot lifter orthosis	Reliable proof of concept
Li et al., 2012 [134]	Humanoid robot control thanks to BCI	None	Identification of mental activities when the subject is thinking "turning right, " "turning left, " or "walking forward."

Zhang et al., 2011 [133]	EEG (SSVEP) + CPG	None	Walk rehabilitation system which recognizes five types of intention related to human walking. Successful classification accuracy above 80%. Functional using online EEG data.
-----------------------------	-------------------	------	---

Table 9.5: A few applications.

9.5 Discussion and Future Works

Recently, several studies dedicated to rehabilitation purposes have emerged in the non-invasive BCI field. It appears that investigations for upper limbs are more often realized than for lower limbs. This is probably due to both the inherent experimental difficulty of measuring EEG signals in ambulatory context and the challenging goal of balance control in walk rehabilitation tasks. Another reason is that walk may be considered as an automatic movement merely based on reflexes governed at the spinal level. However, it has been recently confirmed that the motor cortex is particularly active during specific phases of the gait cycle, particularly before the foot comes in contact with the ground [135]. Tremendous progress in understanding human locomotion control has been made thanks to invasive studies and neuroimaging techniques, giving the opportunity to build a bridge from BCI to new rehabilitation systems and strategies.

Indeed, traditional approaches aiming at walk recovery after stroke, for instance, may be considered as bottom-up approaches: they focus on the physical level (bottom) in order to influence the neural system (top), being able to rehabilitate the patients due to the mechanisms of neural plasticity. How these mechanisms are established is not well understood. Recently, some authors have promoted the top-down approach, which consists in defining the rehabilitation therapies based on the state of the brain after stroke [136]. Mental simulation of movement engages the primary motor cortex in a similar way that motor execution does. This mental exercise, called motor imagery (MI), induces distinctive modulations of sensorimotor rhythms which can be detected online. A specific BCI technology based on such MI paradigm can thus be used to help patients in cognitively rehearsing their physical skills in a safe, repetitive manner, even in the case of no residual motor function [136]. This is an example in which BCI are extensively exploited to promote neuroplasticity in combination with traditional physiotherapy and robot-aided therapy.

Nevertheless, before developing fully efficient neuronal prosthesis control systems, several challenging problems remain to be solved. These have already been mentioned throughout this review. They are summarized below.

According to the recent results presented in the previous sections, it seems quite possible to successfully detect intention of walking on the basis of EEG signals only (go/no-go detection) [108]. However, determining the precise orientation of the movement by analysing the shape of the Bereitschaftspotential happens to be much more challenging, given the weak difference between the BP associated to forward and backward movements [61].

Successful conversion of brain signals into limb kinematics has been achieved with monkeys, on the basis of invasive measurements [72]. Recently, an attempt to realize a similar conversion with EEG signals in humans has been made [71], but the statistical significance of the obtained results remains to be clearly established [77]. In particular, the question arises if the effective bit rate that can be achieved with EEG technology is sufficient to constantly drive a robotic arm or leg.

By contrast, non-invasive EEG signals can be effectively exploited to run standard brain-computer interfaces. These BCI can be designed to decode high level orders (like for instance 'go faster', 'go slower', 'turn left', 'stop', ...) while adapted algorithms such as PCPG provide the rehabilitation system actuators with meaningful limb kinematics [120, 121]. It was shown in several publications that standard BCI paradigm performances are not much affected by the

numerous artefacts polluting EEG signals recorded under “gentle” ambulatory conditions [75, 127]. The use of external visual stimuli (with P300 or SSVEP BCI paradigms) may, however, be considered as cumbersome and too tiring by patients.

In order to develop better BCI for walk rehabilitation, fundamental research aiming at detecting the precise role of motor cortex during the gait cycle (and other movements like stair climbing) should be pursued. It is indeed important to figure out what can effectively and non-ambiguously be measured using EEG: descending commands from the motor cortex? Integration of ascending sensorimotor information? Artefacts? Probably a mix of these different contributions, but in which proportions? In this context, it seems necessary to define several experimental protocols in order to disentangle the different signals.

To this end, we propose to characterize the descending brain commands which are involved in human walk control in a *static* approach (inspired by [65]), in order to ensure absence of EEG motion artefacts. To this aim, the EEG signals of subjects sitting on a chair would be recorded. The subjects would then be asked to produce voluntary rhythmic foot movements, staying at the same tempo. The feet will not be in contact with the ground, to ensure a minimal sensorimotor feedback. Several tempos would be produced. Also, EEG should be recorded when the subject is sitting and not moving the feet, to define a baseline, necessary when using brain imagery tools like LORETA [137]. To assess the presence (or absence) of motion artefacts, an accelerometer should be placed on the neck. A complete characterization of these data could then be realized, by analysing the event-related spectral perturbations (ERSP) combined with a time-warping transformation [87], and by computing directed corticomuscular coherence and in particular delays between EEG and EMG time series (to assess the information flow direction). Then, characterization of EEG signals caused by somatosensory information coming from the feet of the subject when sitting (again, to prevent any motion artefacts) should be undertaken. More precisely, the same experiment as above could be realized, with the feet in contact with ground, this time. By comparing the two states (contact/no contact), it would be possible to emphasize the contribution of sensory feedback. Alternatively, one could use special tactors to stimulate the feet, mimicking the sensation of walk and study the properties of the EEG signals that are phase-locked with this stimulation. Finally, if motion artefacts are correctly rejected, provided we know the signals due to descending commands (voluntary rhythmic movements) and those due to tactile stimulation (tactors, mimicking the sensation of walk), we should be able to disentangle the contribution of posture and balance control when the subject is standing and walking.

Directed coherence (Granger causality) is a promising way to disentangle descending from ascending contributions in EEG signals. Unlike coherence, which measures correlation and therefore does not allow to identify the direction of interaction between two signals, Granger causality can provide information about possible causal relationships. Using such analysis, directed coherence in both descending (EEG to EMG) and ascending (EMG to EEG) directions was found in beta frequencies, in human subjects performing a precision grip task [138]. This study provides, for the first time, clear evidence of bidirectional corticomuscular coherence in man. Such analysis should also be made in the context of bipedal walking.

Of course, another crucial research axis to further develop deals with the adequate cleaning of motion artefacts in EEG signals. The first available option consists in mathematically correcting corrupted signals. The most popular method is Independent Component Analysis (ICA), which

consists in separating EEG into subcomponents (independent components) in such a way that these are all statistically independent from each other. By discarding components related to artefacts, it is possible to reconstruct cleaned EEG signals [139]. While this technique is really powerful to eliminate basic artefacts (like eye motion or blink artefacts), it seems not so well adapted to motion artefacts produced during walk, since these cannot be completely separated from cortical signals, as explained in [76]. Furthermore, the weak point of this technique resides in the arbitrary nature of the choice of independent components to eliminate. Therefore, improved cleaning methods are desirable, especially if the goal is to directly convert EEG signals into lower limb kinematics. On the other hand, it has been demonstrated that motion artefacts do not dramatically impact low complexity P300-based BCI under ambulatory conditions [75], for instance. Interestingly, it has been shown that artefact resistant measures could be computed in order to detect cognitive EEG activity during locomotion [73]. This may constitute a useful perspective for future. Finally, one could also mention the idea to develop a device able to determine online the motion artefacts corrupting the EEG electrode, in order to correct them with adaptive filtering by optimal projection [140].

From a fundamental point of view, we would like to underline the fact that the mechanism of gait control may change as a function of the walking speed, since the kinematics and EMG patterns during the gait cycle vary significantly in shape under 3 km/h [2]. Thus, it should be interesting to systematically compare EEG signals during walking at very low, normal and high walking speeds.

To conclude, it is really exciting to see that new BCI applications are being developed in the field of rehabilitation. These realizations are based on the considerable knowledge acquired over time in the field of brain sciences. In this review, we have summarized the main principles of human locomotion control, described the first non-invasive BCIs dedicated to walk rehabilitation systems and identified the main technical challenges ahead in the field. We must also not forget that the patients should always be put at the heart of the development process [141], by integrating their personal needs and preferences, in order to produce the best possible benefit for their rehabilitation.

Bibliography

- [1] Eric Kandel, James Schwartz, and Thomas Jessell. *Principles of Neural Science*. McGraw-Hill Medical, 2000.
- [2] H. van Hedel and V. Dietz. Rehabilitation of locomotion after spinal cord injury. *Restorative Neurology and Neuroscience*, 28(1):123 – 134, 2010.
- [3] S Grillner and P Wallen. Central pattern generators for locomotion, with special reference to vertebrates. *Annual Review of Neuroscience*, 8(1):233–261, 1985.
- [4] Jacques Duysens and Henry W.A.A Van de Crommert. Neural control of locomotion; part 1: The central pattern generator from cats to humans. *Gait & Posture*, 7(2):131 – 141, 1998.
- [5] Jens Bo Nielsen. How we walk: Central control of muscle activity during human walking. *The Neuroscientist*, 9(3):195–204, 2003.
- [6] M.R. Dimitrijevic, Y. Gerasimenko, and M.M. Pinter. Evidence for a spinal central pattern generator in humans. *Annals of the New York Academy of Sciences*, 860:360–376, 1998.
- [7] Jaynie F. Yang and Monica Gorassini. Spinal and brain control of human walking: Implications for retraining of walking. *The Neuroscientist*, 12(5):379–389, 2006.
- [8] Andre Thomas, S Autgaerden, Spastics Society. Medical Education, and Information Unit. *Locomotion from pre- to post-natal life: how the newborn begins to acquire psycho-sensory functions, preface by R. C. Mac Keith*. London : Spastics Society Medical Education and Information Unit in association with Heinemann Medical, 1966.
- [9] J.I.P. de Vries, G.H.A. Visser, and H.F.R. Prechtl. The emergence of fetal behaviour. i. qualitative aspects. *Early Human Development*, 7(4):301 – 322, 1982.
- [10] Yuri P. Ivanenko, Nadia Dominici, Germana Cappellini, Ambrogio Di Paolo, Carlo Giannini, Richard E. Poppele, and Francesco Lacquaniti. Changes in the spinal segmental motor output for stepping during development from infant to adult. *The Journal of Neuroscience*, 33(7):3025–3036, 2013.
- [11] Scott R. Robinson and William P. Smotherman. Fundamental motor patterns of the mammalian fetus. *Journal of Neurobiology*, 23(10):1574–1600, 1992.

- [12] J. Westergaard and A. Gramsbergen. Development of locomotion in the rat: the significance of early movements. *Early Human Development*, 34(1–2):89 – 100, 1993.
- [13] Stephen M. Ho. Rhythmic motor activity and interlimb co-ordination in the developing pouch young of a wallaby (*macropus eugenii*). *The Journal of Physiology*, 501(3):623–636, 1997.
- [14] Jaynie F. Yang, Marilee J. Stephens, and Rosie Vishram. Transient disturbances to one limb produce coordinated, bilateral responses during infant stepping. *Journal of Neurophysiology*, 79(5):2329–2337, 1998.
- [15] Nadia Dominici, Yuri P. Ivanenko, Germana Cappellini, Andrea d’Avella, Vito Mondi, Marika Cicchese, Adele Fabiano, Tiziana Silei, Ambrogio Di Paolo, Carlo Giannini, Richard E. Poppele, and Francesco Lacquaniti. Locomotor primitives in newborn babies and their development. *Science*, 334(6058):997–999, 2011.
- [16] Gordon Holmes. The goulstonian lectures on spinal injuries of warfare. *British Medical Journal*, 2(2865):769–774, 11 1915.
- [17] Robert A. Kuhn. Functional capacity of the isolated human spinal cord. *Brain*, 73(1):1–51, 1950.
- [18] Blair Calancie, Belinda Needham-Shropshire, Patrick Jacobs, Keith Willer, Gregory Zych, and Barth A. Green. Involuntary stepping after chronic spinal cord injury: Evidence for a central rhythm generator for locomotion in man. *Brain*, 117(5):1143–1159, 1994.
- [19] Richard M. Coleman Phd, Charles P. Pollak, and Elliot D. Weitzman. Periodic movements in sleep (nocturnal myoclonus): Relation to sleep disorders. *Annals of Neurology*, 8(4):416–421, 1980.
- [20] E Lugaresi, F Cirignotta, G Coccagna, and P Montagna. Nocturnal myoclonus and restless legs syndrome. *Advances in neurology*, 43:295–307, 1986.
- [21] M.L. Shik, G.N. Orlovskii, and F.V. Severin. Locomotion of the mesencephalic cat elicited by stimulation of the pyramids. *Biophysics*, 13(1):143–152, 1968.
- [22] I.P. Gerasimenko, A.N. Makarovskii, and O.A. Nikitin. Control of the human and animal locomotor activity in the absence of supraspinal effects. *Ross Fiziol Zh Im I M Sechenova*, 86(11):1502–11, 2000.
- [23] Y.P. Gerasimenko, V.D. Avelev, O.A. Nikitin, and I.A. Lavrov. Initiation of locomotor activity in spinal cats by epidural stimulation of the spinal cord. *Neurosci Behav Physiol*, 33(3):247–54, 2003.
- [24] I.Y. Dorofeev, V.D. Avelev, N.A. Shcherbakova, and Y.P. Gerasimenko. The role of cutaneous afferents in controlling locomotion evoked by epidural stimulation of the spinal cord in decerebrate cats. *Neurosci Behav Physiol*, 38(7):695–701, 2008.

- [25] J. Duysens, F. Clarac, and H. Cruse. Load-regulating mechanisms in gait and posture: Comparative aspects. *Physiological Reviews*, 80(1):83–133, 2000.
- [26] Marco Y C Pang and Jaynie F Yang. The initiation of the swing phase in human infant stepping: importance of hip position and leg loading. *The Journal of Physiology*, 528(2):389–404, 2000.
- [27] Henry W.A.A Van de Crommert, Theo Mulder, and Jacques Duysens. Neural control of locomotion: sensory control of the central pattern generator and its relation to treadmill training. *Gait & Posture*, 7(3):251 – 263, 1998.
- [28] E. D. Schomburg, N. Petersen, I. Barajon, and H. Hultborn. Flexor reflex afferents reset the step cycle during fictive locomotion in the cat. *Experimental Brain Research*, 122:339–350, 1998.
- [29] Keir G Pearson. Proprioceptive regulation of locomotion. *Current Opinion in Neurobiology*, 5(6):786 – 791, 1995.
- [30] E. Paul Zehr and Jacques Duysens. Regulation of arm and leg movement during human locomotion. *The Neuroscientist*, 10(4):347–361, 2004.
- [31] L. O. D. Christensen, H. Morita, N. Petersen, and J. Nielsen. Evidence suggesting that a transcortical reflex pathway contributes to cutaneous reflexes in the tibialis anterior muscle during walking in man. *Experimental Brain Research*, 124(1):59–68, 1999.
- [32] H. Geyer and H. Herr. A muscle-reflex model that encodes principles of legged mechanics produces human walking dynamics and muscle activities. *Neural Systems and Rehabilitation Engineering, IEEE Transactions on*, 18(3):263–273, 2010.
- [33] Patrick J Whelan. Control of locomotion in the decerebrate cat. *Progress in Neurobiology*, 49(5):481 – 515, 1996.
- [34] Larry M. Jordan, Carol A. Pratt, and John E. Menzies. Locomotion evoked by brain stem stimulation: occurrence without phasic segmental afferent input. *Brain Research*, 177(1):204 – 207, 1979.
- [35] E. Eidelberg, J.G. Walden, and L.H. Nguyen. Locomotor control in macaque monkeys. *Brain*, 104(4):647–663, 1981.
- [36] H. Barbeau and S. Rossignol. Recovery of locomotion after chronic spinalization in the adult cat. *Brain Research*, 412(1):84 – 95, 1987.
- [37] K. G. Pearson and S. Rossignol. Fictive motor patterns in chronic spinal cats. *Journal of Neurophysiology*, 66(6):1874–1887, 1991.
- [38] H. Barbeau, C. Chau, and S. Rossignol. Noradrenergic agonists and locomotor training affect locomotor recovery after cord transection in adult cats. *Brain Research Bulletin*, 30(3–4):387 – 393, 1993.

- [39] S. Rossignol and H. Barbeau. Pharmacology of locomotion: an account of studies in spinal cats and spinal cord injured subjects. *The Journal of the American Paraplegia Society*, 16(4):190–196, 1993. cited By (since 1996)29.
- [40] H. Forssberg and S. Grillner. The locomotion of the acute spinal cat injected with clonidine i.v. *Brain Research*, 50(1):184 – 186, 1973.
- [41] N T Petersen, J E Butler, V Marchand-Pauvert, R Fisher, A Ledebt, H S Pyndt, N L Hansen, and J B Nielsen. Suppression of emg activity by transcranial magnetic stimulation in human subjects during walking. *J Physiol*, 537(Pt 2):651–6, 2001.
- [42] Sten Grillner, Peter Wallén, Kazuya Saitoh, Alexander Kozlov, and Brita Robertson. Neural bases of goal-directed locomotion in vertebrates—an overview. *Brain Research Reviews*, 57(1):2 – 12, 2008.
- [43] Bruce H. Dobkin, Ann Firestone, Michele West, Kaveh Saremi, and Roger Woods. Ankle dorsiflexion as an fmri paradigm to assay motor control for walking during rehabilitation. *NeuroImage*, 23(1):370 – 381, 2004.
- [44] T. Harada, I. Miyai, M. Suzuki, and K. Kubota. Gait capacity affects cortical activation patterns related to speed control in the elderly. *Experimental Brain Research*, 193(3):445–454, 2009.
- [45] D. M. Halliday, B. A. Conway, L.O.D. Christensen, N. L. Hansen, N. P. Petersen, and J. B. Nielsen. Functional coupling of motor units is modulated during walking in human subjects. *Journal of Neurophysiology*, 89(2):960–968, 2003.
- [46] Charles Capaday. The special nature of human walking and its neural control. *Trends in Neurosciences*, 25(7):370 – 376, 2002.
- [47] Jens Bo Nielsen. Motoneuronal drive during human walking. *Brain Research Reviews*, 40(1–3):192 – 201, 2002.
- [48] Chandana Paul, Mario Bellotti, Sašo Jezernik, and Armin Curt. Development of a human neuro-musculo-skeletal model for investigation of spinal cord injury. *Biological Cybernetics*, 93(3):153–170, 2005.
- [49] Hidenao Fukuyama, Yasuomi Ouchi, Shigeru Matsuzaki, Yasuhiro Nagahama, Hiroshi Yamauchi, Masafumi Ogawa, Jun Kimura, and Hiroshi Shibasaki. Brain functional activity during gait in normal subjects: a spect study. *Neuroscience Letters*, 228(3):183 – 186, 1997.
- [50] Takashi Hanakawa, Yukinori Katsumi, Hidenao Fukuyama, Manabu Honda, Takuya Hayashi, Jun Kimura, and Hiroshi Shibasaki. Mechanisms underlying gait disturbance in parkinson's disease: A single photon emission computed tomography study. *Brain*, 122(7):1271–1282, 1999.

- [51] Ichiro Miyai, Hiroki C. Tanabe, Ichiro Sase, Hideo Eda, Ichiro Oda, Ikuo Konishi, Yoshio Tsunazawa, Tsunehiko Suzuki, Toshio Yanagida, and Kisou Kubota. Cortical mapping of gait in humans: A near-infrared spectroscopic topography study. *NeuroImage*, 14(5):1186 – 1192, 2001.
- [52] M. Suzuki, I. Miyai, T. Ono, I. Oda, I. Konishi, T. Kochiyama, and K. Kubota. Prefrontal and premotor cortices are involved in adapting walking and running speed on the treadmill: an optical imaging study. *Neuroimage*, 23(3):1020 – 1026, 2004.
- [53] Francine Malouin, Carol L. Richards, Philip L. Jackson, Francine Dumas, and Julien Doyon. Brain activations during motor imagery of locomotor-related tasks: A pet study. *Human Brain Mapping*, 19(1):47–62, 2003.
- [54] Klaus Jahn, Angela Deutschländer, Thomas Stephan, Michael Strupp, Martin Wiesmann, and Thomas Brandt. Brain activation patterns during imagined stance and locomotion in functional magnetic resonance imaging. *NeuroImage*, 22(4):1722 – 1731, 2004.
- [55] C. Sahyoun, A. Floyer-Lea, H. Johansen-Berg, and P.M. Matthews. Towards an understanding of gait control: Brain activation during the anticipation, preparation and execution of foot movements. *NeuroImage*, 21(2):568–575, 2004.
- [56] B.M. de Jong, K.L. Leenders, and A.M.J. Paans. Right parieto-premotor activation related to limb-independent antiphase movement. *Cerebral Cortex*, 12(11):1213–1217, 2002.
- [57] L.O.D. Christensen, P. Johannsen, T. Sinkjaer, N. Petersen, H.S. Pyndt, and J.B. Nielsen. Cerebral activation during bicycle movements in man. *Experimental Brain Research*, 135(1):66–72, 2000.
- [58] C. la Fougère, A. Zwergal, A. Rominger, S. Förster, G. Fesl, M. Dieterich, T. Brandt, M. Strupp, P. Bartenstein, and K. Jahn. Real versus imagined locomotion: A [18f]-fdg pet-fmri comparison. *NeuroImage*, 50(4):1589–1598, 2010.
- [59] I. Miyai, H.C. Tanabe, I. Sase, H. Eda, I. Oda, I. Konishi, Y. Tsunazawa, T. Suzuki, T. Yanagida, and K. Kubota. Cortical mapping of gait in humans: A near-infrared spectroscopic topography study. *NeuroImage*, 14(5):1186–1192, 2001.
- [60] Shogo Yazawa, Hiroshi Shibasaki, Akio Ikeda, Kiyohito Terada, Takashi Nagamine, and Manabu Honda. Cortical mechanism underlying externally cued gait initiation studied by contingent negative variation. *Electroencephalography and Clinical Neurophysiology/Electromyography and Motor Control*, 105(5):390 – 399, 1997.
- [61] Omar Feix do Nascimento, Kim Dremstrup Nielsen, and Michael Voigt. Influence of directional orientations during gait initiation and stepping on movement-related cortical potentials. *Behavioural Brain Research*, 161(1):141 – 154, 2005.
- [62] M. Bakker, C. C. P. Verstappen, B. R. Bloem, and I. Toni. Recent advances in functional neuroimaging of gait. *Journal of Neural Transmission*, 114:1323–1331, 2007.

- [63] Serge Rossignol, Réjean Dubuc, and Jean-Pierre Gossard. Dynamic sensorimotor interactions in locomotion. *Physiological Reviews*, 86(1):89–154, 2006.
- [64] György Buzsáki and Andreas Draguhn. Neuronal oscillations in cortical networks. *Science*, 304(5679):1926–1929, 2004.
- [65] Jan Raethjen, R.B. Govindan, Sabine Binder, Kirsten E. Zeuner, Günther Deuschl, and Henning Stolze. Cortical representation of rhythmic foot movements. *Brain Research*, 1236:79 – 84, 2008.
- [66] M. Wieser, J. Haefeli, L. Bütler, L. Jäncke, R. Riener, and S. Koeneke. Temporal and spatial patterns of cortical activation during assisted lower limb movement. *Experimental Brain Research*, 203:181–191, 2010.
- [67] A-H Do, P-T Wang, C-E King, A. Abiri, and Z. Nenadic. Brain computer interface controlled functional electrical stimulation system for ankle movement. *Journal of NeuroEngineering and Rehabilitation*, 8(49), 2011.
- [68] Christa Neuper and Gert Pfurtscheller. Post-movement synchronization of beta rhythms in the EEG over the cortical foot area in man. *Neuroscience Letters*, 216(1):17 – 20, 1996.
- [69] Teodoro Solis-Escalante, Gernot Müller-Putz, and Gert Pfurtscheller. Overt foot movement detection in one single laplacian eeg derivation. *Journal of Neuroscience Methods*, 175(1):148 – 153, 2008.
- [70] J.T. Gwin, K. Gramann, S. Makeig, and D.P. Ferris. Electrocortical activity is coupled to gait cycle phase during treadmill walking. *NeuroImage*, 54(2):1289 – 1296, 2011.
- [71] A. Presacco, R. Goodman, L. Forrester, and J. Contreras-Vidal. Neural decoding of treadmill walking from non-invasive, electroencephalographic (EEG) signals. *Journal of Neurophysiology*, 2011.
- [72] Nathan Fitzsimmons, Mikhail Lebedev, Ian Peikon, and Miguel A.L Nicolelis. Extracting kinematic parameters for monkey bipedal walking from cortical neuronal ensemble activity. *Frontiers in Integrative Neuroscience*, 3, 2009.
- [73] Troy Lau, Joseph Gwin, Kaleb McDowell, and Daniel Ferris. Weighted phase lag index stability as an artifact resistant measure to detect cognitive eeg activity during locomotion. *Journal of NeuroEngineering and Rehabilitation*, 9(1):47, 2012.
- [74] Scott E. Kerick, Kelvin S. Oie, and Kaleb McDowell. Assessment of EEG signal quality in motion environments. *Army Research Laboratory Report*, (ARL-TR-4866), 2009.
- [75] T. Castermans, M. Duvinage, M. Petieau, T. Hoellinger, C.D. Saedeleer, K. Seetharaman, A. Bengoetxea, G. Cheron, and T. Dutoit. Optimizing the performances of a p300-based brain-computer interface in ambulatory conditions. *Emerging and Selected Topics in Circuits and Systems, IEEE Journal on*, 1(4):566–577, 2011.

- [76] J.T. Gwin, K. Gramann, S. Makeig, and D.P. Ferris. Removal of movement artifact from high-density EEG recorded during walking and running. *Journal of Neurophysiology*, 103(6):3526–3534, 2010.
- [77] Javier M. Antelis, Luis Montesano, Ander Ramos-Murguialday, Niels Birbaumer, and Javier Minguez. On the usage of linear regression models to reconstruct limb kinematics from low frequency eeg signals. *PLoS ONE*, 8(4):e61976, 04 2013.
- [78] H.A. Agashe and J.L. Contreras-Vidal. Reconstructing hand kinematics during reach to grasp movements from electroencephalographic signals. In *Engineering in Medicine and Biology Society, EMBC, 2011 Annual International Conference of the IEEE*, pages 5444–5447, 2011.
- [79] Trent J. Bradberry, Rodolphe J. Gentili, and José L. Contreras-Vidal. Reconstructing three-dimensional hand movements from noninvasive electroencephalographic signals. *The Journal of Neuroscience*, 30(9):3432–3437, 2010.
- [80] Trent J Bradberry, Rodolphe J Gentili, and José L Contreras-Vidal. Fast attainment of computer cursor control with noninvasively acquired brain signals. *Journal of Neural Engineering*, 8(3):036010, 2011.
- [81] M. Severens, B. Nienhuis, P. Desain, and J. Duysens. Feasibility of measuring event related desynchronization with electroencephalography during walking. In *Engineering in Medicine and Biology Society (EMBC), 2012 Annual International Conference of the IEEE*, pages 2764–2767, 2012.
- [82] G. Pfurtscheller and F.H. Lopes da Silva. Event-related eeg/meg synchronization and desynchronization: basic principles. *Clinical Neurophysiology*, 110(11):1842 – 1857, 1999.
- [83] Johanna Wagner, Teodoro Solis-Escalante, Peter Grieshofer, Christa Neuper, Gernot Müller-Putz, and Reinhold Scherer. Level of participation in robotic-assisted treadmill walking modulates midline sensorimotor EEG rhythms in able-bodied subjects. *NeuroImage*, 63(3):1203 – 1211, 2012.
- [84] R.B. Govindan, J. Raethjen, F. Kopper, J.C. Claussen, and G. Deuschl. Estimation of time delay by coherence analysis. *Physica A: Statistical Mechanics and its Applications*, 350(2-4):277 – 295, 2005.
- [85] Thierry Castermans, Matthieu Duvinage, Guy Cheron, and Thierry Dutoit. Eeg and human locomotion - descending commands and sensory feedback should be disentangled from artifacts thanks to new experimental protocols position paper. In Sabine Van Huffel, Carlos Manuel B. A. Correia, Ana L. N. Fred, and Hugo Gamboa, editors, *BIOSIGNALS*, pages 309–314. SciTePress, 2012.
- [86] T. H. Petersen, M. Willerslev-Olsen, B. A. Conway, and J. B. Nielsen. The motor cortex drives the muscles during walking in human subjects. *The Journal of Physiology*, 590(10):2443–2452, 2012.

- [87] Joseph T. Gwin, Klaus Gramann, Scott Makeig, and Daniel P. Ferris. Electrocortical activity is coupled to gait cycle phase during treadmill walking. *NeuroImage*, 54(2):1289 – 1296, 2011.
- [88] M. Iosa, A. Fusco, F. Marchetti, G. Morone, C. Caltagirone, S. Paolucci, and A. Peppe. The golden ratio of gait harmony: Repetitive proportions of repetitive gait phases. *BioMed Research International*, 2013, 2013.
- [89] S.S Smith. Step cycle-related oscillatory properties of inferior olivary neurons recorded in ensembles. *Neuroscience*, 82(1):69 – 81, 1997.
- [90] Vladimir Marlinski, Wijitha U. Nilaweera, Pavel V. Zelenin, Mikhail G. Sirota, and Irina N. Beloozerova. Signals from the ventrolateral thalamus to the motor cortex during locomotion. *Journal of Neurophysiology*, 107(1):455–472, 2012.
- [91] Irina N. Beloozerova, Bradley J. Farrell, Mikhail G. Sirota, and Boris I. Prilutsky. Differences in movement mechanics, electromyographic, and motor cortex activity between accurate and nonaccurate stepping. *Journal of Neurophysiology*, 103(4):2285–2300, 2010.
- [92] J.F Marsden, P Ashby, J.C Rothwell, and P Brown. Phase relationships between cortical and muscle oscillations in cortical myoclonus: electrocorticographic assessment in a single case. *Clinical Neurophysiology*, 111(12):2170 – 2174, 2000.
- [93] M.J. Vansteensel, M.G. Bleichner, L.T. Dintzner, E.J. Aarnoutse, F.S.S. Leijten, D. Hermes, and N.F. Ramsey. Task-free electrocorticography frequency mapping of the motor cortex. *Clinical Neurophysiology*, 124(6):1169 – 1174, 2013.
- [94] Johanna Ruescher, Olga Iljina, Dirk-Matthias Altenmüller, Ad Aertsen, Andreas Schulze-Bonhage, and Tonio Ball. Somatotopic mapping of natural upper- and lower-extremity movements and speech production with high gamma electrocorticography. *NeuroImage*, 81(0):164 – 177, 2013.
- [95] Takufumi Yanagisawa, Masayuki Hirata, Youichi Saitoh, Tetsu Goto, Haruhiko Kishima, Ryohei Fukuma, Hiroshi Yokoi, Yukiyasu Kamitani, and Toshiki Yoshimine. Real-time control of a prosthetic hand using human electrocorticography signals. *Journal of Neurosurgery*, 114(6):1715–1722, 2011.
- [96] Duk Shin, Hidenori Watanabe, Hiroyuki Kambara, Atsushi Nambu, Tadashi Isa, Yukio Nishimura, and Yasuharu Koike. Prediction of muscle activities from electrocorticograms in primary motor cortex of primates. *PLoS ONE*, 7(10):e47992, 10 2012.
- [97] H.L. Benz, Huaijian Zhang, A. Bezerianos, S. Acharya, N.E. Crone, Xiaoxiang Zheng, and N.V. Thakor. Connectivity analysis as a novel approach to motor decoding for prosthesis control. *Neural Systems and Rehabilitation Engineering, IEEE Transactions on*, 20(2):143–152, 2012.
- [98] Tobias Pistohl, Thomas Sebastian Benedikt Schmidt, Tonio Ball, Andreas Schulze-Bonhage, Ad Aertsen, and Carsten Mehring. Grasp detection from human ecog during natural reach-to-grasp movements. *PLoS ONE*, 8(1):e54658, 01 2013.

- [99] Arun Singh, Stefan Kammermeier, Annika Plate, Jan H. Mehrkens, Josef Ilmberger, and Kai Bötzel. Pattern of local field potential activity in the globus pallidus internum of dystonic patients during walking on a treadmill. *Experimental Neurology*, 232(2):162 – 167, 2011.
- [100] L.A. Farwell and E. Donchin. Talking off the top of your head: toward a mental prosthesis utilizing event-related brain potentials. *Electroencephalography and Clinical Neurophysiology*, 70(6):510 – 523, 1988.
- [101] Jonathan R. Wolpaw, Niels Birbaumer, Dennis J. McFarland, Gert Pfurtscheller, and Theresa M. Vaughan. Brain-computer interfaces for communication and control. *Clinical Neurophysiology*, 113(6):767 – 791, 2002.
- [102] Robert Leeb, Doron Friedman, Gernot R. Müller-Putz, Reinhold Scherer, Mel Slater, and Gert Pfurtscheller. Self-Paced (Asynchronous) BCI Control of a Wheelchair in Virtual Environments: A Case Study with a Tetraplegic. *Computational Intelligence and Neuroscience*, 2007:1–8, 2007.
- [103] Gert Pfurtscheller, Gernot R. Müller, Jörg Pfurtscheller, Hans Jürgen Gerner, and Rüdiger Rupp. ‘Thought’ - control of functional electrical stimulation to restore hand grasp in a patient with tetraplegia. *Neuroscience Letters*, 351(1):33 – 36, 2003.
- [104] Anatole Lécuyer, Fabien Lotte, Richard B. Reilly, Robert Leeb, Michitaka Hirose, and Mel Slater. Brain-computer interfaces, virtual reality, and videogames. *Computer*, 41:66–72, October 2008.
- [105] Jose del R. Millán, Rudiger Rupp, Gernot Mueller-Putz, Roderick Murray-Smith, Claudio Giugliemma, Michael Tangermann, Carmen Vidaurre, Febo Cincotti, Andrea Kubler, Robert Leeb, Christa Neuper, Klaus R Mueller, and Donatella Mattia. Combining brain-computer interfaces and assistive technologies: State-of-the-art and challenges. *Frontiers in Neuroscience*, 4(0):12, 2010.
- [106] F Pichiorri, F De Vico Fallani, F Cincotti, F Babiloni, M Molinari, S C Kleih, C Neuper, A Kübler, and D Mattia. Sensorimotor rhythm-based brain–computer interface training: the impact on motor cortical responsiveness. *Journal of Neural Engineering*, 8(2):025020, 2011.
- [107] Fabrizio De Vico Fallani, Floriana Pichiorri, Giovanni Morone, Marco Molinari, Fabio Babiloni, Febo Cincotti, and Donatella Mattia. Multiscale topological properties of functional brain networks during motor imagery after stroke. *NeuroImage*, 83(0):438 – 449, 2013.
- [108] Pouya Ahmadian, Stefano Cagnoni, and Luca Ascoli. How capable is non-invasive eeg data of predicting the next movement? a mini review. *Frontiers in Human Neuroscience*, 7(124), 2013.
- [109] Priya Velu and Virginia R de Sa. Single-trial classification of gait intent from human eeg. *Frontiers in Neuroscience*, 7(84), 2013.

- [110] M. Duvinage, R. Jiménez-Fabián, T. Castermans, O. Verlinden, and Thierry Dutoit. An active foot lifter orthosis based on a PCPG algorithm. In *12th International IEEE Conference on Rehabilitation Robotics*, 2011.
- [111] M.-F. Lucas, C. Doncarli, D. Farina, and O.F. do Nascimento. Optimization of a set of wavelets for classification of imaginary movement-related cortical potentials. In *Applied Sciences on Biomedical and Communication Technologies, 2008. ISABEL '08. First International Symposium on*, pages 1–3, 2008.
- [112] Vera Kaiser, Ian Daly, Floriana Pichiorri, Donatella Mattia, Gernot R. Müller-Putz, and Christa Neuper. Relationship between electrical brain responses to motor imagery and motor impairment in stroke. *Stroke*, 43(10):2735–2740, 2012.
- [113] Imran Khan Niazi, Ning Jiang, Olivier Tiberghien, Jørgen Feldbæk Nielsen, Kim Dremstrup, and Dario Farina. Detection of movement intention from single-trial movement-related cortical potentials. *Journal of Neural Engineering*, 8(6):066009, 2011.
- [114] Valerie Morash, Ou Bai, Stephen Furlani, Peter Lin, and Mark Hallett. Classifying eeg signals preceding right hand, left hand, tongue, and right foot movements and motor imageries. *Clin Neurophysiol*, 119(11):2570–8, 2008.
- [115] Christine King, Po Wang, Luis Chui, An Do, and Zoran Nenadic. Operation of a brain-computer interface walking simulator for individuals with spinal cord injury. *Journal of NeuroEngineering and Rehabilitation*, 10(1):77, 2013.
- [116] A.H. Do, P.T. Wang, C.E. King, A. Schombs, S.C. Cramer, and Z. Nenadic. Brain-computer interface controlled functional electrical stimulation device for foot drop due to stroke. In *Engineering in Medicine and Biology Society (EMBC), 2012 Annual International Conference of the IEEE*, pages 6414–6417, 2012.
- [117] Dawn M. Taylor, Stephen I. Helms Tillery, and Andrew B. Schwartz. Direct cortical control of 3d neuroprosthetic devices. *Science*, 296(5574):1829–1832, 2002.
- [118] Meel Velliste, Sagi Perel, M. Chance Spalding, Andrew S. Whitford, and Andrew B. Schwartz. Cortical control of a prosthetic arm for self-feeding. *Nature*, 453(7198):1098–1101, 2008.
- [119] E. Tanaka, S. Saegusa, and L. Yuge. Development of a whole body motion support type mobile suit and evaluation of cerebral activity corresponding to the cortical motor areas. *Journal of Advanced Mechanical Design, Systems and Manufacturing*, 7(1):82–94, 2013.
- [120] M. Duvinage, T. Castermans, T. Hoellinger, G. Cheron, and T. Dutoit. Modeling human walk by pcpg for lower limb neuroprosthesis control. In *Neural Engineering (NER), 2011 5th International IEEE/EMBS Conference on*, pages 317–321, 2011.
- [121] G. Cheron, M. Duvinage, C. De Saedeleer, T. Castermans, A. Bengoetxea, M. Petieau, K. Seetharaman, T. Hoellinger, B. Dan, T. Dutoit, F. Sylos Labini, F. Lacquaniti, and Y. Ivanenko. From spinal central pattern generators to cortical network: Integrated bci for walking rehabilitation. *Neural Plasticity*, 2012, 2012.

- [122] Rachel Cowan, Benjamin Fregly, Michael Boninger, Leighton Chan, Mary Rodgers, and David Reinkensmeyer. Recent trends in assistive technology for mobility. *Journal of NeuroEngineering and Rehabilitation*, 9(1):20, 2012.
- [123] A.M. Dollar and H. Herr. Lower extremity exoskeletons and active orthoses: Challenges and state-of-the-art. *Robotics, IEEE Transactions on*, 24(1):144–158, 2008.
- [124] L.F. Nicolas-Alonso and J. Gomez-Gil. Brain computer interfaces, a review. *Sensors*, 12(2):1211–1279, 2012.
- [125] Anne-Marie Brouwer and Jan B F Van Erp. A tactile p300 brain-computer interface. *Frontiers in Neuroscience*, 4(19), 2010.
- [126] Auke Jan Ijspeert. Central pattern generators for locomotion control in animals and robots: a review. *Neural Networks*, 21(4):642–653, 2008.
- [127] Fabien Lotte, Junya Fujisawa, Hideaki Touyama, Rika Ito, Michitaka Hirose, and Anatole Lécuyer. Towards ambulatory brain-computer interfaces: a pilot study with p300 signals. In *Proceedings of the International Conference on Advances in Computer Entertainment Technology*, ACE ’09, pages 336–339, New York, NY, USA, 2009. ACM.
- [128] K. Gramann, J.T. Gwin, N. Bigdely-Shamlo, D.P. Ferris, and S. Makeig. Visual evoked responses during standing and walking. *Frontiers in Human Neuroscience*, 4, 2010.
- [129] M. Duvinage, T. Castermans, R. Jimenez-Fabian, T. Hoellinger, C. De Saedeleer, M. Petieau, K. Seetharaman, G. Cheron, O. Verlinden, and T. Dutoit. A five-state p300-based foot lifter orthosis: Proof of concept. In *Biosignals and Biorobotics Conference (BRC), 2012 ISSNIP*, pages 1–6, 2012.
- [130] Matthieu Duvinage, Thierry Castermans, Mathieu Petieau, Thomas Hoellinger, Karthik Seetharaman, Guy Cheron, and Thierry Dutoit. A preliminary fundamental study of ambulatory ssvep. In *TOBI Workshop IV*, 2013, 2013.
- [131] Yuan-Pin Lin, Yijun Wang, and Tzzy-Ping Jung. A mobile ssvep-based brain-computer interface for freely moving humans; the robustness of canonical correlation analysis to motion artifacts. In *Engineering in Medicine and Biology Society (EMBC), 2013 Annual International Conference of the IEEE*, 2013.
- [132] A.J. McDaid, Song Xing, and S.Q. Xie. Brain controlled robotic exoskeleton for neurorehabilitation. In *Advanced Intelligent Mechatronics (AIM), 2013 IEEE/ASME International Conference on*, pages 1039–1044, 2013.
- [133] Dingguo Zhang, Lin Yao, Ying Wang, and Xiangyang Zhu. Functional interface between brain and central pattern generator for application in human-machine system. In *Robotics and Biomimetics (ROBIO), 2011 IEEE International Conference on*, pages 1873–1877, 2011.

- [134] Wei Li, C. Jaramillo, and Yunyi Li. Development of mind control system for humanoid robot through a brain computer interface. In *Intelligent System Design and Engineering Application (ISDEA), 2012 Second International Conference on*, pages 679–682, 2012.
- [135] T. Castermans and M. Duvinage. Corticomuscular coherence revealed during treadmill walking: Further evidence of supraspinal control in human locomotion. *Journal of Physiology*, 591(6):1407–1408, 2013.
- [136] Juan-Manuel Belda-Lois, Silvia Mena-del Horno, Ignacio Bermejo-Bosch, Juan Moreno, Jose Pons, Dario Farina, Marco Iosa, Marco Molinari, Federica Tamburella, Ander Ramos, Andrea Caria, Teodoro Solis-Escalante, Clemens Brunner, and Massimiliano Rea. Rehabilitation of gait after stroke: a review towards a top-down approach. *Journal of Neuro-Engineering and Rehabilitation*, 8(1):66, 2011.
- [137] R.D. Pascual-Marqui. Standardized low-resolution brain electromagnetic tomography (sloreta): technical details. *Methods Find. Exp. Clin. Pharmacol.*, 24(D):5–12, 2002.
- [138] Claire L. Witham, C. Nicholas Riddle, Mark R. Baker, and Stuart N. Baker. Contributions of descending and ascending pathways to corticomuscular coherence in humans. *The Journal of Physiology*, 589(15):3789–3800, 2011.
- [139] A. Delorme and S. Makeig. EEGLAB: An open source toolbox for analysis of single-trial EEG dynamics including independent component analysis. *Journal of Neuroscience Methods*, 134(1):9–21, 2004.
- [140] S. Boudet, L. Peyrodié, G. Forzy, A. Pinti, H. Toumi, and P. Gallois. Improvements of adaptive filtering by optimal projection to filter different artifact types on long duration eeg recordings. *Computer Methods and Programs in Biomedicine*, 108(1):234–249, 2012.
- [141] M. Duvinage, T. Castermans, M. Petieau, K. Seetharaman, T. Hoellinger, G. Cheron, and T. Dutoit. A subjective assessment of a p300 bci system for lower-limb rehabilitation purposes. In *Engineering in Medicine and Biology Society (EMBC), 2012 Annual International Conference of the IEEE*, pages 3845–3849, 2012.

Chapter 10

An analysis of EEG signals during voluntary rhythmic foot movements

Contents

10.1 Introduction	243
10.2 Experimental procedure and data analysis	244
10.2.1 Data collection	244
10.2.2 Pre-processing	244
10.2.3 Ensemble averaged time-frequency analysis	245
10.3 Results and discussion	245
10.3.1 Description of results	245
10.3.2 Discussion	246
10.4 Conclusion	249

Abstract

Human locomotion is based on complex interactions of several cortical and subcortical structures. Over the years, the main underlying mechanisms have been partially unveiled thanks to standard functional neuroimaging techniques as well as electroencephalography (EEG). However, a complete picture is still lacking to date, due to particularly challenging experimental difficulties arising on top of the inherent complexity of the involved mechanisms.

In this context, the aim of this Chapter is to investigate the EEG dynamics associated to the production of voluntary rhythmic foot movements only. An experimental protocol drastically limiting the presence of movement artefacts in the EEG signals compared to real walk on a treadmill is used. Time-frequency analysis is performed, based on a time-warping method allowing for an ensemble averaging of the data of 3 subjects.

Characteristic alternation of power increases and decreases in the alpha, beta and gamma bands during the movement cycle is shown, as well as the emergence of two different neural coordination schemes related to in-phase and anti-phase foot movements.

This chapter is based upon the following publication:

- T. CASTERMANS, M. DUVINAGE, T. HOELLINGER, M. PETIEAU, T. DUTOIT, G. CHERON, 2011, *An analysis of EEG signals during voluntary rhythmic foot movements*, Proceedings of the 5th International IEEE/EMBS Neural Engineering Conference, Fiesta Americana Grand Coral Beach Cancun, Mexico, April 27 - May 1, pp. 584-587.

10.1 Introduction

As explained in the previous Chapter, human locomotion has been proven to be a particularly complex mechanism, implying the coordinated activity of several cortical and subcortical structures [1], [2], [3]. Experimental investigation of the cerebral activity elicited during walk is highly challenging. Indeed, head movements constitute strong limiting factors for most of the standard functional neuroimaging techniques, like single photon emission computed tomography (SPECT), functional magnetic resonance imaging (fMRI) or positron emission tomography (PET). The strategy used to overcome these experimental difficulties generally consists in focusing on simplified foot or leg movements which imply common cerebral processes with gait. Results from several studies show that several brain areas are involved in the higher control of bipedal gait: the supplementary motor cortex (SMA), the primary somatosensory cortex (S1), the primary motor cortex (M1), the cerebellum and parts of the basal ganglia (see for instance [4] for a review).

Electroencephalography (EEG) with a high temporal resolution represents an interesting complementary technique for investigating the dynamics of neural processes governing walk. However, movements of the head and body give rise to oscillations of the EEG wires and electrodes, strongly affecting the EEG signals quality. Again, most of the studies found in the literature describe experimental protocols wherein the subjects are mainly static, producing only limited lower limb movements.

For instance, the cortical activity associated to bilateral anti-phase and in-phase rhythmic foot movements was investigated in [5]. In their study, the authors found significant corticomuscular coherence between EEG signals and the anterior tibial muscles, at the stepping frequencies in the central midline region, extending further to the frontal mesial area. During isometric cocontraction of the calf muscles, coherence appeared between 15 and 30 Hz, concentrated on the central midline area. The main conclusion of this work is that there exists a representation of rhythmic motor patterns in the cortex, transmitted to the muscles and fed back to the cortex with delays compatible with fast corticospinal transmission, which may be important also for gait control.

Assisted lower limb movements have also been investigated using electroencephalography [6]. In this study, subjects performed standardized, assisted stepping movements in an upright position, while being secured to a tilt table. Sources associated to the movement-related potential were localized in the primary motor cortex, the premotor cortex, the supplementary motor cortex, the cingulate cortex, the primary somatosensory cortex and the somatosensory association cortex. The authors demonstrated that a clear succession of activations and deactivations was present in the movement-related potential, in direct relationship with specific phases of the gait-like leg movements. In particular, it was shown that cortical activity was the greatest during transition between flexion and extension of the legs and vice versa. A study of EEG during pedaling, another locomotor-like task, led to similar conclusions [7].

In this general context, the aim of this Chapter is to investigate the EEG dynamics associated to the production of voluntary rhythmic foot movements only. We decided to use an experimental protocol analog to the one described in [5], limiting drastically the presence of movement artefacts in the EEG signals compared to real walk on a treadmill. A time-frequency analysis (which was

missing in the latter study) is presented here, based on the time-warping method originally proposed in [8] and applied in [9]. The interest of this methodology lies in the fact that the focus is put on the mechanism involved in the generation of voluntary rhythmic foot movements itself, without superimposing other cerebral processes like balance control for instance, which would affect the EEG signals directly or indirectly. In addition to the understanding of the mechanism itself, this experiment gives us also the opportunity to study to what extent information extracted from the EEG signals can be exploited to drive an active neural foot-ankle orthosis based on a programmable central pattern generator (PCPG) algorithm [10]. In Section 10.2, the experiment is described and the data analysis is detailed. In Section 10.3, a discussion about the results is provided.

10.2 Experimental procedure and data analysis

10.2.1 Data collection

Three healthy volunteers without any known physical or neurological disorders participated in this experiment (age-range: 25-33 years). Each subject was seated comfortably and as relaxed as possible, with the feet in contact with the ground. They were asked to perform two series of rhythmic stepping movements with their feet: the first series consisted in lifting alternatively the heels and toes (referred to as the *anti-phase movement* experimental condition), whereas in the second series the two feet were moving the same way (referred to as the *in-phase movement* experimental condition). Each series of movement was executed during 90 seconds, at a frequency chosen by the subjects themselves, the only instruction being to keep the rhythm constant. Spontaneously, all the subjects moved their feet at a frequency close to 1 Hz and stayed in rhythm reasonably well (on average 1.013 ± 0.054 Hz and 1.014 ± 0.053 Hz for the *in-phase* and *anti-phase* movements respectively).

During all the recordings, the subjects kept their eyes open, gazing at a fixed point straight ahead on their eyes' level. EEG was recorded using a 128-electrode cap connected to the ANT acquisition system (Advanced Neuro Technology, ANT, Enschede, The Netherlands) digitizing the signals at 2048 Hz. Left ear was chosen as reference. Electrode impedance was measured and maintained under $20\text{ k}\Omega$ for each channel using electrode gel. In parallel, the kinematics of the lower limb movements was recorded using a system of six infrared cameras (Bonita, Vicon, Los Angeles, USA) determining at a frequency of 100 Hz the 3D cartesian coordinates (x , y and z) of 23 passive markers disposed on the subjects. Kinematics and EEG data were synchronized using a common trigger signal sent to the two acquisition systems.

10.2.2 Pre-processing

In a first step, the angles of elevation of both feet were computed as a function of time. A peak-detection algorithm was used to localize precisely the successive maximal and minimal angles, in order to define events of interest in each movement cycle. This procedure was straightforward as the computed kinematics curves were regular and smooth.

EEG signals were processed using the EEGLAB toolbox [11]. They were first detrended and downsampled to 100 Hz. This value was chosen for two reasons: first, it corresponds to the sampling frequency of the Vicon system and, secondly, we considered that the signal to noise ratio above 50 Hz was too small to get significant results. After downsampling, EEG signals were epoched on the basis of the successive movement cycles, by defining a time-window of 2 seconds around each maximal angle of elevation. taking the maximal angles of elevation as equal to zero, and by setting the epoch bounds at -1 and +1 second with respect to the reference time. Each epoch was visually inspected, rejected in case of obvious presence of eye or muscle artefacts, and finally detrended once again.

10.2.3 Ensemble averaged time-frequency analysis

The movements executed by the different subjects were only quasi-periodic, i.e. the lengths of the different movement cycles were not strictly identical. The production of ensemble averaged event-related spectral perturbation (*ERSP*) plots was thus not straightforward. We first generated spectrograms for each EEG channel during each epoch for each subject, as described in [9]. All the single-trial spectrograms were then linear time-warped in such a way that the minimal angles of elevation (preceding and following the maximal angles, located at time $t=0$ in each epoch by definition) occurred at the same adjusted latencies, namely -500 ms and 500 ms. After this operation, spectrograms were ensemble averaged for all subjects. The average log spectrum for all movement cycles was subtracted from the log spectrogram for each movement cycle. The resulting changes from baseline are the ERSP plots presented below, as a function of the percentage of the normalized movement cycle. Significant ERSPs ($p < 0.05$) were computed using a bootstrapping method implemented in EEGLAB, and represented as contours on Figures 10.1 and 10.2.

10.3 Results and discussion

10.3.1 Description of results

EEG activity recorded at scalp electrodes reflects the partial synchrony of local field potentials across a compact cortical domain (on the order of a square centimetre) that is a good reflection of the fluctuation of the membrane potential of synchronized neurons [12]. The event-related spectral perturbation maps (Figures 10.1,10.2, center) allow to decipher by warm colors the increase (ERS) of the EEG power, indicating an increase in the degree of local synchrony, or by cool colors the decrease (ERD) of the power relative to the mean baseline, interpreted as a decrease of local synchrony. For a “yielding” rhythm as the alpha or mu, an ERD is interpreted as an increase of the neural activity reflecting the increase of cortical inhibition [13].

When the cyclic movements of the feet were performed in-phase, three significant ERS clusters (at the frequency of 20-30 Hz, 30-40 Hz and 40-50 Hz) occurred during the 20-30% period of the movement cycle. This period corresponds to the ascending (flexion of the ankle) phase of the movement. A significant ERD in the 5-15 Hz frequency range occurred in the same period of

the cycle indicating a relative increase of the cortical activity of the sensorimotor area of the feet (in close proximity to electrode Cz) and implicated in the generation of the mu rhythm (around 10 Hz). The superimposition of the curves in Figure 10.1 (bottom), representing the ERSP temporal evolution of these frequency bands, shows that the beta (20-30 Hz) and the gamma (30-40 Hz) occurred in perfect synchrony and in opposition with the alpha band during the ascending phase of the cycle (from 0 to 50 %). During the descending phase (from 50 to 100 %), the beta and gamma oscillations were not synchronous and the alpha-mu rhythm presented an important ERS, indicating cortical relaxation.

In contrast, when the foot movements were performed out of phase (as mimicking walking steps), another type of coordination between the EEG rhythms occurred for the same three main frequency bands. In this case, the beta and the gamma bands occurred in opposition, the beta ERS preceding the gamma ERS and the alpha-mu rhythm alternation being not present anymore. Although the rate of the cyclic movements was the same in both experimental conditions, it appears that the coordination of the EEG-related activity significantly differs in function of the type of movement coordination.

10.3.2 Discussion

It is well established that different brain rhythms may operate dynamically in order to produce a broad range of observable behaviours [14] such as locomotion or repetitive cyclic movement. These motor behaviours are characterized by the stability of the relative phase (collective variable) specifying the coordinated behavioural pattern [15]. Recently, it was demonstrated that (1) EEG activity in the beta-gamma range is directly coupled to gait cycle phase [9] and (2) EMG-EEG coherence in the same frequency band originates from the motor and frontal cortex [5]. This is reminiscent of a same type of cortical involvement during rhythmic movement of the hand [16] and suggests that cortical oscillations are involved in the rhythmic control of human locomotion. Moreover, functional neuroimaging techniques [17], [18], [19], movement-related electrocortical recordings [6] and transcranial magnetic stimulation studies [20] have largely confirmed specific involvements of primary sensorimotor and association areas during locomotion. In this context the recent studies of [9] revealed intra-stride cortical dynamics during steady-speed human walking indicating the existence of event-related spectral perturbations in the alpha, beta and gamma bands. By applying similar treatment of the EEG recorded at Cz, we here demonstrated the existence of characteristic rhythmic EEG activity associated to voluntary rhythmic foot movements. This is expressed by alternation of power increase (ERS) and decrease (ERD) in the alpha, beta and gamma bands inside of the movement cycle during the steady state execution of cyclic movements of the feet. Interestingly, the comparison between the in-phase (the feet are flexed and extended at the same time) and anti-phase (one foot is flexed when the other was extended) demonstrates the emergence of two different coordination between the related cortical rhythms. Namely, the fact that beta and gamma EEG oscillations increased or decreased their power at the same time during the in-phase cycle movement while they do the opposite during the anti-phase cycle movement proves that the modulation of the EEG rhythm is probably related to the coordination function of the foot movements. When the same movement is programmed to be

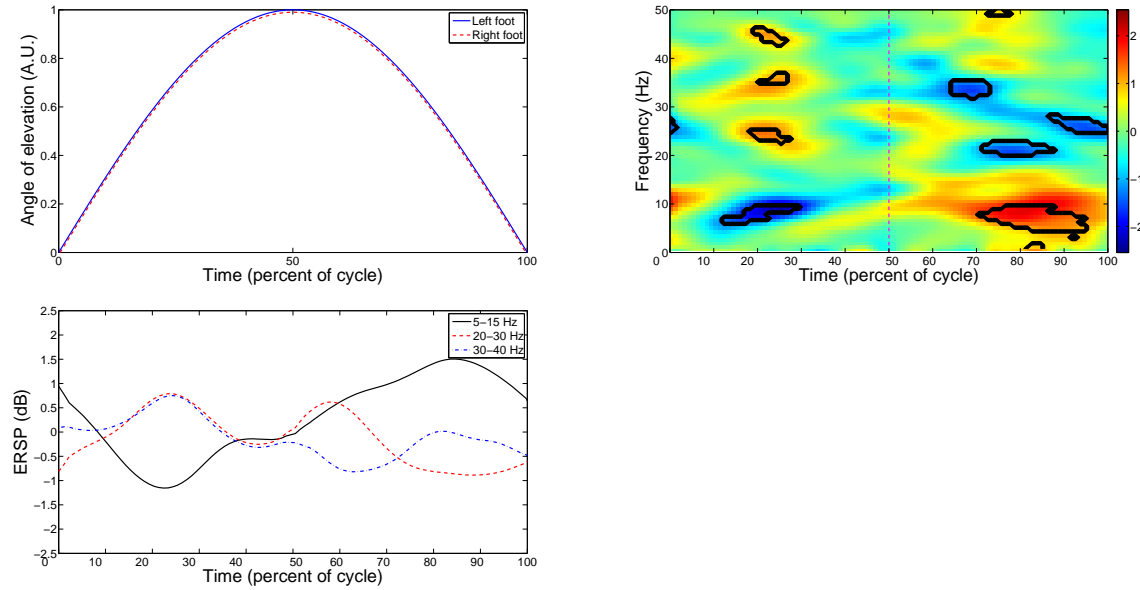


Figure 10.1: In-phase movement experimental condition: typical kinematics of the feet during one movement cycle (top); corresponding event-related spectral perturbation (ERSP) plot at electrode Cz (center); time course of the ERSP projections in different frequency bands (bottom). Contours indicate significant ERSPs ($p < 0.05$).

executed in phase by the two feet, a single global rhythm emerges in the sensorimotor cortex of both side linking in phase the beta and the gamma ERS in conjunction to an alpha-mu ERD. In contrast, when two opposite movements are programmed, another rhythmic distribution of the frequency band occurs and probably results from opposed contributions of the two sensorimotor areas.

Although the present analysis is limited to one recording channel (Cz), the origin of the EEG modulation at this locus is likely multiple and also suffers from volume conduction problems and the spurious synchrony it gives rise to. However, these uncertainties would equally obscure our data to the same extent whatever the movement type (in- or anti-phase) suggesting that after appropriate and additional analysis throughout a larger scale of recordings (128 electrodes are already available), the revealed EEG rhythm difference between in- and anti- phase movement would be confirmed. Further analysis of these data by means of a new version of swLORETA [21] will permit to decipher the present ERSP sources and then to describe the true synchrony between the different cortical sources as proposed by different methods [22], [23].

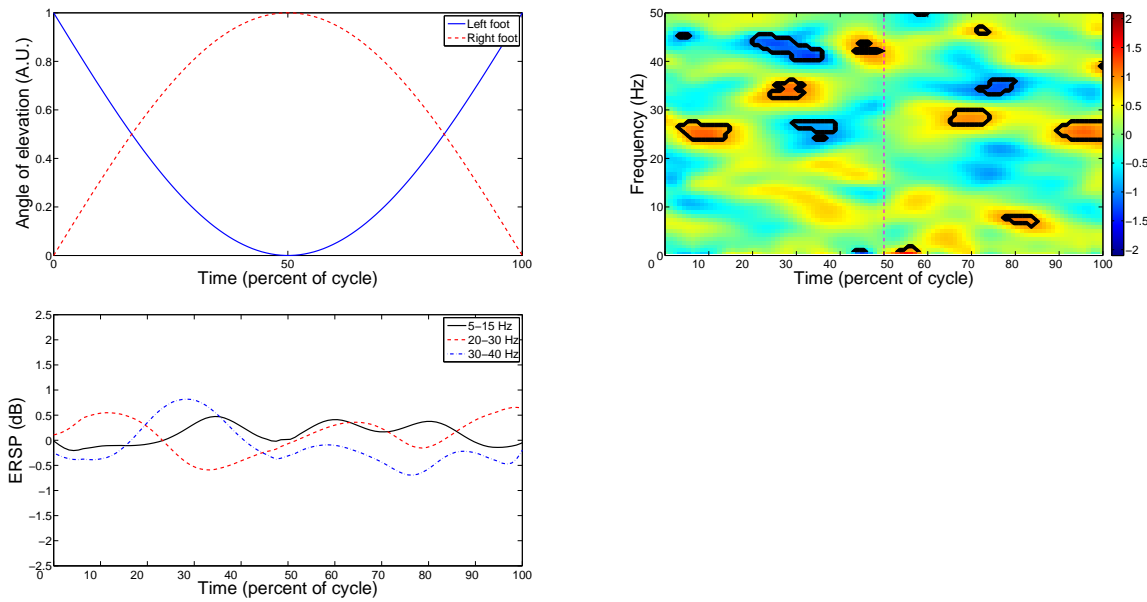


Figure 10.2: Anti-phase movement experimental condition: typical kinematics of the feet during one movement cycle (top); corresponding event-related spectral perturbation (ERSP) plot at electrode Cz (center); time course of the ERSP projections in different frequency bands (bottom). Contours indicate significant ERSPs ($p < 0.05$).

10.4 Conclusion

In this Chapter, we investigate the EEG dynamics associated to the performance of voluntary rhythmic foot movements in in-phase and anti-phase conditions. The chosen experimental protocol ensures that no movement artefact affects the quality of EEG signals. A time-warping method validated in the literature is used in order to compute an ensemble averaged time-frequency decomposition of all the data collected for three subjects (preliminary study).

Our study gives direct evidence of the existence of characteristic rhythmic EEG activity associated to voluntary rhythmic foot movements. In particular, we observe an alternation of power increases (ERS) and decreases (ERD) in the alpha, beta and gamma bands during the steady state execution of cyclic movements of the feet. To some extent, this behaviour is analog to recent findings of intra-stride cortical dynamics during steady-speed human walking. Interestingly, the comparison between the in-phase and anti-phase demonstrates the emergence of two different coordination schemes between the related cortical rhythms.

Several future works would be promising. First, the study of a higher population is essential to check the reproducibility of the results. Then, further analysis could be performed by means of other signal processing technique. For instance, Granger Causality or inverse solution algorithms could help to determine the neural flow of information between brain areas and better identify the electrocortical sources responsible of the production of rhythmic foot movements. The feasibility of developing an active foot-ankle orthosis driven by the patient's intentions could be assessed.

Bibliography

- [1] Hidenao Fukuyama, Yasuomi Ouchi, Shigeru Matsuzaki, Yasuhiro Nagahama, Hiroshi Yamadauchi, Masafumi Ogawa, Jun Kimura, and Hiroshi Shibasaki. Brain functional activity during gait in normal subjects: a spect study. *Neuroscience Letters*, 228(3):183 – 186, 1997.
- [2] V. Dietz. Spinal cord pattern generators for locomotion. *Clinical Neurophysiology*, 114(8):1379 – 1389, 2003.
- [3] Takashi Hanakawa. Neuroimaging of standing and walking: Special emphasis on parkinsonian gait. *Parkinsonism and Related Disorders*, 12(Supplement 2):S70 – S75, 2006. Proceedings of the 1st International Symposium on Dopaminergic and Nondopaminergic Mechanisms in Parkinson’s Disease (ISDNMPD).
- [4] M. Bakker, C. C. P. Verstappen, B. R. Bloem, and I. Toni. Recent advances in functional neuroimaging of gait. *Journal of Neural Transmission*, 114:1323–1331, 2007. 10.1007/s00702-007-0783-8.
- [5] Jan Raethjen, R.B. Govindan, Sabine Binder, Kirsten E. Zeuner, Günther Deuschl, and Henning Stolze. Cortical representation of rhythmic foot movements. *Brain Research*, 1236:79 – 84, 2008.
- [6] M. Wieser, J. Haefeli, L. Bütler, L. Jäncke, R. Riener, and S. Koeneke. Temporal and spatial patterns of cortical activation during assisted lower limb movement. *Experimental Brain Research*, 203:181–191, 2010.
- [7] Sanket G. Jain. EEG during pedaling: Brain activity during a locomotion-like task in humans. Master’s thesis, Marquette University, 2009.
- [8] S. Makeig, J. Onton, T. Sejnowski, and H. Poizner. Prospects for mobile, high-definition brain imaging: spectral modulations during 3d-reaching. In *Hum. Brain Mapp. Chicago, IL*, 2007.
- [9] J.T. Gwin, K. Gramann, S. Makeig, and D.P. Ferris. Electrocortical activity is coupled to gait cycle phase during treadmill walking. *NeuroImage*, 54(2):1289 – 1296, 2011.
- [10] M. Duvinage, T. Castermans, T. Hoellinger, J. Reumaux, and T. Dutoit. Modeling human walk by PCPG for lower limb neuroprostheses control. In *submitted to this conference*, 2011.

- [11] Arnaud Delorme and Scott Makeig. EEGLAB: an open source toolbox for analysis of single-trial EEG dynamics including independent component analysis. *Journal of Neuroscience Methods*, 134(1):9 – 21, 2004.
- [12] James F. Poulet and Carl C. Petersen. Internal brain state regulates membrane potential synchrony in barrel cortex of behaving mice. *Nature*, 454(7206):881–885, August 2008.
- [13] Wolfgang Klimesch, Paul Sauseng, and Simon Hanslmayr. Eeg alpha oscillations: The inhibition-timing hypothesis. *Brain Research Reviews*, 53(1):63 – 88, 2007.
- [14] György Buzsáki and Andreas Draguhn. Neuronal Oscillations in Cortical Networks. *Science*, 304(5679):1926–1929, June 2004.
- [15] Kelly J. Jantzen, Fred L. Steinberg, and J. A. Scott Kelso. Coordination dynamics of large-scale neural circuitry underlying rhythmic sensorimotor behavior. *J. Cognitive Neuroscience*, 21:2420–2433, December 2009.
- [16] B. Pollok, J. Gross, M. Dirks, L. Timmermann, and A. Schnitzler. The cerebral oscillatory network of voluntary tremor. *J. Physiol.*, 554:871–878, 2004.
- [17] L.O.D. Christensen, P. Johannsen, T. Sinkjaer, N. Petersen, H.S. Pyndt, and J.B. Nielsen. [without title]. *Experimental Brain Research*, 135:66–72, 2000.
- [18] Bruce H. Dobkin, Ann Firestone, Michele West, Kaveh Saremi, and Roger Woods. Ankle dorsiflexion as an fmri paradigm to assay motor control for walking during rehabilitation. *NeuroImage*, 23(1):370 – 381, 2004.
- [19] Sofie Heuninckx, Nicole Wenderoth, and Stephan P. Swinnen. Systems neuroplasticity in the aging brain: recruiting additional neural resources for successful motor performance in elderly persons. *The Journal of Neuroscience*, 28(1):91–99, January 2008.
- [20] N.L. Hansen and J.B. Nielsen. The effect of transcranial magnetic stimulation and peripheral nerve stimulation on corticomuscular coherence in humans. *J. Physiol. Lond.*, (561):295–306, 2004.
- [21] A.M. Cebolla, E. Palmero-Soler, B. Dan, and G. Cheron. Frontal phasic and oscillatory generators of the n30 somatosensory evoked potential. *NeuroImage*, 54(2):1297 – 1306, 2011.
- [22] Guido Nolte, Ou Bai, Lewis Wheaton, Zoltan Mari, Sherry Vorbach, and Mark Hallett. Identifying true brain interaction from eeg data using the imaginary part of coherency. *Clinical Neurophysiology*, 115(10):2292 – 2307, 2004.
- [23] Emmanuelle Tognoli and J.A. Scott Kelso. Brain coordination dynamics: True and false faces of phase synchrony and metastability. *Progress in Neurobiology*, 87(1):31 – 40, 2009.

Chapter 11

Automatic Detection of EEG-based Gait Intent

Contents

11.1 Introduction	255
11.2 Background	255
11.3 Experiment	256
11.3.1 Gait Intent Paradigm	256
11.3.2 Acquisition Material	256
11.3.3 Experiment Description	257
11.3.4 Statistical Note	257
11.4 Methods	258
11.4.1 Preprocessing	258
11.4.2 Feature Extraction	258
11.4.3 Classifiers	259
11.5 Results	259
11.5.1 Fundamental Analysis	259
11.5.2 MRP Analysis	259
11.5.3 Classifier Performances	260
11.6 Conclusion	268

Abstract

For decades, the hope of paraplegic people has been to fully recover the control of their lower limbs. In order to develop new walk rehabilitation systems, a nearly perfect prediction of the patient's intent is obviously required.

In the Electroencephalographic signals (EEG), some Event-Related Desynchronization (ERD) and a Bereitschaftspotential (BP), which is a slow negative potential occurring before the movement onset can be detected. Therefore, we here study different strategies to automatically decode these electrical brain signal related to gait initiation.

Four healthy subjects participated in this experiment, which consisted of forward and backward walking and standing. First, a fundamental analysis is proposed showing the type of signals and their localization. Then, five classifiers and six feature extraction techniques are investigated using only the potentials recorded at Cz electrode opening the way for very low complexity embedded devices.

The results show that the movement vs baseline detection comparison can reach around 80 % and 60 % accuracy in average for BP and ERD detection respectively. However, the direction of the movement only reaches at most 60 %. High variability between subjects was observed. By further analysis, it was shown that muscle and ocular artefacts are not impacting the results. Other evidences indicate that these results could be translated in real-time.

This chapter is based upon the following publication:

- M. DUVINAGE, T. CASTERMANS, T. HOELLINGER, M. PETIEAU, G. CHERON, T. DUTOIT, 2014, *Automatic Detection of EEG-based Gait Intent*, IEEE Transaction in Biomedical Engineering [Major Revision]

11.1 Introduction

One major issue of current non-invasive Brain-Computer Interfaces (BCIs) is the unrelated task to the wanted impact. Indeed, most of the currently widely used paradigms imply an interaction which is not natural and requires a specific task. For instance, in the Steady-State Visual Evoked Potential (SSVEP), the subject has to look at a flickering stimulus. After detecting this flickering frequency in the occipital area, the device executes the requested action, which is unrelated to the paradigm itself. This approach could be considered as strongly unnatural and disturbing when the patient desires to grasp an object [1]. Following this spirit, the prediction of the next movement onset, type and direction is of first interest as it could activate devices in a fully natural way.

In this Chapter, a quantitative study of several automatic gait intent detection techniques using ERD/ERS and BP signals is studied. Indeed, although the available review is extremely valuable [2], there are several limits. First, few are reported on lower-limb movements and no study report about classification of different type of lower-limb movements. Moreover, as the different reviewed studies were performed by other researchers, there is not a common framework for fair comparison between the brief reported performances. Additionally, no detailed time-frequency analysis of ERD/ERS produced for that particular movement is given. Afterwards, the evaluation of the performance is not always properly performed. For instance, the respect of training, testing and validation data is seldom applied. There is also sometimes no study of the impact of EMG and EOG pollution, which could partially explain the obtained performance. Then, different pipeline and types of feature extraction may allow to compare their stability. Finally, a pure off-line study at the time of onset is not enough compete to estimate online performance. Section 11.2 deals with the state-of-the-art methods. Section 11.3 provides information about the experiment paradigm, the acquisition material and the experiment description. In Section 11.4, the used pipelines are detailed. Finally, in Section 11.6, the results are divided in a fundamental analysis, an MRP analysis and a discussion about the classifier performance.

11.2 Background

As reviewed in [2], several researchers have succeeded in automatically detecting such events. Most of the studies focus on the upper limb (finger, wrist, arm). Only one study tackles the ankle dorsiflexion movement without cues [3] and another one shows the classification of the type of movement between right-hand, left-hand, tongue or right-foot move [4]. To detect the movement intention, researchers have basically two options: the BP itself or the event-related (de)synchronisation (ERD/ERS). A slow surface negative signal, the Bereitschafts potential (BP), can be obtained by averaging EEG occurring before repeated self-paced movements and time-locked to the movement onset [5, 6]. BP starts about 1.5 s prior to movement onset and is symmetrically recorded with a maximum over the supplementary motor area (SMA) and followed by an asymmetrical negative potential starting about 0.4 s and originating from the contralateral primary motor cortex [6, 7]. The ERS/ERD correspond to a power increase/decrease in the μ (8-12 Hz) and β (12-30 Hz) bands. As reviewed by [8, 9], for automatic detection, several standard approaches have been used for feature extraction and classification: spatial and temporal filtering, template building, wavelet/Fourier transform, Independent Component Analysis

(ICA), Linear Discriminant Analysis (LDA), Support Vector Machine (SVM), Bayesian classifier, thresholding/correlation and multinomial logistic regression.

Although very few gait intent analyses [10, 11, 12, 13] and detection studies are available [8, 9], predicting the leg movement could be helpful to adequately control an orthosis/prosthesis. Indeed, from a mechanical point of view, one interest of using brain signals to control a prosthesis would be to detect early willingness for the next move [14]. Thereby, the whole device could anticipate the movement and adjust the mechanical system as precisely as possible, which is not possible using only physical sensors that are causal to the move.

11.3 Experiment

11.3.1 Gait Intent Paradigm

Two major events occur before the movement onset: the BP or Movement-Related Potential (MRP) and the event-related desynchronization (ERD) [2]. First, the BP or MRP potential is a negative cortical potential that starts around 1.5 s to 1 s before onset. As shown in Figure 1.11, the BP potential can be divided into three different parts. First, in the pre-BP section, the brain signals are not affected by the movement intent yet. Then, in the BP section or *early BP*, the negative potential slowly appears at about 1.5 s before movement onset and is more prominent in the central-medial areas. Second, a negative steeper slope (NS) or *late BP* corresponding to the activity of the primary motor cortex (M1) starts around 400 ms prior to movement onset. These potentials are also detected in imaginary movement intention and observed movements [15].

In a recent study [16], the BP signal was analysed during gait intent. Five different tasks were performed: gait/stepping forward, gait and stepping backward and stepping laterally. As shown in Figure 1.13 from [16], the measured potentials are slightly different and observed at the top of the head, which matches the motor and sensorimotor leg representation of the homunculus.

Second, the ERD is observed by a short-lasting decrease of power in some specific frequency bands [2]. This decrease could start as early as 2 s before onset. In the EEG, there are several frequency bands of interest that correspond to physiological or pathological interpretations. In this Chapter, the μ (8-12 Hz) and β (12-30 Hz) bands are directly linked to movement planning and execution. These frequency limits may vary depending on the subject [17].

11.3.2 Acquisition Material

In this experiment, several types of signals were recorded: EEG/EOG, EMG and kinematics. First, the EEG signal was recorded using a 128-electrode cap (only Cz electrode was used because no additional conclusions or strong outperformance could be made from the full EEG recordings) thanks to the ANT amplifier system (Advanced Neuro Technology, ANT, Enschede, The Netherlands). The sampling rate was 512 Hz downsampled for processing at 128 Hz (not for time-frequency analysis). Left ear were chosen as references. Electrode impedance was measured and maintained under 20 k Ω for each channel using electrode gel. Additionally, the EOG was recorded to detect eye movements during the experiment. Six channels were recorded to measure vertical eye movements of both eyes and horizontal movements. This allows to assess how much this signal pollutes the gait intent detection.

Following the same spirit as for EOG, the EMG signal was recorded on the neck using again the ANT device. This would give an indication about the impact of these EMG signals of the neck (superior region of the left and right trapezia) on EEG and would help interpreting the results. Moreover, 4 additional EMG signals were recorded on the right leading leg muscles: Rectus Femoris, Semitendinosus, Tibialis Anterior, Gastrocnemius Lateralis. Automatic decisions based on these sensors would provide a baseline comparison to the EEG-based brain signals. All these leg EMG signals were recorded at a 1000 Hz sampling rate using the BTS EMG device.

Kinematics was also recorded during this experiment to allow synchronization and gait event detection. First, a footswitch was placed at the heel of the right foot in order to measure heel strike/off. Additionally, the elevation angles of the tibia, the shank and the foot of both legs were computed using the positions of 23 passive markers disposed on the subject and determined thanks to six infrared Bonita Vicon cameras sampling at 100 Hz. Generally, a strong agreement between the footswitch and the measured kinematics was found.

11.3.3 Experiment Description

Four healthy subjects without any known physical or neurological disorders participated in this experiment (4M, age-range: 26-36 years). For each trial, the subject was asked to look at a fixed point in front of his eyes. Then, he performed four tasks: 1) Walking forward (three strides), 2) Imagine the previous task, 3) Walking backward (three strides) and 4) Imagine the previous task again. This means that data for resting, moving forward and moving backward are available in each trial. All these tasks were separated by an average of 5 to 10 seconds break to avoid interferences of the current task by the previous one. This was done without counting and without external stimuli to avoid evoking undesired potentials. To help subjects estimating this duration, they were trained to wait for such duration. In the recorded data, there are always at least 5 second rest meaning that no trial had to be removed. After visual inspection trial rejection, out of the 100 recorded trials, 40 were used for training, 25 for testing and 30 for independent validation. In average, the experiment lasted one hour and a half to 2 hours and the equipment set-up and removal took around 2 hours per subject. Because no synchronized imaginary ERPs could be produced, we did not further analyse this part of the data. To get data in a baseline condition, subjects were asked to stand for two minutes without performing any movement or special thinking. A windowing without overlap was performed to generate baseline trials. All procedures were approved by the Université Libre de Bruxelles Internal Review Board and complied with the standards defined in the Declaration of Helsinki.

11.3.4 Statistical Note

As nicely introduced in [18], reported results should be taken with care. In a two class problem, the actual significant threshold at 5% is not at 50%. By modelling the pipeline performance by a binomial distribution with 30 trials per class as used here, the computed threshold is set at 62.5%. For a three class paradigm, the threshold is around 43%. Therefore, the following results should be observed keeping in mind these points of reference.

11.4 Methods

11.4.1 Preprocessing

Several preprocessing steps are necessary to get the best classification performance: re-referencing, visual inspection, filtering and eye movement artefact removal. The electrodes on the ears were chosen as reference [19]. Then, by visual inspection, a few strong artefacts were detected and removed in order to prevent any influence on the system performance. To allow fair comparison, the number of analysed trials in each condition was decreased to 95. Afterwards, high-pass filtering (0.05 Hz cutoff) and notch filtering (around 50 Hz) were applied to remove the continuous component from the biological drift and the 50 Hz electrical noise. Finally, to remove the eye movement pollution of the EEG signals, Independent Component Analysis (ICA) was used. This widely used technique allows to remove obvious saccades and blinks to prevent them from impacting the performance. No specific algorithm was used and the artefacts were visually detected.

11.4.2 Feature Extraction

To extract the most relevant information for classification, several features can be computed: raw data, low-pass filter, Daubechies Wavelet Transform (MRP), envelope, Short Term Fourier Transform, Daubechies Wavelet Transform (ERD/ERS). Additionally, the dimensionality of the features can be reduced by applying Principal Component Analysis.

First, the most simple feature extraction technique is to use the data themselves. This means that no further processing is applied to the MRP (1 s window). Second, because the MRP signal frequency content is mainly observed at low-frequencies, a low-pass filter with a 3 Hz cut-off frequency was applied before using the obtained waveform as features. Third, Daubechies Wavelet Transform (DWT) up to the 4th order can be computed. By getting these coefficients, the 0 to 4 Hz interval can be deeper analysed. Fourth, the envelope is particularly interesting when the ERD/ERS has to be detected. By computing the square of the bandpass filtered EEG signal (α and β), this signal will actually sharply increase when a burst appears at an ERS (and vice versa) leading to an easy threshold-based detection. Fifth, by using the Short-Term Fourier Transform (STFT), ERD/ERS can also be detected [20]. STFT is computed using a windowing of 0.25 s with a 50% overlap. Then, the detection is based on the squared mean values matching the 8-12 Hz and 12-30 Hz coefficients. Finally, a Discrete Wavelet Transform (DWT) decomposition can be used in the μ and β bands as an enhanced Fourier analysis [20].

As proposed by [9], dimension reduction can be considered using Principal Component Analysis (PCA). Because the number of features is quite huge, reduction methods could be helpful for the classifier step. By removing redundant information, the classifier parameters can be reduced and better estimated. In this study, the PCA components representing 90 % of the variability were retained for each class (baseline, move forward/backward). This led to 15 component variables if 5 components per class are retained. In terms of interpretation, this approach tends to find the combination of the most relevant times and electrodes for representation of the signal. In the end, a better representation should lead to a better classification.

11.4.3 Classifiers

To make a decision between classes, several classifiers can be used: Linear Discriminant Analysis (LDA), Support Vector Machine (SVM), Hidden Markov Model (HMM), Perceptron and Multi-Layer Perceptron (MLP). LDA and SVM (linear kernel) classifiers find a linear frontier that splits features to be splitted according to a linear frontier. The perceptron and the MLP (with a hidden layer) are neuron-based models that are able to generate non-linear frontiers. Finally, the HMM technique was investigated given its particular characteristics: state-based and temporal considerations. Given the specificity of the BP and ERD/ERS features, the HMM could perform better than other classifiers.

11.5 Results

11.5.1 Fundamental Analysis

In this fundamental analysis, three different points of view are provided. First, topographic plots show a global view before the movement onset. Second, the MRP signal is more closely analysed. Finally, ERD/ERS are studied based on ERSP analysis.

Topographic Analysis

In Figures 11.1, a brain topographic view of the ERP analysis is depicted. To obtain these results, the voltage at each electrode is averaged over 95 trials. As predicted, we observe a major negative MRP in central electrodes regardless of the direction of movement. The ERP potentials of each electrode appear similar to those in [16]. The most important contribution corresponds to Cz but all the neighbour electrodes show a significant BP response. In the context of a low complexity and ambulatory algorithm, the Cz electrode seems sufficient.

11.5.2 MRP Analysis

As shown in Figure 11.2, the ERP analysis is made for each condition for one representative subject. The analyses range from -4 s to +2 s around the movement onset (time 0) and focuses on the Cz electrode. For each condition, the 95 % interval of the MRP signals is illustrated.

The ERP analysis shows a clear difference between the anticipation of movement when compared to the baseline, whereas the difference between forward and backward conditions is hard to see. Indeed, the BP is starting around 1 s to 1.5 s before onset. Considering the variance of the BP potential and the relative decrease in potential magnitude, it should be relatively easy to detect movement anticipation against baseline. However, as expected, the slight difference implied by the move direction is too small relative to the BP distribution.

Finally, the acceleration in the gait initiation could influence the potential shift magnitude, which could be related to findings in [21]. In one subject, the slope of the *late BP* was steeper. One potential explanation could be that this subject had a different starting speed of the foot. To confirm this speculation, dedicated future work would be required.

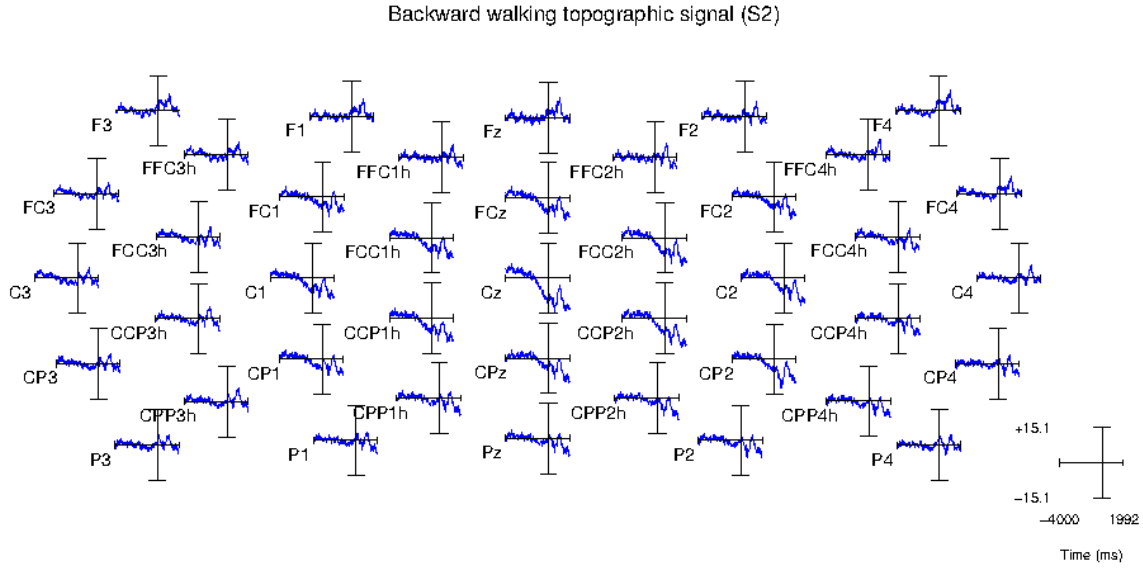


Figure 11.1: For one representative subject, the most important contribution of the slow cortical potential is located around Cz, which has the most powerful response.

ERD/ERS Analysis

Based on Event-Related Spectral Perturbation (ERSP) analysis, which is a time-frequency analysis of averaged trials around a given event (here, move of the foot) [22], the ERD (blue)/ERS (red) observations show mixed results. To remove some potential statistical noise in this time-frequency analysis, a standard 5 % bootstrap was applied. After the movement onset, a large frequency ERS (from 50 Hz to 128 Hz) is observed on every subject. This could be a mix of the expected ERS after a movement and some movement artefacts as discussed in [23]. In comparison, the ERSP before movement onset is strongly subject dependent. Regarding before the onset, results are strongly subject dependent. Sometimes, ERSP plots exhibit the expected μ and β ERDs as illustrated for Subject 2 in Figure 11.3; but for Subject 3, no such ERDs were observed as depicted in Figure 11.3. When present, the ERD starts around -500 ms before onset. Overall, the strength of the observed ERDs was lower than expected and it should lead to a low recognition rate.

11.5.3 Classifier Performances

In this subsection, the classifier performance is studied in depth. First, the dimension reduction technique and the parameter optimisation is tackled. Second, the two and three class performance is assessed. Finally, artefact pollution is considered. Everything has been implemented in Matlab.

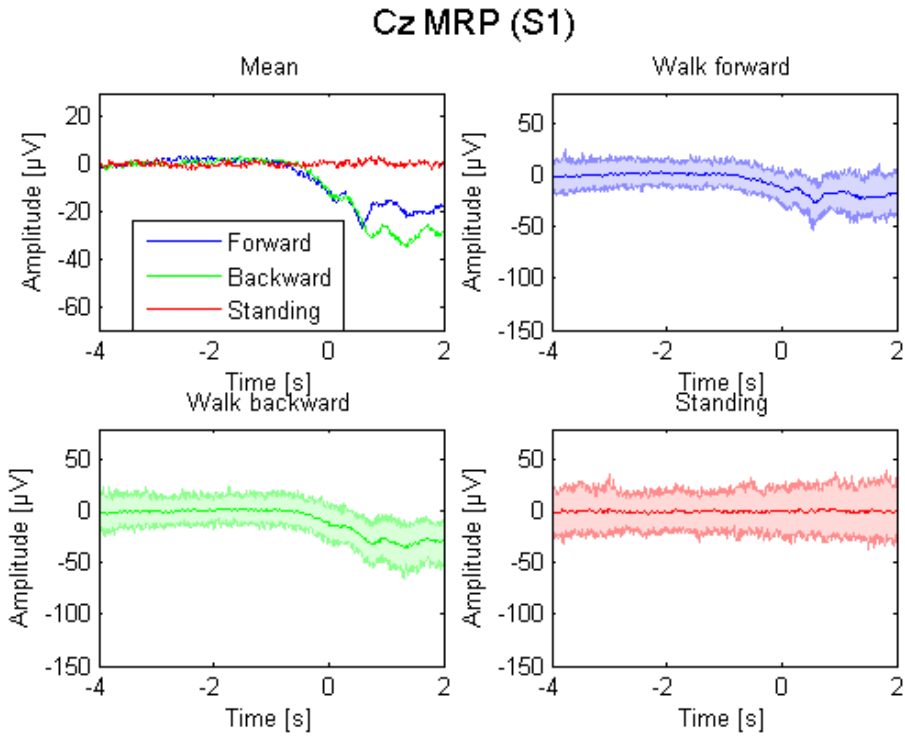


Figure 11.2: The obtained MRPs are obviously different between gait intent and baseline. However, the relative difference between forward and backward walking is too small to get high performance.

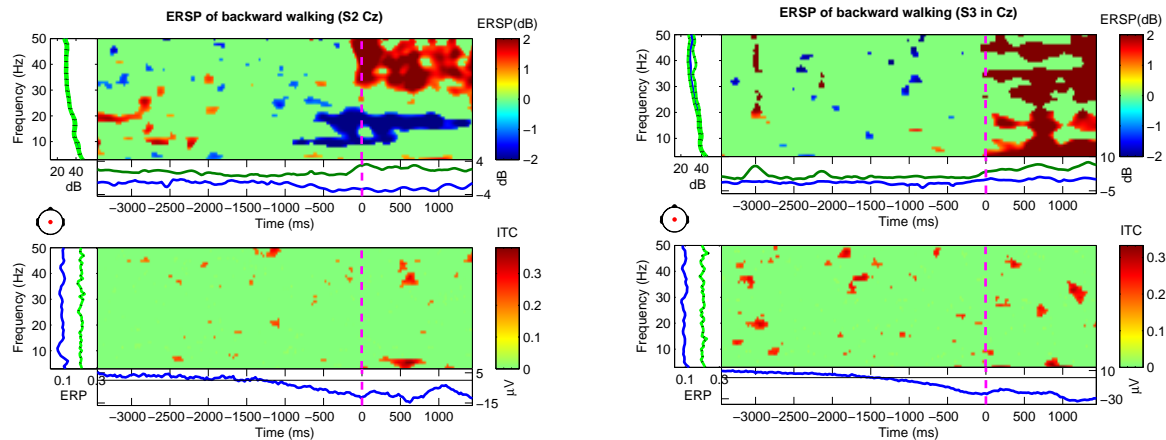


Figure 11.3: On the left: Subject 2 shows two clear ERDs starting 500 ms before onset in the μ and β bands. On the right: Subject 3 does not have any observable ERD.

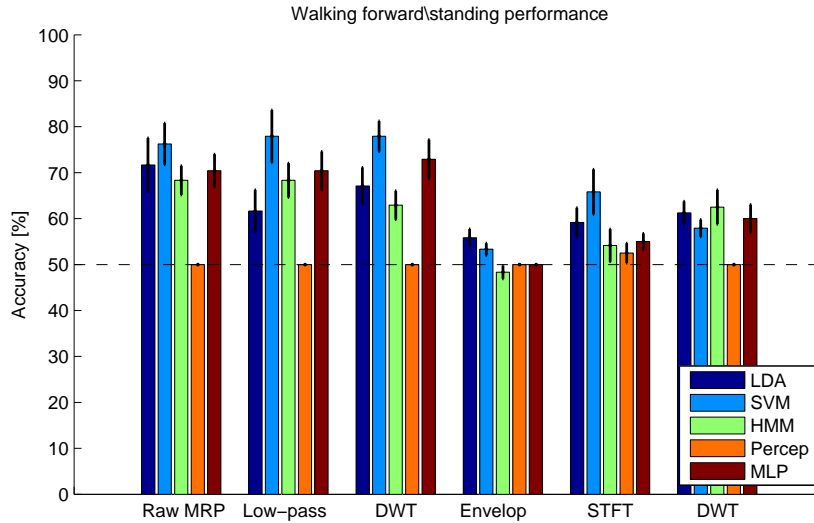


Figure 11.4: The results are generally increased by adding several electrodes (FC1, FC2, FCz, C1, C2, CP1, CP2, CPz). However, there is not a huge gain in performance. This could be due to the central origin of the data. Error bars are standard errors.

Framework and Dimension Reduction Technique

To properly assess the performance, the 95 trials were split into three datasets: training (40), testing (25) and validation (30). This allows to optimize the parameters such as window size, filtering, number of hidden neurons, etc, while avoiding spurring the present results. Therefore, all the displayed results in this section refer to the validation dataset, which was only used once for reporting the performance.

From these optimisation tests, several main conclusions can be drawn. First, the Cz electrode appears sufficient in terms of performance. We did not see a huge gain in the classification accuracy by adding other responsive electrodes in the motor and sensorimotor areas for BP detection. For ERD detection, there was only a small increase in performance that was slightly more favourable for the STFT extraction feature. Contrary to left and right hand movements, leg movement response has its origin in the central area. This may explain why increasing the number of electrodes has less effect. The corresponding results can be seen in Figure 11.4 and in Figure 11.5. Anyway, the use of specific spatial filter that magnifies the measured signal by finding an optimal linear combination between electrodes could be an interesting solution as the proposed pipeline may fail in this task. The most efficient window size and position was found from -1 s to the time of the onset (0 s). Second, except for the LDA classifier, the PCA-based dimension reduction method does not seem to bring much enhancements. While considering the effect of this technique on moving forward vs baseline, little change is observed. The same conclusion arises for the other conditions.

2- and 3- Class Performance

As shown in Figure 11.5 for a two-class classification, the recognition accuracy is smaller when comparing directions of movement. Indeed, this result was expected from the fundamental analysis. Because testing and validation results were quite closed, no overfitting was present. Overall, all the subjects have good MRP detection except Subject 2. This subject had a higher 95 % interval of the MRP potentials. Note that overall, the performance are coherent with [9]. Regarding the classifiers themselves, the perceptron does not provide satisfying results contrary to its multi-layer extension (the training failed). Globally, most of the classifiers obtained satisfying and similar results. But, it appears that the SVM with MRP extraction features is the most stable solution. The underperformance of the perceptron is a bit surprising. Indeed, we train it with Levenberg-Marquardt, gradient descent and resilient backpropagation and each time obtained close to random level results. Finally, the feature extraction methods show a clear difference between ERD/ERS and MRP-based detection methods. As foreseen in the fundamental analysis, the predictive power of ERD/ERS methods is lower than the MRP ones. While classifying forward gait movement against the baseline, the best MRP method (HMM and low-pass filter) provides 79 % accuracy in average whereas its ERS/ERD equivalent approach (HMM and DWT) only displays a 61 % recognition rate. The combination of both these techniques did not enhance the results. Note that the ERD-based approaches provide two subjects around 70-75 % accuracy and two others at chance level whereas the MRP allows to get a [60-90] % accuracy. This was suggested by [17]. Overall, their performance are linked to the strength of the observed ERD in the fundamental analysis: when a clear ERD appeared, a good performance was obtained.

When considering the 3-class problem displayed in Figure 11.6, similar conclusions arise while getting a logical lower performance. The ERD/ERS methods are still locked around the chance level (33 %). It is obvious that the low level of the absolute performance will not be sufficient for a daily life application.

Artefact Considerations

To determine whether artefacts are affecting the performance of our system, we compared the different detection performances of a sliding window using the EMG, EEG and EOG signals as input. In this approach, a 1-s sliding window is used by a 0.125 s increment. For each window, a training was performed and the validation result is reported at the last time of this window in Figure 11.7. This means that the performance indicated at time -1 s corresponds to a [-2 s,-1 s] window.

The major conclusion is that artefact is unlikely to contribute to the classification rate. In Figure 11.7, above chance results start increasing much before the movement onset. On the other hand, although the artefact-based (EOG or EMG) classification can sometimes be found above chance level at the onset, the difference is too small to have an impact on the Cz electrodes. Indeed, the classification accuracy is much higher with EEG than with the EOG signals. Moreover, on the ERSP analysis (not depicted in this study), no such pollution was observed. Anyway, the EOG artefacts were removed in the preprocessing by ICA.

In terms of decision time, the EEG is advantageous compared to EMG or EOG. Indeed, the EEG performance is above chance much before the movement onset. As depicted in Figure 11.8, the leg EMG results only increase 250 ms before movement. For the EMG-based detection,

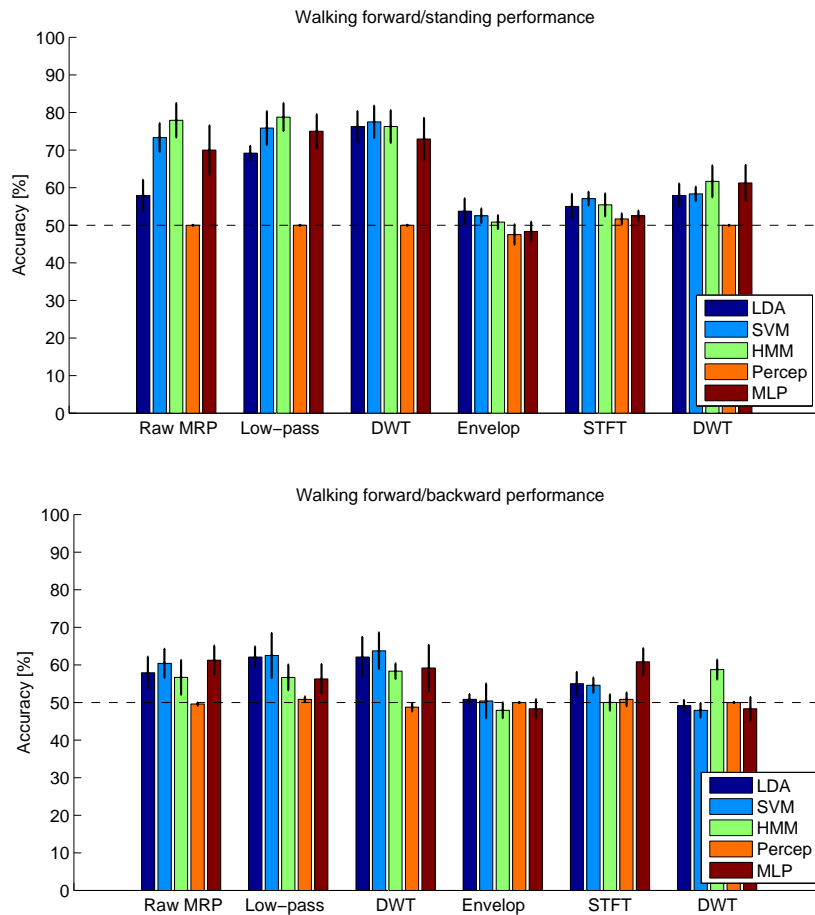


Figure 11.5: On the top: Forward vs baseline detection shows fair results around 75 %. MRP based techniques appears more effective than ERD/ERS ones. On the bottom: The similar conclusion can be drawn but at a lower level. This is due to the relative small difference between both conditions and high variance. Error bars are standard errors.

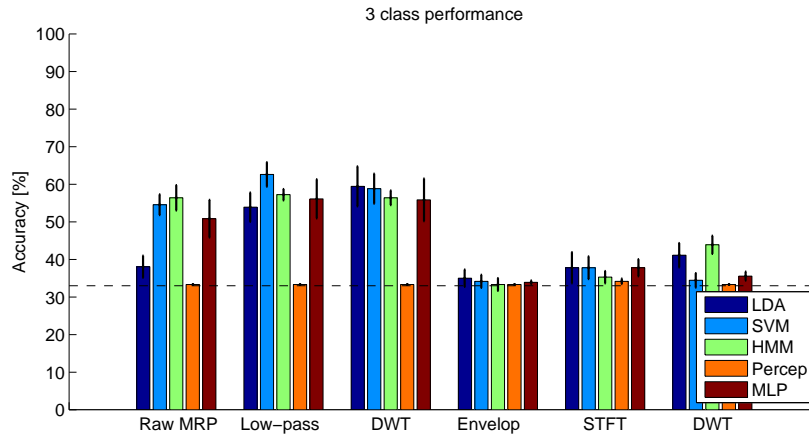


Figure 11.6: The obtained MRPs are obviously different between gait intent and baseline. However, the relative difference between forward and backward walking is too small to get high performance. Error bars are standard errors.

only ERD/ERS methods have meaningful results given the nature of the signal. Indeed, this kind of signal does not have any drift associated to movements but there are alike bursts. This corresponds much more to ERD/ERS like signals.

Pseudo-Online Classification

As shown in Figure 11.9, the pseudo-online classification suggests that good performance is possible in real-time application. The analysis is similar to the sliding window except that the training is performed only once with the window starting 1 s before onset. Basically, the detection of the MRP starts around 0.5 s before onset. Logically, the MRP is detected earlier than the ERD.

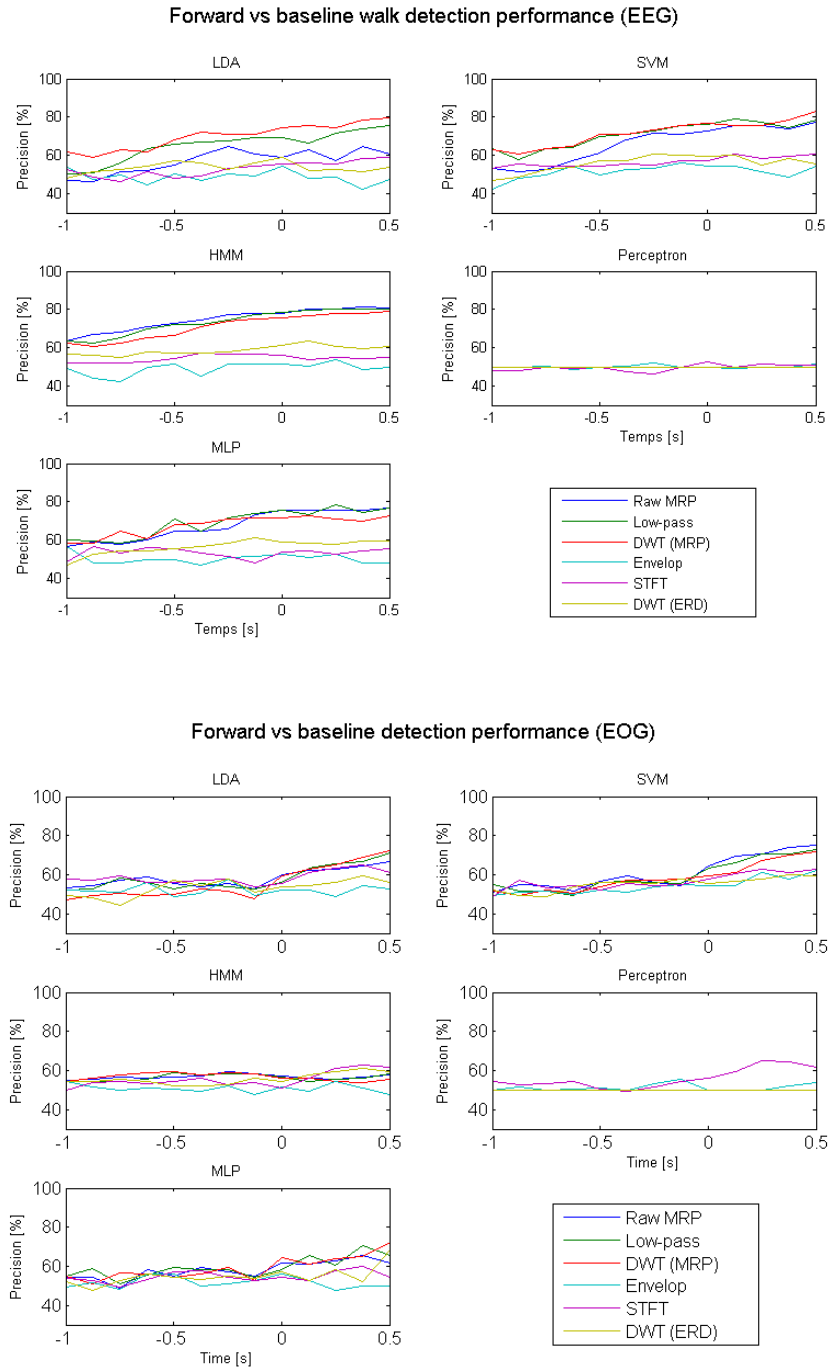


Figure 11.7: On the left: Forward vs baseline detection based on the EEG signals shows an increasing recognition rate as the analysis window comes closer to the movement onset. On the right, the EOG signal does not seem to top the chance level. Similar results were obtained for EMG signals.

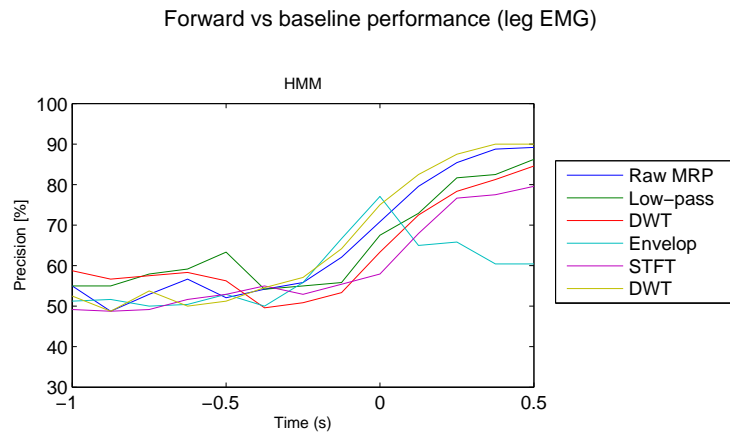


Figure 11.8: The leg EMG signals start to outperform chance level at around 250 ms before onset. Overall, the EEG signals allow to get a better decision at much before the onset.

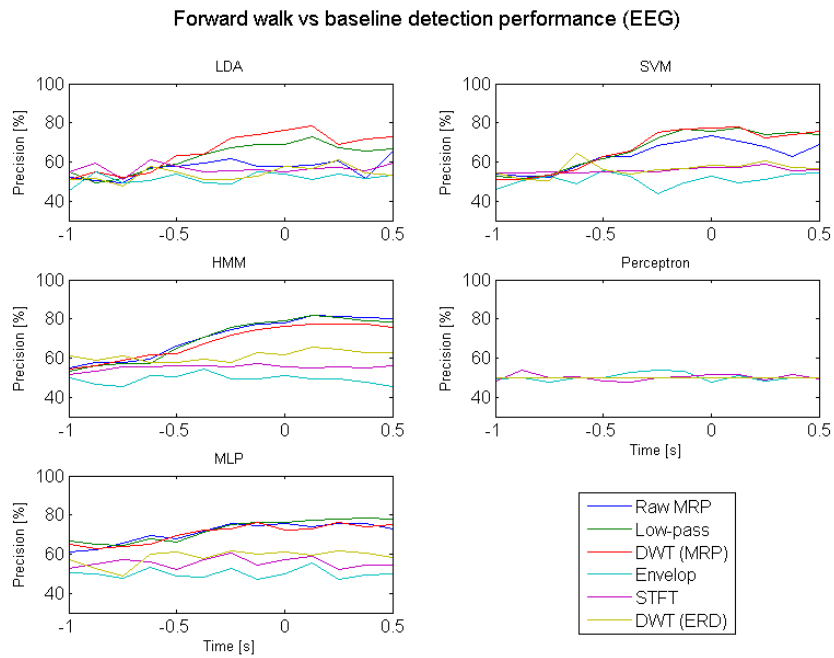


Figure 11.9: The pseudo-online performance indicates that real-time application should be viable.

11.6 Conclusion

To activate a prosthesis or a rehabilitation device, gait intent detection using EEG signals could be helpful. Therefore, a quantitative comparison of several detection techniques is first proposed and followed by an experimental study. Four healthy subjects realised three different tasks: starting moving forward/backward and standing. Four main contributions are performed: a fundamental study of EEG signals, a quantitative comparison of several automatic detection pipelines following a common assessment framework, an evaluation of the impact of artefacts on the performance and the potential performance in close to online conditions.

As no complete study of gait intent paradigm is available, in a first step, a fundamental analysis was performed. From a standing baseline, the slow movement related potential (MRP) was clearly visible. The highest SNR was seen on Cz, though it was also observable in surrounding electrodes. Classification was difficult between moving forward and moving backward tasks, possibly because the measured MRPs were too similar to be discriminated. The ERD/ERS were also observed but not on all subjects and with a highly variable SNR.

For classification purposes (using the Cz electrode), the results are consistent with the literature. Six feature extraction methods were used: three for MRPs (raw MRPs, low-pass filter and wavelet decomposition) and three for ERDs (envelope detection, short-term Fourier transform and wavelet decomposition). Additionally, five different classifiers were tested (LDA, SVM, HMM, perceptron, MLP). Classification of the movement direction only reaches a 60 % rate (two classes). At the opposite, movement initiation compared to standing was more easily detected with classification accuracies up to 80 %. Among the best features extraction, it is clear that MRP features are more classifiable and stabler than ERD features. This is mainly due to the weakness of the observed ERD in our data. Furthermore, the combination of those two types of phenomena does not provide any enhancements. Regarding the classifiers, they basically provide similar results except the perceptron. This basically comes from a lack of convergence in the training due to the Matlab toolbox failure. On the other hand, the SVM classifier coupled to the MRP features seems to be more stable. Adding electrodes did not strongly increase performance. Pseudo-online results show the performance should be maintained in real-time.

Finally, neck muscles and eye movements did not affect the performance. However, although the leg EMG signals allow to detect gait intent before onset, the EEG-based approach provides quicker and better performance before onset. In addition, the detection of EMG may not be possible in pathological states in which muscle activation signals are disrupted or too weak.

In future work, several main points can be looked at. First, other classification pipelines could be proposed. A spatial filter based on xDawn or Common Spatial Pattern (CSP) algorithms may be better at capturing BP and ERD signals, respectively [24, 25]. A dynamic recurrent neural network could be tested as suggested by [26, 27] Second, it would be interesting to examine whether the starting acceleration impacts on the MRP signal [21]. Third, although it is unlikely to completely modify the conclusions between ERD and MRP signals by adding subjects, it could be interesting to propose a demographic study to determine which proportions of people are able to generate usable signals for both approaches. The final step would be to integrate these results toward a rehabilitation device or prosthesis/orthosis.

Bibliography

- [1] R. Ortner, B.Z. Allison, G. Korisek, H. Gaggl, and G. Pfurtscheller. An ssvep bci to control a hand orthosis for persons with tetraplegia. *Neural Systems and Rehabilitation Engineering, IEEE Transactions on*, 19(1):1–5, 2011.
- [2] Pouya Ahmadian, Stefano Cagnoni, and Luca Ascari. How capable is non-invasive eeg data of predicting the next movement? a mini review. *Frontiers in Human Neuroscience*, 7(124), 2013.
- [3] Imran Khan Niazi, Ning Jiang, Olivier Tiberghien, Jørgen Feldbæk Nielsen, Kim Dremstrup, and Dario Farina. Detection of movement intention from single-trial movement-related cortical potentials. *Journal of Neural Engineering*, 8(6):066009, 2011.
- [4] Valerie Morash, Ou Bai, Stephen Furlani, Peter Lin, and Mark Hallett. Classifying eeg signals preceding right hand, left hand, tongue, and right foot movements and motor imageries. *Clin Neurophysiol*, 119(11):2570–8, 2008.
- [5] HansH. Kornhuber and Lüder Deecke. Hirnpotentialänderungen bei willkürbewegungen und passiven bewegungen des menschen: Bereitschaftspotential und reafferente potentiale. *Pflüger's Archiv für die gesamte Physiologie des Menschen und der Tiere*, 284(1):1–17, 1965.
- [6] H Shibasaki, G Barrett, and E. Halliday. Components of the movement-related cortical potential and their scalp topography. *Electroencephalography and Clinical Neurophysiology*, 49(3):213–226, 1980.
- [7] Shibasaki Hiroshi and Hallett Mark. What is the bereitschaftspotential? *Clinical Neurophysiology*, 117(11):2341 – 2356, 2006.
- [8] P. Ahmadian, S. Sanei, L. Ascari, L. Gonzalez-Villanueva, and M.A. Umita. Constrained blind source extraction of readiness potentials from eeg. *Neural Systems and Rehabilitation Engineering, IEEE Transactions on*, 21(4):567–575, 2013.
- [9] Priya Velu and Virginia R de Sa. Single-trial classification of gait intent from human eeg. *Frontiers in Neuroscience*, 7(84), 2013.
- [10] Hiroshi Shibasaki, Hidenao Fukuyama, and Takashi Hanakawa. Neural control mechanisms for normal versus parkinsonian gait. 143:199 – 205, 2004.

- [11] M. Vidailhet, PR. Atchison, F. Stocchi, PD. Thompson, Rothwell JC., and CD. Marsden. The bereitschaftspotential preceding stepping in patients with isolated gait ignition failure. *Mov. Disord.*, 10(1):18–21, 1995.
- [12] M. Vidailhet, F. Stocchi, J. C. Rothwell, P. D. Thompson, B. L. Day, D. J. Brooks, and C. D. Marsden. The bereitschaftspotential preceding simple foot movement and initiation of gait in parkinson’s disease. *Neurology*, 43(9):1784, 1993.
- [13] Shogo Yazawa, Hiroshi Shibasaki, Akio Ikeda, Kiyohito Terada, Takashi Nagamine, and Manabu Honda. Cortical mechanism underlying externally cued gait initiation studied by contingent negative variation. *Electroencephalography and Clinical Neurophysiology/Electromyography and Motor Control*, 105(5):390 – 399, 1997.
- [14] M. Duvinage, R. Jimenez-Fabian, T. Castermans, O. Verlinden, and T. Dutoit. An active foot lifter orthosis based on a pcpg algorithm. In *Rehabilitation Robotics (ICORR), 2011 IEEE International Conference on*, pages 1–7, 2011.
- [15] Omar Feix do Nascimento and D. Farina. Movement-related cortical potentials allow discrimination of rate of torque development in imaginary isometric plantar flexion. *Biomedical Engineering, IEEE Transactions on*, 55(11):2675–2678, 2008.
- [16] Omar Feix do Nascimento, Kim Dremstrup Nielsen, and Michael Voigt. Influence of directional orientations during gait initiation and stepping on movement-related cortical potentials. *Behavioural Brain Research*, 161(1):141 – 154, 2005.
- [17] Teodoro Solis-Escalante, Gernot Müller-Putz, and Gert Pfurtscheller. Overt foot movement detection in one single laplacian EEG derivation. *Journal of Neuroscience Methods*, 175(1):148 – 153, 2008.
- [18] Gernot R. Müller-putz, Reinhold Scherer, Clemens Brunner, Robert Leeb, and Gert Pfurtscheller. Better than random: a closer look on bci results. *International Journal of Bioelectromagnetism*.
- [19] Bruce Fisch. *Fisch and Spehlmann’s EEG Primer: Basic Principles of Digital and Analog EEG*, 3e. Elsevier, 1999.
- [20] Chih-Wei Chen, Chou-Ching K. Lin, and Ming-Shaung Ju. Detecting movement-related {EEG} change by wavelet decomposition-based neural networks trained with single thumb movement. *Clinical Neurophysiology*, 118(4):802 – 814, 2007.
- [21] N. Robinson, A.P. Vinod, Kai Keng Ang, Keng Peng Tee, and C.T. Guan. Eeg-based classification of fast and slow hand movements using wavelet-csp algorithm. *Biomedical Engineering, IEEE Transactions on*, 60(8):2123–2132, 2013.
- [22] Arnaud Delorme and Scott Makeig. Eeglab: an open source toolbox for analysis of single-trial eeg dynamics including independent component analysis. *Journal of Neuroscience Methods*, 134:9–21, 2004.

- [23] Thierry Castermans, Matthieu Duvinage, Guy Cheron, and Thierry Dutoit. About the cortical origin of the low-delta and high-gamma rhythms observed in eeg signals during treadmill walking [submitted]. *Neuroscience Letters*, 2013.
- [24] B. Rivet, A. Souloumiac, V. Attina, and G. Gibert. xDAWN Algorithm to Enhance Evoked Potentials: Application to Brain Computer Interface. *Biomedical Engineering, IEEE Transactions on*, 56(8):2035 –2043, 2009.
- [25] Yijun Wang, Shangkai Gao, and Xiaorong Gao. Common spatial pattern method for channel selelction in motor imagery based brain-computer interface. In *Engineering in Medicine and Biology Society, 2005. IEEE-EMBS 2005. 27th Annual International Conference of the*, pages 5392–5395, 2005.
- [26] G. Cheron, M. Duvinage, C. De Saedeleer, T. Castermans, A. Bengoetxea, M. Petieau, K. Seetharaman, T. Hoellinger, B. Dan, T. Dutoit, F. Sylos Labini, F. Lacquaniti, and Y. Ivanenko. From Spinal Central Pattern Generators to Cortical Network: Integrated BCI for Walking Rehabilitation. *Neural Plasticity*, 2012:1–13, 2012.
- [27] Thomas Hoellinger, Mathieu Petieau, Matthieu Duvinage, Thierry Castermans, Karthik Seetharaman, Ana-Maria Cebolla, Ana Bengoetxea, Yuri P Ivanenko, Bernard Dan, and Guy Cheron. Biological oscillations for learning walking coordination: dynamic recurrent neural network functionally models physiological central pattern generator. *Frontiers in Computational Neuroscience*, 7(70), 2013.

Chapter 12

Towards A Hardware Framework for EEG Motion Artefact Estimation in Movement Conditions

Contents

12.1	Introduction	275
12.2	Material and Methods	275
12.2.1	Acquisition Device and Analysis Approach	275
12.2.2	Brain Electrical Model for Motion Artefact Estimation	276
12.3	Results	278
12.4	Discussion	281
12.5	Conclusion	284

Abstract

More and more researchers are studying movement-related brain activities thanks to the Electro-Encephalogram (EEG) signal. However, brain activity may be coupled to potential artefacts coming from muscles, eyes or movement itself.

In this Chapter, we propose a first hardware prototype that aims at decoupling movement artefacts and spontaneous brain signals. Tests were made with two subjects walking at four different speeds on a treadmill.

Results show that there is an overlap in observed time-frequency analysis between the artefact and the corresponding EEG recordings from the same subjects. Moreover, the same conclusion arises from gait-related studies from other researchers. This suggests that specific care should be taken with movement-related artefacts. Moreover, by injecting simulated EEG signals into the hardware system, this framework should also allow the assessment of the efficiency of artefact removal methods. This could lead to a more objective evaluation of such methods. For instance, the lack of objectivity is a known disadvantage when using Independent Component Analysis (ICA). Future work will be devoted to the development of a real-time artefact-removal EEG cap.

This chapter is based upon the following publication:

- M. DUVINAGE, T. CASTERMANS, T. DUTOIT, G. CHERON, 2014, *Towards A Hardware Framework for EEG Motion Artefact Estimation in Movement Conditions*, IEEE Transaction in Biomedical Engineering [in preparation]

12.1 Introduction

Artefact processing is always a challenge while dealing with electroencephalographic signal (EEG). Different types of artefacts can be observed and corrected: muscular, ocular and mechanical artefacts. Muscular artefacts arise when electrical activities from the muscles pollute the EEG signal through the skin. The contaminated frequency band is usually starting from 10/15 Hz up to high frequencies. Ocular artefacts come from the cornea/retina dipole whose movement creates potential variations in the frontal part of the EEG recordings. Most of the spectrum power is detected below 20 Hz. Finally, motion artefacts are mainly movement dependent. For instance, under constant-speed walking conditions, quasi-periodic electrode movements create quasi-synchronized movement artefacts. In this specific case, the affected spectrum fundamentally matches the stepping frequencies and its harmonics. Moreover, as the electrode system is not linear, more complex frequencies are also present making them difficult to remove.

Typically, when studying unknown spontaneous EEG signal synchronized with movement and related artefacts, the standard artefact removal methods cannot be used, at least, directly. Indeed, these methods may also remove the studied spontaneous EEG signals making it impossible to analyse them. For instance, in an offline method to remove gait-related artefact proposed by [1], the artefact was obtained by computing a template aligned with the gait cycle by a time warping technique. Although interesting, this approach may obviously subtract the synchronized gait control/feedback signal [2]. Moreover, this method does not consider a direct measure of the artefact. As proposed by [3], another method to remove artefacts based on Canonical Correlation Analysis (CCA) shows interesting results. However, as stated by the authors, one can not be sure about the full elimination of the artefacts from the studied signals.

In this paper, in order to come to a clearer distinction between artefacts and brain signals, we propose a first prototype of a hardware solution to this coupling problem. It aims at obtaining an estimation of the artefact signal (excluding any brain signals) and at benchmarking artefact removal methods. In Section 12.2.1, the material and methods are explained. In Section 13.3, the preliminary results under ambulatory conditions are briefly exposed. In Section 12.4, a discussion is proposed about the device results and its limitations. In Section 12.5, conclusions and future work are provided.

12.2 Material and Methods

12.2.1 Acquisition Device and Analysis Approach

The signal was acquired at 256 Hz thanks to an ANT device (Advanced Neuro Technology, ANT, Enschede, The Netherlands). Based on the international 10-20 locations, 5 Ag/AgCl electrodes (Fz, Cz, T7, T8, Oz) were recorded. Additionally, a footswitch, which is connected to ANT as an auxiliary channel, was placed on the right heel. During this experiment, two healthy subjects walked on a treadmill at different walking speeds; 1.5, 3, 4.5 and 6 km/h (around 100 gait cycles). This approach aimed at estimating gait-related movement artefacts. Additionally, EEG results with a non-modified cap were recorded during a complementary experiment under the same conditions.

The analysis was based on both Event-Related Spectrum Perturbation (ERSP) and Event-Related Potential (ERP). In both approaches, the epoching was made around the right heel strike event at time 0 ($[-1\text{ s}, +1.5\text{ s}]$). Only the significant results from a bootstrap analysis are displayed (at a 5% level). The EEGLAB software was used to analyse data in this study [4].

12.2.2 Brain Electrical Model for Motion Artefact Estimation

Motion artefacts are problematic because they often have large amplitude, no defined shape and are not confined to a small passband. Therefore, they cannot be removed by normal filtering, as is often the case for other types of artefacts (e.g. for the 50/60 Hz). Motion artefacts can be extremely frequent, especially in the case of ambulatory recording, intensive care units (ICU), recording of restless patients or children, etc., and have therefore long been a problem in biopotential measurements [5].

Our objective was to focus on motion artefact, and in this regard we needed to isolate it from the EEG signal. An electrode/gel/skin interface model was realized in order to simulate this interface after a typical EEG exam preparation: an Ag/AgCl electrode is placed on skin coated with a conductive gel. The electrode/gel/skin interface was then isolated from the scalp of the subject to ensure that the recording would only include artefacts and no EEG signal.

The electrode/gel/skin interface plays a role in motion artefacts propagation through three effects: 1) the variation of the parasitic current flowing into the skin/gel/electrode interface, 2) the skin/gel/electrode potential variation and 3) the skin/gel/electrode impedance variation. The following paragraphs provide a short review of the literature that determines the key features to model and their typical values.

Electrode leads are usually unshielded and therefore susceptible to the effects of ambient magnetic and electric fields [6, 7]. A geometric change of the leads alters magnetic and capacitive coupling, therefore producing a variation of parasitic current flowing into the leads [8]. Furthermore, movement of other persons around the patient also generates artefacts of capacitive origin [9]. Finally, electrostatic current generated by the friction and deformation of the cable insulation, which acts as a piezoelectric movement transducer, has also been observed [7, 10]. All those parasitic currents flowing into the leads produce a parasitic voltage drop due to the skin/gel/electrode impedance [6]. In this study, a value of $20\text{ k}\Omega$ was chosen for the skin/gel-/electrode impedance, corresponding to a typical value [6]. In a typical situation, a mean current of 10 nA peak-to-peak is measured in the wires with a 50% variation [6], leading to a $100\text{ }\mu\text{V}$ peak-to-peak interference.

Potential variation resulting from a sudden change in the contact potential of the skin/gel-/electrode interface can also produce interference [7, 11, 12]. However, potential variation can be minimized in two ways. First, using a nonpolarizable electrode, such as an Ag/AgCl electrode, reduces the motion artefact in the skin/gel/electrode interface by a factor of ten [7, 12]. Second, abrasion of the skin before applying the electrode, even if it is very light, eliminates skin/gel/electrode artefacts due to potential variation [5, 7, 12, 13]. Impedance variation has also been observed during motion artefacts [13, 14, 15, 16]. The work of de Talhouet [14] allows for the estimation of a 5% change in impedance when stretching the skin with a 1 kg weight for skin/gel/electrode impedance lower than $80\text{ k}\Omega$. This 5% value seems largely overestimated for a practical EEG exam since typical EEG leads only weigh a few grams. Therefore, a typical



(a) The conductor component was tinned to mitigate oxidation-reduction. This component allows mimicking the scalp when connected to a 20 kohm resistance.



(b) A conductor component was plugged in each cupule of interest fixed by Scotch tape and separated from the scalp by an insulating plate.



(c) All the reference cables were linked to a 20 kohm resistance in order to mimic the scalp electrical behaviour. Scotch tape was used to avoid at most the cable movement artefacts. Each cable was connected thanks to a staple.



(d) A profile picture of the whole system is depicted. Artefact introduction due to this part of the setup should be strongly mitigated.

Figure 12.1: The major components of the artefact measurement system are illustrated. By mimicking the scalp while being insulated from the brain, the device is able to record artefact.

situation with a mean current of 10 nA peak-to-peak in the wires leads to an interference far lower than 10 μ V peak-to-peak.

Therefore, when using Ag/AgCl electrodes and assuring careful skin preparation, only the first effect is predominant. In this study, the electrode/gel/skin impedance was modelled by a 20 k Ω resistor. It was followed by an Ag/AgCl layer coated with conductive gel that allows the electrode to be placed on it. Typical Ag/AgCl cupule electrodes were placed. Five derivations were placed on the head (Fz, Cz, T7, T8 and Oz applied according to the standard 10/20 system of electrode placement), as well as a reference electrode (FCZ) and a mastoid. Additionally, a footswitch, which is connected to the ANT amplifier as an auxiliary channel, was placed on the right heel.

Figure 12.1 shows an illustration of the practical implementation of the electrode/gel/skin interface model. In Figure 12.1(a), a tinned conductor component was placed in each of the corresponding cupules. Each cupule was isolated from the scalp using and insulating plate fixed by scotch tape as shown in Figure 12.1(b) and connected to a 20 k Ω resistance used to model the interface. All cupules were connected to a common reference using cables placed with scotch tape to mitigate their movement, which could add unwanted artefacts 12.1(c). Conducting gel was used to establish an electrical link between the electrodes and the tined conductor component (care was taken to avoid any electric link to the scalp). No EEG signal was observed when generating standard muscular, ocular artefacts and alpha rest experiment.

12.3 Results

As depicted in Figure 12.2 at 4.5 km/h for subject 1 (similar conclusions hold at other speeds), large Event-Related Desynchronizations (ERD)/Synchronizations (ERS) are observed on the 1-s gait cycle. On this subject, a heel-strike phase-locked artefact (at time 0s) is observed, e.g. at Cz and Oz electrodes. This observation was also made for every electrode of subject 2 as partially illustrated on Figure 12.3. Other observations are related to main gait events. The frequency range of artefacts was different between subjects and speeds (increase with the speed) and was detected up to 40 Hz at 3 km/h and above 100 Hz at 6 km/h for some electrodes (typically Cz). For both subjects, there is somehow an overlap between the real EEG and the measured artefacts. This should be an indication of artefact pollution in EEG data and it shows that, based on ERSP analysis, the correct removal of artefacts using standard Independent Component Analysis (ICA) appears prone to failures. However, we observed a strong difference with these conclusions at 1.5 km/h shown in Figure 12.4. There was much less overlap between the recorded artefact and the EEG signals. This could be due to a smaller artefact impact at low speeds (less shocks).

Moreover, the Event-Related Potential (ERP) analysis shows different but similar behaviours between electrodes whereas the Inter-Trial Coherence (ITC) are strong around main gait events. The ERP signal depending on the gait cycle could be interpreted (at first order) as the distance fluctuation of the electrodes around the equilibrium. On the other hand, ITC values, whose spread and strength are increasing with speed, are not very different between the observed electrodes. Among both subjects and speeds, there was a coherence in the results although the shape of the ERP and alternation of ERD/ERS could differ as depicted in Figures 12.2 and 12.4.

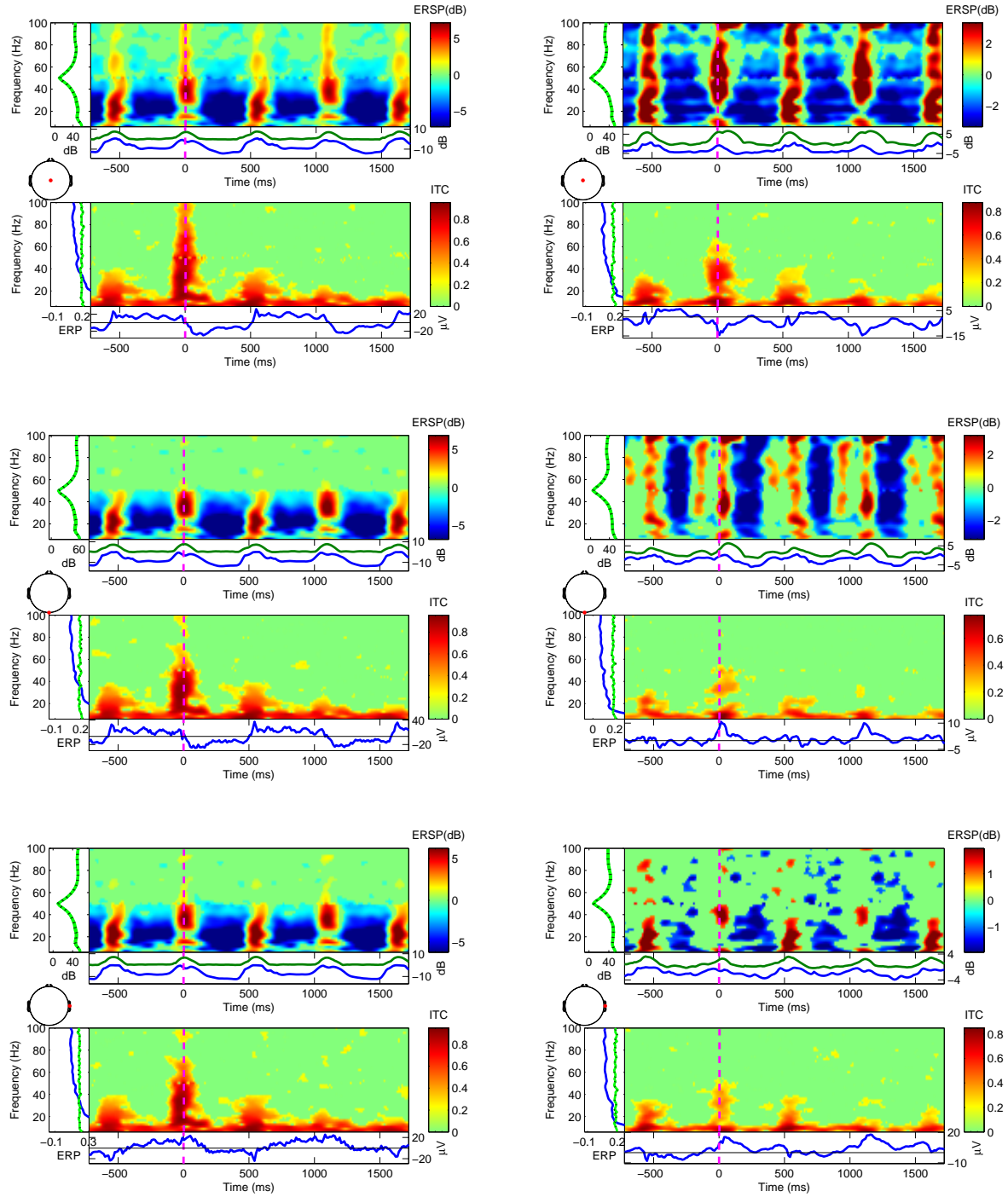


Figure 12.2: Time frequency analyses for several electrodes are illustrated on Subject 1 at 4.5 km/h. On the left: for all the electrodes of the artefact cap (only Cz, Oz and T8 electrodes are shown; $t = 0$ is the heel strike), ERD (blue)/ERS (red) due to artefacts were observed around main gait events. ERP signals show different but similar behaviours while being consistent across trials. On the right: the obtained EEG-based brain signals have some strong overlaps with the artefact measures.

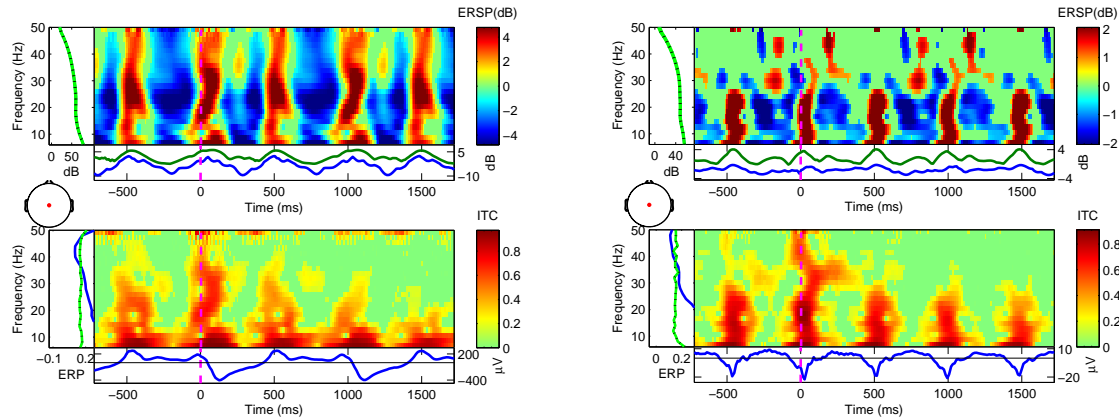


Figure 12.3: On Subject 2, similar observations arise between the brain signal time-frequency analysis (on the right) and the artefact signal (on the left) at 4.5 km/h.

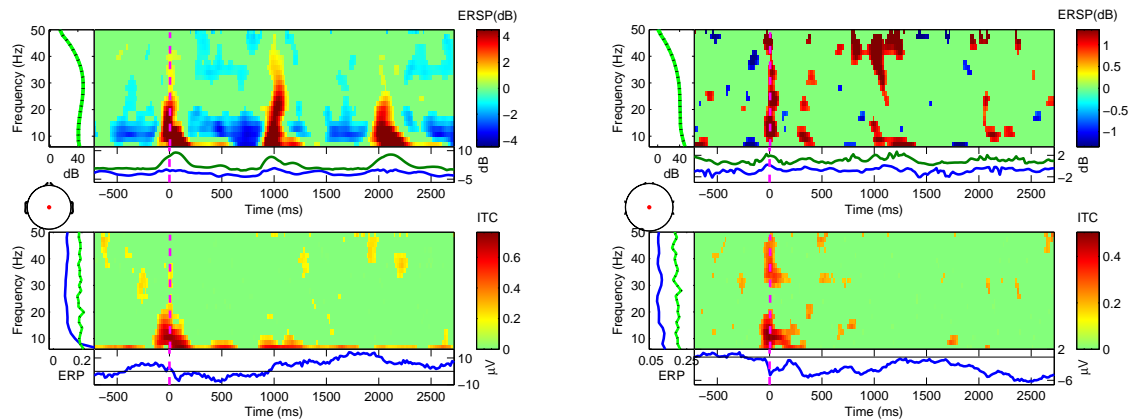


Figure 12.4: The brain signal time-frequency analysis (on the right) and the artefact signal (on the left) are differing at 1.5 km/h (here for Subject 1).

12.4 Discussion

The observed ERD/ERS in the artefact data are somehow similar to those obtained in gait-related studies [3, 17, 18] and have overlap with their respective EEG measures. Actually, there is an overlap of the ERD/ERS frequency bands and timings between the recorded artefacts and the results of those previous studies. This is particularly true for the large frequency band ERS and the alternation of ERD/ERS shown in Figure 12.5 as reported in [17]. In Figure 12.6 from [3], a heel strike coincides with an ERS up to 20 Hz, which is observed in our analysis. In Figure 12.7 depicted in [18], these frequency bands and timings are also consistent with Figure 12.2. However, interestingly, at a given timing, there is an alternation of ERD/ERS in frequency: when an ERS is detected in the 25–35 Hz, an ERD is observed below 10 Hz. This behaviour was not observed in our experiment. This may suggest that some of the data, at least, are not artefacts. Overall, all of these matching observations clearly indicate that a specific care should be considered when studying spontaneous activity related to a movement: effects other than physiological artefacts can pollute the data in both low and high frequency bands.

Theoretically, the electrodes can be affected by different types of movements that are dealt with gait-related artefacts. First, a single electrode can be rendered ineffective by rotation, sliding and compression vibration modes. Some of these factors are more common depending on their location. For instance, occipital electrodes are more commonly prone to a strong sliding contribution whereas central electrodes close to the midline are often under a more important compression contribution. Second, a coupling between all of the electrodes is increasing the vibration mode intensity. Given each electrode is linked to other ones by the textile cap, the overall system could be seen as a multiple coupled oscillator problem. However, in practice, we do not see strong variations across electrodes. Over the two subjects, there were obvious differences between different electrodes (especially in magnitude, phase and sometimes in shape), but they were not that large. It could be interesting to study how these variations are consistent with the assumption of identical distribution of artefacts over the scalp made in [19].

Finally, as a complementary proposition of this hardware system, the same system could be used to benchmark a given artefact reduction/correction method. After recording the data from the artefact measurement headset, one can inject simulated EEG signals offline as performed in [20]. Then, the assessment will objectively compare the signal to noise ratio computed after performing several artefact removal techniques. This will measure how well the artefact is removed and if the useful signal itself is affected by this process. For instance, as depicted in Figure 12.8, the first ICA components have some rhythmic behaviours. Moreover, similar results were found on both subjects and with corresponding EEG data.

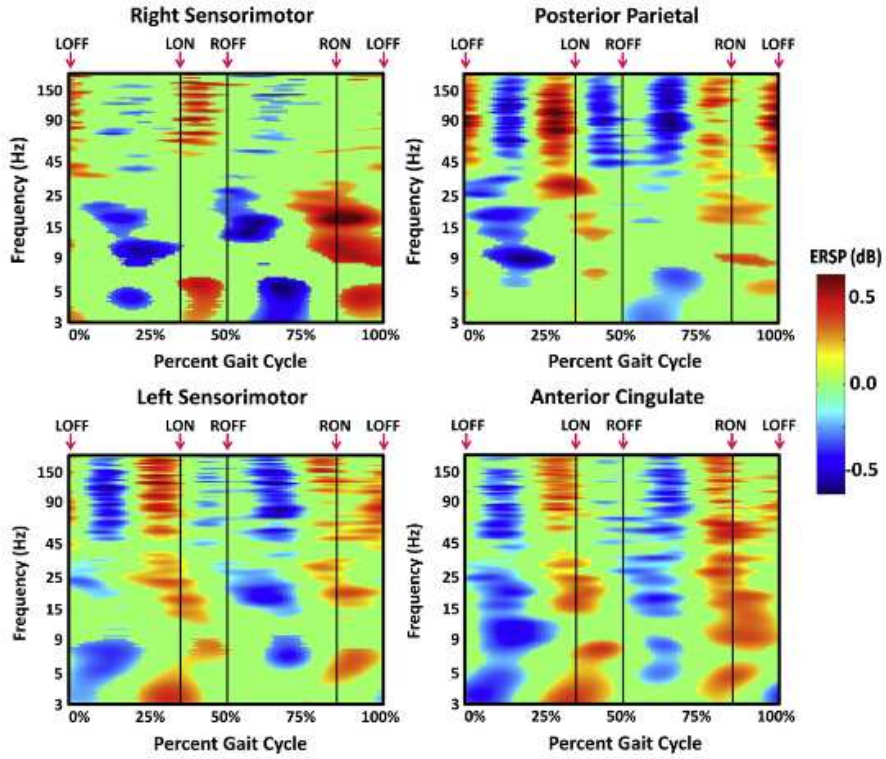


Figure 12.5: In a time-frequency EEG analysis of a gait cycle, the alternation between widely spread ERD and ERS is clearly visible [17].

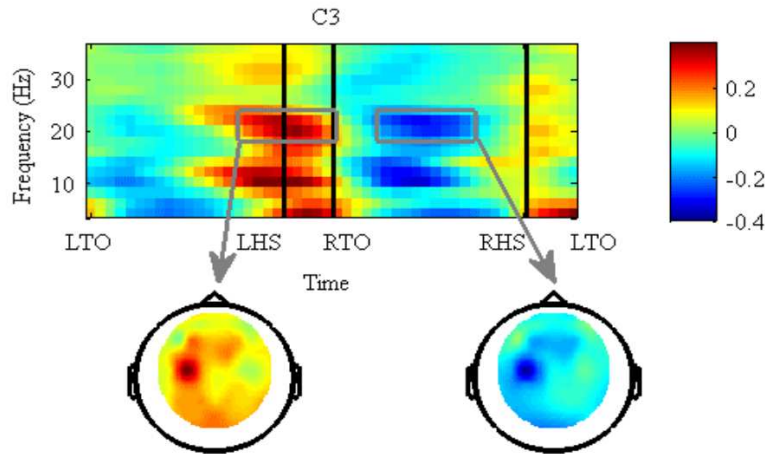


Figure 12.6: After Canonical Correlation Analysis to remove artefacts, an ERS is observed up to 20 Hz, which is overlapping the artefact measures [3]. As stated by the authors, there may still have artefacts.

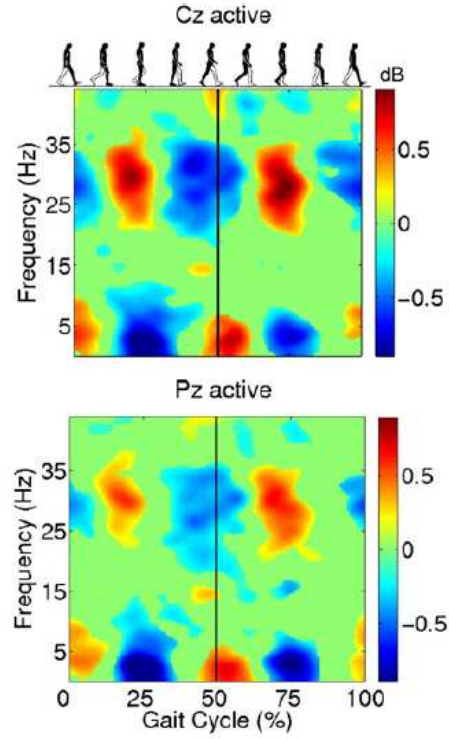


Figure 12.7: Again, there is an overlap in the time frequency analysis with our analysis [18]. However, there is an alternation of ERD/ERS between above and below 10 Hz that was not obtained by the artefact system.

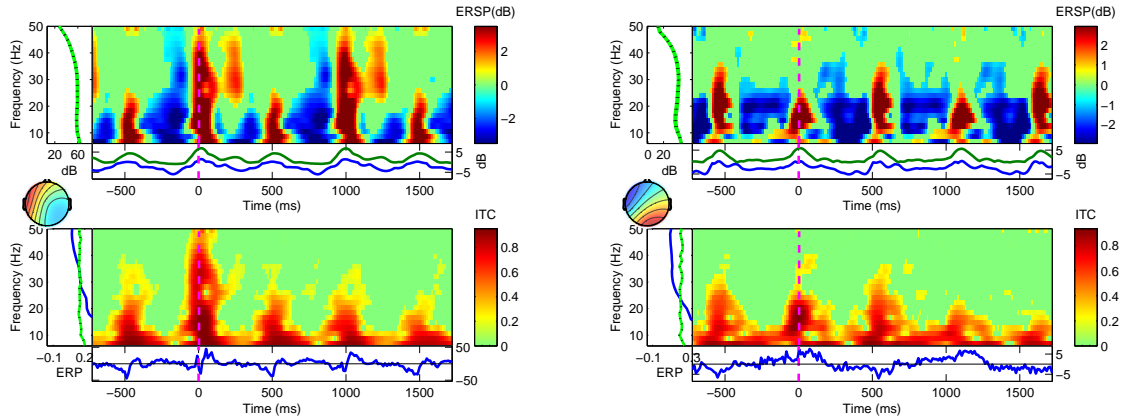


Figure 12.8: At 4.5 km/h, several major ICA components were found in the artefact data. There were similarities between both subjects. The corresponding EEG-based ICA also appeared to be similar.

12.5 Conclusion

In this Chapter, a first step towards a hardware framework to estimate movement artefacts synchronized with brain activity and to assess the efficiency of artefact removal methods was proposed. In this experiment, two subjects were recorded using new EEG cap prototype based on the ANT acquisition system (Advanced Neuro Technology, ANT, Enschede, The Netherlands) under ambulatory conditions.

The measured artefacts have some time-frequency overlaps with previous studies and recorded EEG signal from the same subjects. For instance, a large frequency-band ERS at heel-strike time was observed as in previous works. This shows that non-physiological artefacts may strongly contaminate the measured EEG signals. This information should be cautiously considered by current researchers working in this field. These warnings are complementary to those formulated about the underlying neural origin in an EEG arm movement decoding [21].

By injecting known EEG data in the system, this artefact cap would also allow the objective measurement of the relevancy of artefact removal methods. Indeed, the computation of the Signal-to-Noise Ratio after applying each method will lead to a more objective assessment of the artefact removal technique performance. As used in [20], the cortico-muscular coherence between EMG (Electromyographic) and EEG signals that is able to differentiate whether the signal is cortical could be properly assessed by this prototype. This procedure could also be applied to a claimed artefact resistant measure [22]. In a final version, our framework would be able to experimentally check if artefact removal methods approach work well in the environment of interest.

One future task will be to integrate this approach in a final system. Several hardware devices could be assessed to determine whether they are intrinsically more resistant to artefacts. For instance, the use of a wireless EEG cap could also be a way to mitigate artefacts. Another task would be to use this artefact estimation to correct the polluted signal. This could easily be performed by measuring artefacts with our hardware and by recording EEG around these measurements. By computing ICA or other reference-based signal cancelling method as suggested by [23], one should be able to remove the artefact part of the recorded EEG signal for further analysis. Finally, once the efficiency of an artefact removal technique is proven, cortical gait movements could be properly studied.

Bibliography

- [1] Joseph T. Gwin, Klaus Gramann, Scott Makeig, and Daniel P. Ferris. Removal of movement artifact from high-density eeg recorded during walking and running. *Journal of Neurophysiology*, 103(6):3526–3534, 2010.
- [2] T. Castermans, M. Duvinage, M. Petieau, T. Hoellinger, C.D. Saedeleer, K. Seetharaman, A. Bengoetxea, G. Cheron, and T. Dutoit. Optimizing the performances of a p300-based brain-computer interface in ambulatory conditions. *IEEE JETCAS*, 1(4):566–577, 2011.
- [3] M. Severens, B. Nienhuis, P. Desain, and J. Duysens. Feasibility of measuring event related desynchronization with electroencephalography during walking. In *EMBC, 2012 Annual International Conference of the IEEE*, pages 2764–2767, 2012.
- [4] Arnaud Delorme and Scott Makeig. Eeglab: an open source toolbox for analysis of single-trial eeg dynamics including independent component analysis. *Journal of Neuroscience Methods*, 134:9–21, 2004.
- [5] H. Tam and J.G. Webster. Minimizing electrode motion artifact by skin abrasion. *Biomedical Engineering, IEEE Transactions on*, BME-24(2):134–139, 1977.
- [6] A. C. Metting van Rijn, A. Peper, and C. A. Grimbergen. High-quality recording of bioelectric events. Part 1. Interference reduction, theory and practice. *Medical & Biological Engineering & Computing*, 28(5):389–397, September 1990.
- [7] J.G. Webster. Reducing motion artifacts and interference in biopotential recording. *Biomedical Engineering, IEEE Transactions on*, BME-31(12):823–826, 1984.
- [8] Karl E. Misulis MD PhD and Thomas C. Head MD. *Essentials of Clinical Neurophysiology*, 3e. Butterworth-Heinemann, 2003.
- [9] T. L. Lee-Chiong. *Sleep: A Comprehensive Handbook*. Wiley-Liss, 2005.
- [10] David H. Gordon. Triboelectric interference in the ecg. *Biomedical Engineering, IEEE Transactions on*, BME-22(3):252–255, 1975.
- [11] A Searle and L Kirkup. A direct comparison of wet, dry and insulating bioelectric recording electrodes. *Physiological Measurement*, 21(2):271, 2000.
- [12] John G. Webster. *Medical Instrumentation Application and Design fourth edition*. 2009.

- [13] DanielP. Burbank and JohnG. Webster. Reducing skin potential motion artefact by skin abrasion. *Medical and Biological Engineering and Computing*, 16(1):31–38, 1978.
- [14] Hughes de Talhouet and John G Webster. The origin of skin-stretch-caused motion artifacts under electrodes. *Physiological Measurement*, 17(2):81, 1996.
- [15] Trevor Thompson, Tony Steffert, Tomas Ros, Joseph Leach, and John Gruzelier. {EEG} applications for sport and performance. *Methods*, 45(4):279 – 288, 2008. Neuroimaging in the sports sciences.
- [16] S. Ödman. Potential and impedance variations following skin deformation. *Medical and Biological Engineering and Computing*, 19(3):271–278, 1981.
- [17] Joseph T. Gwin, Klaus Gramann, Scott Makeig, and Daniel P. Ferris. Electrocortical activity is coupled to gait cycle phase during treadmill walking. *NeuroImage*, 54(2):1289 – 1296, 2011.
- [18] Johanna Wagner, Teodoro Solis-Escalante, Peter Grieshofer, Christa Neuper, Gernot Müller-Putz, and Reinhold Scherer. Level of participation in robotic-assisted treadmill walking modulates midline sensorimotor {EEG} rhythms in able-bodied subjects. *NeuroImage*, 63(3):1203 – 1211, 2012.
- [19] Alessandro Presacco, Ronald Goodman, Larry Forrester, and Jose Luis Contreras-Vidal. Neural decoding of treadmill walking from noninvasive electroencephalographic signals. *Journal of Neurophysiology*, 106(4):1875–1887, 2011.
- [20] A. Nonclercq and P. Mathys. Quantification of motion artifact rejection due to active electrodes and driven-right-leg circuit in spike detection algorithms. *Biomedical Engineering, IEEE Transactions on*, 57(11):2746–2752, 2010.
- [21] J. Antelis, L. Montesano, A. Ramos-Murgialday, N. Birbaumer, and J. Minguez. On the usage of linear regression models to reconstruct limb kinematics from low frequency eeg signals. *Plos One, In press*, 2013.
- [22] Troy Lau, Joseph Gwin, Kaleb McDowell, and Daniel Ferris. Weighted phase lag index stability as an artifact resistant measure to detect cognitive eeg activity during locomotion. *Journal of NeuroEngineering and Rehabilitation*, 9(1):47, 2012.
- [23] Samuel Boudet, Laurent Peyrodie, Philippe Gallois, and Christian Vasseur. Filtering by optimal projection and application to automatic artifact removal from {EEG}. *Signal Processing*, 87(8):1978 – 1992, 2007. Independent Component Analysis and Blind Source Separation.

Chapter 13

About The Cortical Origin of The Low-Delta and High-Gamma Rhythms Observed in EEG Signals During Treadmill Walking

Contents

13.1 Introduction	289
13.2 Material and Methods	289
13.2.1 Data Collection	289
13.2.2 Pre-Processing and Spectral Analysis	290
13.2.3 Ensemble Averaged Time-Frequency Analysis	291
13.3 Results	291
13.4 Discussion	293
13.5 Conclusions	297

Abstract

This Chapter presents a spectral and time-frequency analysis of EEG signals recorded on seven healthy subjects walking on a treadmill at three different speeds. An accelerometer was placed on the head of the subjects in order to record the shocks undergone by the EEG electrodes during walking.

Our results indicate that up to 15 harmonics of the fundamental stepping frequency may pollute EEG signals, depending on the walking speed and also on the electrode location. This finding may call into question some conclusions drawn in previous EEG studies where low-delta band (especially around 1 Hz, the fundamental stepping frequency) had been announced as being the seat of angular and linear kinematics control of the lower limbs during walk. Additionally, our analysis reveals that EEG and accelerometer signals exhibit similar time-frequency properties, especially in frequency bands extending up to 150 Hz, suggesting that previous conclusions claiming the activation of high-gamma rhythms during walking may have been drawn on the basis of insufficiently cleaned EEG signals. Our results are put in perspective with recent EEG studies related to locomotion and extensively discussed in particular by focusing on the low-delta and high-gamma bands.

This chapter is based upon the following publication:

- T. CASTERMANS, M. DUVINAGE, G. CHERON, T. DUTOIT, February 2014, *About the cortical origin of the low-delta and high-gamma rhythms observed in EEG signals during treadmill walking*, Neuroscience Letters, Pages 166–170.

13.1 Introduction

Recently, numerous experimental results have indicated a strong involvement of the brain during locomotion. Significant changes in motor and cognitive demands (i.e. spatial attention) have been observed in the context of bipedal walking in unknown or cluttered dynamic environments [1, 2, 3, 4]. Functional neuroimaging studies have shown that the primary motor cortex is recruited during rhythmic foot or leg movements [5, 6, 7, 8, 9, 10]. Additionally, the technique of functional near-infrared spectroscopy (fNIRS) has allowed to detect involvement of frontal, premotor and supplementary motor areas during walking [11, 12].

All those results were obtained using imagery techniques which are characterized by a good spatial but poor temporal resolution. In contrast, electroencephalography (EEG) is a measurement technique offering a sufficiently good temporal resolution to study the dynamics of brain. However, EEG study of cortical activity elicited during walk is highly challenging: EEG signals are by essence noisy and may be affected by different artefacts generated either by extracerebral physiological activity or by the gait itself [13].

Two strategies have thus been developed in the literature in order to overcome these experimental difficulties. The *static approach* consists in focusing on simplified foot or leg movements which imply common cerebral processes with gait. In these experimental protocols, subjects are mainly static and produce only limited lower limb movements. On the other hand, the *dynamic approach* consists in recording EEG signals from subjects walking on a treadmill. In this case, a powerful analysis technique to discriminate the different artefact contributions from the real cortical signals is of course required. Regrettably, the results of those different analyses are most of the time partially, if not totally, incompatible regarding both the location of the brain areas activated and the frequency bands of interest [14, 15].

In this paper, the EEG signals recorded during treadmill walking are analysed and compared with data acquired by an accelerometer placed on the head of each subject. Similarities between both types of signals are presented and extensively discussed in order to bring new clues in the general understanding of EEG signals recorded during human locomotion, in particular for the very low and very high frequency bands. In Section 13.2, the data collection, the pre-processing and spectral analysis and the ensemble averaged time-frequency analysis are detailed. Then, Section 13.3 exposes the results and Section 13.4 discusses these results by the light of current brain research studies related to gait.

13.2 Material and Methods

13.2.1 Data Collection

Seven healthy volunteers (5 males and 2 females) without any known physical or neurological disorders participated in this experiment (age-range: 25-33 years) whose protocol was extensively described elsewhere [13]. Basically, one of the objectives of this data collection was to assess the feasibility of developing a brain-computer interface under ambulatory conditions. Therefore, each subject walked bare feet on a treadmill at 1.5, 3 and 4.5 km/h wearing an EEG cap (32 passive electrodes) connected to the Advanced Neuro Technology amplifier (ANT, Enschede, The Netherlands) digitizing the signals at 512 Hz. Additionally, a piezoelectric accelerometer

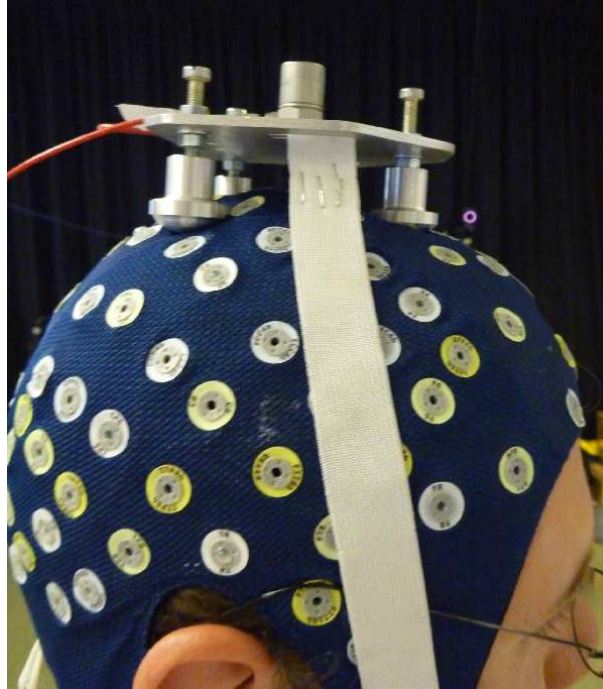


Figure 13.1: Piezoelectric accelerometer was placed on the head of the subjects to record acceleration undergone during gait.

(Dytran 3100B) was fixed to a rigid plate mounted on a three-point linkage, firmly strapped on the head of the subject with an elastic band and plugged into the ANT system (see Figure 13.1). This montage ensured the correct transmission of shocks to the accelerometer. Simultaneously, the kinematics of the lower limb movements was recorded using a system of six infrared cameras (Bonita, Vicon, Los Angeles, USA). Each EEG recording (i.e. 3 per subject) lasted about 12 minutes. All procedures were approved by the Université Libre de Bruxelles Internal Review Board and complied with the standards defined in the Declaration of Helsinki.

13.2.2 Pre-Processing and Spectral Analysis

In a first step, the times of important gait events were determined with the kinematics data. Two principal events are defined in human locomotion: the *heel strike*, which is the time of the first contact of the foot with the ground, and the *toe off*, which is the last instant of contact of the foot with the ground. Consequently, 4 typical events follow one another during a gait cycle: the *right heel strike* (RHS), the *left toe off* (LTO), the *left heel strike* (LHS) and finally the *right toe off* (RTO) before the next RHS. During walking on the treadmill, the heel strike time is defined when the position of the malleolus marker is the most forward (in the treadmill axis direction), while the toe off time is defined when the fifth metatarsal marker is in the most backward position [16].

EEG signals were processed using the EEGLAB toolbox [17]. A standard spectral analysis (FFT) was made in order to compare the frequency contents of EEG electrodes and the ac-

celerometer. The goal of such analysis was to check the possible presence of common harmonics associated to the stepping frequency of each subject. We focused on Cz, Oz and T8, for the diversity of their spatial localizations (top, back and left side of the head respectively) and thus for the diversity of the brain areas which are monitored.

13.2.3 Ensemble Averaged Time-Frequency Analysis

A time-frequency analysis was conducted in order to compare the signals coming from the EEG electrodes and the accelerometer, on a gait cycle basis. With this aim, EEG data were first detrended and then epoched by defining a time-window of 2 seconds around each left heel strike. Each epoch was visually inspected, rejected in case of obvious presence of eye or muscle artefacts.

As the lower limb movements during locomotion are only quasi-periodic, the stride length varies from one step to the other. The generation of precise ensemble averaged event-related spectral perturbation (ERSP) plots is thus not straightforward. We first computed spectrograms for each EEG channel during each epoch for each subject, as described in [18]. All the single-trial spectrograms were then linear time-warped so that the times of heel strikes and toe off events occurred at the same adjusted latencies. After this operation, spectrograms were ensemble averaged for all subjects. The average log spectrum for all movement cycles was subtracted from the log spectrogram for each movement cycle. The resulting changes from baseline are the ERSP plots presented in next section, as a function of the percentage of the normalized gait cycle. Significant ERSPs ($p < 0.05$) were computed using a bootstrapping method [17].

13.3 Results

Common harmonics were found in the spectra of EEG electrodes and the accelerometer. These harmonics correspond to the fundamental stepping frequency of the subjects, which ranges from about 0.6 Hz at 1.5 km/h to 1 Hz roughly at 4.5 km/h. Box-plots shown in 13.2 clearly indicate that the number of harmonics present in the spectra is monotonously increasing with the walking speed. Here, harmonics with Signal to Noise Ratio > 2 are considered, the signal being the peak amplitude at frequency f and the noise being the background amplitude evaluated in the $[f - 0.5, f + 0.5]$ Hz interval. At 4.5 km/h, up to 15 harmonics are observed in the EEG electrode spectra and almost twice as much in the accelerometer spectra. More precisely, harmonics are produced up to 15 Hz and 30 Hz in EEG and accelerometer signals respectively. In these conditions, delta, theta, alpha and low beta bands are impacted. Also, the distributions of harmonic numbers are obviously differing from one electrode to the other, meaning that the phenomenon giving rise to the harmonics most likely depends on the electrode spatial localization.

Regarding the time-frequency analysis, it appears that an event-related synchronization (ERS) is produced in the accelerometer signal at each heel strike, during the double support phase of gait, while an event-related desynchronization (ERD) appears during each swing phase (cf. 13.3), regardless of the walking speed. Both ERD and ERS occur in a large frequency interval ranging from low-delta band up to high-gamma band (150 Hz) without any discontinuity (although inaccurate for an accelerometer, we use the terms ERS and ERD to describe more easily our observations). The same characteristic alternation (i.e. ERD-ERS) is visible in EEG

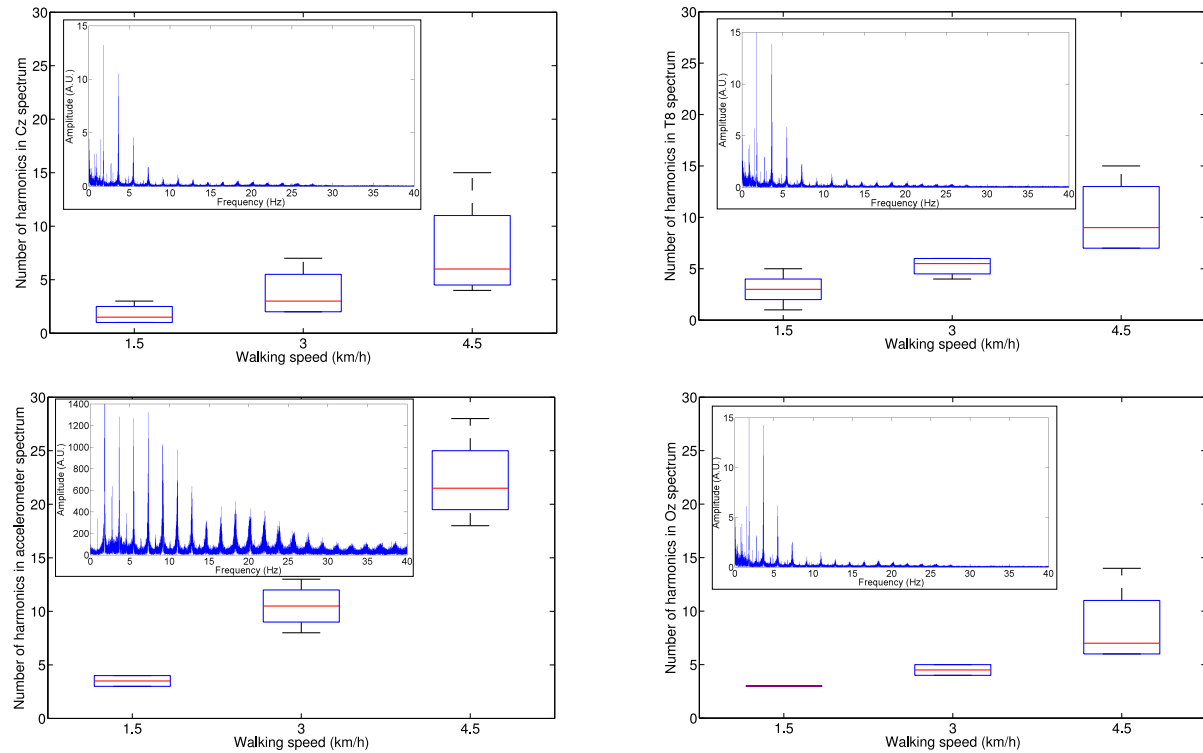


Figure 13.2: The number of harmonics present in the EEG electrode and accelerometer spectra is monotonously increasing with walking speed. Also, the distributions are differing according to the spatial localization on the head. Examples of spectra for one subject walking at 4.5 km/h are inserted.

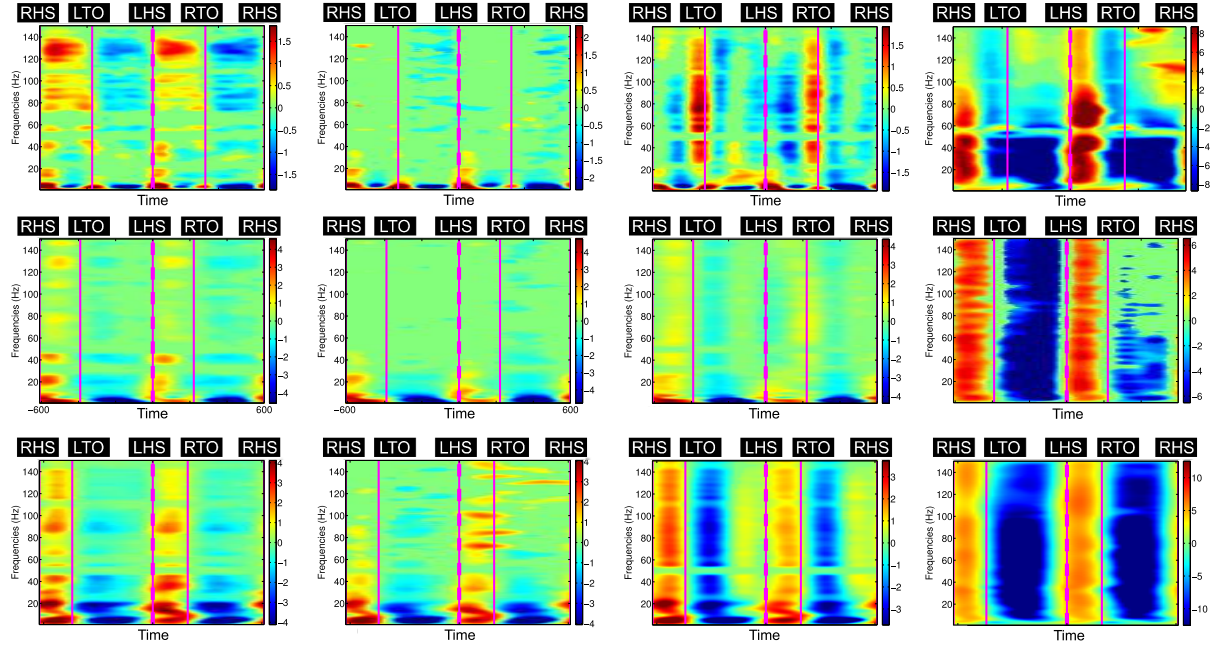


Figure 13.3: The ERSP analyses for both EEG electrodes (Cz on column 1, T8 on column 2, Oz on column 3) and the accelerometer (column 4) during walking indicate successive synchronizations (in red) and desynchronizations (in blue) along the gait cycle. Rows 1, 2, 3 correspond to 1.5, 3 and 4.5 km/h respectively. The color scale is in dB.

electrodes Cz, Oz and T8 at 3 and 4.5 km/h, but with discontinuities along the frequency axis which vary both in number and localization according to the EEG electrode. Interestingly, the results obtained for the lowest walking speed (1.5 km/h) look different. Indeed, a specific succession of ERS-ERD-ERS occurs below 10 Hz, starting at each gait event (i.e. both heel strikes and toe offs) in all EEG electrodes, while the standard ERD-ERS alternation found at higher walking speeds is seen in the accelerometer channel. After applying by Independent Component Analysis (ICA) in Figure 13.4, artefacts are importantly reduced by manual cleaning. However, some activities non related to spontaneous signal are still visible (e.g. Oz electrodes).

13.4 Discussion

In addition to "traditional" EEG artefacts (ocular, muscular, power line, ...), EEG recordings realized in ambulatory conditions are degraded by specific sources of noise [13, 15]. *Triboelectric* noise is generated by movement, friction and flexion of the cable components, resulting in a static or piezoelectric movement transducer effect [19]. *Electrode movements* are produced by movements of the head, but also by the shocks undergone by the whole body at each step, which - albeit significantly attenuated - are transmitted to the head [20]. These movements modify the magnetic and capacitive coupling of the user and the electrode leads, leading to an alteration of the parasitic current flowing into the leads [21]. A resulting parasitic voltage drop is then

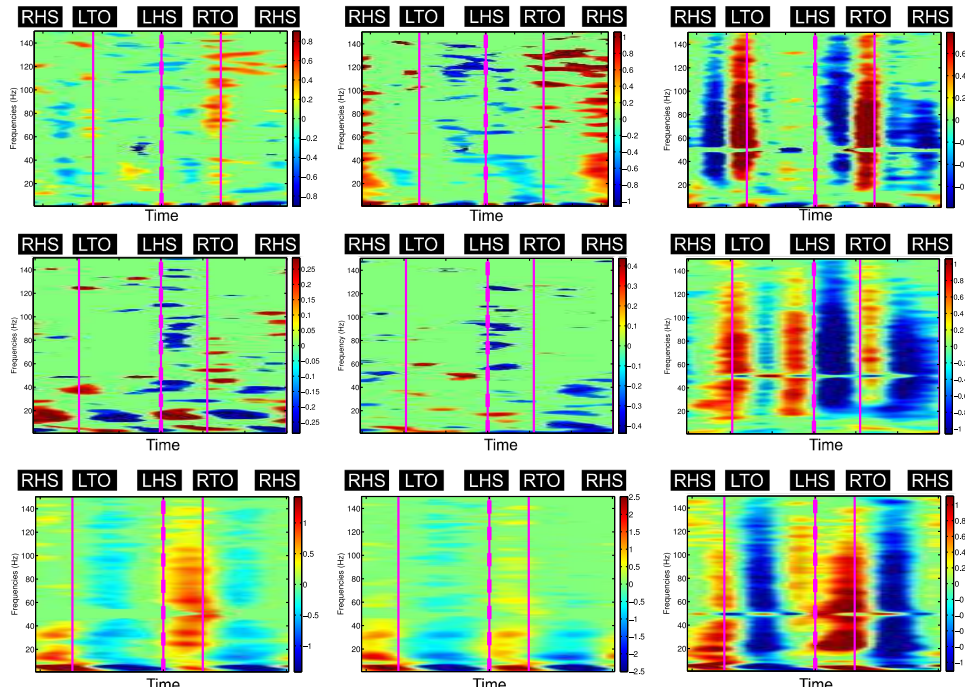


Figure 13.4: ICA manual cleaning helps to drastically reduce the amplitudes of the ERD-ERS. However, spurious rhythmic alternations remain e.g. in Oz electrode, which is not related to motor control (same convention as in Figure 13.3 for the plot presentation).

produced in the electrode/gel/skin interface which interferes with the EEG signal [22]. Finally, electrode movements can also cause impedance variation which directly affects the electrode voltage offset [23]. Unfortunately, our results indicate that all these *motion artefacts* are not limited to a small spectral band, so they cannot be simply removed by frequency filtering. This first conclusion is in total agreement with [24]. Therefore, motion artefacts should be eliminated using a specific treatment, which should be more sophisticated than a simple low-, high- or band-pass filter. In addition, the fact that distributions of harmonic numbers differ from one electrode to the other means that the way motion artefacts affect EEG spectra depends on the electrode spatial localization. This should also be taken into account when correcting motion artefacts.

With these considerations in mind, we are inclined to suspect that several published EEG analyses of walk may be strongly polluted by motion artefacts. For instance, [25] did not use any specific motion artefact cleaning in their EEG decoding. In order to reconstruct the kinematics of lower limbs during treadmill walking, they applied a simple band-pass filter between 0.1 and 2 Hz to the raw EEG signals. Note that this frequency range perfectly coincides with the stepping frequency of human locomotion, as mentioned in this paper and in [20]. Then, [25] used a linear Wiener filter to reconstruct lower limb kinematics during treadmill walking. From a mathematical point of view, though, it may not be surprising that lower limb elevation angles can be accurately reconstructed from a signal containing their first harmonics by determining a set of parameters. In order to rule out the presence of motion artefacts, the authors computed the phase-locking values (PLV) among sensors. The rationale was that potential motion artefacts due to EEG wires or the subject's motion would affect all sensors equally. In their logic, the authors claim that mechanical artefacts did not play a role in their decoding because the PLV values they found ranged from about 0.55 in the walking condition (around 1 and 2 Hz) to 0.4 in the baseline (rest) condition. According to them, these low PLV values (found in both conditions) suggest lack of mechanical coupling due to concerted wire movement. However, our results indicate that motion artefacts do not affect the electrodes located on the top of the head and those on the head circumference in the same way. Thus, the low PLV values argument should not be considered as a direct proof of the absence of motion artefacts. Consequently, it still remains to be confirmed (or infirmed) that EEG delta band contains information about angular and linear kinematics of the lower limb during walk.

This last point is supported by a recent paper from [26]. These authors have focused on several publications in which are reported successful reconstructions of different limb kinematics from EEG using the low frequency activity of the EEG and linear regression models [27, 28, 29]. [26] showed that the mathematical properties of the linear regression model and of the correlation metric used in these studies could explain the good reported results. Moreover, they demonstrated that correlation results obtained with real EEG signals, shuffled or random EEG data were not statistically different. This means that the linear models developed in [27, 28, 29] are able to provide the same results irrespectively of the presence or absence of limb velocity information in EEG signals.

Other recent studies dedicated to EEG analysis during a locomotion task may be added to this discussion. [30] investigated the possibility of measuring ERD and ERSPs during walking on treadmill. After cleaning EMG artefacts using canonical correlation analysis (CCA), they found an ERD in the mu band above the central motor cortex (electrode Cz) and in the beta band above the lateral motor cortex (electrodes C3 and C4). In addition, they found that ERSPs in

mu and beta bands were coupled to the gait cycle with significant differences between left swing, right swing and double support phase of the gait cycle. They did not report any signal of cortical origin at low frequency. Indeed, as the low frequency modulations they found in the ERSPs were also visible in the occipital channels, the authors explained these were very unlikely related to brain activity and probably due to remaining artefacts.

[31] also showed that mu and beta rhythms are suppressed during active walking in the Lokomat, a robotic gait orthosis. They also provided evidence of modulations of the lower gamma band (25 to 40 Hz), localized in central midline areas and related to the phases of the gait cycle. For different reasons, the authors speculate that these activations and deactivations might be related to sensorimotor processing of the lower limbs in the complex motor pattern of human locomotion. Although their ERSPs plots exhibit ERD and ERS around and below 5 Hz, they neither comment them nor claim that these originate from cortical activity.

The first analysis of EEG during walk on treadmill was actually published by [18]. Successive synchronizations (ERS) and desynchronizations (ERD) were found for the first time, in phase with the gait cycle, present in different regions of the brain and in numerous frequency bands comprised between 3 and more than 150 Hz. By using a method based on independent component analysis (ICA) combined with an inverse modelling approach, the authors claimed they could discriminate electrocortical sources, muscle sources and other artefacts from the raw EEG signals. However, the very same authors previously stated [32] *using the very same dataset*, clearly stated that: "Unlike more spatially stationary artefacts in EEG signals arising from eye movements, scalp muscles, fMRI gradients, etc., which may be resolved by ICA decomposition into a subspace of one or more independent components, we found that gait-related movement artefact remained in many if not most of the independent components. This prevented us from removing only a small subset of components capturing the movement artefacts." For this reason, they considered the removal of motion artefacts from EEG during walking and running on treadmill using an artefact template subtraction method. Such method allowed to enhance the detection of P300 potentials in ambulatory conditions. Nevertheless, the study of cerebral processes involved in human locomotion is not possible using a subtraction method, as it would undoubtedly remove interesting signal from the EEG recordings. For this reason, the authors used only the ICA approach to clean the EEG signals in [18]. No mention is made of specific motion artefacts, nor of any particular treatment to reject them. Thus, it may be doubted that the time-frequency analysis plots shown in that paper do not contain any motion artefact contribution. Figure 13.3 clearly shows that periodic power spectral changes over large frequency bands can be observed in the accelerometer signal, in a similar way to the results obtained after ICA by [18].

Finally, spectral analysis does not allow to determine which cortical region is directly involved in the transmission of motor commands to the muscles. In contrast, coherence analysis reveals anatomical coupling between cortical activity and the motor output to the muscles by detecting common rhythmicities in EMG and EEG signals. According to the significant coherence values (24-40 Hz around Cz) found by [33], the multiple ERD-ERS detected by [18] in the 3-24 and 40-76 Hz bands are obviously not indicative of a direct corticospinal drive, at least, not to the tibialis anterior. Thus, one may think that these signals, if not affected by residual artefacts, would rather reflect the control of sensory afferents (i.e. one of the hypotheses formulated by [18] themselves). It is interesting to note that the studies by [31] and [30] do not report multiple ERD-ERS in α , β and γ bands and are in line with the coherence study made by [33].

13.5 Conclusions

Despite the inherent difficulties arising when analysing EEG signals under ambulatory conditions, several groups have recently published papers about EEG decoding of movements or the fundamental analysis of mechanisms taking place in the brain during locomotion. However, the cortical or artefact nature of the signal is rarely definitely set, which puts some doubts on the results.

By simultaneously recording the data coming both from a conventional EEG cap and from an accelerometer placed on the head of subjects walking at different speeds on a treadmill, we demonstrated that motion artefacts in phase with the fundamental stepping frequency could exhibit harmonics impacting EEG signals up to 15 Hz. This pollution of signals is dependent on the electrode location, which renders the motion artefact cleaning step more complex than applying a general band-pass filter. For this reason, we suspect that several studies published in the literature present results that are based on insufficiently cleaned EEG data. As the EEG decoding of gait proposed by [25] was realized on the basis of raw data, it should be considered in no way as a proof that EEG delta band contains information about kinematics of the lower limbs. Such statement still needs to be confirmed or infirmed. In addition, we have shown that our time-frequency analysis results for the real EEG electrodes and for the accelerometer data are similar and exhibit, in particular, large and rhythmic activities spreading over wide frequency bands (up to 150 Hz). This suggests that these large extensions in high gamma band, previously reported by [18], might be due in fact to motion artefacts as well. Consequently, researchers conducting future EEG studies during locomotion should take a great care in the cleaning procedure, as data in this context are strongly affected by an entanglement of downgoing, upgoing and artefactual contributions [15].

Bibliography

- [1] Julia T. Choi and Amy J. Bastian. Adaptation reveals independent control networks for human walking. *Nature Neuroscience*, 10(8):1055–1062, July 2007.
- [2] Sten Grillner, Peter Wallén, Kazuya Saitoh, Alexander Kozlov, and Brita Robertson. Neural bases of goal-directed locomotion in vertebrates - an overview. *Brain Research Reviews*, 57(1):2 – 12, 2008.
- [3] Jens Bo Nielsen. How we walk: Central control of muscle activity during human walking. *The Neuroscientist*, 9(3):195–204, 2003.
- [4] Serge Rossignol, Martin Schwab, Michal Schwartz, and Michael G. Fehlings. Spinal cord injury: Time to move? *The Journal of Neuroscience*, 27(44):11782–11792, 2007.
- [5] L. O. D. Christensen, Jacob Buus Andersen, Thomas Sinkjær, and J. Nielsen. Transcranial magnetic stimulation and stretch reflexes in the tibialis anterior muscle during human walking. *Journal of Physiology*, 531(2):545–557, 2001.
- [6] B. H. Dobkin, A. Firestone, M. West, K. Saremi, and R. Woods. Ankle dorsiflexion as an fMRI paradigm to assay motor control for walking during rehabilitation. *Neuroimage*, 23(1):370–381, September 2004.
- [7] S. Heuninckx, N. Wenderoth, F. Debaere, R. Peeters, and S. P. Swinnen. Neural basis of aging: the penetration of cognition into action control. *J Neurosci*, 25(29):6787–96, Jul 20 2005.
- [8] Sofie Heuninckx, Nicole Wenderoth, and Stephan P. Swinnen. Systems neuroplasticity in the aging brain: recruiting additional neural resources for successful motor performance in elderly persons. *The Journal of Neuroscience*, 28(1):91–99, January 2008.
- [9] Andreas R. Luft, Gerald V. Smith, Larry Forrester, Jill Whitall, Richard F. Macko, Till-Karsten Hauser, Andrew P. Goldberg, and Daniel F. Hanley. Comparing brain activation associated with isolated upper and lower limb movement across corresponding joints. *Human Brain Mapping*, 17(2):131–140, 2002.
- [10] C Sahyoun, A Floyer-Lea, H Johansen-Berg, and P.M Matthews. Towards an understanding of gait control: brain activation during the anticipation, preparation and execution of foot movements. *NeuroImage*, 21(2):568 – 575, 2004.

- [11] Taeko Harada, Ichiro Miyai, Mitsuo Suzuki, and Kisou Kubota. Gait capacity affects cortical activation patterns related to speed control in the elderly. *Experimental Brain Research*, 193(3):445–454, 2009.
- [12] Mitsuo Suzuki, Ichiro Miyai, Takeshi Ono, and Kisou Kubota. Activities in the frontal cortex and gait performance are modulated by preparation. An fNIRS study. *NeuroImage*, 39(2):600–607, January 2008.
- [13] T. Castermans, M. Duvinage, M. Petieau, T. Hoellinger, C.D. Saedeleer, K. Seetharaman, A. Bengoetxea, G. Cheron, and T. Dutoit. Optimizing the performances of a p300-based brain-computer interface in ambulatory conditions. *Emerging and Selected Topics in Circuits and Systems, IEEE Journal on*, 1(4):566–577, 2011.
- [14] T. Castermans and M. Duvinage. Corticomuscular coherence revealed during treadmill walking: further evidence of supraspinal control in human locomotion. *The Journal of Physiology*, 591(6):1407–1408, 2013.
- [15] Thierry Castermans, Matthieu Duvinage, Guy Cheron, and Thierry Dutoit. Eeg and human locomotion - descending commands and sensory feedback should be disentangled from artifacts thanks to new experimental protocols position paper. In Sabine Van Huffel, Carlos Manuel B. A. Correia, Ana L. N. Fred, and Hugo Gamboa, editors, *BIOSIGNALS*, pages 309–314, 2012.
- [16] J.A. Zeni Jr., J.G. Richards, and J.S. Higginson. Two simple methods for determining gait events during treadmill and overground walking using kinematic data. *Gait & Posture*, 27(4):710 – 714, 2008.
- [17] Arnaud Delorme and Scott Makeig. EEGLAB: An open source toolbox for analysis of single-trial {EEG} dynamics including independent component analysis. *Journal of Neuroscience Methods*, 134(1):9–21, 2004.
- [18] Joseph T. Gwin, Klaus Gramann, Scott Makeig, and Daniel P. Ferris. Electrocortical activity is coupled to gait cycle phase during treadmill walking. *NeuroImage*, 54(2):1289 – 1296, 2011.
- [19] Trevor Thompson, Tony Steffert, Tomas Ros, Joseph Leach, and John Gruzelier. EEG applications for sport and performance. *Methods*, 45(4):279 – 288, 2008.
- [20] Robert J. Ratcliffe and Kenneth G. Holt. Low frequency shock absorption in human walking. *Gait & Posture*, 5(2):93 – 100, 1997.
- [21] Karl E. Misulis MD PhD and Thomas C. Head MD. *Essentials of Clinical Neurophysiology*, 3e. Butterworth-Heinemann, 2003.
- [22] A. C. Metting van Rijn, A. Peper, and C. A. Grimbergen. High-quality recording of bioelectric events. Part 1. Interference reduction, theory and practice. *Medical & Biological Engineering & Computing*, 28(5):389–397, September 1990.
- [23] Hughes de Talhouet and John G Webster. The origin of skin-stretch-caused motion artifacts under electrodes. *Physiological Measurement*, 17(2):81, 1996.

- [24] *Assessment of EEG Signal Quality in Motion Environments*, Army Research Laboratory Report, 2009.
- [25] Alessandro Presacco, Ronald Goodman, Larry W Forrester, and Jose L. Contreras-Vidal. Neural decoding of treadmill walking from non-invasive, electroencephalographic (eeg) signals. *Journal of Neurophysiology*, 2011.
- [26] J. Antelis, L. Montesano, A. Ramos-Murguialday, N. Birbaumer, and J. Minguez. On the usage of linear regression models to reconstruct limb kinematics from low frequency eeg signals. *Plos One, In press*, 2013.
- [27] H.A. Agashe and J.L. Contreras-Vidal. Reconstructing hand kinematics during reach to grasp movements from electroencephalographic signals. In *Engineering in Medicine and Biology Society, EMBC, 2011 Annual International Conference of the IEEE*, pages 5444–5447, 2011.
- [28] Wolf Schweitzer. Technical Below Elbow Amputee Issues - Reconstructing Three-Dimensional Hand Movements from Noninvasive Electroencephalographic Signals [science fiction / research], March 2010.
- [29] Trent J Bradberry, Rodolphe J Gentili, and José L Contreras-Vidal. Fast attainment of computer cursor control with noninvasively acquired brain signals. *Journal of Neural Engineering*, 8(3):036010, 2011.
- [30] M. Severens, B. Nienhuis, P. Desain, and J. Duysens. Feasibility of measuring event related desynchronization with electroencephalography during walking. In *Engineering in Medicine and Biology Society (EMBC), 2012 Annual International Conference of the IEEE*, pages 2764–2767, 2012.
- [31] Johanna Wagner, Teodoro Solis-Escalante, Peter Grieshofer, Christa Neuper, Gernot R. Müller-Putz, and Reinhold Scherer. Level of participation in robotic-assisted treadmill walking modulates midline sensorimotor eeg rhythms in able-bodied subjects. *NeuroImage*, 63(3):1203–1211, 2012.
- [32] Joseph T. Gwin, Klaus Gramann, Scott Makeig, and Daniel P. Ferris. Electrocortical activity is coupled to gait cycle phase during treadmill walking. *NeuroImage*, 54(2):1289 – 1296, 2011.
- [33] T. H. Petersen, M. Willerslev-Olsen, B. A. Conway, and J. B. Nielsen. The motor cortex drives the muscles during walking in human subjects. *The Journal of Physiology*, 590(10):2443–2452, 2012.

Part IV

General Conclusion

Chapter 14

General Conclusion

Contents

14.1 Contributions of this thesis	305
14.2 Perspectives	309
14.3 Research Statement	312

14.1 Contributions of this thesis

This thesis presented several advances in lower-limb rehabilitation related applications. First, ambulatory Brain-Computer Interfaces (BCI) using SSVEP, P300 and eye-movements have been deeply investigated and the feasibility of a real-time system has been proven. Second, two gait models have been proposed and show interesting properties for orthosis control. Third, brain spontaneous signals related to gait movement have been studied and a review of current knowledge and challenges has been proposed. Finally, several contributions to other research areas have been made. The original contributions of this thesis are the following:

- **Programmable Central Pattern Generator (PCPG)-based Gait Modelling**

A modified Programmable Central Pattern Generator (PCPG)-based Gait Model has been proposed and implemented in an orthosis. First, we demonstrate that human walk periodic patterns can be modelled by a PCPG whose parameters are adapted thanks to a low-level order polynomial interpolation as a function of speed. However, although good similarity indices were observed between real walk and generated kinematics, results suggest that walk would be advantageously modelled by two PCPGs.

Second, a foot lifter orthosis prototype dedicated to people suffering from foot drop driven by this modified PCPG algorithm and based on biomechanical sensors has been developed. After a learning phase, the PCPG output is used to drive the orthosis actuator during the swing phase, in order to help patients (the orthosis just follows the movement during the stance phase). In practice, given that human gait is not perfectly periodic, the phase of this control signal needs to be reset with actual movement. Therefore, two phase-resetting procedures were studied: one standard hard phase-resetting leading to discontinuities and

one original soft phase-resetting allowing to recover the correct phase in a smooth way. Simulated tests on a chirp and a steep speed modifications show that the prototype is working as expected.

- **Dynamic Recurrent Neural Network (DRNN)-based Gait Modelling** We describe the use of a dynamic recurrent neural network (DRNN) mimicking the natural oscillatory behaviour of human locomotion for reproducing the planar covariation rule in both legs at different walking speeds. Neural network learning was based on sinusoid signals integrating frequency and amplitude features of the first three harmonics of the sagittal elevation angles of the thigh, shank and foot of each lower limb. We verified the biological plausibility of the neural networks.

Best results were obtained with oscillations extracted from the first three harmonics in comparison to oscillations outside the harmonic frequency peaks. Physiological replication steadily increased with the number of neuronal units from 1 to 80, where similarity index reached 0.99. Analysis of synaptic weighting showed that the proportion of inhibitory connections consistently increased with the number of neuronal units in the DRNN. This emerging property in the artificial neural networks resonates with recent advances in neurophysiology of inhibitory neurons that are involved in central nervous system oscillatory activities. The main message of this Chapter is that this type of DRNN may offer a useful model of physiological central pattern generator for gaining insights in basic research and developing clinical applications.

- **Ambulatory Steady-State Visual Evoked Potential (SSVEP) Analysis**

A fundamental study of the Steady-State Visual Evoked Potential (SSVEP) distribution under different conditions was performed: sitting on a chair/walking on a treadmill at 3 km/h and a normal/maximal luminosity of the LED panel. In this experiment, eight healthy subjects had to look at a LED panel whose flickering frequency ranged from 10 Hz to 46 Hz by 2 Hz step. It was shown that the average SNR in the occipital area under walking condition is significantly worse than under sitting conditions. Muscle artefacts from the neck strongly affect the SSVEP response in this area. Several unexpected behaviours, which are unlikely linked to artefacts, were observed. In conclusion, without any artefact removal techniques, results suggest that gait is not a transparent process for the SSVEP paradigm. However, the walking conditions should be able to reach similar performance as the sitting conditions using an optimal artefact correction method (still to be designed). Several behaviours that were observed could be helpful for the design of ambulatory BCIs in order to increase the performance of such systems.

- **Ambulatory P300 Analysis**

A deep study of the possibility to develop a P300-based BCI system under ambulatory conditions has been proposed. The study is based on experimental data recorded with seven subjects executing a visual P300 speller-like discrimination task while simultaneously walking at three different speeds on a treadmill. It is demonstrated that a P300-based BCI is definitely feasible in such conditions. Different artefact correction methods relying on independent component analysis and template subtraction are described and discussed in

details. However, none of the methods outperforms the filtered raw data. Additionally, for real-time applications requiring low-complexity, the results suggest to use seven electrodes as a good trade-off between performance and compactedness.

- **Ambulatory P300 and SSVEP Objective and Subjective Comparison**

A comparison of a four-state SSVEP BCI plus a non-control state for lower-limb rehabilitation purposes and a similar P300 interface has been investigated. The comparison relies on the subjective and objective performances assessed by usability and workload. After performing a real-time treadmill speed control, the System Usability Scale and the NASA Task Load Index questionnaires were administered to five healthy subjects. Results show that the SSVEP BCI has better attributes than its P300 counterpart. Major contributors to this increased performance are the higher reactivity, the asynchronous interface and the lighter cognitive load for command generation.

- **Assessment of a Low-Cost Emotiv Headset**

A statistical comparison between a medical-grade system, the ANT device, and the Emotiv Epop headset by determining their respective performances in a P300 BCI using the same electrodes has been proposed. Nine healthy subjects participated in this experiment during which the ANT and the Emotiv systems are used in two different conditions: sitting on a chair and walking on a treadmill at constant speed. The Emotiv headset performs significantly worse than the medical device; observed effect sizes vary from medium to large. The Emotiv headset has higher relative operational and maintenance costs than its medical-grade competitor. Although this low-cost headset is able to record EEG data in a satisfying manner, it should only be chosen for non critical applications such as games, communication systems, etc. For rehabilitation or prosthesis control, this lack of reliability may lead to serious consequences. For research purposes, the medical system should be chosen except if a lot of trials are available or when the Signal-to-Noise Ratio is high.

- **Eye Movement-based Control Scheme: Principles and Review**

We propose an original and biologically-inspired leg prosthesis control scheme consisting of: an EOG-based eye tracker and a Programmable Central Pattern Generator (PCPG). Additionally, we propose to compare two widely known techniques (the standard R. Barea (RB) and A. Bulling (AB)'s works) with several potential improvements and the implementation of a speech-recognition based method that were all assessed according to the F1-score. Additionally, we investigate 3 different target configurations on the screen: 3x3, 3x5 and 5x5 to detect which configuration can reach the best bitrate. Finally, double blink and wink detectors are evaluated to estimate their relevancy as a mouse click.

In this 8-healthy-subject experiment, we observed that both RB and AB methods provide fairly similar results. According to the bitrate analysis while considering complexity, the 3x3 is the most suitable interface. Among the different potential enhancements, none of the methods seems to outperform the fixed grid. The speech tool-based method provides unexpected good results. Regarding the eye mouse click detectors, their performance should be high enough to be used in a reliable interface.

- **Locomotion and Brain Signals: a Review**

A deep review of the progress made in the development of non-invasive BCIs dedicated to motor rehabilitation systems has been proposed. In a first part, the main principles of human locomotion control are presented. The paper then focuses on the mechanisms of supra-spinal centers active during gait, including results from electroencephalography, functional brain imaging technologies (NIRS, fMRI, PET, SPECT) and invasive studies. The first BCI applications to gait rehabilitation are then presented, with a discussion about the different strategies developed in the field. The challenges to raise for future systems are identified and commented. Finally, we present some proposals to address these challenges, in order to contribute to the improvement of BCI for gait rehabilitation.

- **Gait-like Movement Brain Analysis**

The EEG dynamics associated to the production of voluntary rhythmic foot movements only has been studied. An experimental protocol limiting drastically the presence of movement artefacts in the EEG signals compared to real walk is used. A time-frequency analysis is performed, based on a time-warping method allowing an ensemble averaging of the data of 3 subjects. Alternation of power increases and decreases in the α , β and γ bands during the movement cycle is shown as well as the emergence of two different neural coordination schemes related to in-phase and anti-phase foot movements.

- **Gait Intent Detection** A quantitative comparison of different strategies to automatically decode brain signals related to gait initiation has been performed. In the Electroencephalographic signals (EEG), some Event-Related Desynchronization (ERD) and a Bereitschaftspotential (BP), which is a slow negative potential occurring before the movement onset can be detected. Four healthy subjects participated in this experiment, which consisted in forward/backward walking and standing. First, a fundamental analysis is proposed showing the type of signals and their localization. Then, five classifiers and six feature extraction techniques are investigated using only the potentials recorded at Cz electrode opening the way for very low complexity embedded devices.

The results show that the movement vs baseline classification results can reach around 80 % and 60 % in average for BP and ERD respectively. However, the direction of the movement only reaches at most 60 %. A high variability between subjects was observed. By further analysis, it was shown that muscle and ocular artefacts are not impacting the results. Other evidences indicate that these results could be translated in real-time.

- **Artifact Estimation** A first hardware prototype that aims at decoupling movement artefacts and spontaneous brain signals has been proposed. Tests were made with two subjects walking at four different speeds on a treadmill. Results show that there is an artefact overlap in observed time-frequency analysis with the corresponding EEG recordings and gait-related studies from other researchers. This suggests that specific care should be taken with movement-related artefacts. Moreover, by injecting simulated EEG signals, this framework should also allow the assessment of the efficiency of artefact removal methods. This could lead to a more objective evaluation of such methods. Subjectivity is a known disadvantage when using Independent Component Analysis (ICA).

- **Low-delta and High-gamma Rhythms Origins** A spectral and time-frequency analysis of EEG signals recorded on seven healthy subjects walking on a treadmill at three different speeds was performed. An accelerometer was placed on the head of the subjects in order to record the shocks undergone by the EEG electrodes during walking.

Our results indicate that up to 15 harmonics of the fundamental stepping frequency may pollute EEG signals, depending on the walking speed and also on the electrode location. This finding may call into question some conclusions drawn in previous EEG studies where low-delta band (especially around 1 Hz, the fundamental stepping frequency) had been announced as being the seat of angular and linear kinematics control of the lower limbs during walk. Additionally, our analysis reveals that EEG and accelerometer signals exhibit similar time-frequency properties, especially in frequency bands extending up to 150 Hz, suggesting that previous conclusions claiming the activation of high-gamma rhythms during walking may have been drawn on the basis of insufficiently cleaned EEG signals. Our results are put in perspective with recent EEG studies related to locomotion and extensively discussed in particular by focusing on the low-delta and high-gamma bands.

In conclusion, several recommendations can be drawn. First, although DRNN-based CPG provides good overall properties, it has currently less capabilities to adapt to unforeseen events. Indeed, the DRNN output is not currently considering the actual movement (no phase-resetting). Therefore, the PCPG-based gait modelling is suggested as the current most promising solution. Second, in terms of BNCI control, the EOG-based approach appears quick, reliable and asynchronous. However, an online test has still to be performed. On the other hand, for a pure BCI control, the SSVEP is obviously the best solution for similar reasons. Third, for brain-decoding, even if several tools are existing, the use of a PCPG is still encouraged. This will help to integrate a robust output able to manage external perturbations. Obviously, to drive the PCPG, the decoded signal should embed a sort of speed information and, ideally, a phase information.

14.2 Perspectives

This thesis succeeded in providing several major contributions about the feasibility of ambulatory BCIs and potential results for rehabilitation related applications. However, it also paves the way for further investigations that can be summarized as follows:

- **Gait Model and Orthosis Development**

Proposed gait models can still be improved. First, our DRNN-based model has still to be studied regarding stability over time and for robustness to perturbations, e.g. in terms of recovery time. Second, the PCPG algorithm could be improved by using non-linear filtering to consider the modification of the gait pattern shape over speeds. This would allow to further refine the similarity index curve.

On the other side, the second orthosis prototype will be assessed by the MECARA team (UMons) on real patients to provide further insights on what to improve.

- **Ambulatory BCIs**

Some more advanced signal processing methods and interfaces could be used to improve the reactivity of the device. For instance, recent research on Canonical Correlation Analysis (CCA) coupled to Independent Component Analysis (ICA) suggests that it should be possible to eliminate artefacts in the SSVEP paradigms. Regarding the interface itself, the phase-shift SSVEP [1], which consists in using the same frequency with a time delay, could focus on the best performing frequency. The P300 interface could also be accelerated in order to provide a quicker response while keeping low false positive rate.

Additionally, other paradigms could be investigated while considering both objective and subjective measures. For instance, EOG-based eye movements could lead to a lower decision time. Similarly to motor imagery, the self-paced aspect of EOG should be appreciated by subjects.

- **Spontaneous Gait-Related Brain Signals**

The main purposes of this research area are to disentangle the artefact and brain control signal of the lower limbs in real-time but also to characterize the time-frequency features of the artefact. When these goals are achieved, a proper understanding of the brain control signal while walking will be available. It would not be surprising that different behaviours occur at low and high speeds. This important step will obviously lead to develop numerous outcomes such as rehabilitation systems and lower-limb orthosis/prostheses design. Moreover, if the full characteristics of the ambulatory artefact is available, it will pave the way for establishing efficient artefact removal methods and enhancing performance of out-of-the-lab methods. In the end, when rehabilitation is targeted, a more spontaneous approach would be advised to reactivate the plasticity of the injured brain area and to accelerate recovery.

From previous Chapters, several characteristics of the artefact are known. 1) When a subject was walking on a treadmill, it was shown that there was a significant coherence between the muscle electromyographic (EMG) and the brain electroencephalographic (EEG) signals. This coherence analysis was performed using the imaginary part, which is known as artefact resistant by displaying complex relationship that artefact is unlikely to produce. 2) By construction of the artefact signal, it is likely phase-locked to the gait cycle events (heel strike and toe off). This assumption was made by [2], who proposed a template subtraction based method. However, their method is likely to remove gait-related brain activity too. Logically, standard Independent Component Analysis (ICA) is not appropriate. Indeed, to blindly separate sources, ICA is using statistical independence as a criterion. Obviously, as explained in [3], this assumption does not hold when the two signals of interest are phased-locked. 3) The artefact is likely to have a highly complex structure. It was shown in [4] that an accelerometer put on the head exhibits a similar time-frequency behaviour to EEG electrodes recording on subjects walking on a treadmill. The properties are positive and negative modifications of the power from very low frequencies to more than 150 Hz. A similar behaviour was observed in a fundamental analysis proposed by [5]. Furthermore, in [4], using a specific hardware device insulated from the brain, which only records the artefacts, we showed that the same widely spread frequency response was obtained. This shows that

artefact pollution is likely to occur in current gait-related studies and that simple filtering methods should not be able to remove artefacts. Furthermore, this also means that the transfer function from movement to artefact is not straightforward. Finally, a reference signal of the movement artefact is hard to get: only an accelerometer signal put on the head and EMG signals from muscles around the head could give some insights about the current underlying artefact. 4) Phase-based measures should be of first interest. Indeed, in [6], it was shown that the phase-lag weighted index was an artefact resistant measure while performing an odd-ball paradigm under walking conditions. In [7], other authors also suggest that the movement artefact should affect all the electrodes the same way, implying relative similar phases between electrodes.

As a solution, a better artefact estimator prototype could be designed by better integrating reference cables and by adding real measurements. Hence, a precise artefact measurement could be coupled to an EEG measurement to be corrected in real-time. Additionally, two major strategies are envisaged: - First, similarly to a currently submitted paper about removing artefacts while having an external reference signal, using an accelerometer, a series of algorithms could be investigated to remove this artefact. The external signals that could be used are the accelerometer and the neck EMG signals. - Second, introducing phase, synchrony, coherence with an EMG signal from lower limbs in BSS criteria is an interesting option. Indeed, one strong lack of Peterson's study is that it does not give any information on a time-frequency analysis [8]. This is why using a modified BSS method would help getting the temporal signal of interest and not only part of its characteristics. This will pave the way for further analysis. Additionally, as proposed in the conclusion of [9], several experiments can be conducted to further confirm or infirm the obtained results.

In terms of work packages, several main tasks could be proposed:

WP1 - Accelerometer and EMGs-based Artefact Removal Noise Cancellation is a variation of optimal filtering that involves producing an estimate of the noise by filtering the reference input and then subtracting this noise estimate from the primary input containing both signal and noise. According to this scheme, the reference signal is supposed to be correlated to the noise to be cancelled. Obviously, the reference signal should be uncorrelated to the signal of interest; otherwise, the latter will be removed too.

Reference signals that can mimic the movement artefact should somehow measure the head movement. Hence, an accelerometer put on the head as well as EMG signals from the neck are interesting options as proposed in Chapter 5 for P300 detection. Methods like Independent Component Analysis (ICA), adaptive filtering, template subtraction, ARMAX model and orthogonal subspace projection, information transfer/Granger Causality could be applied.

As the artefact signal reference is not available, to evaluate the relevancy of the approach, three validation methods are available. First, getting the artefact using one specific method, this signal can be added on data. Then, the known artefact can be compared to the obtained signal from other methods. Second, as cortico-muscular

coherence is significant between the brain signal and lower limb EMGs, a very low value computed from the obtained artefact signal will show no control brain signal is available. Third, based on [10], the study of the decoding capability of both types of signals will determine their artefactual nature.

WP2 - Phase and cortico-muscular coherence-based BSS However, although ICA is a powerful BSS algorithm, as stated in [3], independence of the sources is not a valid assumption here, because phase-locked sources are highly dependent. Thus, a source separation of phase-locked subspaces method was proposed by the same authors. By implementing a two-stage method, the authors succeed in fairly disentangling phase-locked signal.

As a first step, this method may be applied to the data. A similar validation scheme as proposed in WP1 will be followed. By comparing the obtained signal from WP1 and from this analysis, some insights of the method capability will be available.

Second, to enforce convergence of the algorithm to split artefact and signal, we propose to add the maximisation/minimisation of the cortico-muscular coherence in this method criteria. Hence, the algorithm convergence will lead to the automatic splitting of highly/weakly coherent signal with lower limb muscles indicating a high/low part of brain control signals.

WP3 - Artefact Signal Description After WP1 and WP2, the artefact signal will be compared and fully analysed. By using Fourier and Wavelet analysis, the time-frequency response of the artefact signal will be given. A specific focus will be around gait events such as heel strike and toe off as major contribution in brain recordings were suggested by other researchers. Furthermore, more advanced signal processing techniques like ICA and empirical mode decomposition (EMD) would be essential to completely describe this artefact.

14.3 Research Statement

Lower limb impairment is an important cause of dependence, reduced earnings and costs for our society. Sometimes, these impairments can lead to isolation and instability. Therefore, during my PhD thesis, my research focus was on investigating several strategies to develop a lower limb prosthesis/orthosis and rehabilitation systems using non-invasive and portable technologies. This topic was highly challenging because the electroencephalographic brain signals (EEG) strongly suffer from movement artefacts. Brain-Computer Interfaces (BCIs) have been used to help disabled people to communicate or control devices just by thoughts without using muscular activities. This approach has been successfully applied to control wheelchair, hand orthosis and communication. One of the drawbacks of such a technique is the low signal to noise ratio. Indeed, in previous works, to avoid artefacts from muscles, movements, etc., any movement was forbidden or polluted signals were discarded (e.g. by visual inspection) in order to get the best performance. To address these ambulatory conditions, I investigated several strategies in signal processing part and computer brain interface aspects.

First, I reviewed several famous BCI/BNCI paradigms (e.g. P300, SSVEP) under ambulatory conditions. One of the most important conclusions is that gait does not impact that much the performance of the P300 potential interface. By proposing several artefact removal methods dedicated to movement artefacts, no result outperformance was observed. Additionally, as the cost of EEG devices is still high, I proposed a comparative study between the low-cost and widely spread Emotiv EPOC headset and a medical device. This shows that the low-cost device is able to produce satisfying results but not enough reliable for critical applications. Regarding the SSVEP paradigm, by a signal-to-noise ratio analysis, I showed that the muscle artefacts are affecting the occipital area, in the back of the head. This suggests that mobile SSVEP BCI is feasible but requires some dedicated pre-processing. As a proof of concept, I implemented an online P300 and SSVEP BCI where the subjects were able to control the treadmill speed while walking on it. By assessing subjective performances relying on some standard questionnaires (SUS, NASA-TLX), I was able to compare both BCI paradigms from the user point of view. Finally, I compared several eye-movement detection methods based on Electrooculography (EOG) as no such comparison was available in the literature.

Second, the analysis of spontaneous gait-related brain activity should lead to a more natural interface. Actually, standard BCI interfaces are often far from being natural leading to a high abandonment rate. Therefore, I also studied this more spontaneous way. First, I co-wrote a deep review of current knowledge in ambulatory brain-computer interfaces. Second, it is known that before movement, a slow decrease in the brain potential arises (readiness potential) and decrease in power in some frequency bands. Thus, as few studies were performed while standing, I used several pipelines to predict the leg movement onset and the direction of the move using the brain signals. Results show the direction estimation (forward/backward walking) is too challenging to get fair performance but the movement onset can be relatively well predicted against standing. This would mean the prosthesis or orthosis may be activated properly depending on the willingness of the patient. Besides, to get a full control of the prosthesis, the cortical signals have to be decoded while walking. I am currently participating to the discussion about the decoding and the origins of lower limb control. With some colleagues, we proposed a critical point of view of current studies that somehow expose incoherent results. Furthermore, to disentangle artefacts and cortical signals (both are inherent and synchronized during gait), I proposed to develop a hardware device, that only measure artefacts using the same cap while insulating the brain from the electrodes. This system should give valuable information to determine what the gait related cortical signal is based on ERP/ERSP analysis. We also assess the transmission of artefacts to the electrodes from an accelerometer signal put on the head. Third, to convert the gait intent signals into a usable device, a gait model is required. Thus, we developed two methods based on a Programmable Central Pattern Generator (PCPG) and a Dynamic Recurrent Neural Network (DRNN). The PCPG was adapted to fit a lower-limb orthosis developed with some mechanical colleagues in the University of Mons. By modelling the central pattern generator from the spinal cord, the DRNN shows similar properties to neurophysiological CPGs. Thanks to these approaches, good kinematics can be obtained. Finally, I have worked at the Ecole Polytechnique Fédérale de Lausanne. I am working on firing rates and spiking point process tuning synchronous to gait cycle. This encompasses cross correlation, coherence, Granger analysis between neurons in multi-unit and single unit analysis.

As main future research areas, I am strongly interested in multidisciplinary research bridging the gap between neuroscience findings and applications/clinical practice thanks to engineering. This research includes participating in more fundamental research, developing and implementing innovative engineering modelling, machine learning and signal processing methods. Obviously, when the technology will be sufficiently mature, a transfer to the industry or the creation of spinoffs is a must. The following research topics are matching these requirements and are potential future projects.

First, rehabilitation (and prosthetic) has been a hot topic for decades. By using bio-imaging techniques and robotics, the recovery of patients could be accelerated (e.g. after stroke). After a better understanding of brain gait control, the development of a hardware solution integrating those discoveries would allow observing whether it enhances the patient's recovery.

Second, automatic disease/disability detection and its current stage assessment, i.e. diagnosis, could be an interesting research opportunity (same partners). For instance, the detection of the type and stage of schizophrenia and how well medicines are working could be a good multidisciplinary challenge. It could also help to uniform the diagnosis across doctors and provide more reliable biological indicators for sensitive cases (e.g. in court). Another topic of investigation could be linked to hyperactivity and loss of attention (e.g. ADHD: attention deficit hyperactivity disorder) and Alzheimer disease. As a final example, vocal tract pathologies could be investigated. A microphone-based disease detection could help decreasing the cost and increasing the standard of living by early screening.

Third, studying high-level sports is another topic I am interested in. What is the difference between a good and an exceptional sportsman? Is the difference linked to brain activity, muscles? By dealing with the acquired data, the understanding of these differences could help predicting the success of a given sportsman. It could also contribute to develop new training method.

To achieve these long-term goals, collaborations with hospitals, doctors and patients are highly desired. Additionally, I already have several collaborations that could help in these research projects. Guy Cheron is a neuroscientist and full professor working on a large panel of research topics that includes biomechanics, movement related cortical activity and its mapping to kinematics, rat brain analysis. He is also the co-founder of the "Human Wave" company, which is advising top sportsmen to enhance their performance. This company is also involved in a BioWin project (Neuroatt) on the development of a diagnosis tool for ADHD and a brain wave trainer.

As a conclusion, I propose you several promising research directions in neuroengineering. All these projects are linked to potential biomedical applications that should enhance the patient standard of living. They include the understanding of the underlying mechanism to be translated into relevant feedback. The rehabilitation-related potential outcomes are obviously of first interest in an aging population, which is prone to a higher level of disability. Furthermore, biological-based diagnosis tools could help decreasing the overall cost by early screening and the same approach could help curing patients. All these projects are obviously in areas that are considered as promising by the economic leaders. This suggests higher funding will be available in the coming years and decades. Additionally, research about understanding and improving sport performance should also find some funding from professional sport teams.

Bibliography

- [1] Hung-Yi Wu, Po-Lei Lee, Hsiang-Chih Chang, and Jen-Chuen Hsieh. Accounting for phase drifts in ssvep-based bcis by means of biphasic stimulation. *Biomedical Engineering, IEEE Transactions on*, 58(5):1394–1402, May 2011.
- [2] Joseph T. Gwin, Klaus Gramann, Scott Makeig, and Daniel P. Ferris. Removal of movement artifact from high-density eeg recorded during walking and running. *Journal of Neurophysiology*, 103(6):3526–3534, 2010.
- [3] M. Almeida, J.-H. Schleimer, R. V. Vigário, and J. Dias. Source separation and clustering of phase-locked subspaces. *IEEE Trans. on Neural networks*, 22(9):1419–1434, September 2011.
- [4] Thierry Castermans, Matthieu Duvinage, Guy Cheron, and Thierry Dutoit. About the cortical origin of the low-delta and high-gamma rhythms observed in {EEG} signals during treadmill walking. *Neuroscience Letters*, 561(0):166 – 170, 2014.
- [5] Joseph T. Gwin, Klaus Gramann, Scott Makeig, and Daniel P. Ferris. Electrocortical activity is coupled to gait cycle phase during treadmill walking. *NeuroImage*, 54(2):1289 – 1296, 2011.
- [6] Troy Lau, Joseph Gwin, Kaleb McDowell, and Daniel Ferris. Weighted phase lag index stability as an artifact resistant measure to detect cognitive eeg activity during locomotion. *Journal of NeuroEngineering and Rehabilitation*, 9(1):47, 2012.
- [7] A. Presacco, R. Goodman, L. Forrester, and J. Contreras-Vidal. Neural decoding of treadmill walking from non-invasive, electroencephalographic (EEG) signals. *Journal of Neurophysiology*, 2011.
- [8] T. H. Petersen, M. Willerslev-Olsen, B. A. Conway, and J. B. Nielsen. The motor cortex drives the muscles during walking in human subjects. *The Journal of Physiology*, 590(10):2443–2452, 2012.
- [9] Thierry Castermans, Matthieu Duvinage, Guy Cheron, and Thierry Dutoit. Towards effective non-invasive brain-computer interfaces dedicated to gait rehabilitation systems. *Brain Sciences*, 4(1):1–48, 2013.
- [10] Javier M. Antelis, Luis Montesano, Ander Ramos-Murguialday, Niels Birbaumer, and Javier Minguez. On the usage of linear regression models to reconstruct limb kinematics from low frequency eeg signals. *PLoS ONE*, 8(4):e61976, 04 2013.

Part V

Other Research Contributions

Chapter 15

Inverse Reinforcement Learning to Control a Robotic Arm Using a Brain-Computer Interface

Abstract

A self-paced BCI such as a motor imagery based-BCI allows the subject to give orders at any time to freely control a device. Even after a long training, however, the accuracy of the classifier used to recognize the order is not 100%.

While a lot of studies try to improve the accuracy by using a preprocessing stage that improves the feature extraction, we work on a post- processing solution to control a JACO robotic arm developed by Kinova in a Brain-Computer Interface (BCI). The classifier used to recognize the mental commands will provide as outputs a value for each command such as the posterior probability. But the executed action will not depend on this information only. A decision process will also take into account the position of the robotic arm and previous trajectories into account. More precisely, the decision process will be obtained applying an Inverse Reinforcement Learning (IRL) on a subset of trajectories specified by an expert.

Although the approach appears promising, the convergence of the inverse reinforcement algorithm has not been achieved. Nevertheless, we developed a whole processing chain based on OpenViBE for controlling 2D- movements and we present how to deal with this high dimensional time series problem with a lot of noise which is unusual for the IRL community.

Future work will be devoted to make the IRL algorithm converge. Then, a comparative study will be undertaken.

This chapter is based upon the following publications:

- L. BOUGRAIN, M. DUVINAGE, E. KLEIN, 2012, *Inverse reinforcement learning to control a robotic arm using a Brain-Computer Interface*, Proceedings of the 8th International Summer Workshop on Multimodal Interfaces - eINTERFACE'12, pp. 83-88, July, Metz, France.

Chapter 16

Bacteria Hunt: A Multimodal, Multi-paradigm Brain-Computer Interfacing Game

Abstract

Even if brain-computer interfaces (BCI) were first designed for rehabilitation and control, they now have a lot of applications in games. By using a BCI, researchers want to increase the user experience and fun for gamers. As gamers are more demanding users, several more complex aspects of the interaction have to be studied. The multimodal, multi-paradigm brain-computer interfacing (BCI) game Bacteria Hunt was used to evaluate two aspects of BCI interaction in a gaming context. One goal was to examine the effect of feedback on the ability of the user to manipulate his mental state of relaxation. This was done by having one condition in which the subject played the game with real feedback, and another with sham feedback. The second goal was to look into possible interactions between the two BCI paradigms used in the game: steady-state visually-evoked potentials (SSVEP) as an indicator of concentration, and alpha activity as a measure of relaxation. SSVEP stimulation activates the cortex and can thus block the alpha rhythm. In addition to the main goals, a new SSVEP detection algorithm was developed and evaluated.

First, feedback did not seem to affect the game experience (such as sense of control and tension) or the objective indicators of relaxation, alpha activity and heart rate. The results are discussed with regard to clinical neurofeedback studies. Second, contrary to what was expected, subjects were able to keep their alpha power up, in compliance with the instructed relaxation task. Finally, the proposed SSVEP algorithm provides interesting features compared to a standard method. The main advantage over the standard method is the independence of prior baseline recordings.

This chapter is based upon the following publications:

- C. MÜHL, H. GÜRKÖK, D. PLASS-OUDE BOS, M.E. THURLINGS, L. SCHERFFIG, **M. DUVINAGE**, A.A. ELBAKYAN, S. KANG, M. POEL, D.K.J. HEYLEN, 2010, *Bacteria Hunt: Evaluating multi-paradigm BCI interaction*, Journal on Multimodal User Interfaces (JMUI), Springer Berlin/Heidelberg.
- C. MÜHL, H. GÜRKÖK, D. PLASS-OUDE BOS, M.E. THURLINGS, L. SCHERFFIG, **M. DUVINAGE**, A.A. ELBAKYAN, S. KANG, M. POEL, D.K.J. HEYLEN, 2009, *Bacteria Hunt: A multimodal, multiparadigm BCI game*, Proceedings of the 5th International Summer Workshop on Multimodal Interfaces - eENTERFACE'09, pp. 41-62, July 13th - August 7th, 2009, Genoa, Italy.

Chapter 17

Online Emotion Classification From Electroencephalographic Signals : A First Study Conducted In A Realistic Movie Theater

Abstract

New affordable electroencephalographic (EEG) devices dedicated to the game industry have recently appeared on the market. Consequently, more and more artists inspired by these promising technologies imagine the possibility to directly integrate human emotions in their performance through measurement of the brain waves. In this Chapter, we describe a first attempt to detect the valence (positive or negative value) of emotions provoked by different video excerpts amongst several spectators seated in a realistic movie theater, on the basis of their EEG signals only. Preliminary results obtained with consumer grade EEG headsets indicate that positively and negatively valenced video excerpts may be discriminated in the training data set but not on an independent data set. These results are extensively discussed as well as further studies and developments that should be made to improve performance in the future.

This chapter is based upon the following publications:

- T. CASTERMANS, M. DUVINAGE, N. RICHE, 2013, "Online emotion classification from electroencephalographic signals : a first study conducted in a realistic movie theater", 12th International Conference on Artificial Intelligence and Soft Computing ICAISC 2013, Zakopane, Pologne, June 9-13.

Appendix A

Statistical Performance Assessment of Japanese Candlesticks and Contrarian-based Investment Strategies

Abstract

In the Asset Management industry, every actor wants to beat the market, i.e. obtaining a an excess return in comparison to the benchmark indexes such as the CAC40 or the MSCI world. Indeed, this excess return has to justify the active portfolio management costs. Contrary to an indexed-based strategy, e.g. a passive CAC40 investment for a given period of time, active management actors are always looking for new opportunities that should lead to abnormal excess returns. Different kinds of information can be retrieved to this end: fundamental or technical analysis indicators. Fundamental analysis rely on balance sheet data. It looks for (current and estimated future) financial ratios such as debt ratios or price earning ratio (PER), i.e. the ratio between the share price and the profit. On the other hand, technical analysis considers that the Efficient Market Hypothesis (EMH) is not supported by the market. This basically means that trend identification and trend modifications can be found by price movement pattern analysis. Although this approach could be strange at first for non-investors, this kind of strategy has been largely used and implemented in both robot and human-based trading systems and investment strategies. Therefore, in this Chapter, this is the latter analysis also known in Finance as the Graal Quest, which is used to find evidence of outperformance. Two different approaches are assessed: Japanese candlesticks and contrarian strategies.

First, we develop market timing strategies and trading systems to test the intraday predictive power of Japanese candlesticks at the 5-minute interval on the 30 constituents of the DJIA index. Around a third of the candlestick rules outperforms the buy-and-hold strategy at the conservative Bonferroni level. After adjusting for trading costs, just a few rules remain significant however. When we correct for data snooping by applying the SSPA test on double-or-out market timing strategies, no single candlestick rule beats the buy-and-hold strategy after transaction costs. We also design fully automated trading systems by combining the best performing candlestick rules. No evidence of outperformance is found after transaction costs. Although Japanese candlesticks can somewhat predict intraday returns on large US caps, we show that such predictive power is too limited for active portfolio management to outperform the buy-and-hold strategy when luck, risk, and trading costs are correctly measured.

Second, we develop 200 contrarian trading strategies based on significant market variations to test whether it is possible to benefit from the well-known psychological bias of overreaction that plagues investors. We conduct the most recent and appropriate statistical tests to ensure that none of these active strategies beats the buy-and-hold strategy due to pure luck only. Each of these strategies are tested on 15 different underlying assets, including exchange rates, stock indexes, and individual stocks. When both transaction and borrowing costs are taken into account, our empirical results suggest that the use of significant market variations as daily reversal signals does not lead to any abnormal profit.

This chapter is based upon the following publications:

- **M. DUVINAGE**, P. MAZZA, M. PETITJEAN, 2013, *The intraday performance of market timing strategies and trading systems based on Japanese candlesticks*, Quantitative Finance.
- **M. DUVINAGE**, P. MAZZA, M. PETITJEAN, 2014, *Testing the profitability of contrarian trading strategies based on the overreaction hypothesis*, [Submitted].

Appendix B

RARE2012: A Multi-Scale Rarity-Based Saliency Detection With Its Comparative Statistical Analysis

Abstract

For the last decades, computer-based visual attention models aiming at automatically predicting human gaze on images or videos have exponentially increased. Even if several families of methods have been proposed and a lot of words like centre-surround difference, contrast, rarity, novelty, redundancy, irregularity, surprise or compressibility have been used to define those models, they are all based on the same and unique idea of information innovation in a given context.

In this Chapter, we propose a novel saliency prediction model, called RARE2012, which selects information worthy of attention based on multi-scale spatial rarity. RARE2012 is then evaluated using two complementary metrics, the Normalized Scanpath Saliency (NSS) and the Area Under the Receiver Operating Characteristic (AUROC) against 13 recently published saliency models. It is shown to be the best for NSS metric and second best for AUROC metric on three publicly available datasets (Toronto, Koostra and Jian Li).

Finally, based on an additional comparative statistical analysis and the effect-size Hedge' g^* measure, RARE2012 outperforms, at least slightly, the other models while considering both metrics on the three databases as a whole.

This chapter is based upon the following publications:

- N. RICHE, M. MANCAS, M. DUVINAGE, M. MIBULUMUKINI, B. GOSSELIN, T. DUTOIT, 2013, *RARE2012: A multi-scale rarity-based saliency detection with its comparative statistical analysis*, Signal Processing: Image Communication.

Appendix C

Towards A Unified Framework For Saliency Model Assessment

Abstract

Visual saliency has been an increasingly active research area in the last ten years with dozens of saliency models recently published. Nowadays, one of the big challenges in the field is to find a way to fairly evaluate all of these models. Two parameters are assessed. First, two ground truths can be used for assessment: eye fixations thanks to an eye-tracker or region labelled manually by subjects. In this Chapter, it is shown that although there is a significant difference in terms of ranking, a fairly similar concordance is observed meaning that the effect is small. Second, it is also shown that the size of the salient region impacts on the metric value. This bias is stronger when using region labelled ground truth.

Then, on human eye fixations, we compare the ranking of 12 state-of-the art saliency models using 12 similarity metrics. The comparison is done on Jian Li database containing several hundreds of natural images. Based on Kendall concordance coefficient, it is shown that some of the metrics are strongly correlated leading to a redundancy in the performance metrics reported in the available benchmarks. On the other hand, other metrics provide a more diverse picture of model overall performance. As a recommendation, three similarity metrics should be used to obtain a complete point of view of saliency model performance.

This chapter is based upon the following publications:

- N. RICHE, M. DUVINAGE, M. MANCAS, B. GOSSELIN, T. DUTOIT, 2013, *A study of parameters affecting visual saliency assessment*, Proceedings of the 6th International Symposium on Attention in Cognitive Systems (ISACS'13), Beijing, China, August 3-5.
- N. RICHE, M. DUVINAGE, M. MANCAS, B. GOSSELIN, T. DUTOIT, 2013, *Saliency and Human Fixations: State-of-the-art and Study of Comparison Metrics*, Proceedings of the 14th International Conference on Computer Vision (ICCV 2013), Sydney, Australia, December 1-8.

Appendix D

Publications

D.1 Book Chapter

- G. CHERON, M. DUVINAGE, T. CASTERMANS, F. LEURS, A.M. CEBOLLA, A. BENGOETXEA, C. DE SAEDELEER, M. PETIEAU, T. HOELLINGER, K. SEETHARAMAN, J.-P. DRAYE, B. DAN, 2011, *Recurrent Neural Networks for Temporal Data Processing*, Recurrent Neural Networks, chapter 5, pp.67-80.

D.2 Patents

- T. CASTERMANS, T. DUTOIT, M. DUVINAGE, 2013, *Method to Determine an Artificial Limb Movement from an Electroencephalographic Signal*, US2013046715 (A1).
- M. DUVINAGE, T. CASTERMANS, T. DUTOIT, 2012, *Method for Determining an Artificial Periodic Patterned Signal*, WO2012107096 (A1).

D.3 Regular papers in Journals

- M. DUVINAGE, T. CASTERMANS, M. PETIEAU, T. HOELLINGER, G. CHERON, T. DUTOIT, 2013, *SSVEP Response Distribution Under Different Luminosity and Movement Conditions*, Journal of NeuroEngineering [Under Review].
- M. DUVINAGE, T. CASTERMANS, T. DUTOIT, G. CHERON, 2014, *Towards A Hardware Framework for EEG Motion Artefact Estimation in Movement Conditions*, IEEE Transaction in Biomedical Engineering [in preparation]
- M. DUVINAGE, T. CASTERMANS, M. PETIEAU, T. HOELLINGER, G. CHERON, T. DUTOIT, 2014, *Comparative Objective and Subjective Assessment of Ambulatory SSVEP and P300 Treadmill Control* [To submit]
- M. DUVINAGE, T. CASTERMANS, T. HOELLINGER, M. PETIEAU, G. CHERON, T. DUTOIT, 2014, *Automatic Detection of EEG-based Gait Intent*, IEEE Transaction in Biomedical Engineering [Major Revision]

- M. DUVINAGE, T. CASTERMANS, M. PETIEAU, T. HOELLINGER, G. CHERON, T. DUTOIT, 2013, *SSVEP Response Distribution Under Different Luminosity and Movement Conditions*, Journal of NeuroEngineering [Under Review].
- M. DUVINAGE, T. CASTERMANS, M. PETIEAU, T. HOELLINGER, C. DE SAEDELEER, K. SEETHARAMAN, G. CHERON, T. DUTOIT, 2012, *Testing the profitability of contrarian trading strategies based on the overreaction hypothesis*, [Submitted].
- T. CASTERMANS, M. DUVINAGE, 2013, Corticomuscular coherence revealed during treadmill walking: another evidence of supraspinal control in human locomotion, Journal Club of Journal of Physiology, [IF=4.9].
- T. HOELLINGER, M. PETIEAU, M. DUVINAGE, T. CASTERMANS, K. SEETHARAMAN, A.M. CEBOLLA, A. BENGOETXEA, Y. IVANENKO, B. DAN, G. CHERON, 2013, *Biological oscillations for learning walking coordination: dynamic recurrent neural network functionally models physiological central pattern generator*, Frontiers in Computational Neuroscience, 29 May 2013, [IF=2.15].
- M. DUVINAGE, T. CASTERMANS, M. PETIEAU, T. HOELLINGER, G. CHERON, T. DUTOIT, 2013, *Performance of the Emotiv EPOC headset for P300-based applications*, BioMedical Engineering OnLine, Volume 12:56, Published: 25 June 2013.
- N. RICHE, M. MANCAS, M. DUVINAGE, M. MIBULUMUKINI, B. GOSSELIN, T. DUTOIT, 2013, *RARE2012: A multi-scale rarity-based saliency detection with its comparative statistical analysis*, Signal Processing: Image Communication.
- M. DUVINAGE, P. MAZZA, M. PETITJEAN, 2013, *The intraday performance of market timing strategies and trading systems based on Japanese candlesticks*, Quantitative Finance, [Ranked C-CNRS/C-ABS].
- T. CASTERMANS, M. DUVINAGE, G. CHERON, T. DUTOIT, 2013, *Towards Effective Non-Invasive Brain-Computer Interfaces Dedicated to Gait Rehabilitation Systems*, Brain Sciences, 2014; 4(1):1-48.
- G. CHERON, M. DUVINAGE, C. DE SAEDELEER, T. CASTERMANS, A. BENGOETXEA, M. PETIEAU, K. SEETHARAMAN, T. HOELLINGER, B. DAN, T. DUTOIT, F. SYLOS LABINI, F. LACQUANITI, Y. IVANENKO, 2012, *Forthcoming Strategies for Clinical Translation in Neurorehabilitation: From spinal central pattern generators to cortical network: integrated BCI for walking rehabilitation*, Neural Plasticity [IF=2], Volume 2012, Article ID 375148.
- M. DUVINAGE, T. CASTERMANS, R. JIMÉNEZ-FABIÁN, T. HOELLINGER, M. PETIEAU, O. VERLINDEN, G. CHERON, T. DUTOIT, 2012, *Human Walk Modeled by PCPG to Control a Lower Limb Neuroprosthesis by High-Level Commands*, Journal of Systemics, Cybernetics and Informatics, volume 10, number 3, pp. 70-80, [Extended version of the 5

- T. CASTERMANS, **M. DUVINAGE**, M. PETIEAU, T. HOELLINGER, C. DE SAEDELEER, K. SEETHARAMAN, A. BENGOETXEA, G. CHERON, T. DUTOIT, 2012, *Optimizing the performances of a P300-based Brain-Computer Interface in ambulatory conditions*, IEEE Journal on Emerging and Selected Topics in Circuits and Systems, vol. 4, n. 4, December 2011, pp. 566 - 577.
- C. MÜHL, H. GÜRKÖK, D. PLASS-OUDE BOS, M.E. THURLINGS, L. SCHERFFIG, **M. DUVINAGE**, A.A. ELBAKYAN, S. KANG, M. POEL, D.K.J. HEYLEN, 2010, *Bacteria Hunt: Evaluating multi-paradigm BCI interaction*, Journal on Multimodal User Interfaces (JMUI), Springer Berlin/Heidelberg.

D.4 Papers in Conference Proceedings

- **M. DUVINAGE**, T. CASTERMANS, M. PETIEAU, T. HOELLINGER, K. SEETHARAMAN, G. CHERON, T. DUTOIT, 2013, *A Preliminary Fundamental Study of Ambulatory SSVEP*, Proceedings of the TOBI IV workshop, Sion, Switzerland, January 23-25.
- **M. DUVINAGE**, J. CUBETA, T. CASTERMANS, M. PETIEAU, T. HOELLINGER, G. CHERON, T. DUTOIT, 2013, *A Quantitative Comparison of the Most Sophisticated EOG-based Eye Movement Recognition Techniques*, Proceedings of the IEEE SSCI series, Singapore, April 16-19.
- N. RICHE, **M. DUVINAGE**, M. MANCAS, B. GOSSELIN, T. DUTOIT, 2013, "A study of parameters affecting visual saliency assessment", Proceedings of the 6th International Symposium on Attention in Cognitive Systems (ISACS'13) , Beijing, China, August 3-5.
- T. CASTERMANS, **M. DUVINAGE**, N. RICHE, 2013, *Online emotion classification from electroencephalographic signals : a first study conducted in a realistic movie theater*, 12th International Conference on Artificial Intelligence and Soft Computing ICAISC 2013, Zakopane, Pologne, June 9-13.
- N. RICHE, **M. DUVINAGE**, M. MANCAS, B. GOSSELIN, T. DUTOIT, 2013, *Saliency and Human Fixations: State-of-the-art and Study of Comparison Metrics*, Proceedings of the 14th International Conference on Computer Vision (ICCV 2013), Sydney, Australia, December 1-8 [to appear].
- **M. DUVINAGE**, T. CASTERMANS, R. JIMÉNEZ-FABIÁN, T. HOELLINGER, C. DE SAEDELEER, M. PETIEAU, K. SEETHARAMAN, G. CHERON, O. VERLINDEN, T. DUTOIT, 2012, *A Five-State P300-based Foot Lifter Orthosis: Proof of Concept*, Proceedings of the 3rd IEEE Biosignals and Biorobotics conference (ISSNIP), Manaus, Brazil, January 9-11.
- **M. DUVINAGE**, T. CASTERMANS, M. PETIEAU, T. HOELLINGER, C. DE SAEDELEER, K. SEETHARAMAN, G. CHERON, T. DUTOIT, 2012, *A P300-Based Quantitative Comparison Between the Emotiv Epoc Headset and a Medical EEG Device*, Proceedings of the 9th IASTED International Conference on Biomedical Engineering.

- M. DUVINAGE, T. CASTERMANS, M. PETIEAU, K. SEETHARAMAN, T. HOELLINGER, G. CHERON, T. DUTOIT, 2012, *A Subjective Assessment of a P300 BCI System for Lower-Limb Rehabilitation Purposes*, Proceedings of the 34th Annual International Conference of the IEEE Engineering in Medicine and Biology Society (EMBC 2012), San Diego, USA, August 28 - September 1.
- M. DUVINAGE, T. CASTERMANS, M. PETIEAU, G. CHERON, T. DUTOIT, 2012, *Are current gait-related artifact removal techniques useful for low-complexity BCIs?*, IEEE World Congress On Computational Intelligence (IEEE WCCI), Brisbane, Australia, June 10-15.
- T. CASTERMANS, M. DUVINAGE, G. CHERON, T. DUTOIT, 2012, *EEG AND HUMAN LOCOMOTION: Descending Commands and Sensory Feedback should be Disentangled from Artifacts Thanks to New Experimental Protocols*, Proceedings of the 5th International Joint Conference on Biomedical Engineering Systems and Technologies (BIOSTEC), Vilamoura, Algarve, Portugal, February 1-4.
- L. BOUGRAIN, M. DUVINAGE, E. KLEIN, 2012, *Inverse reinforcement learning to control a robotic arm using a Brain-Computer Interface*, Proceedings of the 8th International Summer Workshop on Multimodal Interfaces - eINTERFACE'12, pp. 83-88, July, Metz, France.
- Q. OGGERO, O. VERLINDEN, R. JIMÉNEZ-FABIÁN, M. DUVINAGE, T. CASTERMANS, A. CLARINVAL, C. ENGEL, 2012, *Prototype of active ankle orthosis with specific actuator design and capitalizing on additive manufacturing*, Proceedings of the HFR2012 – 5th International Workshop on Human-Friendly Robotics, Brussels, Belgium, October 18-19.
- M. DUVINAGE, R. JIMÉNEZ-FABIÁN, T. CASTERMANS, O. VERLINDEN, T. DUTOIT, 2011, *An active foot lifter orthosis based on a PCPG algorithm*, Proceedings of the IEEE 12th International Conference on Rehabilitation Robotics (ICORR 2011), ETH Zurich, Switzerland, June 29 - July 1, pp 116-122.
- T. CASTERMANS, M. DUVINAGE, T. HOELLINGER, M. PETIEAU, T. DUTOIT, G. CHERON, 2011, "An analysis of EEG signals during voluntary rhythmic foot movements", Proceedings of the 5th International IEEE/EMBS Neural Engineering Conference, Fiesta Americana Grand Coral Beach Cancun, Mexico, April 27 - May 1, pp. 584-587.
- M. DUVINAGE, T. CASTERMANS, T. DUTOIT, 2011, *Control of a lower limb active prosthesis with eye movement sequences*, Proceedings of the IEEE Symposium on Computational Intelligence, Cognitive Algorithms, Mind, and Brain (CCMB), Paris, France, April 11-15, pp. 136-142.
- M. DUVINAGE, T. CASTERMANS, T. HOELLINGER, J. REUMAUX, 2011, *Human Walk Modeled by PCPG to Control a Lower Limb Neuroprostheses by High-Level Commands*, Proceedings of the 2nd International Multi-Conference on Complexity, Informatics and Cybernetics (IMCIC 2011), March 27-30, Orlando, Florida, USA [Best Session Paper].

- G. CHERON, O. VERLINDEN, T. DUTOIT, A. CLARINVAL, C. RUSTIN, R. JIMÉNEZ-FABIÁN, T. CASTERMANS, **M. DUVINAGE**, C. DE SAEDELEER, M. PETIEAU, 2011, *Integrated Development of an Intellinet Customised Foot Orthosis*, 10th Belgian Day on Biomedical Engineering, joint meeting with IEEE EMBS Benelux Chapter, Brussels, Belgium.
- D. PLASS-OUDE BOS, **M. DUVINAGE**, O. OKTAY, J. DELGADO SAA, H. GU-RULER, A. ISTANBULLU, M. VAN VLIET, B. VAN DE LAAR, M. POEL, L. ROI-JENDIJK, L. TONIN, A. BAHRAMISHARIF, B. REUDERINK, 2011, *Looking Around with your brain in a virtual world*, Proceedings of the IEEE Symposium on Computational Intelligence, Cognitive Algorithms, Mind, and Brain (CCMB), Paris, France, April 11-15, pp. 106-113.
- **M. DUVINAGE**, T. CASTERMANS, T. HOELLINGER, G. CHERON, T. DUTOIT, 2011, *Modeling Human Walk by PCPG for Lower Limb Neuroprostheses Control*, Proceedings of the 5th International IEEE/EMBS Neural Engineering Conference, Fiesta Americana Grand Coral Beach, Cancun, Mexico, April 27 - May 1, pp. 317-321.
- D. PLASS-OUDE BOS, B. VAN DE LAAR, **M. DUVINAGE**, O. OKTAY, J. DELGADO SAA, M. VAN VLIET, M. POEL, L. ROIJENDIJK, A. BAHRAMISHARIF, B. REUDERINK, 2011, *Wild Photoshoot: Applying overt and covert attention: Workshop*, Neuroscience Letters Conference Abstract, Society of applied neuroscience (SAN2011), Thessaloniki, Greece, page 26-27.
- D. PLASS-OUDE BOS, **M. DUVINAGE**, O. OKTAY, J. DELGADO SAA, H. GU-RULER, A. ISTANBULLU, M. VAN VLIET, B. VAN DE LAAR, M. POEL, L. ROI-JENDIJK, L. TONIN, A. BAHRAMISHARIF, B. REUDERINK, 2010, *Looking Around with Your Brain in a Virtual World*, Proceedings of the 6th International Summer Workshop on Multimodal Interfaces - eINTERFACE'10, Amsterdam, The Netherlands, Volume 2, pp. 12-23.
- **M. DUVINAGE**, J.Y. PARFAIT, 2010, *Reconnaissance vocale basée sur les phonèmes voisés*, Actes des 28emes Journées d'Etude sur la Parole (JEP 2010), pages 257-260, 25-28 mai, 2010, Mons, Belgique.
- C. MÜHL, H. GÜRKÖK, D. PLASS-OUDE BOS, M.E. THURLINGS, L. SCHERFFIG, **M. DUVINAGE**, A.A. ELBAKYAN, S. KANG, M. POEL, D.K.J. HEYLEN, 2009, *Bacteria Hunt: A multimodal, multiparadigm BCI game*, Proceedings of the 5th International Summer Workshop on Multimodal Interfaces - eINTERFACE'09, pp. 41-62, July 13th - August 7th, 2009, Genoa, Italy.